Vibration-Based Finite Element Model Updating and Structural Damage Identification

Maung Than Soe

A thesis submitted in partial fulfilment of the requirements of the University of Greenwich for the Degree of Doctor of Philosophy

May 2013

Declaration

I certify that this work has not been accepted in substance for any degree, and is not concurrently being submitted for any degree other than that of Doctor of Philosophy being studied at the University of Greenwich. I also declare that this work is the result of my own investigations except where otherwise identified by references and that I have not plagiarised the work of others.

Signature:

PhD candidate: Maung Than Soe

Signature:

1st supervisor:Dr Hua-Peng Chen

Signature:

2nd supervisor: Prof Amir M Alani

Summary

Damage and material deterioration could lead to structural failure with unknown consequences. Structural health monitoring strategy based on vibration measurements for existing aging structures offers a promising technique for effectively managing the deteriorating structures. The main objectives of this research are to develop a procedure for finite element model updating by using incomplete modal data identified from vibration measurements, to develop real time structural damage detecting method by directly using vibration measurements and then identify the damage at detailed location and extend in the structure on the basis of the validated numerical model.

A steel frame model structure was constructed in the laboratory for finite element model updating and structural damage detection. Forced vibration testing was undertaken on the model structure, and dynamic response such as accelerations were measured by using sensors installed. Modal analyses are then carried out to identify modal parameters such as frequencies, mode shapes and damping from the vibration measurements. Structural damage scenarios were simulated by breaking bracing members of the model structure, and modal parameter of the damaged structures were also identified and analysed.

An effective approach for directly updating finite element model from measured incomplete modal data with a regularised iterative algorithm is then presented.The exact relationship between the perturbation of structural parameters and the modal properties of the dynamic structure is developed. Numerical simulation investigations and experimental study of a

laboratory tested space steel frame model and practical application to the Canton Tower benchmark problem are undertaken to verify the accuracy and effectiveness of the proposed model updating method.

Finally, a new approach for real time structural damage detection by using acceleration measurements is presented. Structural damage is characterised at element level by introducing damage parameters which can indicate the location and severity of damage in the structure. The relationship between the damage parameters and the measured dynamic response is then established from the governing equation of the dynamic structure. Numerical examples of cantilever beams, plane frame, and braced frames are adopted to demonstrate the effectiveness of the proposed method. The new proposed technique performs well and produces stable and reliable results, which could be used for real time damage assessment during the event of earthquake and explosion.

Acknowledgements

Firstly, I am most grateful tomy supervisor Dr. Hua-Peng Chen for his encouragement, valuable advices, and guidance throughout this research project.

Thanks are due to the Head of Civil Engineering Department, Professor Amir M Alani for his valuable advices on various issues.

Thanks are additionally due to colleagues in the laboratory for their assistance in conducting experiments.

I would like to thankto the research committee of University of Greenwich for providing financial support for this research project.

Finally, truly unbounded thanks are due to my parents who encouraged me to be a graduate.

Table of Contents

List of Figures

List of Tables

List of Symbols

B location matrix

b(ξ) row vector representing the relationship between thecurvature of the structural element and the nodal displacements

C damping matrix of undamaged structure

$\mathbf{C}^d$ damping matrix of damaged (tested) structure

C_{ik} mode participation factor

E_{ω}^{i} relative error of updated frequency

E_{ω} average absolute error of all updated frequencies

E_{ϕ}^{i} relative error of updated incomplete mode shape

E_{ϕ} average error ofall updated incomplete mode shapes

F force vector

F(ω) input force as a function of frequency

$\mathbf{FSE}_{ij}$ fractional strain energy

$\mathbf{F}_i$ time dependent applied force of undamaged structure

$\mathbf{F}_i^d$ time dependent applied force of damaged (tested) structure

G gain matrix

H(ω) transfer function as function of frequency

I identity matrix

$\mathbf{K}$ global stiffness matrix

$\mathbf{K}_j$ j^{th} element stiffness matrix

$\mathbf{K}^d$ global stiffness matrix of damaged (tested) structure

$\mathbf{K}_e$ element stiffness matrix of analytical model

$\mathbf{K}_e^b$ e^{th}beam element stiffness matrix of beam of analytical model

$\mathbf{K}_r^b$ element stiffness matrix of beam at integration point r

$\mathbf{K}^{-1}$ flexibility matrix

$\Delta\mathbf{K}_e$ variation ofe^{th} element stiffness matrix

$\Delta\mathbf{K}$ variation ofglobal stiffness matrix

$\Delta\mathbf{K}_e^b$ variation ofe^{th} element stiffness matrix of beam

$\Delta\mathbf{K}^{-1}$ variation of flexibility matrix

$\tilde{\mathbf{K}}$ global stiffness matrix of damaged (tested) structure

$\tilde{\mathbf{K}}_e$ e^{th} element stiffness matrix of damaged (tested) structure

$\tilde{\mathbf{K}}_e^b$ e^{th}beam element stiffness matrix of beam of damaged (tested) structure

$\mathbf{M}$ global mass matrix

$\mathbf{M}^d$ global mass matrix of damaged (tested) structure

$\mathbf{M}_e$ element mass matrix

$\mathbf{M}_j$ j^{th} element mass matrix

$\Delta\mathbf{M}$ change in global mass matrix

$\tilde{\mathbf{M}}$ global mass matrix of damaged (tested) structure

$\Delta\mathbf{P}$ structural parameters residual

$\mathbf{P}_j$ structure parameter

$\mathbf{r}_i$ residual force vector

$\Delta\mathbf{R}$ structural response residual

$\mathbf{S}$ sensitivity matrix

$\mathbf{SE}_i$ strain energy of undamaged structure

$\mathbf{SE}_i^d$ strain energy of damaged structure

$\mathbf{T}_s$ static transformation

$\mathbf{T}_p$ transformation matrix

$\mathbf{u}$ state vector

$\mathbf{U}(\omega)$ displacement response function as function frequency

$\mathbf{U}_i$ time dependent variable displacement

$\Delta\mathbf{U}_i$ time dependent variable incremental displacement,

$\mathbf{U}_i^d$ time dependent variable displacement of damaged (tested) structure

$\dot{\mathbf{U}}_i$ time dependent variable velocity

$\Delta\dot{\mathbf{U}}_i$ time dependent variable incremental velocity

$\dot{\mathbf{U}}_i^d$ time dependent variable velocity of damaged (tested) structure

$\ddot{\mathbf{U}}_i$ time dependent variable acceleration

$\Delta\ddot{\mathbf{U}}_i$ time dependent variable incremental acceleration

$\ddot{\mathbf{U}}_i^d$ time dependent variable acceleration of damaged (tested) structure

$\overline{\ddot{\mathbf{U}}}_i^d$ time dependent noise-free variable acceleration of damaged structure

$\boldsymbol{\phi}_k$ analytical mode shape

$\boldsymbol{\phi}_\kappa^a$ analyticalmode shapes corresponding to the same dimension of measured mode shape readings

$\boldsymbol{\phi}_i^d$ mode shape of damaged (tested) structure

$\boldsymbol{\phi}_k^u$ analytical mode shape associated with unmeasured partition

$\tilde{\boldsymbol{\phi}}_i^u$ unmeasured components of mode shape

$\tilde{\boldsymbol{\phi}}_i$ mode shape of damaged (tested) structure

$\tilde{\boldsymbol{\phi}}_i^a$ incomplete measured mode shape

$\hat{\boldsymbol{\phi}}_i$ updated mode shape

$\hat{\boldsymbol{\phi}}_i^a$ updated incomplete mode shape

$\tilde{\boldsymbol{\psi}}_i$ mode shapereadings of damaged (tested) structure

$\boldsymbol{\Lambda}$ diagonal matrix of associated measured modal frequencies squared

ω_i frequency of analytical model

$\tilde{\omega}_i$ frequency of damaged (tested) structure

$\hat{\omega}_i$ updated frequency

υ_i mode scale factor

θ_e e^{th} stiffness updating parameter

θ_r stiffness updating parameter characterised at critical point level

θ_j j^{th} element stiffness updating parameter

β_j j^{th} element mass updating parameters

α_j j^{th} structural damage parameter

$\boldsymbol{\alpha}$ vector of damage parameters

Chapter 1 Introduction

1.1 Background

Due to structural material deterioration and extreme events on structures, structural health monitoring (SHM) of civil engineering infrastructure has received significant attention in order to assess the safety of structures during their service life. The safety of aging infrastructure and economic considerations have been motivating factors for the development of reliable structural condition assessment methods which can be used to evaluate the deterioration at the earliest stage. Assessment of structural conditions is not only beneficial to the cost effective maintenance strategy but also increases the overall efficiency of operation and life-span of a structure. It can also reduce the risk of loss of human lives due to unexpected structural failures.

In the UK, over 40,000 bridges and tunnels have been constructed for the railway system alone. The average age of the bridges is more than 50 years old and the ages of London underground tunnels are 75-100 years old. Many of the structures are below the required strength and are in need of either strengthening, rehabilitation or replacement. Many researches have being undertaken by researchers for investigating the condition and performance of the structural integrity and functionality. However, inaccurate condition assessment has been identified as the most critical technical barrier for effective structural condition assessment. For example, conditions of structures are typically expressed in terms of subjective indices which are based on visual inspection alone. The difficulties of visually inspecting have proved to be inadequate in order to evaluate an aging structure accurately.

In the past two decades, the amount of research relating to structural health monitoring has increased significantly and various structural health monitoring techniques have been developed to detect the damage in the structures and assess the condition of the structures. Structural health monitoring is the implementation of a damage identification strategy to the civil engineering infrastructure. Damage is defined as changes to the material and/or geometric properties of the structural systems, including changes to the boundary conditions. Damage affects the current or future performance of the structural systems. In 1970s and 1980s, the oil industry introduced vibration-based structural damage detection for offshore platforms but practical problems prevented adaptation and abandoned in early 1980s. In the late 1970s and early 1980s, the aerospace community made contributions in identifying fatigue damage in aircraft components. Cawley and Adams (1979) developed a method to detect damage in composites by using natural frequency shifts. However, the changes in natural frequencies did not provide sufficient information to fully assess or characterize damage in the structure. In the early 1980s, vibration-based damage assessment for bridge structures based on mode shape curvature and dynamic flexibility matrix indices was proposed (Farrar and Worden 2007).

The curvature of the mode shape appears to be more sensitive to the reduction in stiffness caused by structural damage (Farrar and Cone 1995). However, the detection of structural damage may not be practical if the change in stiffness is relatively small and noise exists in the measurements. Most vibration-based damage identification methods have utilised the modal characteristics, i.e., natural frequencies, mode shapes, and damping properties of the structural system which are governed by the physical properties such as stiffness and mass of the structural system. Since the modal characteristics of a structure are functions of its

physical properties, any changes to these physical properties caused by damage will reflect the changes in the modal properties.

In structural damage detection, the measured modal parameters of the damaged structure as well as the original undamaged structure are typically required. In general, the analytical model for the finite element (FE) analysis of the associated actual engineering structure is constructed on the basis of highly idealised engineering design that may not fully represent all the physical and geometrical aspects of the actually built structure. As a result, a significant discrepancy may exist between the modal properties calculated by the constructed finite element model and those identified from the vibration measurements of the actual tested structure. In the 1990s, Mottershad and Friswell (1993) surveyed finite element model updating methods using vibration measurements. The finite element model updating methods are often utilised to adjust the numerical model using the measured modal data to maximize the correlation between the numerical and experimental results. The existing model updating method utilising vibration response data can be classified into two categories (i.e., direct and iterative methods). In direct method, the stiffness and mass matrices of elements are directly constructed utilising vibration measurements by one-step procedure. However, this method may not perform well to represent the actual tested structure concerned in the case of large number of structure parameters need to be updated in the finite element model. The iterative method including sensitivity method updates the structural parameters of finite element model by an optimisation process. The performance of iterative method mainly depends on the selection of objective function and constraints. However, optimisation techniques used in iterative method may not perform well if number of the chosen structure parameters to be updated is large and significant discrepancy exist between initial finite element model and actual tested structure.

Although, the advancement in structural health monitoring techniques based on measured vibration data have been widely utilised for assessing engineering structures, there is still a need to develop more accurate and reliable methods for finite element model updating by directly utilising incomplete modal data without requiring optimisation technique, mode shape expansion or model reduction technique. Moreover, the existing structural damage detecting methods required modal data identified from vibration measurements and may not provided evolution of damage in real time. Thus, it is beneficial to develop real time structural damage detection method to identify both the location and severity evolution of damage in the structure by directly utilising of monitored vibration measurements without requiring modal analysis technique.

1.2 Aim and objectives

The main aim of the research project is to develop aprocedure for finite element model updating, on-line structural damage detection and condition assessment using vibration measurements from installed sensors.

The specific objectives of the project are

1. To undertake vibration testing in the laboratory to investigate dynamic responses of intact and damaged structures.
2. To develop a robust finite element model updating method using incomplete modal data
3. To develop a structural damage identification method for assessing structural condition from vibration measurements.

1.3 Research methodologies

The methodologies used in this research include:

- Laboratory vibration testing of a scaled steel frame model structure. Vibration response data set such as acceleration is obtained from limited installed sensors (i.e., accelerometers) and incomplete modal data is identified by modal analysis technique.
- Developments of new methods for finite element model updating by using incomplete modal data with regularised iterative algorithm and real time structural damage identification method by directly using vibration measurements without requiring modal analysis techniques.
- Applications of the developed methods in validated numeral models and real engineering structures.

The research will extend the modal perturbation method structural condition assessment (Chen and Bicanic 2006). The model updating method, on the basis of a physical-based model of the monitored structure, will be used as a tool for assessing the health and evaluating the condition of the structure by directly updating the finite element model from measured incomplete modal data with regularised iterative algorithms. This method will also be used as a basis to assess the reliability of the structure in performing as expected under uncertain current conditions of existing structures. Furthermore, real time structural damage detection method will be developed based on stiffness coefficients associated with element stiffness matrices (Chen and Bicanic 2006) and time step integration method to obtain dynamic responses such as displacement and velocity from acceleration (Newmark 1959, Kang et al. 2005). Structural damage evolution assessment can be carried out on the basis of

the validated numerical model using vibration measurements which can assess the condition and monitor the reliability or safety of the structures under consideration.

Chapter 2 Literature Review

2.1 Introduction

The performance and behaviour characteristics of civil infrastructure can be affected by degradation resulting from the structural damage caused by loading and extreme events such as earthquake and explosion. Monitoring the integrity of civil infrastructure is of great concern in order to improve the safety and reliability of the structures. Such monitoring processes can provide the necessary information for maintenance, rehabilitation, and other relevant activities to ensure the safety of the structure during its service life. Moreover, assessment of structural condition is also beneficial for on-time decisions which can reduce the probability of catastrophic collapse due to undetected structural failures.The structural health monitoringprocess involves the monitoring of a structure periodically by using structural response measurements obtained from installed sensors, extraction of features from measured data, and statistical analysis of these features to determine the current health condition of the structural system, and timely evaluating the structural performance (Sohn et al. 2003, Farrar 2007).

Material deteriorationof a structural system, adversely affect the performance of the structure. The commonly measured modal parameters (frequencies, mode shapes, and damping) are functions of the physical properties of the structure (mass and stiffness). Therefore, changes in physical properties, such as reductionsof stiffness may cause detectable changes in modal properties (Chang et al. 2003).For example, long-spanned structures such as bridges are more sensitive to flutter instability under wind, earthquake and traffic-induced vibrations which may cause large deflections and considerable structural deterioration.

The structural health monitoring problem can be addressed in the context of a statistical pattern recognition paradigm (Farrar and Doebling 1999). This paradigm can be broken down into four parts:

1. Operational evaluation
2. Data acquisition and cleansing
3. Feature extraction and data compression
4. Statistical model development for feature discrimination

Operational evaluation answers four questions regarding the implementation of a structural health monitoring system:

1. What are the economic and/or life safety motives for performing the monitoring?
2. How is damage defined for the system being monitored?
3. What are the conditions, both operational and environmental, under which the system to be monitored function?
4. What are the limitations on acquiring data in the operational environment?

The data acquisition portion of the structural health monitoring process involves selecting the excitation methods, the types of sensors to be used, the number of sensors, the locations where the sensors should be placed, and the data acquisition hardware. Data cleansing is the process of data selection to pass on to or reject from the feature selection process. Signal processing techniques such as filtering and re-sampling can also be thought of as data cleansing procedures. Feature extraction is the process of identifying damage-sensitive properties, derived from the measured vibration response, which allows distinguishingbetween the undamaged and damaged structure. Statistical model development

is concerned with the implementation of the algorithms that operate on the extracted features to quantify the damage state of the structure.

The damage state of a structural system can be described as a five-step process (Rytter 1993, Yan 2006). The damage state is described by answering the following questions:

1. Is there damage in the system (existence)?
2. Where is the damage in the system (location)?
3. What kind of damage is present (type)?
4. How severe is the damage (extent)?
5. How much useful life remains (prognosis)?

Experimental structural dynamics techniques may be used to address the first two questions. To identify the type of damage, measured data from structures with the specific types of damage can be used. Analytical models are usually needed to answer the fourth and fifth questions. Estimates of the future system loading are also necessary to completely address the fourth and fifth questions.In general, damage identification methods can be classified into two categories: data-based and modal-based methods. The data-based method describes the change in structural properties (mass and stiffness) in terms of structural response data and modal-based method expresses changes in structural properties in terms of modal parameters (natural frequencies, modal damping, and mode shapes) estimated from modal analysis.

2.2 Data-based damage identification methods

2.2.1 Neural networks

The neural network method has been applied successfully in many applications including vibration based damage identification. Spillman et al. (1993) used neural network to identify damage in a steel bridge element. Damage was introduced by cutting the element and bolting

plate reinforcement over top of the cut. With the plate attached, the element was considered to be undamaged. With the bolts loosened, the element was considered to be partially damaged, and when the plate was removed, the element was considered to be fully damaged. There were three sensors mounted to the element: two accelerometers and a fiber optic sensor.

The beam was struck in four different locations with a calibrated impact. A total number of eleven tests were performed. The time-history signal from each sensor was Fourier transformed, and the height and frequency of the first two modal peaks were used as inputs to the neural network. The impact intensity and location were also provided as inputs. A network configuration was selected with the 14 inputs, a hidden layer with 20 neurons, and 3 outputs, one for each of the possible damage states. The body of training data was cycled through the training algorithm until the self-prediction error converged to a minimum. Using all three sensors, the authors found the proportion of correct diagnoses to be 58%.

Liu and Sun (1997) used neural networks to identify damage in a simply supported three-span bridge. The neural networks were trained using simulated data from a finite element model of the bridge. The bridge model was discretized into 30 uniform beam elements. Damage was simulated by reducing element stiffness located in at the middle as well as the sides of the spans. The maxima and minima of the bridge elongation curves were produced by a moving truck traversing the bridge. Five separate neural networks were used to monitor local dynamic characteristics along the total span of the bridge.Nine local elongation curves, calculated at different locations along the bridge, were used as inputs to the five networks. The network outputs were estimated as reductions in terms of percentage. Liu and Sun found that damage influences the extreme values of the elongation curves in different ways,

depending on the damage location in relation to the elongation curve.Liu and Sun concluded that these local bridge elongations from a moving truck were effective features for damage detection.

2.2.2 Wavelet analysis

Wavelet analysis is very suitable to analyse non-stationary signal, so it can be used as a feasible method for processing signal in damage detection to construct the needed feature index of structural damage. Wavelet analysis has various applications in structural damage detection, for example, singular signal detection, signal-to-noise separation, frequency-band analysis and so on. The spectrum graph obtained using wavelet transform can indicate the damage existence (Chang and Chen 2005, Fan and Qiao 2009).Rajasekaran and Varghese (2005) proposed a wavelet based approach for structural damage detection in beams, plates and detection of delamination of composite plates. The main concept used was the breaking down of the dynamic signal of a structural response into a series of local basis function called wavelets, so as to detect the special characteristics of the structure using scaling and transformation property of wavelets.

Lu and Hsu (2002) presented a study based on the wavelet transform for structural damage detection. Through comparing the discrete wavelet transforms of two sets of vibration signals from the undamaged and damaged structures in the space domain, not only the presence of defects can be detected, but also their number and location as well. Numerical results showed that even a minor localised defect can induce significant changes in the wavelet coefficients of the vibration signals.With respect to structural damage condition assessment and structural

health monitoring, wavelet analyses can be used to detect instantaneous changes in structural properties by monitoring online responses.

2.2.3 Genetic algorithm (GA)

The genetic algorithm (GA) is optimization technique based on the Darwin's (1859) theory of evolution and survival of the fittest. This method, originally developed by Holland (1975), operates on an initial population of randomly generated candidate solutions. The applying principle is survival of the fittest to produce better approximations to the solution. At each generation, a new set of approximations is created by the process of selecting individuals according to their level of fitness. A simple Genetic Algorithm consists of three basic operations, selection, crossover and mutation (Perera and Torres 2006). The algorithm begins with a population of individuals each of them representing a possible solution of the problem.

At the selection level, the quality of an individual is measured by its fitness value. In the crossover operation, the genes of pair of individuals are exchanged. The mutation operator introduces a change in one or more of the genes. Therefore, with this operator new material is introduced in the population and its main goal is to prevent the population from converging to a local minimum. The genetic algorithm approach attempts to find the best solution to a given problem by minimizing an objective evaluation function (Silva 2006).

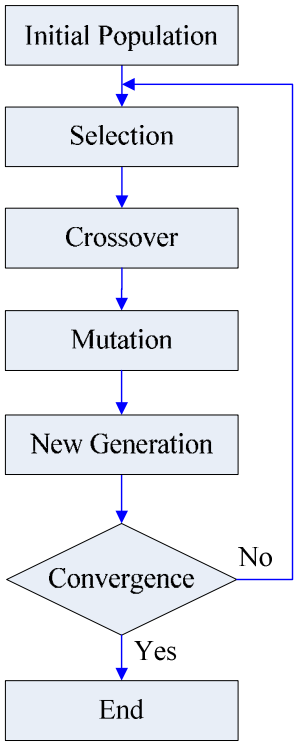

Figure 2.1 Flowchart of simple genetic algorithm

Sazonov et al. (2002) used the genetic algorithm to produce a sufficiently optimized amplitude characteristic filter to extract damage information from strain energy mode shapes. The genetic optimization was performed based on the minimization of the signal-to-distortion ratio. The algorithm progresses with successive generations to reach an optimum solution for the problem.Chou and Ghaboussi (2001) used a genetic algorithm as a method of structural damage detection by optimizing fitness functions formulated in terms of static measured displacements. Xu and Liu (2002) applied genetic algorithm as an effective technique for flaw detection of composites.

The application of genetic algorithm in structural damage assessment is effective, easy to implement, and no special requirement concerning the initial values of unknown parameters

is needed. Furthermore, genetic algorithm uses multiple points to search for the solution rather than single point, and the calculation of the derivative of the error function with respect to the search direction is not required. However, damage detection involves inverse analysis, and noise contaminated data may lead to large error in the damage estimations.

2.3 Modal-based damage identification methods

During the late 1970s and early 1980s vibration based damage detection techniques were started to be developed. The early approaches used were based on correlating numerical models with measured modal properties from undamaged and damaged components. Euring last decade, significant research effort has been applied to condition monitoring with the emergence of a broad range of techniques, algorithms and methods.

Vibration-based structural damage detection methods can be categorized as (Wang and Chan 2009, Fan and Qiao 2011)

1. Change of natural frequency
2. Change of structural vibration mode shape
3. Change of structural flexibility or stiffness
4. Damage index method
5. Frequency response function
6. Modal residual vectors

2.3.1 Change of natural frequency

The presence of damage or deterioration in a structure causes changes in the natural frequencies of the structure. Frequency measurements can be quickly conducted and are often utilized in structural damage detection. Typically, measured frequencies are compared to the predicted frequencies of analytical model to determine the damage in the structure.

Kim et al. (2003) have proposed a method to locate and estimate the size of damage in structures using a few natural frequencies. A damage-localisation algorithm to locate damage from changes in natural frequencies and a damage-sizing algorithm to estimate crack size from natural frequency perturbation were formulated.From the test study of I-40 concrete bridge in Oklahoma, USA, Farrar and Cone (1995) demonstrated that frequency shift was not a sensitive damaged indicator as no significant reductions of modal frequencies were observed although overall stiffness of the bridge cross section was reduced by 21%. Kessler et al. (2002) studied the effect on frequency response of various forms of damage (drilled through holes, impact damage, bending induced cracks and fatigue damage) on clamped composite plates and concluded that the only type of damage distinguishable from the others at low frequency ranges was fatigue damage.De Roeck et al. (2000) monitored the Z24 concrete bridge built between 1961 and 1963 in Switzerland over a year. Its damage pattern was identified using the eigen frequencies and unscaled mode shape data obtained from ambient vibrations. The damage was presented by a reduction in bending and torsion stiffness of the bridge girder.

Lee and Chung (2000) ranked the first four frequencies of a simulated cantilever beam to locate a single crack. The crack depth was then approximated iteratively to match the first

frequency as closely as possible before the location of the crack was finally refined.Yang et al. (2001) used 3D plots of frequency change versus depth and location of a crack to identify a saw cut in an aluminium beam. The contour lines obtained from each frequency change plot were overlain and their intersection gave the true location and depth of the crack.

A review of methods of damage detection using natural frequencies has shown that these approaches are potentially useful for routine integrity assessment of structures. Frequency values obtained from vibration testing could be used to detect structural damage. The most successful applications have been conducted to small laboratory structures. The advantage of using the change of structural natural frequency is its convenient measurement and high accuracy. However, natural frequency changes alone may not provide enough information for structural damage detection. Furthermore, the natural frequency is not often sensitive enough to initial damage in structures. Usually, this method can only ascertain existence of the large damage, but may not be able to detect the detailed location and extend of damage in the structure.

2.3.2 Change of structural vibration mode shape

The frequencies can be measured more accurately than the vibration mode shapes, but the mode shapes are more sensitive to local damage. Structural damage existence can be detected through the information of modal data. Modal analysis techniques are available for the extraction of mode shapes from the measured data. To check for agreement between the measured mode shapes and analytical ones, the Modal Assurance Criterion (MAC) proposed by Allemang and Brown (1983) is used, which is defined as

$$\mathrm{MAC}(k,i) = \frac{\left|\boldsymbol{\phi}_k^T \tilde{\boldsymbol{\phi}}_i\right|^2}{\left|\boldsymbol{\phi}_k^T \boldsymbol{\phi}_k\right|\left|\tilde{\boldsymbol{\phi}}_i^T \tilde{\boldsymbol{\phi}}_i\right|} \tag{2.1}$$

where $\tilde{\boldsymbol{\phi}}_i$ is the measured i^{th} mode shape and $\boldsymbol{\phi}_k$ is the corresponding analytical mode shape.The value of MAC is between "0" and "1". When the two mode shapes are more similar, the MAC value is closer to "1". The MAC value is "0" if two mode shapes are orthogonal with each other.

Nikolakopoulos et al. (1997) used changes in natural frequencies and mode shapes to detect damage in a finite element model of the cable-stayed steel bridge consisting of 5 spans; i.e, 31 m, 64 m, 171 m, 64 m, and 31 m respectively. Damage was simulated by removing the bottom flanges of the longitudinal girders in the end spans. The second vertical bending mode showed a 23% reduction in the corresponding frequency, and the MAC values of the mode shapes differed significantly from unity. Salawu and Williams (1995) tested a reinforced concrete bridge before and after repair. Although the first seven natural frequencies shifted by less than 3%, MAC values showed significant change. Salawu and Williams argued that comparison of mode shapes is a more robust technique for damage detection than shifts in natural frequencies.

Fox (1992) showed that MAC was relatively insensitive to damage in a beam with a saw cut. MAC based on measurement points close to a node point for a particular mode was found to be a more sensitive indicator of changes in the mode shapes caused by damage. Graphical

comparisons of relative changes in mode shapes proved to be the best way of detecting the damage location.

Ettouney et al. (1998) discussed a comparison of three different techniques applied to a complex structure. All three of the techniques were based on knowing the mode shapes and natural frequencies of the damaged and undamaged structure. A finite element model was used to extract modes of up to 250 Hz. The first method was based on monitoring the change of the stiffness matrix of the structure. The stiffness matrix of an undamaged structure can be computed from the measured modal parameters, and the stiffness matrix for the damaged structure can also be computed using the mode shapes and natural frequencies obtained from the damaged structure. The change in the stiffness matrix of the damaged and undamaged states can then be used for damage detection. In second method, the flexibility matrices can be computed from the measured modal parameters. Then, the flexibility change between the damaged and undamaged states can be used for damage detection. In the third method, damage was identified at structural element levels rather than at nodal degrees of freedom. All three methods were applied to a complex steel structure.

Mode shape and natural frequency information was obtained from the analytical models of the damaged and undamaged conditions. Damage was introduced into the model by altering the modulus of elasticity for selected structural elements. All three methods were able to detect the relative location of the damaged elements with acceptable accuracy. However, applications of these methods are limited because the numbers of mode shape and natural frequencies identified from experimental modal analysis are often limited.In summary, changes in the mode shapes could be used to detect damage in the structure, however, the

detection may not be practical if the change in stiffness is relatively small and noise exists in the vibration measurements.

2.3.3 Mode shape curvature

Pandey and Barai (1995) assumed that structural damage only affects the stiffness and not the mass of the structure. For the undamaged condition, the characteristic equation of the structural dynamic system is expressed as

$$(\mathbf{K} - \omega_i^2 \mathbf{M})\boldsymbol{\phi}_i = \mathbf{0} \tag{2.2}$$

where $\mathbf{K}$ and $\mathbf{M}$ are the global stiffness and mass matrices, ω_i and $\boldsymbol{\phi}_i$ are the i^{th} eigenvalue and the associated eigenvector respectively. Similarly, the damaged condition is described as

$$(\mathbf{K}^d - \omega_i^{d^2} \mathbf{M}^d)\boldsymbol{\phi}_i^d = \mathbf{0} \tag{2.3}$$

where *"d"* denotes the damaged structure. Mode shape curvature for a beam in the undamaged and damaged conditions can then be estimated numerically from the mode shapes. For example, a beam cross section at location "*x*"subjected to a bending moment $M(x)$ .The curvature $v''(x)$ at location "*x*" is given by

$$\nu''(x) = \frac{M(x)}{EI} \tag{2.4}$$

where$E$ is the modulus of elasticity and $I$is the second moment of area of the section. The curvature is inversely proportional to the flexural stiffness of the beam. Reduction in the stiffness resulting from damage tends to increase the curvature of the mode shapes in the vicinity of the damage. The mode shape curvature is more sensitive to a change in the stiffness. Structural damage location can be identified by using the change of mode shape curvature. Furthermore, an estimation of the extent of damage can be obtained by measuring the amount of change in the mode shape curvatures.

Maeck and De Roeck (1999) applied a direct stiffness approach to damage detection, localization, and quantification for a bridge structure. The direct stiffness calculation used experimental frequencies and mode shapes in deriving the dynamic stiffness of a structure. The basic relation is that the bending stiffness of a beam is equal to the bending moment divided by the corresponding curvature, which is the second derivative of the bending deflection. A particular advantage of using either modal curvatures or their derivatives is that the modal curvatures tend to be more sensitive to local damage than modal displacements.

2.3.4 Change of structural flexibility or stiffness

Structural damage can be detected based on the change of the flexibility matrix (Jaishi and Ren 2006). According to the difference of the flexibility matrixes before and after structural damage, the largest element value in each column of the matrix can be found, and then the

structural damage location can be ascertained by examining the largest element value in each column of the matrix. The flexibility matrix $\mathbf{K}^{-1}$ is defined as the inverse of the stiffness matrix and, therefore, relates the applied static force $\mathbf{F}$ and structural displacement $\mathbf{U}$ as

$$\mathbf{U} = \mathbf{K}^{-1}\mathbf{F} \tag{2.5}$$

The flexibility matrix $\mathbf{K}^{-1}$ is generally estimated from,

$$\mathbf{K}^{-1} = \tilde{\boldsymbol{\phi}}\,\boldsymbol{\Lambda}^{-1}\tilde{\boldsymbol{\phi}}^{T} \tag{2.6}$$

where $\tilde{\boldsymbol{\phi}}$ is measured mode shapes, and $\boldsymbol{\Lambda}$ is the diagonal matrix of the associated measured modal frequencies squared.Flexibility matrix is usually estimated by using the lower modes due to difficulties in measuring higher modes. Moreover, it is most sensitive to changes in the lower frequency modes because of the inverse relationship to the square of the modal frequencies.The variation matrix $\Delta\mathbf{K}^{-1}$ can be obtained by measuring the flexibility matrices before and after damage.

$$\Delta\mathbf{K}^{-1} = \tilde{\mathbf{K}}^{-1} - \mathbf{K}^{-1} \tag{2.7}$$

where $\tilde{\mathbf{K}}^{-1}$ represents the flexibility matrix of the damaged structure.Yan and Golinval (2005) also presented a damage diagnosis technique based on changes in dynamically measured flexibility and stiffness of structures. The covariance-driven subspace identification technique was applied to identify structural modal parameters, and these were then used to assemble the

flexibility matrix of dimensions corresponding to the measured degrees of freedom. The corresponding stiffness matrix was obtained by a pseudo-inverse of the flexibility matrix. Damage localisation was achieved by a combined assessment of changes in these two measured matrices in moving from the reference state to the damaged state.

Generally, when some damage appears in a structure, the stiffness matrix can offer more information than the mass matrix. The stiffness changes remarkably when big damage appears in a structure. However, if the damage is very small, this method cannot work well.Zhao and DeWolf (1999) examined and compared sensitivity coefficients for natural frequencies, mode shapes and modal flexibility. On application to a simulated five degrees of freedom spring mass system it was found that the modal flexibility was the most sensitive to damage.Farrar and Doebling (1999) did not come to the same positive conclusions when comparing the strain energy, the mode shape curvature and the changes in flexibility based methods in locating damage on the I-40 bridge over the Rio Grande in America. Four controlled damage states were investigated and it was found that the strain energy based method was the most successful one followed by the mode shape curvature based method. The change in flexibility method could only locate damage in the most severe damage scenario.

2.3.5 Damage index method (modal strain energy method)

This method is based on the comparison of modal stain energy before and after damage. Damage causes a reduction in the flexural rigidity of the structure. The strain energy $\mathbf{SE}_i$ in a Bernoulli-Euler beam associated with a particular mode shape can be calculated from (Carden and Fanning 2004, Humar et al. 2006)

$$\mathbf{SE}_i = \frac{1}{2}\int_0^l EI\left(\frac{\partial^2 \boldsymbol{\phi}_i}{\partial x^2}\right)^2 dx \tag{2.8}$$

Assuming that the beam is divided into several numbers of elements, then the strain energy in a element for a given mode shape is

$$\mathbf{SE}_{ij} = \frac{1}{2}\int_{a_j}^{a_{j+1}} EI\left(\frac{\partial^2 \boldsymbol{\phi}_i}{\partial x^2}\right)^2 dx \tag{2.9}$$

where a_j and a_{j+1} are delimitations of element j. From the strain energy related each element and the strain energy of the complete structure for a given mode, the fractional strain energy $\mathbf{FSE}_{ij}$, which is the ratio of the element strain energy and the beam strain energy, can be defined as,

$$\mathbf{FSE}_{ij} = \frac{\mathbf{SE}_{ij}}{\mathbf{SE}_i} \tag{2.10}$$

Similar expressions can be derived for a damaged case as

$$\mathbf{FSE}_{ij}^{d} = \frac{\mathbf{SE}_{ij}^{d}}{\mathbf{SE}_i^{d}} \tag{2.11}$$

$$\mathbf{SE}_i^d = \frac{1}{2}\int_0^l EI^d \left(\frac{\partial^2 \boldsymbol{\phi}_i^d}{\partial x^2} \right)^2 dx \tag{2.12}$$

$$\mathbf{SE}_{ij}^d = \frac{1}{2}\int_{a_j}^{a_{j+1}} EI^d \left(\frac{\partial^2 \boldsymbol{\phi}_i^d}{\partial x^2} \right)^2 dx \tag{2.13}$$

The curvature required for this calculation is commonly extracted from the measured displacement mode shapes using a central difference approximation.

Kim and Stubbs (1995) applied a damage identification algorithm to locate and determine a single crack size in an experimental plate girder. The method was also demonstrated to locate up to two damage sites in a simulated plate girder. The damage indicator was based on the ratio of modal strain energy of elements before and after the damage.Farrar and Doebling (1999) were successful in using Kim and Stubbs (1995) damage index in locating controlled damage in a bridge. They found that this method outperformed the direct comparison of mode shape curvature before and after the damage.The damage index method is fairly successful in predicting damages in the structures. Since the method relies on the computation of modal stain energy in the elements of the structure, damage will not be detected when the damaged member makes very little contribution to the strain energy of the measured modes.

2.3.6 Frequency response function (FRF)

There are many methods available for performing vibration analysis and testing. The frequency response function (FRF) is a particular method. FRF is a transfer function,

expressed in the frequency domain. It expresses the structural response to an applied force as a function of frequency. The response may be given in terms of displacement, velocity, or acceleration (Carden and Fanning 2004). Consider a system as represented by the following diagram.

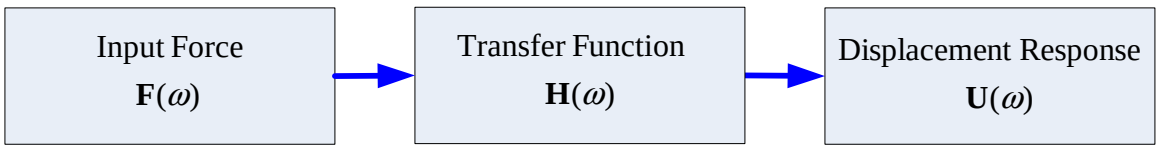

Figure 2.2 Frequency response function diagram

$\mathbf{F}(\omega)$ is the input force as a function of the frequency ω. $\mathbf{H}(\omega)$ is the transfer function. $\mathbf{U}(\omega)$ is the displacement response function. The relationship can be represented by the following equations.

$$\mathbf{H}(\omega) = \frac{\mathbf{U}(\omega)}{\mathbf{F}(\omega)} \tag{2.14}$$

$$\mathbf{U}(\omega) = \mathbf{H}(\omega)\mathbf{F}(\omega) \tag{2.15}$$

Lee and Shin (2002) used both modal and FRF data from a simulated beam to identify up to three damage locations. Damage was simulated by the reduction in the Young's Modulus of sections of a Bernoulli–Euler beam. Modal data from the beam in the undamaged state and FRF data from the beam in the damaged state were used in the identification algorithm. It was found that the multiple-excitation-frequency and multiple-measurement-point approach gave the most reliable results.

Mares et al. (1999) proposed a damage location procedure based on rigid body constraints. A crack in a two-dimensional finite element model of a cantilevered beam was simulated. The beam was discredited into 10 elements along the length. Frequency responses were calculated for the beam's damaged and undamaged states. A crack was introduced at the third element from the fixed end. When the external load was applied at the damaged element, there was no difference in the frequency response functions between the damaged and undamaged states of the cantilever beam.

Since the change of transfer function caused by structural damage is uniquely determined by the damage type and location, one column data is only need to be measured in transfer matrix to detect damage instead of measuring the whole transfer matrix. The advantages of these methods are the numericalmodel, vibration mode measurement and experimental knowledge are not needed. Therefore, this method can be used in online monitoring. The disadvantage is that the accuracy of structural damage detection is prone to be influenced by the amount and position of measurement point.

2.3.7 Modal residual vector

Based on the measured mode shapes and natural frequencies, the eigenvalue equation in Eq.(2.3) for the damaged structure can be rewritten as,

$$(\mathbf{K}^d - \omega_i^{d^2}\mathbf{M}^d)\boldsymbol{\phi}_i^d = \mathbf{0} \tag{2.16}$$

where $\mathbf{K}^d$ and $\mathbf{M}^d$ can be defined as,

$$\mathbf{K}^d = \mathbf{K} + \Delta\mathbf{K} \tag{2.17}$$

$$\mathbf{M}^d = \mathbf{M} + \Delta\mathbf{M} \tag{2.18}$$

where $\Delta\mathbf{K}$ and $\Delta\mathbf{M}$ are changes in stiffness and mass matrices, respectively.It is assumed that damage cause changes in the structural stiffness and structural mass remain unchanged.By substituting $\mathbf{K}^d$ and $\mathbf{M}^d$ into eigenvalue equation Eq.(2.16)and rearranging gives the definition of the residual force vector $\mathbf{r}_i$ for the i^{th} mode,

$$\mathbf{r}_i = (\mathbf{K} - \omega_i^{d^2}\mathbf{M})\boldsymbol{\phi}_i^d \tag{2.19}$$

Each mode provides a single residual force vector. When damage occurs to an element, the entry in the residual force vector becomes very large compared to the other entries where no damage has occurred. Picking out these large terms therefore provides the results for the location of damage.

Chen and Bicanic (2000) identified up to three damage locations in a simulated plate. A mode shape expansion technique was employed and two algorithms were used to identify the damage, one involving the minimisation of the norm of the residual force vector and the second involving the minimisation of the norm of the residual energy vector. Both methods were found to give similar convergence to the correct identification.

2.4 Real time structural damage detection

In the case of extreme event such as earthquake, roads and bridges are fundamental infrastructure to evacuate the affected people and to transport the emergency equipment and materials. Post-earthquake damage assessment of the structures typically requires long time to be completed. There is a need to develop faster and reliable methods to detect local damage evolution during and/or after the earthquake. During the past decades, various damage detection algorithms have been developed. Currently, visual inspection is the standard method used for health assessment of the structures, along with non-destructive damage detection methods such as methods using strain gauge measurements (Moyo et al. 2005), using acoustic for crack detection (Yu et al. 2011) and ground radar penetration (GPR) methods (Hugenschmidt and Mastrangelo 2006). Chase et al. (2004) identified real time changes in structural stiffness using least mean square-based adaptive filtering. Recently, global positioning system (GPS) is employed for real time displacement monitoring of large structures (Safak and Hudnut 2006). However, most of those techniques may not provide immediate assessment of real time damage evolution at detailed level. Development of real time damage detection techniques would be useful for rapid detection of some sudden structural damages and aims to provide real time reliable information regarding the integrity of the structure during and/or after extreme events of earthquakes and impact of blast loading for appropriate repair of structural damage. There is limitation for requirement of vibration response measurements in all degrees of freedom in the structure, which may not be practical due to limited number of sensors are available for measurements.

2.5 Modal testing

Maintenance of civil engineering infrastructure for safe and reliable operation is of paramount important throughout its entire life cycle. Currently, performance of different kinds of structures such as buildings, towers and bridges under different environmental conditionsare under investigation. The long term implementation of a structural health monitoring system by measuring vibration response may address a structural condition and issue an early warning on deterioration prior to a partial or catastrophic collapse.

Modal testing is common practice in structural health monitoring (Wu and Li 2004). In modal testing, the structure needs to be excited by the operational condition (ambient vibration)or artificial vibrations (forced vibration). In general, force vibration is conducted for small scale structures in the laboratory. Ambient vibration is the only practical means of exciting large structures such as tall buildings, towers, and cable-stayed bridges. In structural dynamic testing, dynamic responses of a structure can be obtained from installed sensors. Measured data isanalysed in order to calibrate a finite element model and identify any structural damage.

The purpose of vibration testing is to identify the dynamic characteristics of the structure such as frequencies, mode shapes and damping factors through the information of measured data. The changes in the vibration characteristics can provide the information of structural deterioration. The use of vibration responses to identity the damage is sometime referred to as vibration-based damage identification (Huynh et al. 2005).

In vibration testing, various mechanical devices are available to excite the structure. Among them are, impact hammer and dynamic shaker which are widely used due to their simplicity in their application. Transducers such as accelerometers are usually employed to measure the vibration responses of the structure. Modal properties of the structure are then extracted from the measured data by utilizing modal analysis techniques.

2.5.1 Forced vibration

Impact excitation

Impact excitation offers the advantages of simplicity and speed of execution laboratory testing. The impact equipment typically consists of an impactor, usually with tips of varying stiffness from soft to hard to control its dynamic range, and an attached load cell is used to measure the impulse transmitted to the test structure. The impactor can take the form of a hammer that can be operated by hand, a drop weight mechanism or a spring loaded device.

In structural dynamic testing, the impact hammer is used to excite the structure. Some modes may not be excited based on the location of the excitation. If the impact produces a perfect impulse force, then all modes will be excited.Those missing modes may be excited by using tips of different stiffness and hammers of different mass. The desired frequency range will be increased if stiffer hammer tips and lower hammer masses are used. The choice of desired frequency range is also critical to the accurate measurement of the modes of interest, as a hammer will not excite a structure with any great energy at frequencies above the desired frequency range. Impact excitation is generally convenience to apply to a structure and does

not produce any significant mass loading although the direction of impact is difficult to control accurately (Park et al. 2011).

Shaker excitation

Electro-magnetic shaker, electro-hydraulic shaker, and eccentric mass shaker are also used as excitation sources in forced vibration testing of the structure. The shakers can provide the flexibility to generate different forms of dynamic excitation time histories such as sinusoidal and random.An electro-magnetic shaker converts an input electrical signal into an alternating magnetic field that drives the shaker. It is suitable to generate a lower level force and normally used in laboratory scale structure testing (Ohm et al. 2006). Shakers making use of hydraulic actuators as the driving mechanism offer the potential advantage of incorporating long stroke lengths, enabling larger amplitude motion at the low frequencies. Mechanical shakers make use of a rotating eccentric mass and generate the prescribed forcing due to physical constraints involved in the system. In practice, eccentric mass shakers have rarely been used to apply load in the vertical direction.

All types of shakers require a power supply, amplifier and control software for various input force in operation. The shaker should only provide force to the structure in the direction measured by a transducer and poor attachment of shaker to excite the structure will lead to miss some of the vibration modes. Although shaker excitation is widely employed in structural dynamic testing, this excitation approach is inconvenience in mobility, requires high cost and more time for setting up the equipment than by impact hammer excitation.

Pullback testing

Pullback testing is generally conducted for large-scale structures to determine their response to lateral dynamic excitation that are difficult to excite using other means. For example, in the case of testing a bridge, it is usually difficult to determine its lateral vibration characteristics since normal traffic loads do not significantly excite the bridge in the lateral direction. In this approach, the test structure is pulled by means of a steel cable or rope anchored in the ground or some other fixed object and suddenly releasing the cable to induce the lateral vibration (Robson and Harik 1998).

Accelerometers

An accelerometer is a sensor or transducer which is designed to generate an electrical signal in response to acceleration that is applied along its sensitive axis. Piezoelectric accelerometer typically weighs between 3 and 35 grams with sensitivities spanning from 10 mV/g to 100 mV/g and is generally used in measuring the acceleration. It employs either natural quartz crystals or man-made polycrystalline ceramics as its sensing element. Uni-axial and multi-axial models of accelerometer are available to detect acceleration.

Mounting accelerometers

The mounting technique of an accelerometer on the structure is also important for the accuracy of measurements. The structural dynamic responses are determined by securely mounting the accelerometers in the reference locations of the test structureby variety of methods, such as using studs, screws, adhesive and/or magnets. It is important to prepare a

smooth, clean and flat surface where the accelerometers are to be attached for the measurements.

Stud mounting is suitable for permanent installations, where a very secure attachment of the accelerometer to the test structure is preferred. The stud mounted to a very smooth surface generally yields high accuracy in measurements and, therefore, the broadest usable frequency range. When installing accelerometer onto a thin-walled structure, a cap screw passing through a hole of sufficient diameter is an acceptable means for securing the accelerometer to the structure.

Occasionally, mounting by studs or screws is impractical. For such cases, adhesive or magnet mounting offer an alternative mounting method. Adhesive and magnet mounting methods have the advantage that the accelerometers can be moved around easily. Magnetic mounting of accelerometers offer a very convenient, temporary attachment to magnetic surfaces and can provide higher accuracy in measurements. However, the addition of an adhesive or magnetic mounting base mass to the accelerometer lowers the resonant frequency of the test structure and may affect the accuracy in measurements.

Also, compliant materials, such as a rubber interface pad, can create a mechanical filtering effect by isolating and damping high-frequency transmissibility. Surface flatness, adhesive stiffness, and adhesion strength also affect the measurements accuracy of an accelerometer. Generally, surface irregularities or increase in the thickness of the adhesive decrease the usable frequency ranges.Connecting cables should be securely fastened to the mounting structure with a clamp, tape, or other adhesive to minimize cable whip and connector strain.

Cable whip can introduce noise, especially in high-impedance signal paths (Colombo et al. 2005).

2.5.2 Ambient vibration

When a tall building vibrates by wind or a bridge vibrates continuously under traffic, the input excitation is usually not known and/or can not be measured. This type of vibration is referred to as ambient vibration (Wenzel and Pichler 2005).Ambient vibration testing is the most economical non-destructive testing and only practical means of exciting the large structure as the ability to input significant energy into the structure. It describes the linear behaviour of the structure, since the amplitudes of vibration are small. In the practical application of testing the bridge, either controlled test vehicles or moving traffic loadings can be used to excite the structure. However, traffic excitation may not sufficiently excite the lateral modes of a bridge (Lu et al. 2006).

Advantage is that ambient vibration test is full scale experiment and usually only light equipmentis required. It can provide evaluating the response of the structure to the actual vibration environment. Even a carefully planned laboratory experiment will represent only some aspects of the problem. Disadvantage of using ambient excitation is that this type of input is often non-stationary and not known whether this excitation source can provide the input at the frequencies of interest range.

In a review of various ambient and controlled input excitation methods, Brownjohn (2003) found that shaker excitation yielded the most reliable dynamic data in comparison with vehicle induced response and hammer impact test. However, Peeters and De Roeck (2001)

reported that results from ambient excitation was comparable to those obtained using either a shaker or drop weight impact. On the other hand, Farrar (2000) determined that natural frequencies extracted from impact hammer test data were more promising than those obtained using ambient excitation, and that fewer vibration modes could be successfully identified from ambient testing.

2.5.3 Time, frequency and modal domains

The vibration signal measured at discrete sampling instants can be represented in the time domain. A time domain graph shows how a signal changes over time. Measured signal in time domain can be converted to frequency domain with a pair of mathematical operators called a Fourier transform. Frequency domain is used to describe the signal with respect to frequency, rather than time. For a sampled signal x_k consisting of *N* samples over a time period of *T* seconds, this is defined by (Friswell and Mottershead 1995),

$$\mathrm{x}_k = \mathrm{x}(t_k) = \frac{a_0}{2} + \sum_{j=1}^{N/2} \{a_j \cos\frac{2\pi j t_k}{T} + b_j \sin\frac{2\pi j t_k}{T}\} \tag{2.20}$$

where

$$a_0 = \frac{1}{N}\sum_{k=1}^{N} \mathrm{x}_k \tag{2.21}$$

$$a_j = \frac{1}{N}\sum_{k=1}^{N} \mathrm{x}_k \cos\frac{2\pi j k}{N} \tag{2.22}$$

$$b_j = \frac{1}{N}\sum_{k=1}^{N} \mathrm{x}_k \sin\frac{2\pi jk}{N} \tag{2.23}$$

A Fourier series may be used because the signal is periodic, and the series is of finite length because the signal is sampled. The set of spectral coefficients a_j and b_j are called the discrete Fourier transform of the signal x. In practice the discrete Fourier transform is efficiently calculated by variations to the method given by Cooley and Tukey (1965) which is generally called the Fast Fourier Transform (FFT). The Fourier transform may be considered in the complex domain by writing the transform at the j^{th} frequency, given by $\frac{2\pi j}{T}$, as $a_j + ib_j$ where *"i"* is the square root of -1. The inverse Fourier transform converts the frequency domain function back to a time function.

2.5.4 Experimental modal analysis

After the frequency response functions have been measured, the data may be further processed to obtain the natural frequencies, damping ratios and mode shapes of the experimental structure. Figure 2.3 shows example of modal parameters estimation from FRF (ME'scope VES). This is called experimental modal analysis which is able to accurately identify modal data from frequency response function data (Zivanovic et al. 2006). One major problem with any modal extraction method is the determination of the number of modes in a given frequency range. The experimental modal data should always be compared to the analytical results to give confidence in the measured data.

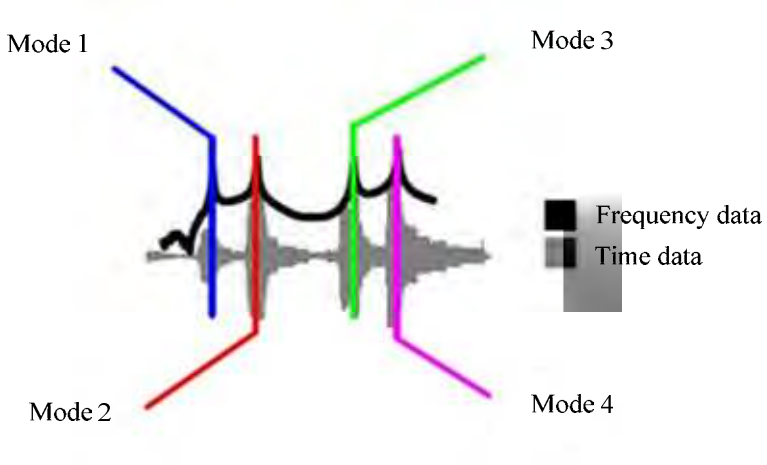

Figure 2.3 Modal parameters estimation from FRF

Input-output modal identification

Conventional modal analysis techniques are typically single-input-multiple-output and based on estimating a set of frequency response functions relating the applied force and corresponding response. In a small and medium size structure, the excitation can be induced by an impact hammer. This device has ability to stimulate different modes of vibration in control manner. Advantage of input-output modal identification is that input excitation can be used in the modal identification (Verboven et al. 2004).On the other hand, it requires more energy to excite some relevant modes of vibration for a large structure and input excitation is difficult to measure. In this case, this traditional modal analysis might not work very well because of unknown input acting on the structure.

Output-only modal identification

In very large, flexible structures like cable-stayed or suspension bridges, the forced excitation requires extremely heavy and difficulty in exciting with sufficient energy for the most

significant modes of vibration in a low range of frequencies. Therefore, output-only modal identification techniques became an alternative of great importance in the field of structural dynamic testing (Rainieri et al. 2012). Recent technological developments are possible to measure the very low levels of dynamic response induced by ambient excitations such as wind or traffic loading without knowing the excitation force. It is also called operational modal analysis (Brownjohn et al. 2010). This new technology is capable of estimating the mode shapes, the natural frequencies and the damping ratio as input-output modal identification techniques.

2.5.5 Measurement noise: random and systematic errors

In finite element model updating, the measured data will be used to update the structural parameters of the analytical model. It is therefore vital to eliminate the likely errors in the measurements (Mohd-Yasin et al. 2009, Hu et al. 2010). Two main types of measurement errors are recognized: (a) random error, in which there are unpredictable random variations in the measured signal. It is often called noise; (b) systematic error, in which every measurement is consistently less than or greater than the correct value by a certain amount.

Any signal corrupted by random noise is, by its nature, unpredictable. The noise may be described by a statistical distribution (Newland 1985, Hogg and Craig 1978). The most commonly used statistical distribution used to present noise is the Gaussian distribution that describes the probability of a random variable falling within a certain range of values. The distribution is totally specified by the mean μ and variance σ^2, respectively. The probability *P*of noise signal x between x_1 and x_2 is given by

$$P(x_1 \le x \le x_2) = \int_{x_1}^{x_2} p(x)dx \tag{2.24}$$

where

$$p(x) = \frac{1}{\sqrt{2\pi\sigma}} \exp\left(\frac{(x-\mu)^2}{2\sigma^2}\right) \tag{2.25}$$

is called the probability density function. Random errors may be reduced by careful preparation for experiments, choice of excitation methods and by smoothing the data. Impact excitation, such as hammer excitation, puts very little energy into a structure and can produce noisy data (Friswell and Mottershead 1995).

In smoothing process, the data points of a signal are modified so that individual points that are higher than the immediately adjacent points are reduced, and the points that are lower than the adjacent points are increased (Girard and Defosse 1993, Baneen et al. 2012). This naturally leads to a smoother signal. Smoothing the data reduces the variance of the noise on the data and so reduces the effect of the noise. The more reduction of noise can be done by larger smooth width but there will be the possibility of distorted signal by the smoothing operation.

Systematic errors are difficult to remove from the data. It is important to model the tested structure as accurately as possible. For example, if a connection of beam in the tested structure is a fixed connection, then every effort must be made to ensure that connection is fixed in the analytical model. Significant errors can arise in the measured data, for example, the connections of brace members are assumed to be flexible in the analytical model, but

those connections in actual tested structureare relatively fixed.Attaching transducers and shakers to the structure may also introduce significant systematic errors. Mass loading or local stiffening due to the attachment system will change the dynamic properties of the structure (Rana 2011). Accelerometers can also produce mass loading and local stiffening problems, particularly with light structures.

2.5.6 Measured incomplete modal data

Finite element model of the tested structure can be very large and consist of several thousand degrees of freedom. In practice, only limited sensors are available and impossible to install sensors in all degrees of freedom. There are often internal nodes which cannot be measured. Rotational degrees of freedom are also very difficult to measure with accuracy. Consequently not all the degrees of freedom in the finite element model will be measured.Therefore, the measured mode shapes obtained from vibration testing are typically incomplete (Rahai et al. 2007, Xu et al. 2012). Comparison of analytical and experimental mode shapes becomes difficult in practice unless some measurements are taken to fill in the missing entries or the order of the model is reduced. There are two ways of overcoming this difficulty, either a model reduction technique has to be applied to the finite element model or measured mode shapes have to be expanded to the full order of the finite element model (Zhang 2007, Chen 2010, Panayirci et al. 2011).

It is important to compare experimental results for the tested structure with predicted results for the corresponding finite element model to ensure the better correlation(Warren et al. 2011). In the comparison, errors may be introduceddue to the large number of degrees of

freedom in the analytical model and limited number of transducers available to measure the response of the structure (Wendy et al. 2007). One of the critical tasks in structural dynamic testing is mode paring. The MAC is a widely used technique to estimate the degree of correlation between analytical and experimental mode shapes (Allemang and Brown 1982, Pastor et al. 2012). The MAC between an analytical mode ϕ_k and measured mode $\tilde{\phi}_i$ is defined in Eq.(2.1).

2.5.7 Model reduction

Due to limited sensors and incomplete measurements, problems arise from comparing measured experimental data with numerically generated data. One way to compare the data is to reduce the number of degrees of freedom in the analytical model to the number of measured degrees of freedom of the tested structure.The idea is to reduce original finite element model to a properly chosen measured degrees of freedom system that has properties similar to the original system (Avitabile 2005). A complex system can thus be approximated by the simpler system involving fewer equations and unknown variables, which can be solved much more quickly than the original problem (Guedri et al. 2006).

Guyan or static reduction

Guyan (1965) reduction has been used for many years as one of the most common tools for the reduction of large analytical models. The state and force vectors, **u** and **f**, and the mass and stiffness matrices, **M** and **K** are split into sub-vectors and matrices relating to the master

degrees of freedom, which are retained, and the slave degrees of freedom, which are eliminated (Friswell and Mottershead 1995), expressed as

$$\begin{bmatrix} \mathbf{M}_{mm} & \mathbf{M}_{ms} \\ \mathbf{M}_{sm} & \mathbf{M}_{ss} \end{bmatrix} \begin{Bmatrix} \ddot{\mathbf{u}}_m \\ \ddot{\mathbf{u}}_s \end{Bmatrix} + \begin{bmatrix} \mathbf{K}_{mm} & \mathbf{K}_{ms} \\ \mathbf{K}_{sm} & \mathbf{K}_{ss} \end{bmatrix} \begin{Bmatrix} \mathbf{u}_m \\ \mathbf{u}_s \end{Bmatrix} = \begin{Bmatrix} \mathbf{f}_m \\ \mathbf{f}_s \end{Bmatrix} \tag{2.26}$$

The subscripts “m” and “s” denote master and slave co-ordinates respectively. Assuming that no force is applied to the slave degrees of freedom and neglecting the inertia terms, Eq. (2.26) becomes static equation as

$$\begin{bmatrix} \mathbf{K}_{mm} & \mathbf{K}_{ms} \\ \mathbf{K}_{sm} & \mathbf{K}_{ss} \end{bmatrix} \begin{Bmatrix} \mathbf{u}_m \\ \mathbf{u}_s \end{Bmatrix} = \begin{Bmatrix} \mathbf{f}_m \\ \mathbf{0} \end{Bmatrix} \tag{2.27}$$

For the second set of equation in Eq**.** (2.27)

$$\mathbf{K}_{sm}\mathbf{u}_m + \mathbf{K}_{ss}\mathbf{u}_s = \mathbf{0} \tag{2.28}$$

which may be used to eliminate the slave degrees of freedom so that

$$\begin{Bmatrix} \mathbf{u}_m \\ \mathbf{u}_s \end{Bmatrix} = \begin{bmatrix} \mathbf{I} \\ -\mathbf{K}_{ss}^{-1}\mathbf{K}_{sm} \end{bmatrix} \{\mathbf{u}_m\} = \mathbf{T}_s\mathbf{u}_m \tag{2.29}$$

where $\mathbf{T}_s$ denotes the static transformation between the full state vector and the master co-ordinates. The reduced mass and stiffness matrices are then written as

$$\mathbf{M}_R = \mathbf{T}_s^T \mathbf{M} \mathbf{T}_s \quad , \quad \mathbf{K}_R = \mathbf{T}_s^T \mathbf{K} \mathbf{T}_s \tag{2.30}$$

where $\mathbf{M}_R$ and $\mathbf{K}_R$ are the reduced mass and stiffness matrices respectively. Guyan reduction depends heavily on the selection of the master degrees of freedom, and a poor selection could yield inaccurate models.

Dynamic reduction

This is an extension to Guyan's method by considering the inertia term. Eq. (2.28) is modified to include inertia forces at the chosen frequency ω_i (Friswell et al. 1995). The transformation to generate the slave co-ordinates from the master co-ordinates is then given by

$$\begin{Bmatrix} \mathbf{u}_m \\ \cdots \\ \mathbf{u}_s \end{Bmatrix} = \begin{bmatrix} \mathbf{I} \\ \cdots \\ -(\mathbf{K}_{ss} - \omega_i^2 \mathbf{M}_{ss})^{-1} (\mathbf{K}_{sm} - \omega_i^2 \mathbf{M}_{sm}) \end{bmatrix} \{\mathbf{u}_m\} = \mathbf{T}_d \mathbf{u}_m \tag{2.31}$$

This transformation matrix $\mathbf{T}_d$ is then used in the same way as the static transformation $\mathbf{T}_s$ to obtain reduced mass and stiffness matrices similar to Eq. (2.30). Yin et al. (2009), Lam et al. (2011)presented a damage detection method based on dynamic reduction by utilizing ambient vibration data measured from a limited number of sensors in a transmission tower. The

transmission tower is divided into sub-structures and damage is identifiedby estimating the equivalent stiffness reduction.

Improved reduced system (IRS)

The IRS method was proposed by O'Callahan (1989) as an improvement of Guyan reduction by introducing the inertia terms. The transformation $\mathbf{T}_i$ used to generate the slave co-ordinates from the master co-ordinates is given by

$$\mathbf{T}_i = \mathbf{T}_s + \mathbf{S}\,\mathbf{M}\,\mathbf{T}_s\mathbf{M}_R^{-1}\mathbf{K}_R \tag{2.32}$$

where

$$\mathbf{S} = \begin{bmatrix} 0 & 0 \\ 0 & \mathbf{K}_{ss}^{-1} \end{bmatrix} \tag{2.33}$$

The reduced mass and stiffness matrices obtained from static reduction (Friswell et al. 1998).Xia and Lin (2004) presented an iterated improved reduced system (IIRS) technique to modify the iterative transformation matrix and achieve faster convergence and obtained the lowest eigensolutions of structures more accurately and efficiently.

System equivalent reduction expansion process (SEREP)

This method was originally introduced by O'Callahan et al. (1989) for the computed mode shapes to produce the transformation between the master and slave co-ordinates. The analytical modes are partitioned into the master and slave co-ordinates as (Li et al. 2008)

$$\boldsymbol{\phi} = \begin{bmatrix} \boldsymbol{\phi}_m \\ \boldsymbol{\phi}_s \end{bmatrix} \tag{2.34}$$

The generalised or pseudo inverse of $\boldsymbol{\phi}_m$ is used to give the transformation as

$$\mathbf{T}_u = \begin{bmatrix} \boldsymbol{\phi}_m \\ \boldsymbol{\phi}_s \end{bmatrix} \boldsymbol{\phi}_m^+ \qquad \text{where} \qquad \boldsymbol{\phi}_m^+ = (\boldsymbol{\phi}_m^T \boldsymbol{\phi}_m)^{-1} \boldsymbol{\phi}_m^T \tag{2.35}$$

The reduced mass and stiffness matrices may be obtained in a similar way to Eq.(2.30). With this method, the reduced model will exactly reproduce the lower natural frequencies of the full model.

Comparison of methods

Static or Guyan reduction is widely used to reduce the number of degrees of freedom in a finite element model but it is exact only at zero frequency and never reproduces frequencies of the original model.The improved version of the Guyan method, called the Improved Reduced System (IRS),produces a reduced model which more accurately estimates the modal data of the full system.The System Equivalent Reduction (SEREP) method produces the natural frequencies correctly but the method has the computational disadvantage of requiring the computation of pseudo inverse.In all reduction techniques, there exists a relation between the measured or master degrees of freedom and the unmeasured or slave degrees of freedom (Friswell and Mottershead 1995).

2.5.8 Mode shape expansion

Model reduction process destroys the original sparse pattern in mass and stiffness matrices and propagates modelling errors. The alternative to model reduction is to expand the measured mode shapes to estimate the data at unmeasured locations (Miguel 2006). Mode shape expansion is the reverse of model reduction, and the methods have some similarities. The easiest way is to fill in the unmeasured components of the experimental modes from the corresponding components of analytical modes (Chen 2010, Liu 2011). To be consistent with the model reduction section, subscripts "m" and "s" will represent measured and unmeasured degrees of freedom respectively. Dynamic characteristic equation of the analytical model with measured and unmeasured components of mass and stiffness matrices can be written as (Friswell and Mottershead 1995)

$$\left(\begin{bmatrix} \mathbf{K}_{mm} & \mathbf{K}_{ms} \\ \mathbf{K}_{sm} & \mathbf{K}_{ss} \end{bmatrix} - \omega_{mj}^2 \begin{bmatrix} \mathbf{M}_{mm} & \mathbf{M}_{ms} \\ \mathbf{M}_{sm} & \mathbf{M}_{ss} \end{bmatrix} \right) \begin{Bmatrix} \boldsymbol{\phi}_{mj} \\ \boldsymbol{\phi}_{sj} \end{Bmatrix} = \begin{Bmatrix} \mathbf{0} \\ \mathbf{0} \end{Bmatrix} \tag{2.36}$$

where $\boldsymbol{\phi}_{sj}$ represents the estimated mode shape at the slave, or unmeasured degrees of freedom, ω_{mj} and $\boldsymbol{\phi}_{mj}$ represent the j^{th} measured natural frequency and the corresponding mode shape at the measured co-ordinates. Rearranging the lower part of the matrix equation produces a solution for the unknown part of the measured mode shape vector, as

$$\boldsymbol{\phi}_{sj} = -(\mathbf{K}_{ss} - \omega_{mj}^2 \mathbf{M}_{ss})^{-1} (\mathbf{K}_{sm} - \omega_{mj}^2 \mathbf{M}_{sm}) \boldsymbol{\phi}_{mj} \tag{2.37}$$

This technique is very similar to the dynamic model reduction method.

2.6 Element types used for numerical examples

The finite element method is often used to solve physical problems in engineering analysis and design. The basic concept of finite element method is dividing up a very complicated problem into small elements that can be solved in relation to each other. A typical finite element analysis requires the following information of a structure system:

- nodal points or geometry of model
- elements connecting the nodal points (e.g truss element, beam element)
- material properties (e.g steel, concrete)
- boundary conditions (e.g fix, pin)
- loadings (e.g point load, uniform load)
- analysis options (e.g static, dynamic)

In this study, truss and beam elements are utilised for numerical examples and numerical modelling of the steel frame model structure.

2.6.1 Plane truss element

Truss element transmits only axial force and has no bending resistance. It has two degrees of freedom (i.e, axial translation at each node). Stiffness and mass matrices of a plane truss element can be expressed respectively, as

$$\mathbf{K}_e = \begin{bmatrix} \frac{AE}{l} & -\frac{AE}{l} \\ -\frac{AE}{l} & \frac{AE}{l} \end{bmatrix} \tag{2.38}$$

$$\mathbf{M}_e = \frac{\rho Al}{420}\begin{bmatrix} 140 & 70 \\ 70 & 140 \end{bmatrix} \tag{2.39}$$

where$A$ and E are cross section area, and modulus of elasticity; l and ρ are length, and density; $\mathbf{K}_e$ and $\mathbf{M}_e$ are stiffness matrix, and mass matrix of the element, respectively.

2.6.2 Plane beam element

Beam element offers resistance to bending under applied load. A beam element differs from a truss element since a beam resists bending moments at the connections. The joints can be assumed to be rigid connection. It has translation and rotation degrees of freedom at each node. Stiffness and mass matrices of plane beam element are given by

$$\mathbf{K}_e = \begin{bmatrix} \frac{12EI}{l^3} & \frac{6EI}{l^2} & -\frac{12EI}{l^3} & \frac{6EI}{l^2} \\ \frac{6EI}{l^2} & \frac{4EI}{l} & -\frac{6EI}{l^2} & \frac{2EI}{l} \\ -\frac{12EI}{l^3} & -\frac{6EI}{l^2} & \frac{12EI}{l^3} & -\frac{6EI}{l^2} \\ \frac{6EI}{l^2} & \frac{2EI}{l} & -\frac{6EI}{l^2} & \frac{4EI}{l} \end{bmatrix} \tag{2.40}$$

$$\mathbf{M}_e = \frac{\rho A l}{420}\left[\begin{array}{cc:cc} 156 & 22l & 54 & -13l \\ 22l & 4l^2 & 13l & -3l^2 \\ \hdashline 54 & 13l & 156 & -22l \\ -13l & -3l^2 & -22l & 4l^2 \end{array}\right] \tag{2.41}$$

where$I$ is moment of inertia.

2.6.3 General plane beam element

Truss and beam element matrix must be combined to form a plane beam element matrix with consideration of axial deformation. Sometime it is called as beam-frame element. It has two translation and one rotation degrees of freedom at each node. Element stiffness and mass matrices can be expressed as

$$\mathbf{K}_e = \left[\begin{array}{ccc:ccc} \frac{AE}{l} & 0 & 0 & -\frac{AE}{l} & 0 & 0 \\ 0 & \frac{12EI}{l^3} & \frac{6EI}{l^2} & 0 & -\frac{12EI}{l^3} & \frac{6EI}{l^2} \\ 0 & \frac{6EI}{l^2} & \frac{4EI}{l} & 0 & -\frac{6EI}{l^2} & \frac{2EI}{l} \\ \hdashline -\frac{AE}{l} & 0 & 0 & \frac{AE}{l} & 0 & 0 \\ 0 & -\frac{12EI}{l^3} & -\frac{6EI}{l^2} & 0 & \frac{12EI}{l^3} & -\frac{6EI}{l^2} \\ 0 & \frac{6EI}{l^2} & \frac{2EI}{l} & 0 & -\frac{6EI}{l^2} & \frac{4EI}{l} \end{array}\right] \tag{2.42}$$

$$\mathbf{M}_e = \frac{\rho A l}{420}\left[\begin{array}{ccc:ccc} 140 & 0 & 0 & 70 & 0 & 0 \\ 0 & 156 & 22l & 0 & 54 & -13l \\ 0 & 22l & 4l^2 & 0 & 13l & -3l^2 \\ \hdashline 70 & 0 & 0 & 140 & 0 & 0 \\ 0 & 54 & 13l & 0 & 156 & -22l \\ 0 & -13l & -3l^2 & 0 & -22l & 4l^2 \end{array}\right] \tag{2.43}$$

From the transformation matrix **T**the relationship between the local and global element stiffness and mass matrices can be described as

$$\mathbf{T} = \left[\begin{array}{ccc:ccc} \cos\vartheta & \sin\vartheta & 0 & 0 & 0 & 0 \\ -\sin\vartheta & \cos\vartheta & 0 & 0 & 0 & 0 \\ 0 & 0 & 1 & 0 & 0 & 0 \\ \hdashline 0 & 0 & 0 & \cos\vartheta & \sin\vartheta & 0 \\ 0 & 0 & 0 & -\sin\vartheta & \cos\vartheta & 0 \\ 0 & 0 & 0 & 0 & 0 & 1 \end{array}\right] \tag{2.44}$$

$$\mathbf{K}_j = \mathbf{T}^T \mathbf{K}_e \mathbf{T} \tag{2.45}$$

$$\mathbf{M}_j = \mathbf{T}^T \mathbf{M}_e \mathbf{T} \tag{2.46}$$

where $\mathbf{K}_j$ and $\mathbf{M}_j$ are j^{th} element of global stiffness mass matrices. The global stiffness matrix $\mathbf{K}$ and mass matrix $\mathbf{M}$ of the structural system can then be obtained by combination of the element stiffness and mass matrices, respectively. They can be expressed as

$$\mathbf{K} = \sum_{j=1}^{NE} \mathbf{K}_j \tag{2.47}$$

$$\mathbf{M} = \sum_{j=1}^{NE} \mathbf{M}_j \tag{2.48}$$

where*NE* represents total number of elements in the structural system.

2.7 Description of Canton Tower benchmark problem

For a case study of model updating, the Canton Tower in Guangzhou, China is selected. Numerical modelling and structural health monitoring system of the Canton Tower have been designed by Hong Kong Polytechnic University. The tower shown inFigure 2.4(a) has a total height of 610m with a 454m high main tower and a 156m high antenna mast (Ni et al. 2009, Chen et al. 2011). The structure comprises a reinforced concrete inner tube and a steel outer tube with concrete-filled columns. The outer structure has a hyperboloid shape, which is generated by opposite rotation of two ellipses, one at the ground level and the other at 454 m above the ground. The tightening caused by the rotation between the two ellipses forms a "waist" and a densification of structure in the tower. The cross-section of the outer structure is 50 m × 80 m at the ground, 20.65 m × 27.5 m at the waist level (280 m high), and 41 m × 55 m at the top (454 m high). The outer structure is made of 24 inclined concrete-filled-tube columns, which are transversely interconnected by steel ring beams and bracings. The antenna mast is a steel structure founded on the top of the main tower.

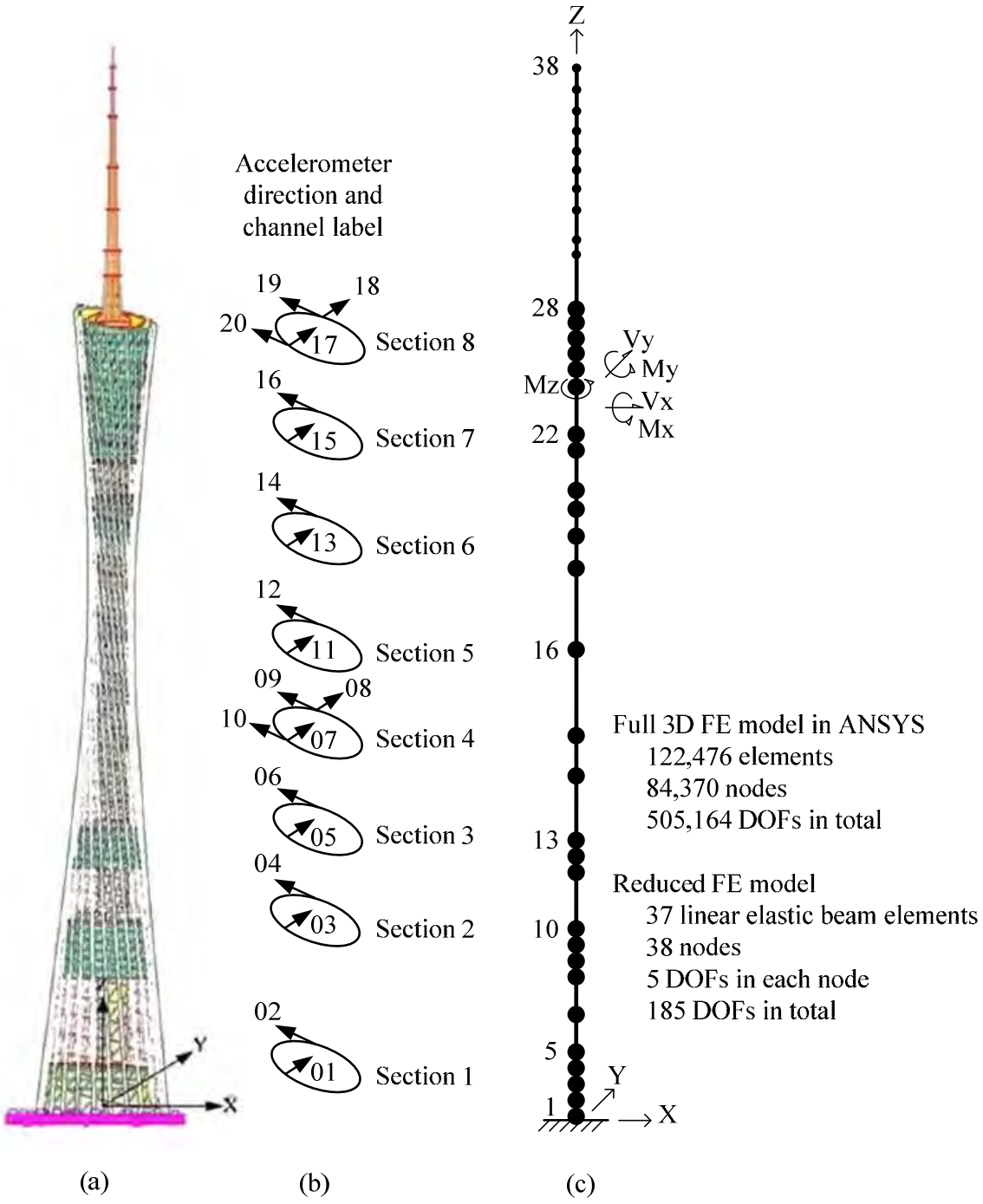

Figure 2.4 The Canton Tower; (a) Finite element model of Canton Tower; (b) Positions of installed accelerometers; (c) Reduced finite element model

A sophisticated long-term structural health monitoring system which consists of over 600 sensors including accelerometers has been designed and implemented by The Hong Kong Polytechnic University for real-time monitoring of the Canton Tower at both in-construction

and in-service stages. Wire and wireless data acquisition network in conjunction with 13 data acquisition units (DAUs) during in-construction monitoring and 5 DAUs during in-service monitoring have been adopted in the structural health monitoring system. A total number of 20 uni-axial accelerometers (Tokyo Sokushin AS-2000C) were installed at eight different levels, as shown inFigure 2.4(b) (Chen et al. 2011). Four uniaxial accelerometers were installed at section 4 and 8, while two uni-axial accelerometers were installed in the rest of the sections in the direction of long and short axes of the inner tube oval. The vibration of the structure is monitored mainly by using a wired cabling network, while a wireless system is also adopted in-situ for complementary vibration monitoring. The detailed information on the structure and the implemented structural health monitoring system can be found in the studies by Chen et al. (2011) and Ni et al. (2009, 2011).

A full-order three dimensional finite element model in ANSYS contains 122,476 elements, 84,370 nodes, and 505,164 degrees of freedom in total. In order to carry out structural health monitoring and associated studies, a reduced-order three dimensional beam model was established by Hong Kong Polytechnic University on the basic of the complex three dimensional full finite element model. In the reduced analytical model, tower is model as a cantilever beam with 38 nodes and 37 beam elements, i.e. 27 elements for main tower and 10 elements for mast, as shown inFigure 2.4(c). The vertical displacement of the structure is omitted in the reduced model and thus each node has 5 degrees of freedom, namely, two horizontal translational degrees of freedom and three rotational degrees of freedom.

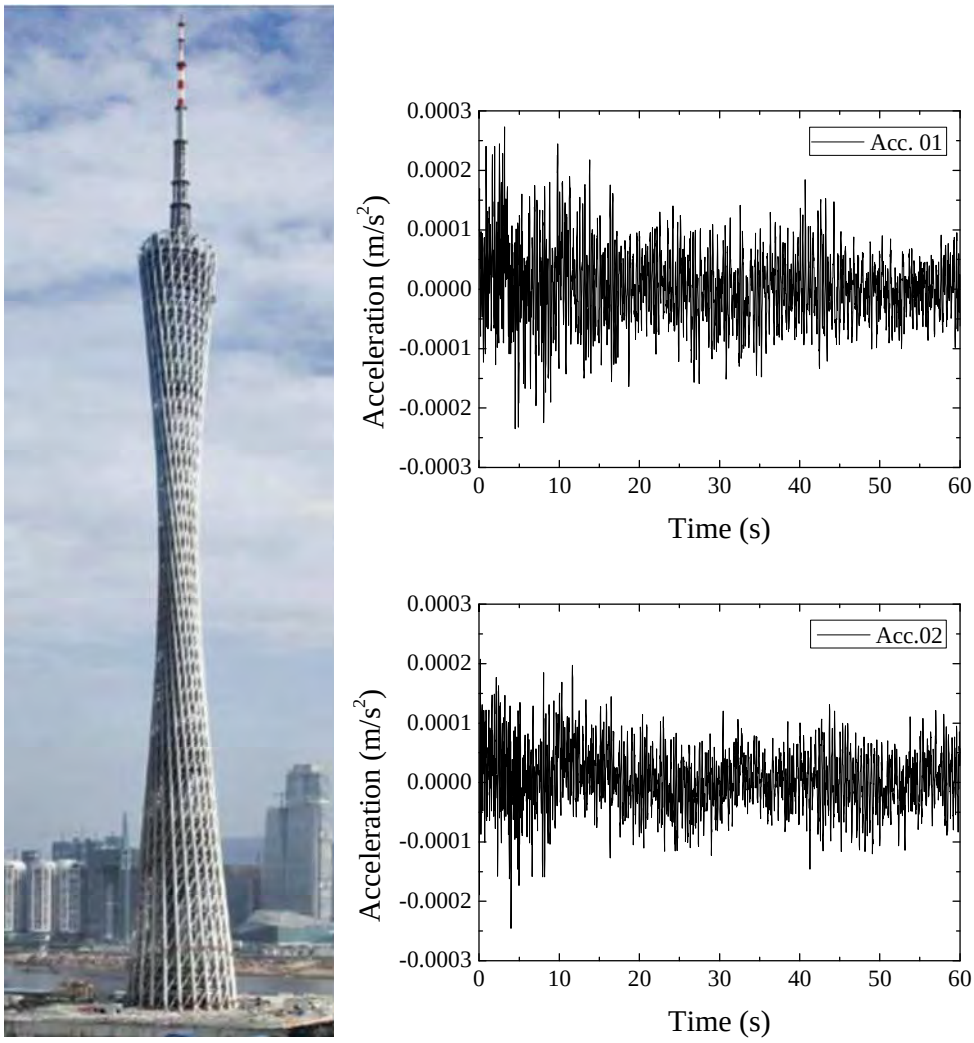

Figure 2.5 The Canton Tower; measured accelerations of accelerometer 01 and 02 at 21:00-22:00

As a result, each beam element has 10 degrees of freedom and the reduced finite element model has a total of 185 degrees of freedom with a fixed end at the base. The reduced analytical model was finely tuned so that its dynamic characteristics match those of the full finite element model as closely as possible. The ambient vibration measurements were recorded through the installed system for 24 hours from 18:00 pm on 19 January to 18:00 pm on 20 January 2010 with a sampling frequency of 50 Hz. The measured data are divided into

24 data sets of one hour equal time interval. These measurements were released for the Phase I of the Benchmark Problem involving the updating of the reduced analytical model. In this study, the ambient vibration measurements recorded from 21:00 pm to 22:00 pm are adopted to identify operational modal properties of the tower, such as frequencies and mode shape measurements, by using the Stochastic Subspace Identification (SSI) technique (Peeters and De Roeck 1999, De Roeck and Peeters 1999, Conte et al.2008). The extracted acceleration measurements recorded by accelerometers 01 and 02 during the first 60 seconds after 21:00 are shown in Figure 2.5.

2.8 Conclusions

Many vibration-based damage detection methods attempt to identify damage by utilising modal data estimated from vibration measurements. The frequency change-based damage identification method can be successfully applied to locate small damage in the simple structure in a controlled laboratory condition. In general, it is not reliable for detecting of structural damage in the real complex structures. Mode shape and mode shape curvature-based methods are only useful for damage localisation and may not be able to detect the quantity of damage in the structure. Moreover, most damage identification methods may not be able to provide accurate predictions for the severity of damage related to stiffness changes with time at specific locations in the structure. Therefore, it is desirable to develop an applicable method for real time detection of structural damage caused by extreme event, such as earthquake, with the consideration of damage indicators to characterise both the location and extend of damage at element level.

In structural dynamic testing, forced vibration testing produces better modal parameter estimation if the input force is known. However, ambient vibration testing is critical for long-term structural health monitoring of the large structures, such as bridges and towers, where input excitations are unknown. Thus, further development of modal parameter extraction techniques without an input record is another important issue for structural damage detection. Furthermore, there are a number of challenges still exist including development of methods to optimally define the number and location of the sensors, and statistical models to distinguish the features from undamaged and damaged structures.

Chapter 3 Dynamic Responses of Intact and Damaged Structures

3.1 Introduction

With growing interest in structural health monitoring, structural dynamic testing can be used as a tool for assessing the integrity of the structure. Laboratory testing techniques, such as impact excitation, shaking table, swept sine or random excitation by electromagnetic exciter, have been widely used in the dynamic testing of civil engineering structures and laboratory scale models (Ewins 2000). Changes in structural properties can cause the changes in dynamic responses of the structure. In this study, a space steel frame model structure is selected for structural dynamic testing in the laboratory. The model structure comprises of rectangular beams and columns, and circular bracings as shown in Figure 3.1. Structural dynamic testing of the intact and damaged structures by using impact excitation is carried out for the following purposes:

- Testing can provides the information about the dynamic characteristic of the tested structures.
- The measurement modal parameters could be used to identify the difference in dynamic responses and integrities of the intact and damaged structures by observation of the changes in the modal parameters.
- Analytical models of the tested structures can be validated and calibrated by using those measured modal parameters.

3.2 Structural model

A small scale steel framemodelstructure was constructed, as shown in Figure 3.1, for numerical simulation investigation and experimental studies of finite element model updating and structural damage identification by using measured modal data.

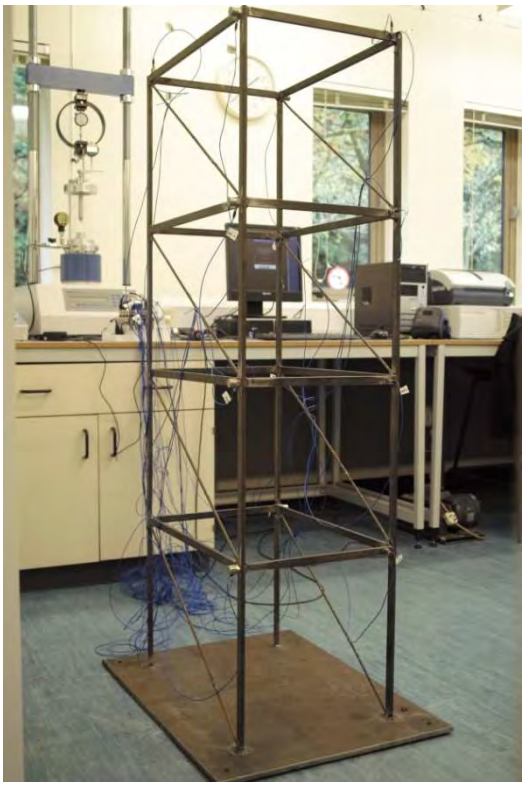

Figure 3.1 Spacesteel frame model structure used in laboratory structural dynamic testing

The associatedfinite elementmodel of the test structure is modelled with the geometric dimensions, the node and element numbering, as shown in Figure 3.2. The structure has four stories comprising of 10 structural members at each storey, i.e. four columns, four beams and two diagonal braces. The columns are fixed at the base and continuous at bean-column joints.

The bracing is formed by inserting diagonal structural members between each story to resist lateral forces and are assumed pin-jointed at both ends and therefore primarily subject to axial force. The beams and columns are modelled as conventional beams and the braces as axial

bar elements. The connection joints of beams and columns are modelled as rigid joints to maintain bending moments. The analytical model has 20 nodes and 40 elements with a total number of 96 degrees of freedom. The column and beam elements have the same rectangular cross section with dimensions of 20 mm × 10 mm, while the brace elements have an identical circular cross section with diameter of 6 mm. The material properties of Young's modulus $E = 2.0 \times 10^{11}$ N/m^2 and density $\rho = 7850$ kg/m^3 are adopted in calculations for all elements.

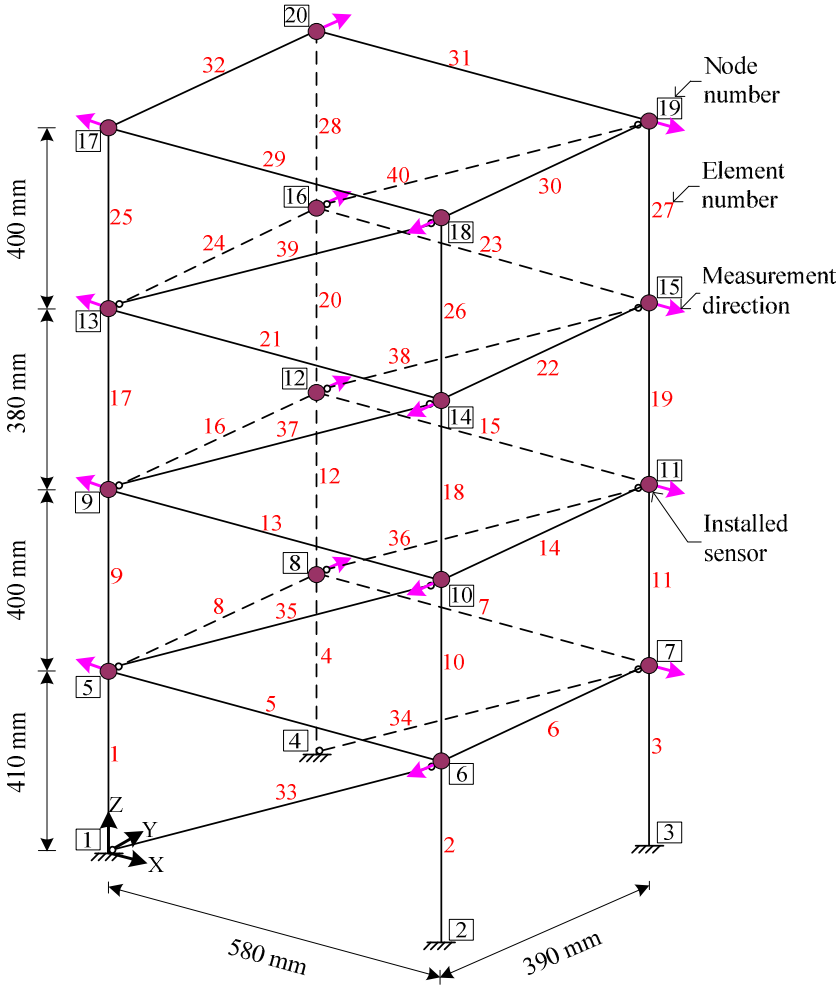

Figure 3.2 The finite element model of the laboratory tested space steel frame model structure with sixteen installed sensors

3.3 Laboratory testing

Structural dynamic testing is undertaken in the laboratory to evaluate the dynamic characteristics of space steel frame structure. The data acquisition system is set up to measure vibration data and to calculate Fast Fourier Transform (FFT) (Brownjohn et al. 2001, Dong and Song 2010). The system consists of sixteen accelerometers, an impact hammer, data acquisition devices and Dell desktop computer loaded with Windows XP platform and modal analysis program. Uni-axial ICP accelerometers model 353B33 and 333B32 manufactured by PCB Piezotronics Ltd, as shown in Figure 3.3, are utilized as sensors. Those accelerometers have sensitivity of 100 mV/g, frequency rate of 1 to 4k Hz for model 353B33 andsensitivityof 100 mV/g, frequency rate of 0.5 to 3k Hz for model 333B32 respectively.

(a) (b)

Figure 3.3 Accelerometers model (a) 353B33; (b) 333B32

3.3.1 Data acquisition

Measured data are acquired by using 4 channel 24-Bit AC/DC input module and cDAQ-9178 data acquisition chassis along with five NI-9234 DAQ signal processing modules from National Instruments. Initially, the test structure is cleaned especially around the nodes of

beam-column joints where the accelerometers are installed. The optimum sensors arrangement is determined from the information of analytical mode shapes and iteratively moving sensor locations that do not effect significantly to the linear independence of the mode shapes (Meo and Zumpano 2005, Flynn and Todd. 2010, Stephan 2012). A total number of 16 uni-axial accelerometers are installed by adhesive mounting to measure only translational displacement readings in horizontal directions as shown in Figure 3.2.

Figure 3.4 Impact hammer model 086D20 with rubber tips

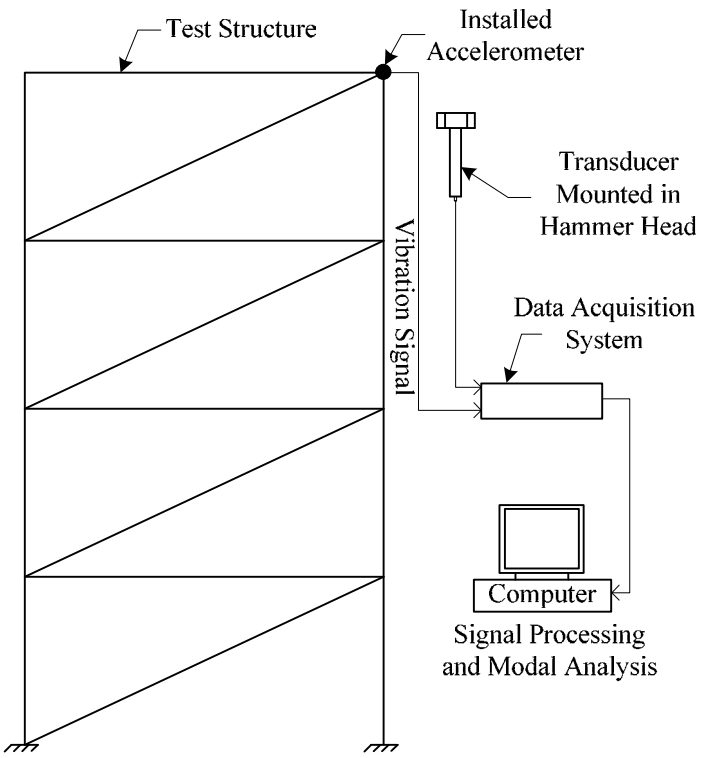

Figure 3.5 The system of structural dynamic testing and data acquisition

Accelerometers are then connected by low noise cable (model 003C20) to the input module. PCB model 086D20 impact hammer mounted transducer is used to excite the structure at specified locations. The mass of the hammer is approximately 1.1 kg and has 5.1 cm diameter head. A super soft rubber hammer tip (model 084A60) is attached in the hammer to broaden the impulse that is imparted to structure in an effort to better excite the lower frequency modes. Transducer at hammer tip has a nominal sensitivity of 0.23 m V/N. Approximately 7 m long coaxial cable (model 012A20) is used to connect the hammer and input module to acquire the impulse measurements. The impact hammer used for structural excitation and structural dynamic testing system are illustrated inFigure 3.4 and Figure 3.5 respectively.

3.3.2 Damage patterns

In this experiment, dynamic properties of intact structure and the damaged structures with four damage patterns are studied. These four damage patterns are defined as

1. No stiffness in the braces of the level 1 (i.e. the braces still contribute mass, but provide no stiffness to the structure)
2. No stiffness in any of the braces in levels 1 and 3
3. No stiffness in any of the braces in levels 1, 2 and 3
4. No stiffness in any of the braces in all stories

Damage patterns of the tested structure are illustrated in Figure 3.6.

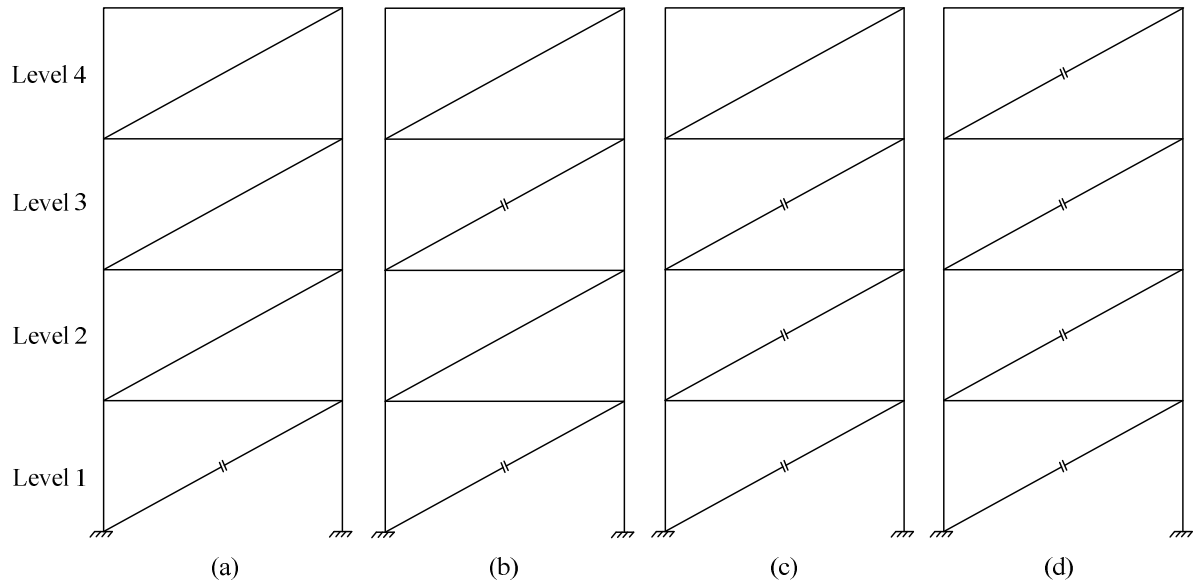

Figure 3.6 The four damage patterns: (a) Damage pattern 1; (b) Damage pattern 2; (c) Damage pattern 3; (d) Damage pattern 4

Finite element models of the tested structure are developed to estimatethe natural frequencies and corresponding mode shapes for both intact and damaged structures in all damage patterns.

3.3.3 Modal parameters identification

In the dynamic testing, the frame steel structure is excited by impact hammer at several places in order to excite all frequencies and mode shapes of interest range (Alwash et al. 2009, Agarwal et al. 2010). When the model structure is excited, the data set of acceleration measurements is recorded by using data acquisition devices and Labview Signalexpress commercial software (Labview 2009). The modal data such as frequencies and mode shape readings at measured degrees of freedom are extracted from the acceleration measurements

through ME'Scope VES modal analysis software (Vibrant Technology 2010, Michel et.al 2008). In order to illustrate the laboratory testing clearly, flowchart diagram of experimental procedure is shown in Figure 3.7.

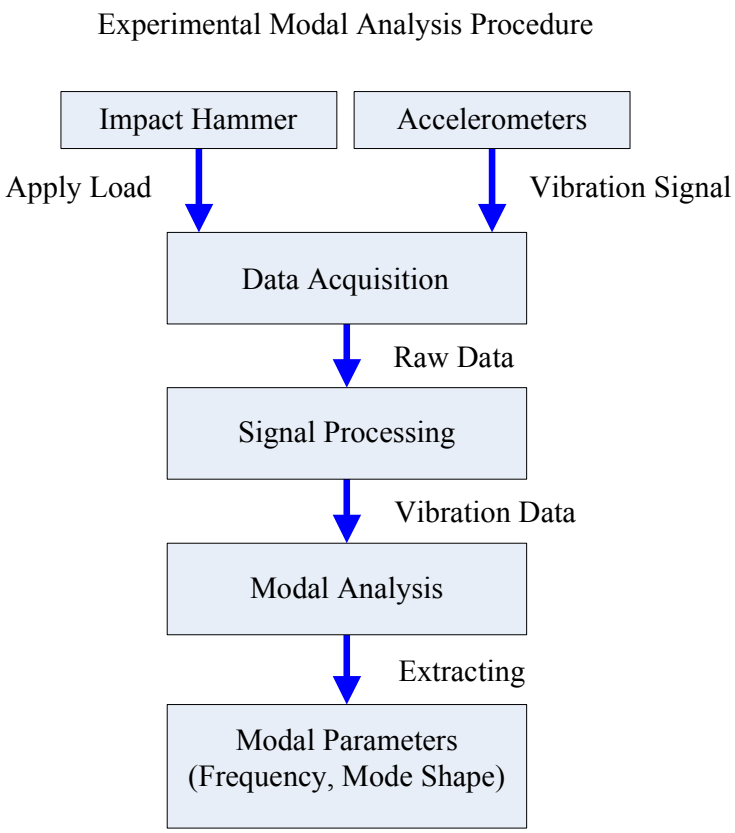

Figure 3.7 Flowchart diagram of structural dynamic testing and modal parameters estimation

3.4 Modal data for intact structure

Structural dynamic testing of intact structure was undertaken at the beginning of the lab testing. The modal properties of the analytical and measured natural frequencies for the first 7 modes along with Modal Assurance Criterion (MAC) values are provided in Table 3.1. It is evident that the natural frequencies could be extracted with a high degree of reliability. The

graphical presentations of measured natural frequencies from installed accelerometer are shown fromFigure 3.8 to Figure 3.23. It can be noticed thatnatural frequencies of mode number 3,4,5 and 6 are missing in the Figure 3.17. This is due to the fact that the selected location of excitation in the structure cannot excite those missing modes during structural vibration although several excitation attempts have been performed by selecting the different locations for impact excitation in the structure. Moreover, the most dominant modal parameters are globally identified based on measured vibration data obtained from all installed sensors rather than single sensor. It might be the cause of unable to identify some modes in the measured data. A similar problem can be found in the Figure 3.19,where frequencies mode number 3,4 and 5 are missing. Additionally, comparisons of the first 7 mode shapes calculated from the finite element model and extracted from the measured data are illustrated inFigure 3.24 to Figure 3.30.

As an indication of the level of agreement between the measured and calculated mode shapes, MAC factorsdefined in Eq.(2.1) is utilised. Good agreements are also found between analytical and measured mode shapes, particularly for the first four fundamental modes as shown in Figure 3.24 to Figure 3.27.5thmode shapes withvery low MAC values of 0.0574 do not correlate well with corresponding analytical mode shape. Similarly, comparisons of 6th and 7th modes do not yield satisfactory condition as MAC values indicate as low as 0.6469 and 0.6098 respectively due to complexity of higher modes.

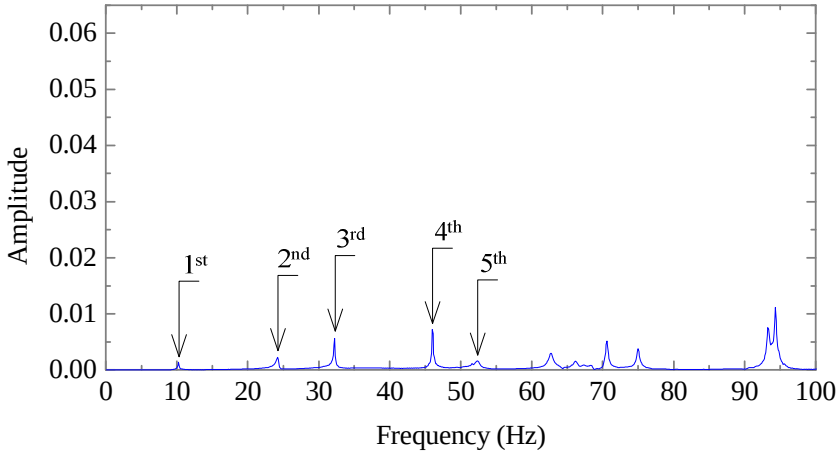

Figure 3.8 Measured frequencies extracted from measured acceleration at node 5 of intact structure

Table 3.1 Analytical and experimental frequencies of intact structure

Mode	Analytical Frequency (Hz)	Experimental Frequency (Hz)	MAC Analytic vs Experiment	ModeDescription
1	10.3552	10.3	0.9961	Y-axis bending
2	25.9379	24.3	0.9823	Y-axis bendingand torsion
3	31.7607	32.2	0.9972	Y-axis bending
4	45.2474	46.0	0.9936	Y-axis bending and torsion
5	51.8178	51.4	0.0574	Y-axis bending
6	65.5715	60.3	0.6469	Y-axis bending and torsion
7	70.6418	70.4	0.6098	Y-axis bending

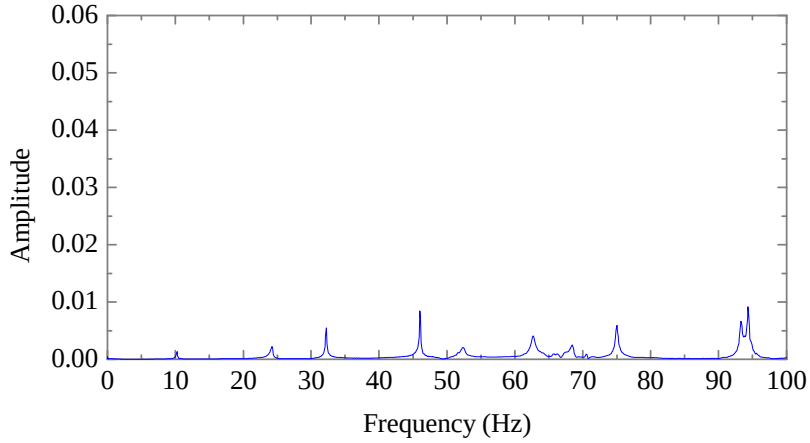

Figure 3.9 Measured frequencies extracted from measured accelerationat node 6 of intact structure

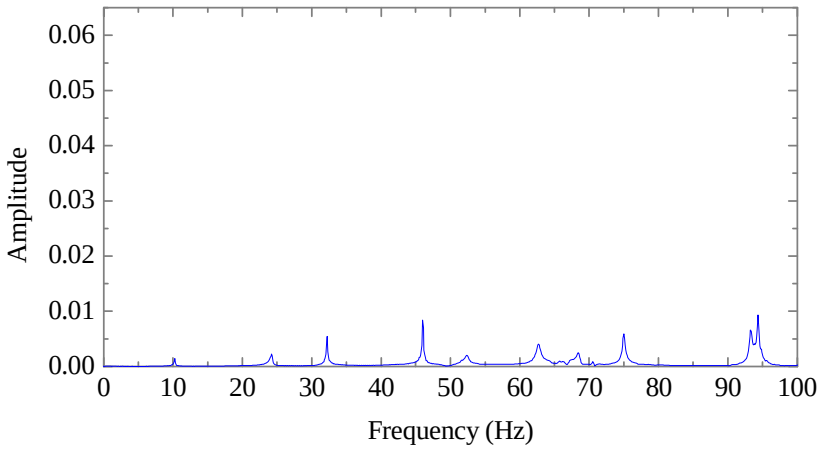

Figure 3.10 Measured frequencies extracted from measured accelerationat node 7 of intact structure

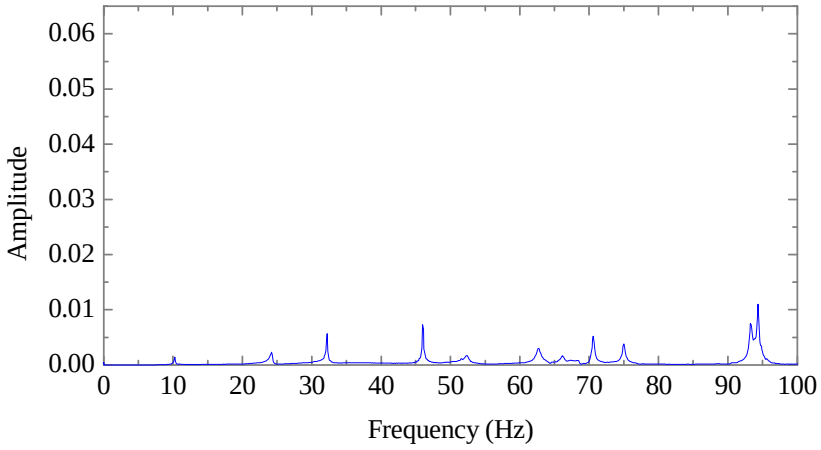

Figure 3.11 Measured frequencies extracted from measured acceleration at node 8 of intact structure

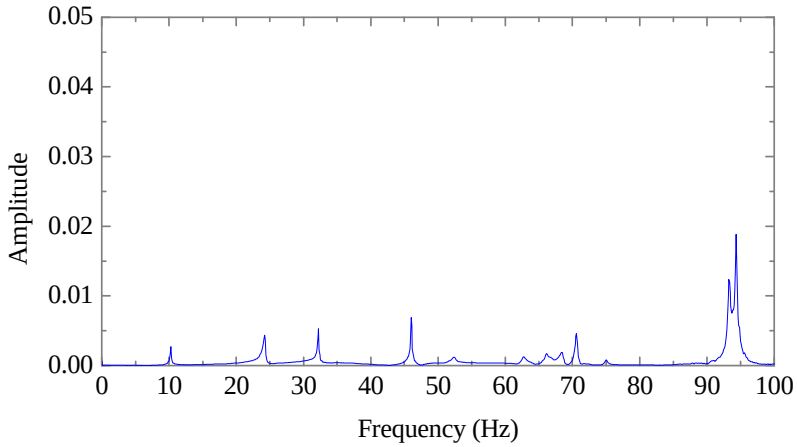

Figure 3.12 Measured frequencies extracted from measured acceleration at node 9 of intact structure

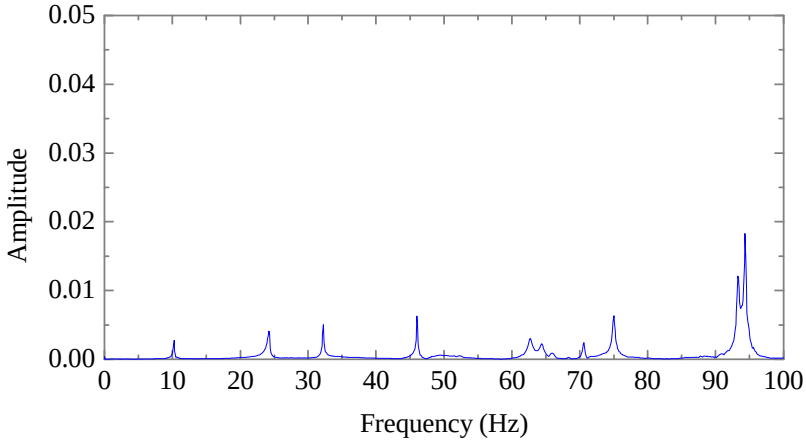

Figure 3.13 Measured frequencies extracted from measured acceleration at node 10 of intact structure

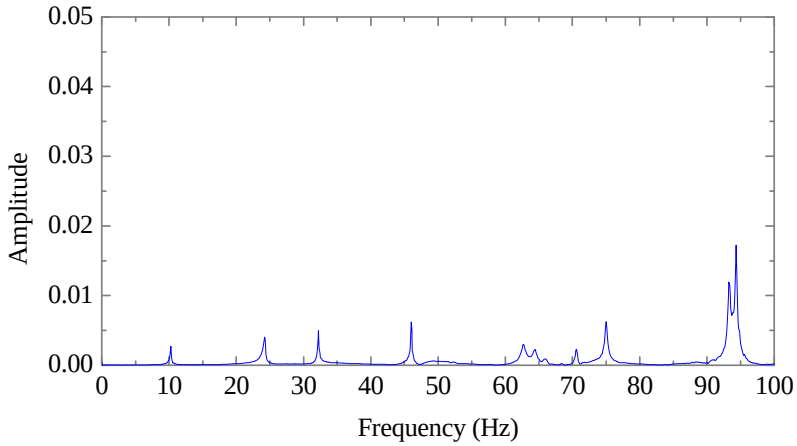

Figure 3.14 Measured frequencies extracted from measured acceleration at node 11 of intact structure

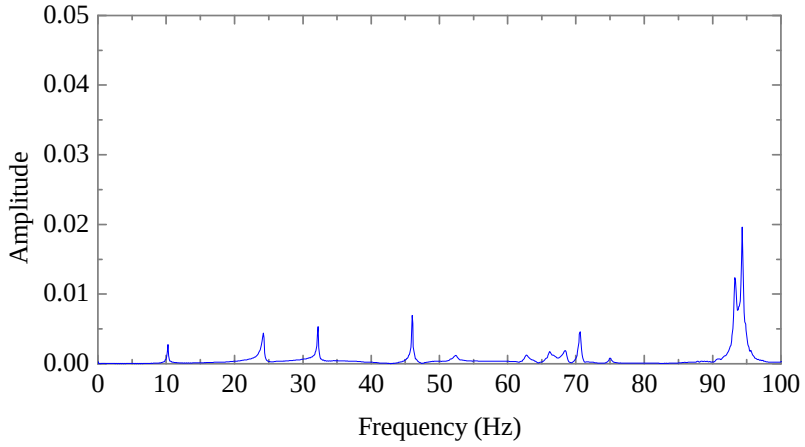

Figure 3.15 Measured frequencies extracted from measured acceleration at node 12 of intact structure

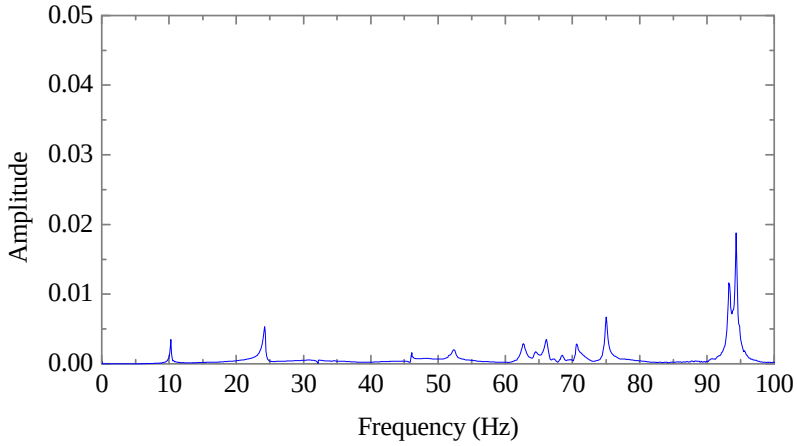

Figure 3.16 Measured frequencies extracted from measured acceleration at node 13 of intact structure

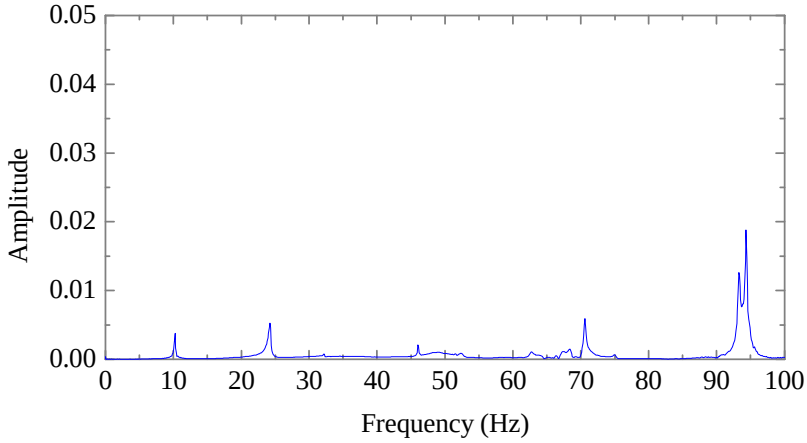

Figure 3.17 Measured frequencies extracted from measured acceleration at node 14 of intact structure

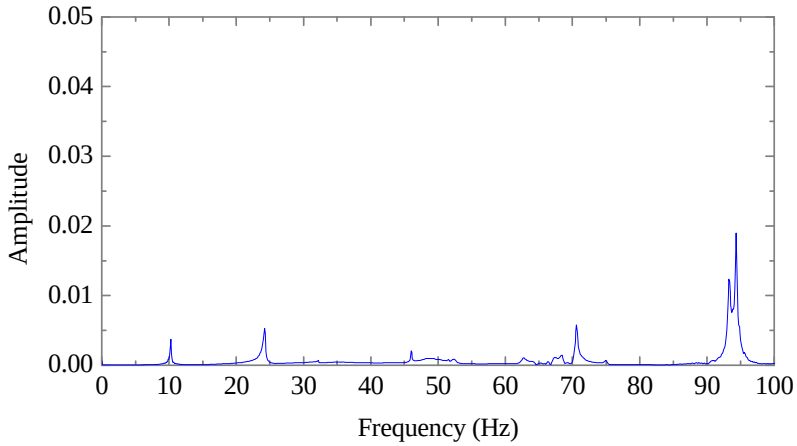

Figure 3.18 Measured frequencies extracted from measured acceleration at node 15 of intact structure

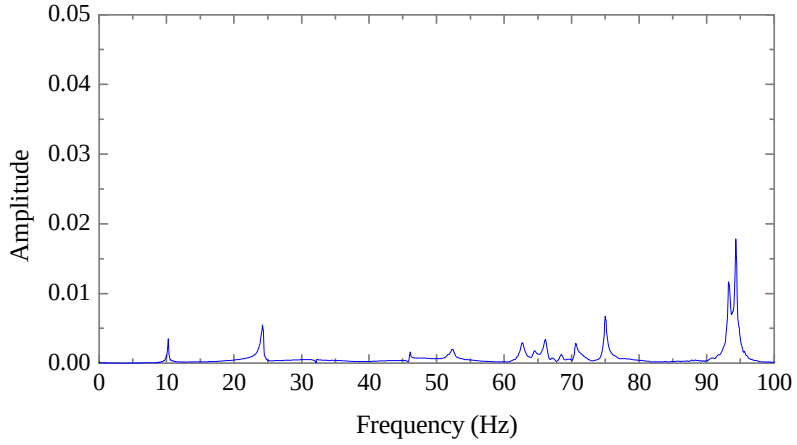

Figure 3.19 Measured frequencies extracted from measured acceleration at node 16 of intact structure

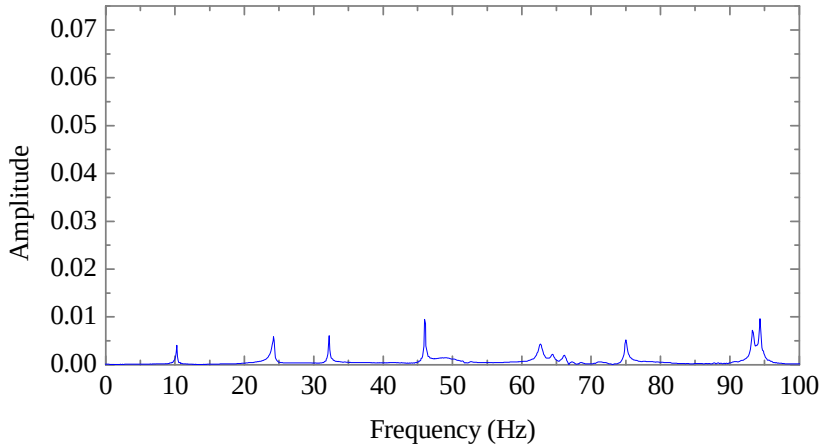

Figure 3.20 Measured frequencies extracted from measured acceleration at node 17 of intact structure

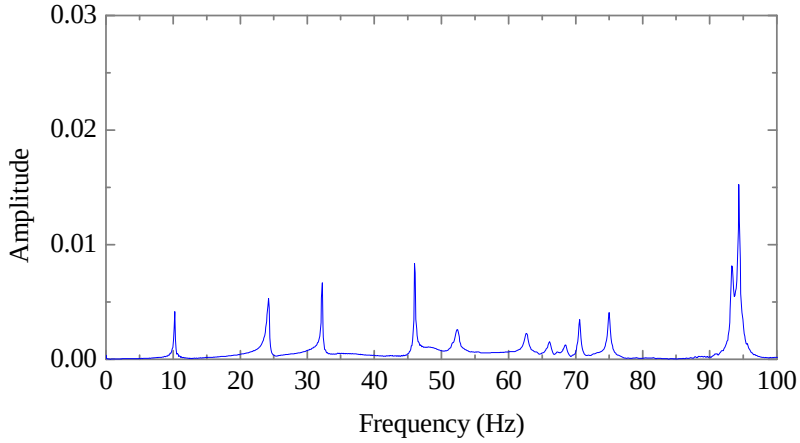

Figure 3.21 Measured frequencies extracted from measured acceleration at node 18 of intact structure

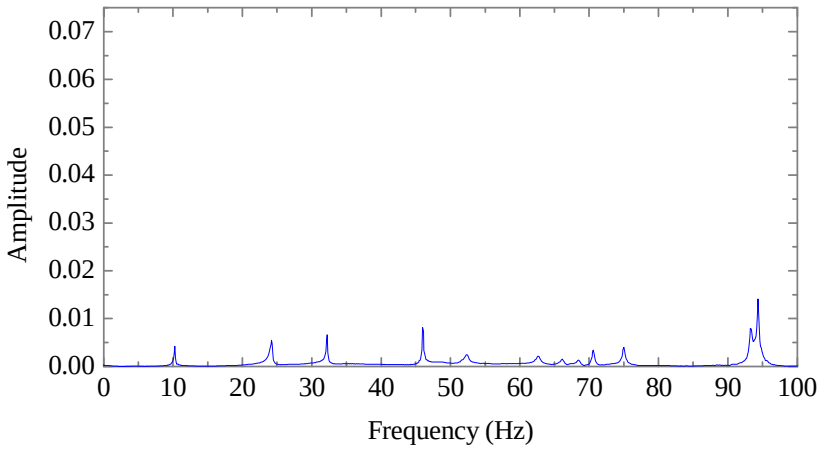

Figure 3.22 Measured frequencies extracted from measured acceleration at node 19 of intact structure

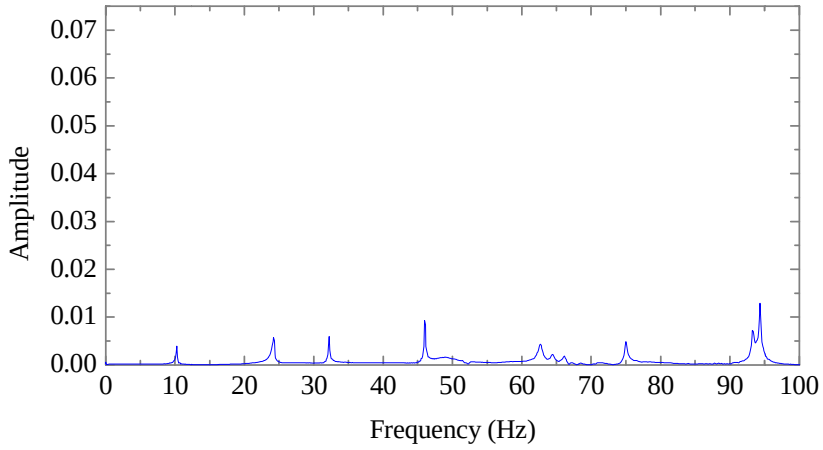

Figure 3.23 Measured frequencies extracted from measured acceleration at node 20 of intact structure

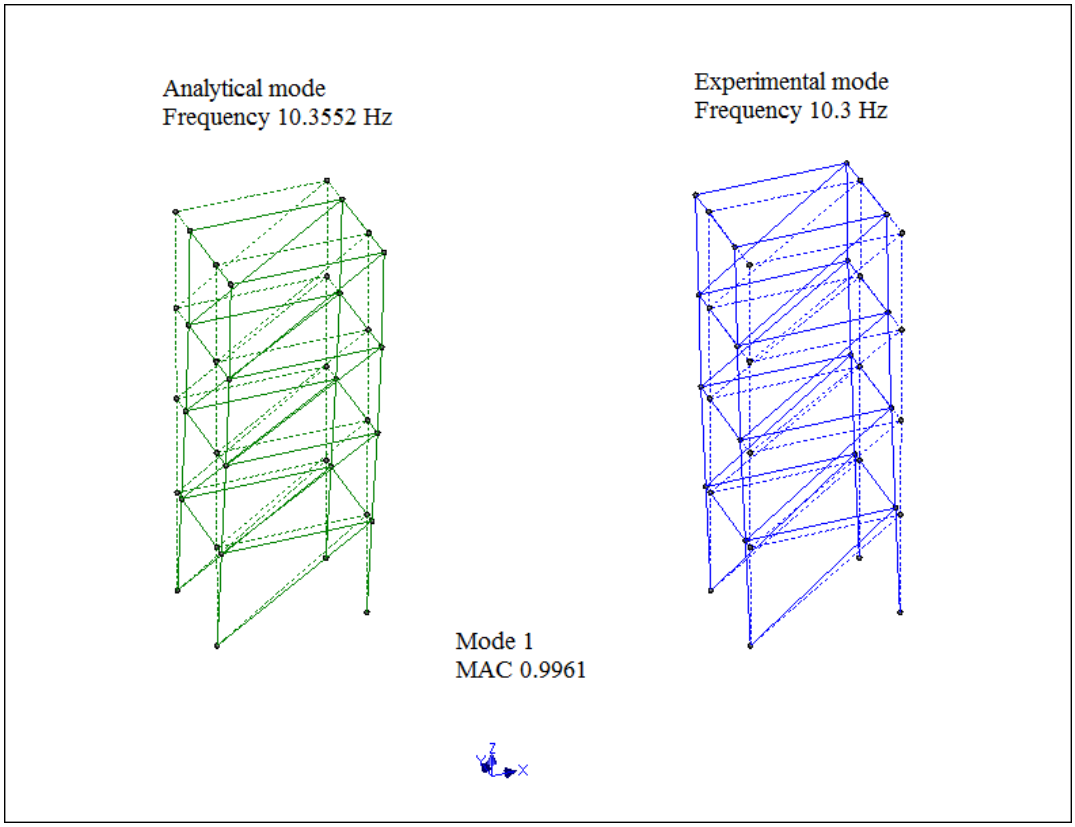

Figure 3.24 Comparison of 1st analytical and experimental mode shapes of intact structure

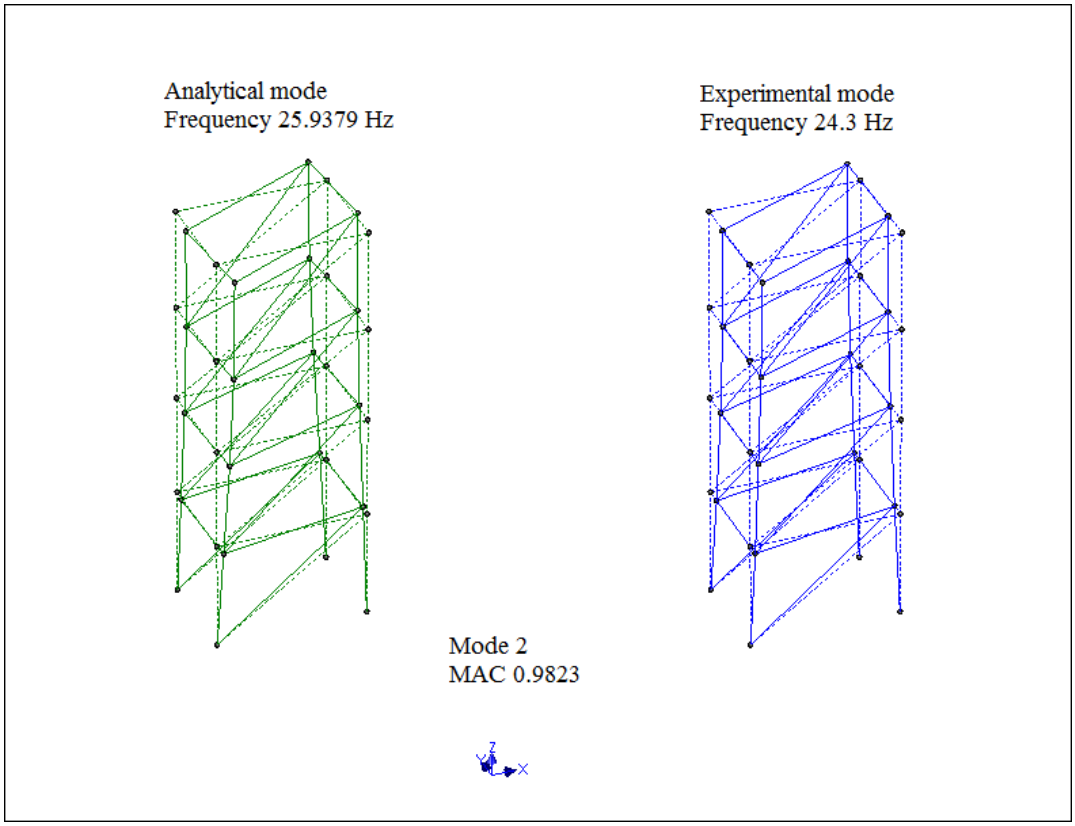

Figure 3.25 Comparison of 2nd analytical and experimental mode shapes of intact structure

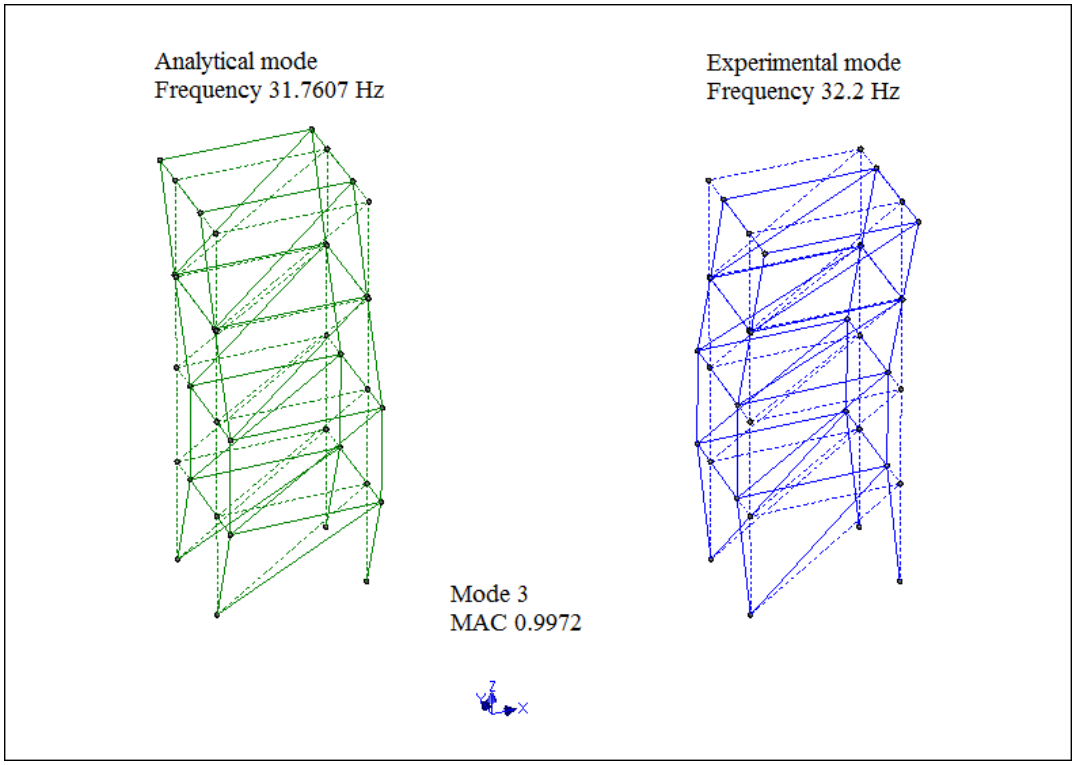

Figure 3.26 Comparison of 3rd analytical and experimental mode shapes of intact structure

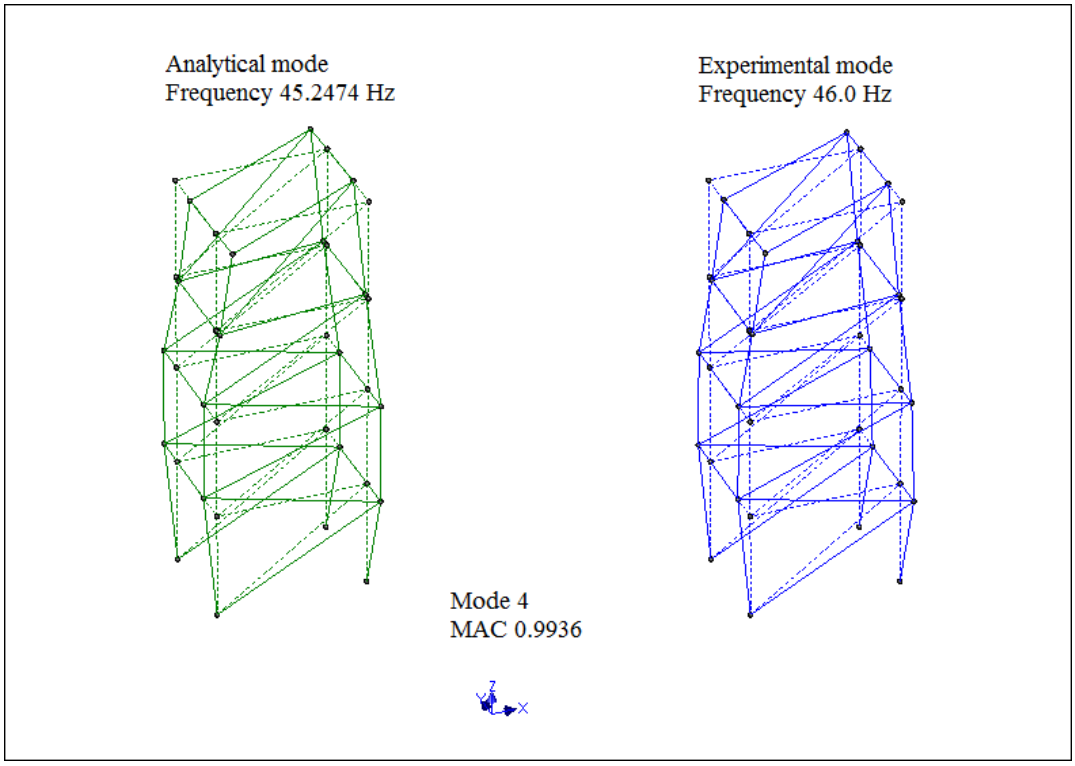

Figure 3.27 Comparison of 4th analytical and experimental mode shapes of intact structure

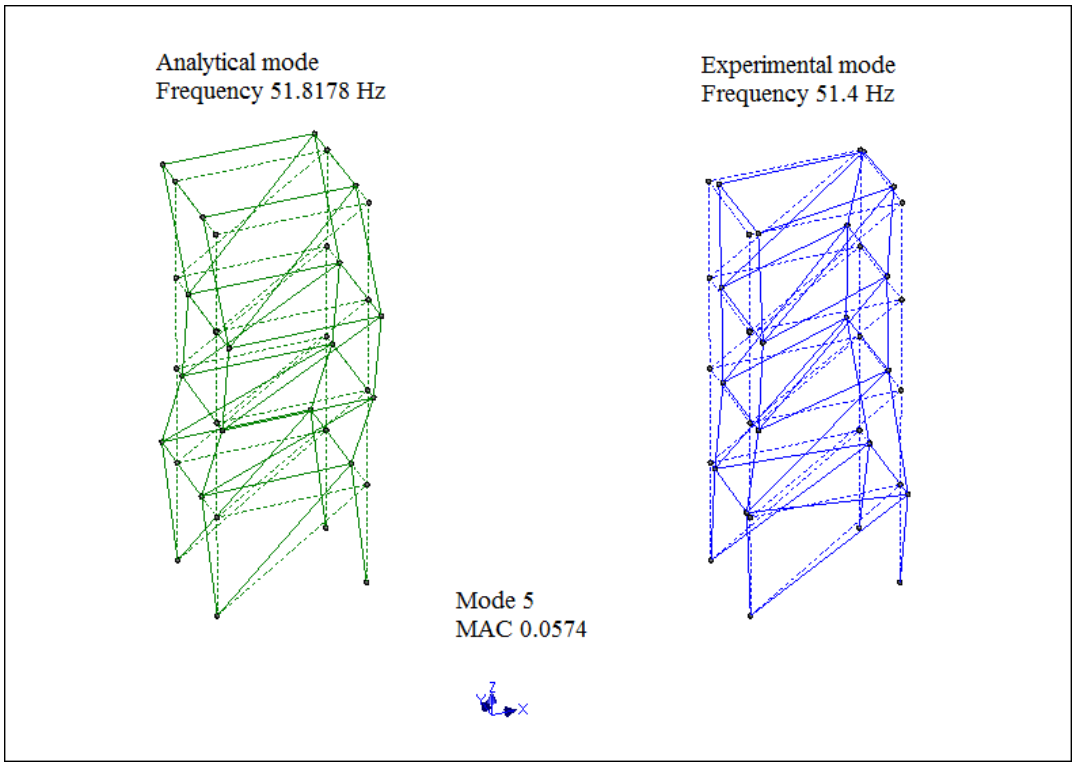

Figure 3.28 Comparison of 5th analytical and experimental mode shapes of intact structure

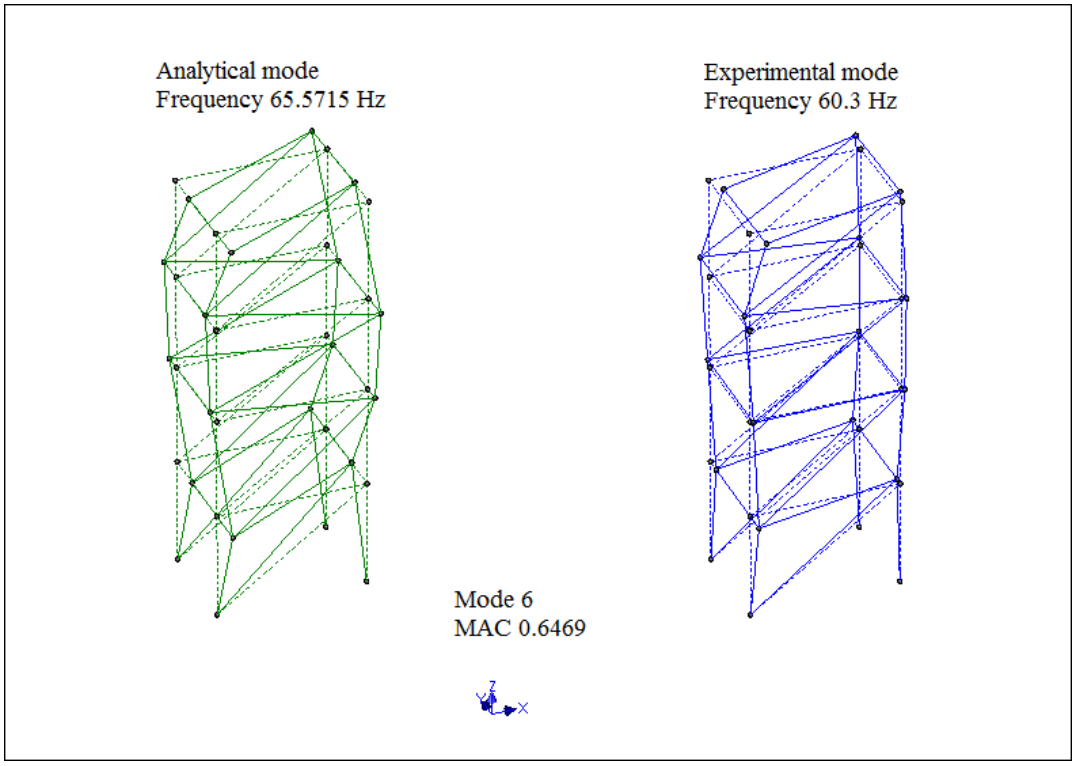

Figure 3.29 Comparison of 6th analytical and experimental mode shapes of intact structure

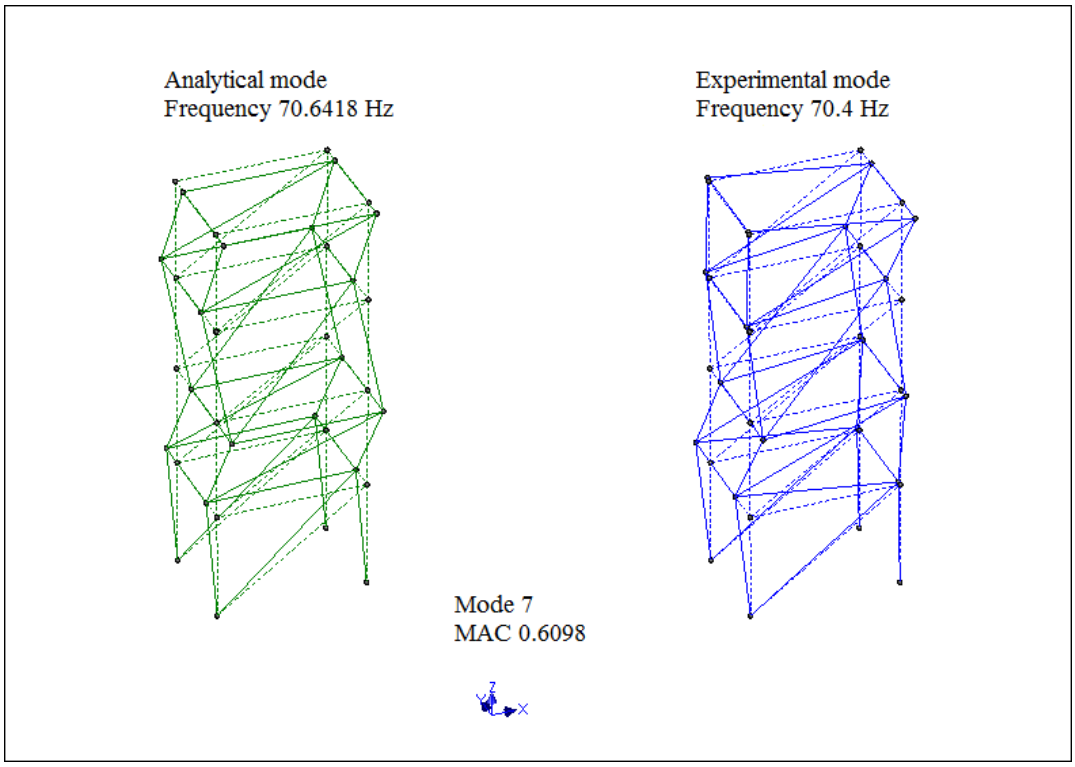

Figure 3.30 Comparison of 7th analytical and experimental mode shapes of intact structure

3.5 Modal data for damaged structures

In the experiment, four damage patterns for damaged structures are defined as summarised in Table 3.2 in order to identify the modal data of the damaged structures.

Table 3.2 Damage patterns defined for space steel frame model structure

Damage pattern	Element number	Damage description
1	33,34	Stiffness reduction
2	33,34,37,38	Stiffness reduction
3	33 to 38	Stiffness reduction
4	33 to 40	Stiffness reduction

3.5.1 Damage pattern 1

In the damage pattern 1, no stiffness exists in the brace members at level 1. Firstly, finite element analysis is performed to obtain the dynamic properties of the damaged structure. Invibration testing, two brace elements in level 1 are cut to reduce the stiffness of braces but the masses are still remained in the structure as shown in Figure 3.6(a). The cut edges of the brace member are slotted in to a small pipe and hold the both cut edges to prevent from local element vibration. Vibration responses through the installed sensors are acquired with the help of data acquisition devices while the impact hammer hit the beam element number 32 at the top floor to excite the modes in the interest range. Natural frequencies and mode shapes are identified by using similar method for the intact structure.

Comparison of analytical and measured frequencies, and MAC values are summarised in Table 3.3. Graphical presentation of measured frequencies is also presented in the Figure 3.31. Although no stiffness in brace members at floor level, the 1st mode frequency do not reduce and in good agreement with corresponding analytical mode. 2nd mode frequency 18.8 Hz is slightly lower than analytical value of 20.0396 Hz. 4th, 5th, and 7th measured frequencies are in well match with corresponding analytical frequencies.It is immediately apparent that some modes are not excited in the dynamic testing of damaged structure due to missing damaged elements. Higher MAC values showthat measured mode shapes are agreeing well with corresponding analytical modes.

Table 3.3 Analytical and experimental frequencies of damaged structure in damage pattern 1

Mode	Analytical Frequency (Hz)	Experimental Frequency (Hz)	MAC Analytic vs Experiment
1	10.3551	10.5	0.9942
2	20.0396	18.8	0.8482
3	27.1367	/	/
4	31.7604	32.3	0.7690
5	45.1850	45.9	0.9723
6	49.1911	/	/
7	51.8190	52.2	0.7233

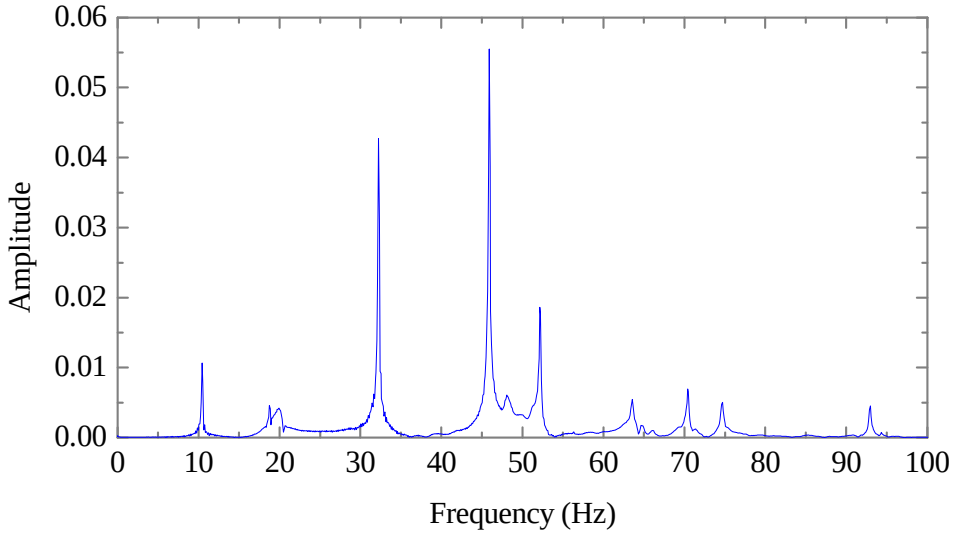

Figure 3.31 Measured frequencies of damaged structure in damage pattern 1

3.5.2 Damage pattern 2

In the damage pattern 2, no stiffness exists in the brace members at the level 1 and 3. For comparison of analytical and measured modal data, mathematical model of damaged structure is developed and finite element dynamic analysis is performed prior to experimental study. In this damage pattern, additional two brace members in floor level 3 are cut to reduce the additional stiffness of braces in damage pattern 1 as shown in Figure 3.6(b). Measured modal data are extracted with the help of modal analysis technique implemented in the modal analysis software. Analytical and measured frequencies as well as MAC values are shown in Table 3.4. Graphical illustration of measured frequencies is also shown in the Figure 3.32.

Table 3.4 Analytical and experimental frequencies of damaged structure in damage pattern 2

Mode	Analytical Frequency (Hz)	Experimental Frequency (Hz)	MAC Analytic vs Experiment
1	10.3550	10.5	0.9710
2	18.7420	18.0	0.7872
3	24.3464	/	/
4	31.7602	32.3	0.9956
5	44.1538	45.0	0.9881
6	48.2108	/	/
7	51.8178	52.8	0.7901

In this damage pattern, 1st measured and analytical frequencies do not change significantly. However, 2nd, 4th, 5th, and 7th measured frequencies agree well with corresponding analytical frequencies. Even though additional stiffness of the brace elements are reduced, all measured frequencies of the damaged structure in damage pattern 2 do not change significantly. Higher MAC values indicate that measured modes are in good correlation with corresponding analytical modes.

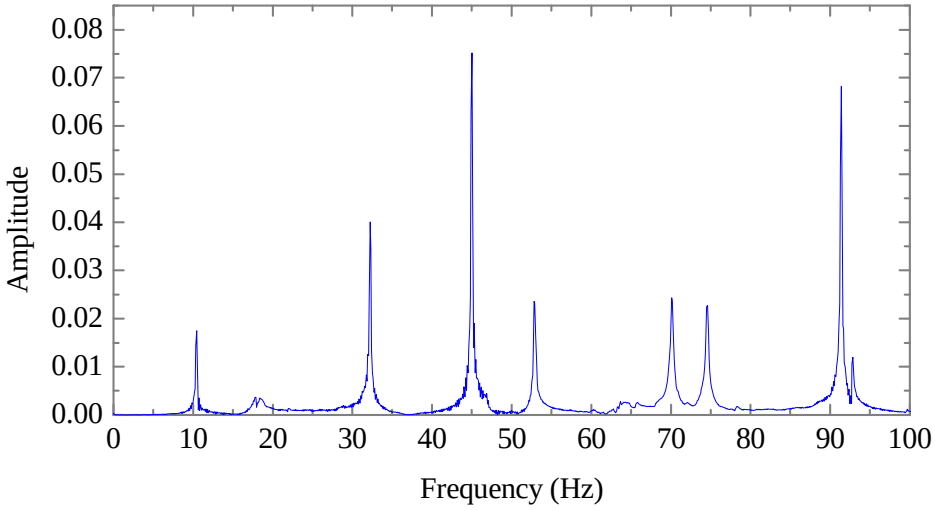

Figure 3.32 Measured frequencies of damaged structure in damage pattern 2

3.5.3 Damage pattern 3

In this damage pattern, brace elements in level 1, 2 and 3 are assumed to be damaged and no stiffness of those elements contribute to the structure system. Two more brace elements at level 2 of tested frame structure are cut in order to reduce further stiffness. Similar to previous damage pattern, comparison of numerically estimated frequencies vs measured frequencies and MAC values are presented in Table 3.5. Extracted frequencies are also plotted in Figure 3.33.Major notice in this damage pattern is 2ndmeasured frequencyis further reduced to 14.9221 Hz.1st, 4th, 6th, and 7th measured frequencies do not change significantly, and agree well with corresponding analytical frequencies. By judging the MAC values closed to unity, measured modes 1 to 6 except missing modes 3 and 5 show well correlations with the corresponding analytical modes. The existence of damage in the structure affects the natural frequencies and corresponding mode shapes of the structure.

Table 3.5 Analytical and experimental frequencies of damaged structure in damage pattern 3

Mode	Analytical Frequency (Hz)	Experimental Frequency (Hz)	MAC Analytic vs Experiment
1	10.3549	10.4	0.9834
2	14.9221	14.9	0.9866
3	15.3495	/	/
4	31.7601	32.7	0.8740
5	43.4155	/	/
6	45.5680	44.2	0.8509
7	51.8175	52.9	0.6378

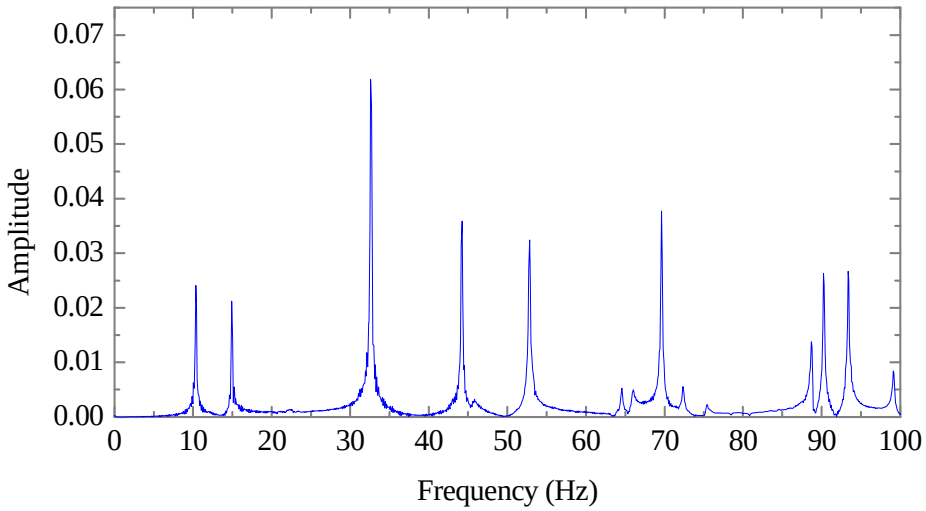

Figure 3.33 Measured frequencies of damaged structure in damage pattern 3

3.5.4 Damage pattern 4

In the last damage pattern, all brace elements are assumed to be damaged and there is no contribution of their stiffness into the structure system. Two brace members at the top floor of the frame structure are cut in addition to damage pattern 3. Finite element analysis and experimental study are undertaken in similar way to previous damaged structures. Numericallyestimated frequencies, measured frequencies, and MAC values are summarised in Table 3.6.Graphical presentation of identified frequencies is also shown in Figure 3.34. In this damage pattern, 1st measured frequency does not change noticeably. The rest measured frequencies except missing 3rd, 6th, and 7th modes are in good agreement with corresponding analytical values. MAC values close to unity show that measured mode shapes are in good correlation with analytical mode shapes.

Table 3.6 Analytical and experimental frequencies of damaged structure in damage pattern 4

Mode	Analytical Frequency (Hz)	Experimental Frequency (Hz)	MAC Analytic vs Experiment
1	10.3548	10.4	0.9934
2	14.2052	14.6	0.9973
3	15.0934	/	/
4	31.7598	32.8	0.9638
5	42.5627	43.0	0.9952
6	45.3228	/	/
7	46.8497	/	/

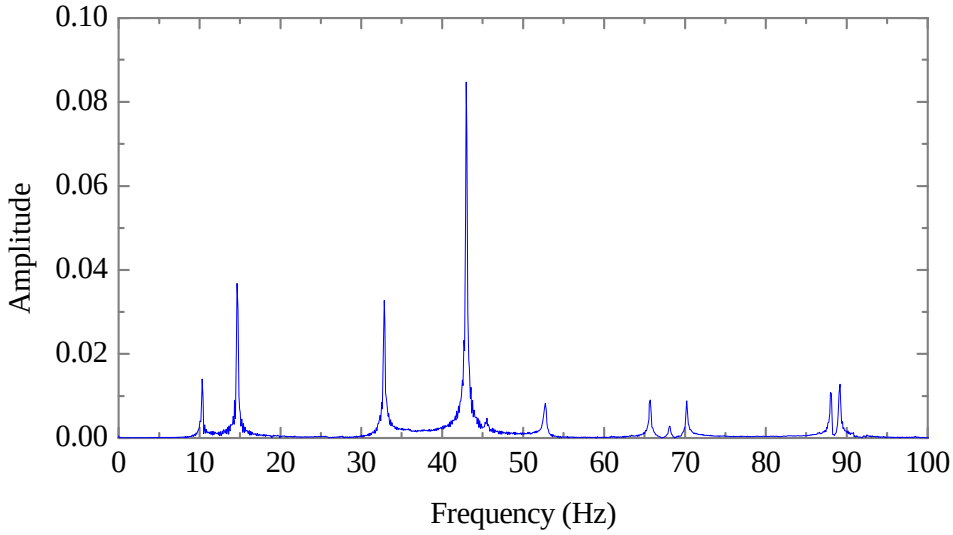

Figure 3.34 Measured frequencies of damaged structure in damage pattern 4

3.6 Comparison of measured frequencies for intact and damaged structures

Comparison of measured frequencies for intact and four damaged structures are indicated in Table 3.7. In the comparison, 1st mode frequencies of all structures do not change significantly. However, 2nd mode frequency of the intact structure reduces from 24.3 Hz to 14.6 Hz of damaged pattern 4 structure where stiffness of all brace elements are reduced in the structural system. Similarly, 4th, 5th, and 7th measured frequencies of damage pattern 1 structure are reduced. However, no significant reductions of frequencies are observedin all four damaged structures although stiffness of brace elements arefurther reduced. It is assumed that stiffness reductions of brace members from a relatively stiffness structural system are not large enough to reduce the measured frequencies significantly. It is apparent that some of the modes are not exciting in the dynamic testing of damaged

structures.Moreover,Figure 3.28 andFigure 3.30 show that 5thand 7th measured modes include torsion effect on bending mode although corresponding analytical modes are pure bending.

Table 3.7 Comparison of measured frequencies identified from measured daata of space steel frame model structures including intact and four damaged structures

Mode	Intact (Hz)	Damage 1 (Hz)	Damage 2 (Hz)	Damage 3 (Hz)	Damage 4 (Hz)
1	10.3	10.5	10.5	10.4	10.4
2	24.3	18.8	18.0	14.9	14.6
3	32.2	/	/	/	/
4	46.0	32.3	32.3	32.7	32.8
5	51.4	45.9	45.0	/	43.8
6	60.3	/	/	44.2	/
7	70.4	52.2	52.8	52.9	/

3.7 Conclusions

Structural dynamic testing of the steel frame model structure was undertaken in the laboratory for the purposes of identifying the dynamic characteristics of the intact and damaged structures. A three dimensional steel frame model structure was constructed with rectangular beam and column elements, and circular brace elements. For damaged structures, four damage patterns were defined by cutting the brace elements of the structure. Local vibration of cut braced members was prevented by using a small plastic pipe holding the both

cut ends of the braced members. The first seven natural frequencies ranging from 10.3 Hz to 70.4 Hz and associated mode shapes were identified from measured acceleration data by utilising experimental modal analysis technique. Those measured modal parameters were validated with the analytical results obtained from finite element dynamic analysis and integrities of the tested structures were determined by observing the changes in modal parameters. For the intact structure, the first four experimental modes correlate well with corresponding analytical modes. However, fifth to seven modes do not agree well with corresponding analytical modes due to complexity of higher modes. Some lower modes were missed and could not be extracted from the measured data due to missing stiffness of damaged braced members in the structure. Moreover, the location of input force to excite the structure also affected the excitation of the experimental modes.

Chapter 4 Finite Element Model Updating Using Incomplete Measured Modal Data

4.1 Introduction

The finite element method is useful for many applications in engineering practice such as structural analysis and structural damage detection (Wu and Li 2006, Friswell 2007, Quek et al. 2009). In general, the analytical model of the associated actual engineering structure may not fully represent all the physical and geometrical aspects of the actually built structure. As a result, discrepancies exist between analytical predictions and experimental results.These discrepancies can occur due to:

- errors in structural modelling caused by imperfection in geometry, member's connection such as bolted or welded connection.
- errors in model order which associated with discretization in the generation of the finite element model.
- errors in structural parameter due to incorrect material properties and boundary conditions.

Many investigations show that the differences between the numerical and experimental frequencies may exceed 10% or sometimes even 40% (Brownjohn and Xia 2000, Jaishi and Ren 2005, Zivanovic et al. 2007). In order to improve the correlation between the analytical predictions and measured data, effective methods for finite elementmodel updating are required to adjust the structural parameters of the initial analytical model by using the measured vibration data of the actual tested structure (Friswell and Mottershead 1995, Teughels et al. 2002, Weng et al. 2011). In this chapter, existing model updating methods are

reviewed and development of a robust model updating method is presented. The proposed model updating method can directly adopt measured incomplete data to update the structural updating parameters at critical point level without requiring mode shape expansion or model reduction techniques.

4.2 Existing model updating methods

4.2.1 Direct method

The direct method, also called model-based method, directly reconstruct the elements stiffness and mass matrices by a one-step procedure (Caesar and Peter 1987, Friswell et al. 1998, Yang and Chen 2009). Incomplete measured modal data could be used for updating structural parameters without using standard modal expansion or model reduction techniques (Carvalho et al. 2007). Apart from the measured modal data, the measured frequency response functions can also be utilised to update the structural parameters of the finite element model by minimizing the residual error between analytical and experimental outputs (Esfandiari et al. 2010). The direct updating methods basically require full degrees of freedom measured data to update the finite element model. When a full set of measurements at all degrees of freedom are available, the model updating problem is algebraically linear and can be solved in one step iteration. However, in practice, it is impossible to measure vibration responses at all degrees of freedom of a large structure. Thus, the numbers of measurable degrees of freedom are limited and the measured data sets are often incomplete. Then, the applicability of the direct method may be restricted to update the large number of structural parameters and the updated physical properties may not truly represent the actual tested structure concerned.

There are some advantages and disadvantages in direct updating methods (Maia and Silva, 1997, Jaishi 2005). The main advantages are:

- the method does not require any iteration and assures the convergence solution.
- the analytical data may be produced exactly as test results.

Disadvantages include:

- precisegeometry of test structure in finite element modelling and accurate finite element modal analysis are required.
- the measured modal data must be expanded to the size of finite element model or reduce the finite element model to the size of measured degrees of freedom of test structure.
- original element matrices before updating are diagonally dominated with couplings since elements connect each other to their neighbour elements. However, the updated matrices are usually polluted due to forced manipulating the test results.
- the method may produce deficiency in connectivity of the structure as all the element matrices in the structure system are changed separately.
- possibility of loss in symmetry of the element matrices and no guarantee for the positive definiteness of the updated matrices.

4.2.2 Matrix mixing method

The matrix mixing approach was proposed by Thoren (1972) and Ross (1971), and further developed by Caesar (1987) and Link et al. (1987). The problem in assembling of stiffness and mass matrices from tested data is that measured mode shapes are usually incomplete. The

unmeasured partitions of mode shape are recovered by using analytical data to construct the full measured mode shapes.

$$\hat{\mathbf{K}}^{-1} = \sum_{i=1}^{m} \frac{\tilde{\boldsymbol{\phi}}_i \tilde{\boldsymbol{\phi}}_i^T}{\tilde{\omega}_i^2} + \sum_{i=m+1}^{n} \frac{\boldsymbol{\phi}_i \boldsymbol{\phi}_i^T}{\omega_i^2} \tag{4.1}$$

$$\hat{\mathbf{M}}^{-1} = \sum_{i=1}^{m} \tilde{\boldsymbol{\phi}}_i \tilde{\boldsymbol{\phi}}_i^T + \sum_{i=m+1}^{n} \boldsymbol{\phi}_i \boldsymbol{\phi}_i^T \tag{4.2}$$

where $\hat{\mathbf{K}}$ and $\hat{\mathbf{M}}$ are updated stiffness and mass matrices, $\tilde{\omega}_i$ and ω_i are i^{th} measured and analytical natural frequencies, $\tilde{\boldsymbol{\phi}}_i$ and $\boldsymbol{\phi}_i$ are associated measured and analytical mode shapes, m and n are number of measured and analytical mode shapes, respectively. The updated stiffness and mass matrices are generally polluted and updated model is not always physically realistic.

4.2.3 Error matrix method

Error matrix methods directly estimate the error in the stiffness and mass matrices by assuming that the error is very small. Sidhu and Ewins (1984) defined an expression for the error matrix $\Delta\mathbf{K}$ as:

$$\Delta\mathbf{K} = \tilde{\mathbf{K}} - \mathbf{K} \tag{4.3}$$

Due to the incompleteness of the measured data, Eq. (4.3) was rearranged and an expression for the error in the stiffness matrix was obtained by expanding the flexibility matrix $\tilde{\mathbf{K}}^{-1}$.

Considering the second order terms in the error matrix were negligible and rearranging produces an estimated error matrix.

$$\Delta \mathbf{K} \approx \mathbf{K}(\mathbf{K}^{-1} - \tilde{\mathbf{K}}^{-1})\mathbf{K} \tag{4.4}$$

Lieven and Ewins (1990) defined the stiffness error matrix in Eq.(4.4) by a modified version of the error matrix method via Singular Value Decomposition (SVD) method.

$$\Delta \mathbf{K} \approx (\tilde{\boldsymbol{\phi}}_i \tilde{\omega}_i^2 \tilde{\boldsymbol{\phi}}_i^T)^+ - (\boldsymbol{\phi}_i \omega_i^2 \boldsymbol{\phi}_i^T)^+ \tag{4.5}$$

where“ + ” refers to SVD. The advantage of this approach is that the structural system matrices computed by finite element analysis are not required.

4.2.4 Eigenstructure assignment method

The eigenstructure assignment method adapted from the control theory has been used to update finite element models. In this method, state feedback is used to describe the right hand side of equation of motion in terms of the displacements and velocity states. Using the state feedback, Moore (1976) formulated the sufficient conditions for simultaneous eigenvalue and eigenvector assignment.Consider mathematical equation of motion of a structural dynamic system as

$$\mathbf{M}\ddot{\mathbf{U}} + \mathbf{C}\dot{\mathbf{U}} + \mathbf{K}\mathbf{U} = \mathbf{B}\mathbf{F} \tag{4.6}$$

where the matrix $\mathbf{B}$ is the location matrix and $\mathbf{F}$ is the input or control force vector on the structure. An arbitrary output $\mathbf{Y}$ can be described by a combination of displacements and velocities as

$$\mathbf{Y} = \mathbf{D}_0\mathbf{U} + \mathbf{D}_1\dot{\mathbf{U}} \tag{4.7}$$

where $\mathbf{D}_0$ and $\mathbf{D}_1$ are the measurement matrices associated with displacement and velocity respectively. The matrices $\mathbf{B}$, $\mathbf{D}_0$, and $\mathbf{D}_1$ have to be chosen. The required input force is produced by actuators based on feedback gain matrix $\mathbf{G}$ such that the closed loop system has the desired eigenvalues and eigenvectors,

$$\mathbf{F} = \mathbf{G}\mathbf{Y} \tag{4.8}$$

The result of this procedure is that the stiffness and damping matrices are modified and the analytical mass matrix remains unchanged. The updated damping and stiffness matrices are given by

$$\hat{\mathbf{C}} = \mathbf{C} + \mathbf{B}\mathbf{G}\mathbf{D}_1 \tag{4.9}$$

$$\hat{\mathbf{K}} = \mathbf{K} + \mathbf{B}\mathbf{G}\mathbf{D}_0 \tag{4.10}$$

The perturbations on the damping and stiffness matrices are given by the matrix triple products $\mathbf{BGD}_1$ and $\mathbf{BGD}_0$. These perturbed matrices will give updated matrices which can reproduce the measured eigendata (Inman and Minas 1990, Mottershead and Friswell 1995).

4.2.5 Iterative method

Another category of finite element model updating method covers the widely used iterative updating method including sensitivity-based approaches. The iterative method update structural parameters of the finite element analytical model by an optimisation process, which requires the eigen solutions and associated sensitivity matrices of the analytical model to be calculated in each iteration (Bakira et.al 2007, Chen and Bicanic 2010). The performance of the iterative method largely depends on the selections of an objective function and constraints, structural updating parameters and optimisation techniques, requiring significant computational effort in the model updating process. The objective function can be taken as the residuals between the measured quantities and the corresponding predictions from the initial finite element model, such as difference in frequencies and mode shape measurements (Modak et al. 2002). The selection of structural parameters to be updated requires considerable physical insight into the tested structure so as to correctly characterise the physical properties at local level such as at connections of structural elements (Palmonella et al. 2005, Zapico-Valle 2012). The global optimisation technique is often employed to obtain optimum structural updating parameters in the model updating process (Bakir et al. 2008, Tu and Lu 2008). However, the sensitivity analysis and optimisation technique used in the iterative model updating methods may not perform well, in particular in the cases when the

number of the chosen structural parameters to be updated is large and the discrepancy between the initial finite element model and the actual tested structure is significant.

4.2.6 Sensitivity-based method

The sensitivity method is probably the most successful approach in finite element model updating of engineering structures. It is developed from Taylor series expansion truncated after the first order term (Mottershead et al. 2011). The error ε between the measured and analytical data can be expressed as

$$\varepsilon = \mathbf{R} - \mathbf{R}_i \tag{4.11}$$

where $\mathbf{R}$ and $\mathbf{R}_i$ are structural responses of experimental and analytical predictions respectively. This can be taken as eigenfrequencies, mode shapes or frequency response functions. The residual $\Delta\mathbf{R}$ at i^{th} iteration is defined as $\Delta\mathbf{R} = \mathbf{R} - \mathbf{R}_i$. The sensitivity matrix $\mathbf{S}$ can be calculated as follows:

$$\mathbf{S}_{ij} = \frac{\partial \mathbf{R}_i}{\partial \mathbf{P}_j} \tag{4.12}$$

where $\mathbf{P}_j$ represent structure parameter. The sensitivity matrix $\mathbf{S}$ is computed at the current value of the complete vector of parameter $\mathbf{P} = \mathbf{P}_i$ where $\mathbf{P}$ and $\mathbf{P}_i$ are the measured and analytical predicted outputs. At each iteration Eq.(4.11) is solved for residual of structural parameters $\Delta\mathbf{P}$ as

$$\Delta \mathbf{P} = \mathbf{P} - \mathbf{P}_i \tag{4.13}$$

$\Delta \mathbf{P}$ is evaluated by dynamic perturbation approach and the model is then updated to next iteration

$$\mathbf{P}_{i+1} = \mathbf{P}_i + \Delta \mathbf{P} \tag{4.14}$$

This procedure continues until consecutive estimates $\mathbf{P}_i$ and $\mathbf{P}_{i+1}$ are sufficiently converged.

4.3 Proposed model updating method

A new robust procedure offinite element model updating method (Maung et al. 2011) is presented. The proposed model updating method is extended based on nonlinear perturbation method structural dynamic (Chen 2005)by using incomplete measured vibration data and regularised algorithm. This method can directly adopt measured incomplete modal data for evaluating the chosen structural updating parameters of the initial finite element model at local level, without requiring mode shape expansion or model reduction techniques. On the basis of the dynamic perturbation method, the exact relationship between the structural parameter modifications and the incomplete measured modal data of the tested structure is generated, without requiring sensitivity analysis and the construction of an objective function. The structural parameters to be updated are properly chosen to characterise the modifications of structural parameters, i.e. differences in stiffness and mass matrices between the analytical model and tested structure. An iterative solution procedure is proposed to estimate the chosen structural updating parameters in the least squares sense, without requiring an optimisation

technique. The Tikhonov regularisation algorithm incorporating the L-curve criterion method for determining the regularisation parameter is employed to reduce the influence of modal measurements uncertainty and then to produce reliable solutions for the structural updating parameters.

4.3.1 Dynamic perturbation method with incomplete mode shapes

The characteristic equation for an undamped dynamic structural system with global stiffness matrix $\mathbf{K}$ and global mass matrix $\mathbf{M}$ of *N* degrees of freedom analytical model in Eq.(2.1) is rewritten as

$$(\mathbf{K} - \omega_i^2 \mathbf{M})\boldsymbol{\phi}_i = \mathbf{0} \tag{4.15}$$

The analytical eigenvectors are assumed to be normalised as unity withrespect to the mass of the analytical model.

In the finite element model updating, the finite element model often has uncertainty in modelling structural parameters such as the stiffness and mass of the associated tested structure due to the complexity of the actually constructed structure. The model uncertainty is mainly related to the unknown perturbations of structural parameters such as differences in stiffness $\Delta\mathbf{K}$ and mass $\Delta\mathbf{M}$ between the analytical model and the tested structure. The global stiffness matrix $\tilde{\mathbf{K}}$ and mass matrix $\tilde{\mathbf{M}}$ of the tested dynamic structure can be expressed as

$$\tilde{\mathbf{K}} = \mathbf{K} + \Delta\mathbf{K} \tag{4.16a}$$

$$\mathbf{M} = \mathbf{M} + \Delta\mathbf{M} \tag{4.16b}$$

Similarly, the characteristic equation for the actual tested structure is expressed as

$$(\tilde{\mathbf{K}} - \tilde{\omega}_i^2 \tilde{\mathbf{M}})\tilde{\boldsymbol{\phi}}_i = \mathbf{0} \tag{4.17}$$

in which $\tilde{\omega}_i$ and $\tilde{\boldsymbol{\phi}}_i$ are the i^{th}frequency and the corresponding modeshape for the tested dynamic system, respectively. From Eq.(4.16) the experimental characteristic equation in Eq.(4.17) becomes

$$[(\Delta\mathbf{K} - \tilde{\omega}_i^2 \Delta\mathbf{M}) + (\mathbf{K} - \tilde{\omega}_i^2 \mathbf{M})]\tilde{\boldsymbol{\phi}}_i = \mathbf{0} \tag{4.18}$$

Pre-multiplying Eq.(4.18) by analytical eigenvector $\boldsymbol{\phi}_k^T$

$$\boldsymbol{\phi}_k^T[(\Delta\mathbf{K} - \tilde{\omega}_i^2 \Delta\mathbf{M}) + (\mathbf{K} - \tilde{\omega}_i^2 \mathbf{M})]\tilde{\boldsymbol{\phi}}_i = \mathbf{0} \tag{4.19}$$

replacing $\mathbf{K} = \omega_k^2 \mathbf{M}$, in Eq.(4.19) becomes

$$\boldsymbol{\phi}_k^T(\Delta\mathbf{K} - \tilde{\omega}_i^2 \Delta\mathbf{M})\tilde{\boldsymbol{\phi}}_i + \boldsymbol{\phi}_k^T(\omega_k^2 \mathbf{M} - \tilde{\omega}_i^2 \mathbf{M})\tilde{\boldsymbol{\phi}}_i = \mathbf{0} \tag{4.20}$$

$$\boldsymbol{\phi}_k^T(\Delta\mathbf{K} - \tilde{\omega}_i^2\Delta\mathbf{M})\tilde{\boldsymbol{\phi}}_i + (\omega_k^2 - \tilde{\omega}_i^2)\boldsymbol{\phi}_k^T\mathbf{M}\tilde{\boldsymbol{\phi}}_i = \mathbf{0} \tag{4.21}$$

Since the analyticaleigenvectors are linearly independent due to the symmetry of the analytical stiffness and massmatrices, the mode shapes of the tested structure canbe expressed as a linear combination of the analytical eigenvectors, namely

$$\tilde{\boldsymbol{\phi}}_i = \sum_{k=1}^{N} C_{ik}\boldsymbol{\phi}_k \tag{4.22}$$

where C_{ik} are mode participation factors. Premultiplying Eq.(4.22)by $\boldsymbol{\phi}_k^T\mathbf{M}$,

$$\boldsymbol{\phi}_k^T\mathbf{M}\tilde{\boldsymbol{\phi}}_i = \sum_{k=1}^{N} C_{ik}\boldsymbol{\phi}_k^T\mathbf{M}\boldsymbol{\phi}_k \tag{4.23}$$

using themass normalisation of the analytical eigenvectors $\boldsymbol{\phi}_k^T\mathbf{M}\boldsymbol{\phi}_k = 1$, yields,

$$C_{ik} = \boldsymbol{\phi}_k^T\mathbf{M}\tilde{\boldsymbol{\phi}}_i \tag{4.24}$$

Assuming that the mode shapes of the tested structure are scaled in the following form

$$\boldsymbol{\phi}_i^T\mathbf{M}\tilde{\boldsymbol{\phi}}_i = 1 \tag{4.25}$$

The mode participation factor C_{ii} becomes $C_{ii}=1$. The mode shapes of the tested structure in Eq.(4.22) is then rewritten as

$$\tilde{\boldsymbol{\phi}}_i = \boldsymbol{\phi}_i + \sum_{k=1,k\neq i}^{N} C_{ik}\boldsymbol{\phi}_k \tag{4.26}$$

From the mode participation factor C_{ik} in Eq.(4.24), the Eq.(4.21) becomes

$$(\tilde{\omega}_i^2 - \omega_k^2)C_{ik} = \boldsymbol{\phi}_k^T(\Delta\mathbf{K} - \tilde{\omega}_i^2\Delta\mathbf{M})\tilde{\boldsymbol{\phi}}_i \tag{4.27}$$

$$C_{ik} = \frac{\boldsymbol{\phi}_k^T(\Delta\mathbf{K} - \tilde{\omega}_i^2\Delta\mathbf{M})\tilde{\boldsymbol{\phi}}_i}{\tilde{\omega}_i^2 - \omega_k^2} \tag{4.28}$$

Substituting the mode participation factors C_{ik} in Eq.(4.28) into Eq.(4.22), yields

$$\sum_{k=1}^{N} \frac{\boldsymbol{\phi}_k^T(\Delta\mathbf{K} - \tilde{\omega}_i^2\Delta\mathbf{M})\tilde{\boldsymbol{\phi}}_i}{\tilde{\omega}_i^2 - \omega_k^2}\boldsymbol{\phi}_k - \tilde{\boldsymbol{\phi}}_i = \mathbf{0} \tag{4.29}$$

In structural dynamic testing, modal data about the natural frequency $\tilde{\omega}_i$ and mode shapereadings $\tilde{\boldsymbol{\psi}}_i$ of the tested structure can be extracted from vibration measurements by modalanalysis techniques. However, in practice, the measured mode shapes are usually incomplete since the numbers of measured degrees of freedom are less than the numbers of degrees of freedom of analytical model due to limited number of sensorsavailable for vibration measurements. The measured modes arepaired to the analytical eigenvectors $\boldsymbol{\phi}_k^a$

(restricted to the same dimensions as $\tilde{\boldsymbol{\psi}}_i$), by usingMAC factors defined in Eq. (2.1).In the application of governing equation Eq. (4.29), the measured incomplete mode shapes of the actual tested structure need to be close to the corresponding part of the original eigenvectors $\boldsymbol{\phi}_k^a$. The measured degrees of freedom readings $\tilde{\boldsymbol{\psi}}_i$ are then scaled by a mode scale factor υ_i

$$\tilde{\boldsymbol{\phi}}_i^a = \upsilon_i \tilde{\boldsymbol{\psi}}_i \quad , \quad \text{where} \quad \upsilon_i = \frac{\left|\boldsymbol{\phi}_i^{a^T} \tilde{\boldsymbol{\psi}}_i\right|}{\left|\tilde{\boldsymbol{\psi}}_i^T \tilde{\boldsymbol{\psi}}_i\right|} \tag{4.30}$$

The remaining unmeasured components $\tilde{\boldsymbol{\phi}}_i^u$ are covered with corresponding parts of analytical model by using Eq.(4.26)

$$\tilde{\boldsymbol{\phi}}_i^u = \boldsymbol{\phi}_i^u + \sum_{k=1,k\neq i}^{N} C_{ik} \boldsymbol{\phi}_k^u \tag{4.31}$$

where $\boldsymbol{\phi}_k^u$ is original eigenvector corresponding to the entries of the unmeasured components. In the calculation of C_{ik} , complete mode shapes of all degrees of freedom are constructed by using measured components of measured mode shapes and unmeasured components from analytical mode shapes. For simplicity and convenience in matrix operations, both the measured components $\tilde{\boldsymbol{\phi}}_i^a$ andthe remaining calculated components $\tilde{\boldsymbol{\phi}}_i^u$ of the i^{th} mode shapes of tested structure areexpanded to full dimension with zeroes at their unknown entries. The i^{th} completeeigenvector of the tested structure, consisting of the measured components and the remainingcalculated components, is then given by

$$\tilde{\boldsymbol{\phi}}_i = \boldsymbol{\varphi}_i^a + \sum_{k=1,k\neq i}^{N} C_{ik}\boldsymbol{\phi}_k^u \tag{4.32}$$

where $\boldsymbol{\varphi}_i^a$ is a known vector of dimension N, defined as

$$\boldsymbol{\varphi}_i^a = \upsilon_i \tilde{\boldsymbol{\psi}}_i + \boldsymbol{\phi}_i^u \tag{4.33}$$

From Eq. (4.32), the mode participation factors C_{ik} in Eq.(4.28) are rewritten as

$$C_{ik} = \frac{\boldsymbol{\phi}_k^T \Delta\mathbf{K}(\boldsymbol{\varphi}_i^a + \sum_{l=1,l\neq i}^{N} C_{il}\boldsymbol{\phi}_l^u) - \tilde{\omega}_i^2 \boldsymbol{\phi}_k^T \Delta\mathbf{M}(\boldsymbol{\varphi}_i^a + \sum_{l=1,l\neq i}^{N} C_{il}\boldsymbol{\phi}_l^u)}{\tilde{\omega}_i^2 - \omega_k^2} \tag{4.34}$$

By using the scaled measured degrees of freedom readings in Eq.(4.30) and the constructed eigenvector in Eq.(4.32), Eq.(4.29) is now restricted to the dimension for the measured components and becomes

$$\sum_{k=1}^{N} \frac{\boldsymbol{\phi}_k^T \Delta\mathbf{K}(\boldsymbol{\varphi}_i^a + \sum_{l=1,l\neq i}^{N} C_{il}\boldsymbol{\phi}_l^u)}{\tilde{\omega}_i^2 - \omega_k^2}\boldsymbol{\phi}_k^a - \tilde{\omega}_i^2 \sum_{k=1}^{N} \frac{\boldsymbol{\phi}_k^T \Delta\mathbf{M}(\boldsymbol{\varphi}_i^a + \sum_{l=1,l\neq i}^{N} C_{il}\boldsymbol{\phi}_l^u)}{\tilde{\omega}_i^2 - \omega_k^2}\boldsymbol{\phi}_k^a - \tilde{\boldsymbol{\phi}}_i^a = \mathbf{0} \tag{4.35}$$

The governing equation in Eq.(4.35) represents the exact relationship between the change in structural parameters and the measured modal properties of the tested structure such as mode shape readings. The governing equation avoids the approximations and complexity in most

existing eigensesitivity-based analysis methods for model updating, without requiring eigensolution derivatives.

4.3.2 Governing equations for model updating

In the proposed model updating method, structural system parameters to be updated, such as parameters for material and geometric properties, are employed to reflect the updating of structural parameters, e.g. stiffness matrix and/or mass matrix. The structural system updating parameters can characterise the structural parameters at element level or at integration point level. In the case where structural updating parameters are chosen at element level, the change in element stiffness matrix $\Delta\mathbf{K}_e$ can be expressed by

$$\Delta\mathbf{K}_e = \tilde{\mathbf{K}}_e - \mathbf{K}_e = \theta_e \mathbf{K}_e \tag{4.36}$$

where θ_e is a stiffness updating parameter characterised at element level to be determined from model updating; $\mathbf{K}_e$ and $\tilde{\mathbf{K}}_e$ are the e^{th} element stiffness matrices for the analytical model and the tested structure, respectively.

For the frame structures, it is difficult to accurately model beam-column joints in the analytical model and the bending stiffness at the joints is often estimated with uncertainty. In order to effectively update the bending stiffness at the ends of beam and column elements, the element stiffness matrix is now calculated from an integral form (Hinton and Owen 1985).

The element stiffness matrix excluding axial stiffness for a conventional beam with bending stiffness *EI* and element length *l* is given by

$$\mathbf{K}_e^b = \int_{-1}^{1} EI\mathbf{b}^T(\xi)\mathbf{b}(\xi)\frac{l}{2}d\xi \tag{4.37}$$

where the dimensionless natural coordinate ξ associated with the longitudinal beam axis *x*is defined as $\xi = \frac{2\bar{x}}{l} - 1$; $\mathbf{b}(\xi)$ is a row vector representing the relationship between thecurvature of the structural element and the nodal displacements, expressed as

$$\mathbf{b}(\xi) = \frac{1}{l^2}[6\xi, (3\xi - 1)l, -6\xi, (3\xi + 1)l] \tag{4.38}$$

By adopting the three-point Newton-Cotes integration rule (Stoer and Bulirsch 1980), the element stiffness matrix in Eq.(4.37) is calculated from the sum of the contributions of integration points at the middle and both ends of the element

$$\mathbf{K}_e^b = \sum_r \mathbf{K}_r^b, \qquad \text{where} \quad \mathbf{K}_r^b = \frac{l}{2} w_r (EI)_r \mathbf{b}^T(\xi_r)\mathbf{b}(\xi_r) \tag{4.39}$$

in which index *r* denotes the integration points at the middle and both ends of the element where $\xi_r = 0$ and $\xi_r = \pm 1$, respectively; Weight coefficients w_r for the three-point Newton-Cotes integration rule at the middle and both ends are w_r = 4/3 and w_r = 1/3, respectively; $(EI)_r$ represents bending stiffness at integration points, i.e. in the middle and at both beam-

column joints of the structural element. The change in element stiffness matrix $\Delta\mathbf{K}_e^b$ between the element stiffness of tested structure $\tilde{\mathbf{K}}_e^b$ and the element stiffness of analytical model $\mathbf{K}_e^b$ for the beam element is given by

$$\Delta\mathbf{K}_e^b = \tilde{\mathbf{K}}_e^b - \mathbf{K}_e^b = \sum_r \theta_r \mathbf{K}_r^b \tag{4.40}$$

where θ_r is stiffness updating parameter characterised at critical point level to be determined from model updating. Consequently, the change of global stiffness matrix between the tested structure and analytical model is written as (Chen and Bicanic 2006, Maung et al. 2011)

$$\Delta\mathbf{K} = \sum_{j=1}^{N\theta} \theta_j \mathbf{K}_j \tag{4.41}$$

where $N\theta$ represents the total number of stiffness updating parameters adopted in calculations; θ_j is stiffness updating parameter characterised at element level or integration point level; $\mathbf{K}_j$ is the contribution of the j^{th} element or integration point to the global stiffness matrix. Similarly, the change of global mass matrix between the tested structure and the analytical model is expressed as

$$\Delta\mathbf{M} = \sum_{j=1}^{N\beta} \beta_j \mathbf{M}_j \tag{4.42}$$

where $N\beta$ represents the total number of mass updating parameters β_j adopted for model updating; $\mathbf{M}_j$ is the j^{th} contribution to the global mass matrix. In order to minimise the computational effort, the sensitivity coefficients associated with the known eigenmodes and structural parameters in the governing equation Eq.(4.35) are defined in a general form as

$$\mathbf{p}^a_{jii} = \sum_{k=1}^{N} \frac{\boldsymbol{\phi}_k^T \mathbf{K}_j \boldsymbol{\varphi}_i^a}{\tilde{\omega}_i^2 - \omega_k^2} \boldsymbol{\phi}_k^a \quad , \quad \mathbf{p}^u_{jil} = \sum_{k=1}^{N} \frac{\boldsymbol{\phi}_k^T \mathbf{K}_j \boldsymbol{\phi}_l^u}{\tilde{\omega}_i^2 - \omega_k^2} \boldsymbol{\phi}_k^a \tag{4.43a}$$

$$\mathbf{q}^a_{jii} = \sum_{k=1}^{N} \frac{\boldsymbol{\phi}_k^T \mathbf{M}_j \boldsymbol{\varphi}_i^a}{\tilde{\omega}_i^2 - \omega_k^2} \boldsymbol{\phi}_k^a \quad , \quad \mathbf{q}^u_{jil} = \sum_{k=1}^{N} \frac{\boldsymbol{\phi}_k^T \mathbf{M}_j \boldsymbol{\phi}_l^u}{\tilde{\omega}_i^2 - \omega_k^2} \boldsymbol{\phi}_k^a \tag{4.43b}$$

from Eq.(4.41) andEq.(4.42) the governing equation Eq.(4.35) is rewritten as

$$\begin{aligned} &\sum_{j=1}^{N\theta} \left[\sum_{k=1}^{N} \frac{\boldsymbol{\phi}_k^T \mathbf{K}_j \boldsymbol{\varphi}_i^a}{\tilde{\omega}_i^2 - \omega_k^2} \boldsymbol{\phi}_k^a + \sum_{l=1, l\neq i}^{N} \sum_{k=1}^{N} \frac{\boldsymbol{\phi}_k^T \mathbf{K}_j \boldsymbol{\phi}_l^u}{\tilde{\omega}_i^2 - \omega_k^2} \boldsymbol{\phi}_k^a C_{il} \right] \theta_j \\ &- \tilde{\omega}_i^2 \sum_{j=1}^{N\beta} \left[\sum_{k=1}^{N} \frac{\boldsymbol{\phi}_k^T \mathbf{M}_j \boldsymbol{\varphi}_i^a}{\tilde{\omega}_i^2 - \omega_k^2} \boldsymbol{\phi}_k^a + \sum_{l=1, l\neq i}^{N} \sum_{k=1}^{N} \frac{\boldsymbol{\phi}_k^T \mathbf{M}_j \boldsymbol{\phi}_l^u}{\tilde{\omega}_i^2 - \omega_k^2} \boldsymbol{\phi}_k^a C_{il} \right] \beta_j - \tilde{\boldsymbol{\phi}}_i^a = \mathbf{0} \end{aligned} \tag{4.44}$$

substituting Eq.(4.43a) and Eq.(4.43b) gives

$$\sum_{j=1}^{N\theta} [\mathbf{p}^a_{jii} + \sum_{k=1, k\neq i}^{N} \mathbf{p}^u_{jik} C_{ik}] \theta_j - \tilde{\omega}_i^2 \sum_{j=1}^{N\beta} [\mathbf{q}^a_{jii} + \sum_{k=1, k\neq i}^{N} \mathbf{q}^u_{jik} C_{ik}] \beta_j - \tilde{\boldsymbol{\phi}}_i^a = \mathbf{0} \tag{4.45}$$

Similarly, define the sensitivity coefficients associated with the known eigenmodes and structural parameters in Eq. (4.34) as

$$g_{kji}^{a} = \boldsymbol{\phi}_k^T \mathbf{K}_j \boldsymbol{\varphi}_i^a \quad , \quad g_{kjl}^{u} = \boldsymbol{\phi}_k^T \mathbf{K}_j \boldsymbol{\phi}_l^u \tag{4.46a}$$

$$h_{kji}^{a} = \boldsymbol{\phi}_k^T \mathbf{M}_j \boldsymbol{\varphi}_i^a \quad , \quad h_{kjl}^{u} = \boldsymbol{\phi}_k^T \mathbf{M}_j \boldsymbol{\phi}_l^u \tag{4.46b}$$

from Eqs.(4.41) and (4.42), the mode participation factors C_{ik} in Eq.(4.34) are thus expressed as

$$C_{ik} = \frac{\sum_{j=1}^{N\theta}\left[\boldsymbol{\phi}_k^T \mathbf{K}_j \boldsymbol{\varphi}_i^a + \sum_{l=1,l\neq i}^{N} \boldsymbol{\phi}_k^T \mathbf{K}_j \boldsymbol{\phi}_l^u C_{il}\right]\theta_j - \tilde{\omega}_i^2 \sum_{j=1}^{N\beta}\left[\boldsymbol{\phi}_k^T \mathbf{M}_j \boldsymbol{\varphi}_i^a + \sum_{l=1,l\neq i}^{N} \boldsymbol{\phi}_k^T \mathbf{M}_j \boldsymbol{\phi}_l^u C_{il}\right]\beta_j}{\tilde{\omega}_i^2 - \omega_k^2} \tag{4.47}$$

and by using Eq. (4.46), rewriting as

$$C_{ik} = \frac{\sum_{j=1}^{N\theta}\left[g_{kji}^{a} + \sum_{l=1,l\neq i}^{N} g_{kjl}^{u} C_{il}\right]\theta_j - \tilde{\omega}_i^2 \sum_{j=1}^{N\beta}\left[h_{kji}^{a} + \sum_{l=1,l\neq i}^{N} h_{kjl}^{u} C_{il}\right]\beta_j}{\tilde{\omega}_i^2 - \omega_k^2} \tag{4.48}$$

On the basis of the governing equations Eq.(4.45) and Eq.(4.48) developed above, an iterative solution procedure is required to solve for the structural updating parameters. In order to accelerate the convergence process, the n^{th} approximations for the structural updating

parameters $\theta_j^{(n)}$ and $\beta_j^{(n)}$ and the mode participation factors $C_{ik}^{(n)}$ are calculated, respectively, from

$$\sum_{j=1}^{N\theta}\left[\mathbf{p}_{jii}^{a}+\sum_{k=1,k\neq i}^{N}\mathbf{p}_{jik}^{u}C_{ik}^{(n-1)}\right]\theta_j^{(n)}-\tilde{\omega}_i^2\sum_{j=1}^{N\beta}\left[\mathbf{q}_{jii}^{a}+\sum_{k=1,k\neq i}^{N}\mathbf{q}_{jik}^{u}C_{ik}^{(n-1)}\right]\beta_j^{(n)}-\tilde{\boldsymbol{\phi}}_i^{a}=0 \tag{4.49}$$

$$\begin{aligned}C_{ik}^{(n)}=&\frac{\sum_{j=1}^{N\theta}g_{kji}^{a}\theta_j^{(n)}+\sum_{l=1,l\neq i}^{k-1}\sum_{j=1}^{N\theta}g_{kjl}^{u}\theta_j^{(n)}C_{il}^{(n)}+\sum_{l=k+1,l\neq i}^{N}\sum_{j=1}^{N\theta}g_{kjl}^{u}\theta_j^{(n)}C_{il}^{(n-1)}}{\tilde{\omega}_i^2-\omega_k^2-\sum_{j=1}^{N\theta}g_{kjk}^{u}\theta_j^{(n)}+\tilde{\omega}_i^2\sum_{j=1}^{N\beta}h_{kjk}^{u}\beta_j^{(n)}}\\&-\tilde{\omega}_i^2\frac{\sum_{j=1}^{N\beta}h_{kji}^{a}\beta_j^{(n)}+\sum_{l=1,l\neq i}^{k-1}\sum_{j=1}^{N\beta}h_{kjl}^{u}\beta_j^{(n)}C_{il}^{(n)}+\sum_{l=k+1,l\neq i}^{N}\sum_{j=1}^{N\beta}h_{kjl}^{u}\beta_j^{(n)}C_{il}^{(n-1)}}{\tilde{\omega}_i^2-\omega_k^2-\sum_{j=1}^{N\theta}g_{kjk}^{u}\theta_j^{(n)}+\tilde{\omega}_i^2\sum_{j=1}^{N\beta}h_{kjk}^{u}\beta_j^{(n)}}\end{aligned} \tag{4.50}$$

where*n* indicates the n^{th} iteration and (*n*-1) indicates the $(n\text{-}1)^{\text{th}}$ iteration. When the $C_{ik}^{(n)}$ are being calculated, the $C_{il}^{(n)}$ where $l<k$ are known, while $C_{il}^{(n)}$ where $l>k$ are not available, but $C_{il}^{(n-1)}$ are known. Therefore the $C_{il}^{(n)}$ where $l<k$ are used for calculating n^{th} iteration $C_{ik}^{(n)}$ to accelerate the iterative procedure. The governing equation Eq.(4.49) is used for evaluating the structural updating parameters, where a regularisation algorithm is often required to obtain stable solutions due to the ill-posed problem (Titurus and Friswell 2008).

4.3.3 Regularised solution to updating parameters

A regularization algorithm is often required to obtain stable solutions for the ill-posed problem defined in the governing equation Eq.(4.49).For the i^{th} measured mode with a total of Ns mode shape readings, that governing equation are rewritten here as

$$\mathbf{A}^{(i)}\mathbf{x}=\mathbf{b}^{(i)} \quad , \quad \mathbf{A}^{(i)} \in R^{Ns x Nx} \quad , \quad \mathbf{x} \in R^{Nx} \quad , \quad \mathbf{b}^{(i)} \in R^{Ns} \tag{4.51}$$

where $\mathbf{A}^{(i)}$ is sensitivity matrix with dimensions of Ns x Nx associated with sensitivity coefficients and the obtained mode participation factor defined in the governing equation Eq.(4.50) for the i^{th} measured mode; $\mathbf{x}$ is unknown vector of dimension Nx containing structural updating parameters θ_j and β_j; $\mathbf{b}^{(i)}$ is known vector of dimension Ns containing degrees of freedom's readings for the i^{th} measured mode. In order to reduce the influence of measurement uncertainty on finite element model updating, the Tikhonov regularisation, one of the most popular regularisation methods (Tikhonov and Arsenin 1993), is adopted, in which the linear equations Eq.(4.51)is replaced by a minimisation problem

$$\min_{\mathbf{x} \in R^{Nx}} \{ \|\mathbf{A}\mathbf{x}-\mathbf{b}\|_2^2 + \lambda^2 \|\mathbf{x}\|_2^2 \} \tag{4.52}$$

where $\lambda \geq 0$ is the regularisation parameter and $\|\bullet\|$ denotes the Euclidean norm. An explicit regularised solution $\mathbf{x}_\lambda$ to the minimisation problem is given by

$$\mathbf{x}_\lambda = \left(\mathbf{A}^T\mathbf{A} + \lambda^2\mathbf{I}\right)^{-1}\mathbf{A}^T\mathbf{b} \tag{4.53}$$

where**I** is the identity matrix. Let Singular Value Decomposition (SVD) of the sensitivity matrix **A** be

$$\mathbf{A} = \mathbf{U}\,\mathbf{\Sigma}\,\mathbf{V}^T = \sum_{j=1}^{Nx} \sigma_j \mathbf{u}_j \mathbf{v}_j^T \tag{4.54}$$

where $\mathbf{\Sigma}$ is a diagonal matrix $\mathbf{\Sigma} = diag\,[\sigma_1, \sigma_2, ..., \sigma_{Nx}]$ in which $\sigma_1 \geq \sigma_2 \geq ... \geq \sigma_{Nx}$; **U**and**V** are orthogonal matrices with $\mathbf{U}\mathbf{U}^T = \mathbf{U}^T\mathbf{U} = \mathbf{I}$ and $\mathbf{V}\mathbf{V}^T = \mathbf{V}^T\mathbf{V} = \mathbf{I}$. By using the SVD of **A**in Eq.(4.54), the regularised solution $\mathbf{x}_\lambda$ is thus given by

$$\mathbf{x}_\lambda = \sum_{j=1}^{Nx} f_j(\lambda) \frac{\mathbf{u}_j^T \mathbf{b}}{\sigma_j} \mathbf{v}_j \tag{4.55}$$

where $f_j(\lambda)$ is the Tikhonov filter, defined as

$$f_j(\lambda) = \frac{\sigma_j^2}{\sigma_j^2 + \lambda^2}\ , \qquad \begin{cases} f_j(\lambda) \approx 1 & \text{if} \quad \sigma_j >> \lambda \\ f_j(\lambda) \approx \dfrac{\sigma_j^2}{\lambda^2} & \text{if} \quad \sigma_j << \lambda \end{cases} \tag{4.56}$$

The regularisation parameter λ in Eq.(4.55)needs to be properly selected in order to filter out enough noise without losing too much information in the regularised solution. Computational experience shows the L-curve criterion can provide suitable values of regularisation parameters in many problems (Hansen and O'Leary 1993), without requiring the priorknowledge of noise in the measured data. The L-curve is a plot in log-log scale of the

corresponding values of the residual norm $\rho(\lambda)$ and solution norm $\eta(\lambda)$ as a function of the regularisation parameter λ , defined in terms of the SVD as

$$\rho(\lambda) = \left\|\mathbf{A}\mathbf{x}_\lambda - \mathbf{b}\right\|_2^2 = \sum_{j=1}^{Nx}[(1-f_j(\lambda))\mathbf{u}_j^T\mathbf{b}]^2 \tag{4.57a}$$

$$\eta(\lambda) = \left\|\mathbf{x}_\lambda\right\|_2^2 = \sum_{j=1}^{Nx}[\, f_j(\lambda)\frac{\mathbf{u}_j^T\mathbf{b}}{\sigma_j}]^2 \tag{4.57b}$$

It can be shown that the L-curve's corner, where the curvature of the L-curve approximately has a maximum value, indicates an optimal regularisation parameter to balance the residual norm error and the solution norm error (Hansen and O'Leary 1993). From Eq.(4.57), the curvature of the L-curve $\kappa(\lambda)$ is given by

$$\kappa(\lambda) = \frac{2\eta\rho}{\eta'}\frac{(\lambda^2\eta'\rho + 2\lambda\eta\rho + \lambda^4\eta\eta')}{(\lambda^4\eta^2 + \rho^2)^{3/2}} \tag{4.58}$$

where η' denotes the first derivative of η with respect to λ and is expressed as

$$\eta' = -4\lambda\sum_{j=1}^{Nx}\frac{\sigma_j^4}{(\sigma_j^2 + \lambda^2)^3}\left(\frac{\mathbf{u}_j^T\mathbf{b}}{\sigma_j}\right)^2 \tag{4.59}$$

A one-dimensional optimisation procedure is adopted to determine the optimal regularisation parameter λ corresponding to the maximum curvature.The iterative solution algorithm and

flowchart for solving for structural updating parameters θ_j and β_j is now summarised as follows.

Algorithm start

1. Calculate and store sensitivity coefficients in Eq.(4.43).

2. Calculate and store sensitivity coefficients in Eq.(4.46).

3. Give initial values $C_{ik}^{(0)} = 0, \quad (k \neq i)$.

4. For n = 1, 2, 3, …

- $\theta_j^{(n)}$ and $\beta_j^{(n)}$ are evaluated from Eq.(4.49), where regularised solutions are obtained from Eq.(4.55) in which λ is determined by maximising Eq.(4.58).
- $C_{ik}^{(n)}$ are calculated from Eq.(4.50)
- Return if solution has not converged.

Algorithm end.

4.3.4 Flowchart for proposed model updating procedure

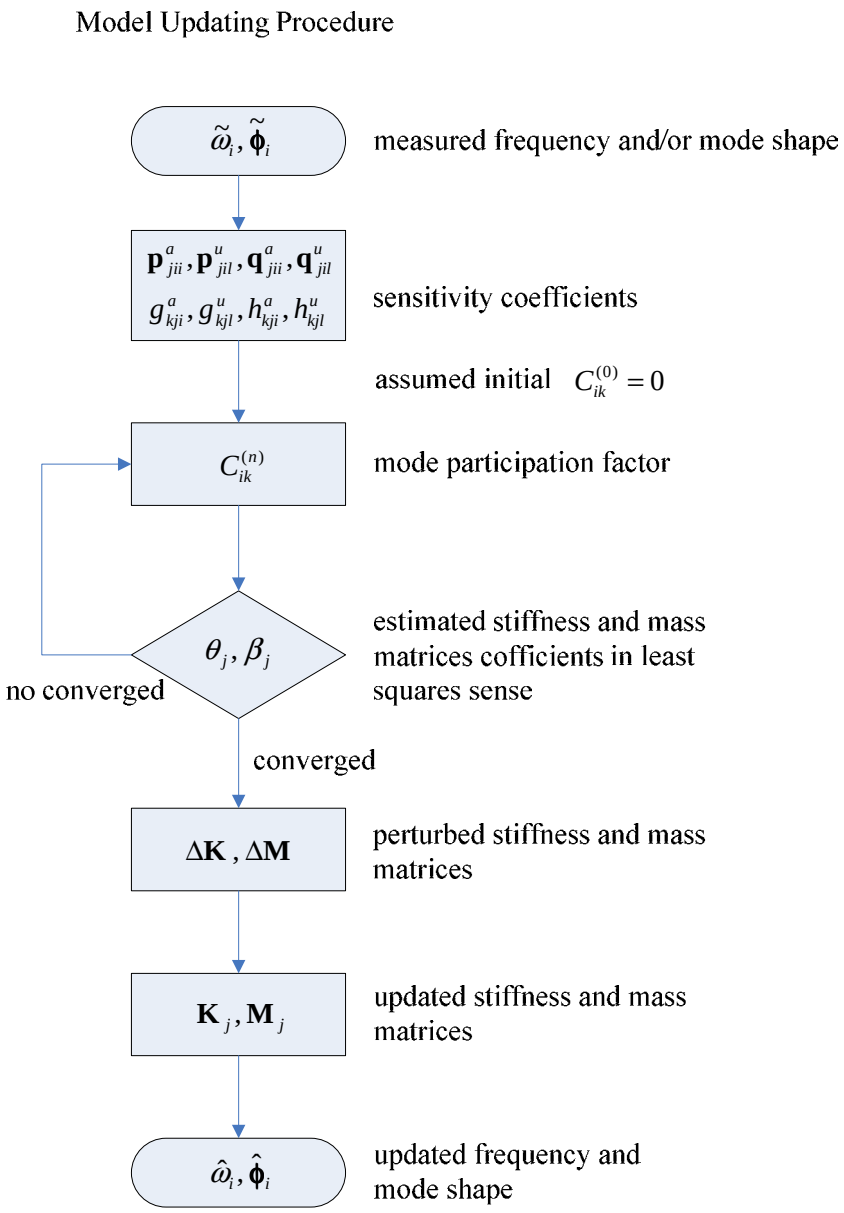

Figure 4.1 Flowchart for modal updating scenario

The above iterative solution algorithm is performed until the convergence for structural updating parameters is achieved, often after only a few iterations. In order to assess the performance of the proposed model updating method, evaluation criteria are introduced to compare the updated modal properties with the measured modal data. The relative error for

the i^{th} updated frequency E_{ω}^{i} and the average absolute error for all updated frequencies E_{ω} are defined, respectively, as

$$E_{\omega}^{i} = \frac{\hat{\omega}_i - \tilde{\omega}_i}{\tilde{\omega}_i} \tag{4.60a}$$

$$E_{\omega} = \frac{1}{N_m} \sum_{i=1}^{Nm} \left| E_{\omega}^{i} \right| \tag{4.60b}$$

where*Nm* is the total number of measured modes and $\hat{\omega}_i$ is the i^{th} updated natural frequency.The relative error for the i^{th} updated incomplete mode shape E_{ϕ}^{i} and the average error forall updated incomplete mode shapes E_{ϕ} are defined, respectively, as

$$E_{\phi}^{i} = \frac{\left| (\hat{\upsilon}_i \hat{\boldsymbol{\phi}}_i^{a} - \tilde{\boldsymbol{\phi}}_i^{a})^{T} (\hat{\upsilon}_i \hat{\boldsymbol{\phi}}_i^{a} - \tilde{\boldsymbol{\phi}}_i^{a}) \right|}{\left| \tilde{\boldsymbol{\phi}}_i^{aT} \tilde{\boldsymbol{\phi}}_i^{a} \right|}, \qquad \text{where } \hat{\upsilon}_i = \frac{\left| \tilde{\boldsymbol{\phi}}_i^{aT} \hat{\boldsymbol{\phi}}_i^{a} \right|}{\left| \hat{\boldsymbol{\phi}}_i^{aT} \hat{\boldsymbol{\phi}}_i^{a} \right|} \tag{4.61a}$$

$$E_{\phi} = \frac{1}{N_m} \sum_{i=1}^{Nm} E_{\phi}^{i} \tag{4.61b}$$

where $\hat{\boldsymbol{\phi}}_i^{a}$ is the i^{th} incomplete mode shape of the updated analytical model.

Chapter 5 Verifications of Proposed Model Updating Method

5.1 Introduction

The effectiveness and applicability of the proposed finite element model updating method presented in Chapter 4 are demonstrated by the numerical simulation investigations and experimental studies of the steel frame model structure for adjusting the stiffness at the joints of structural members. Additionally, the benchmark problem of Canton Tower located in Guangzhou, China (Chen et al. 2011, Ni et al. 2009) established by the Hong Kong Polytechnic University is employed for practical application. Incomplete modal data identified from the recorded ambient vibration measurements are utilized to updated the given finite element model of the Canton Tower.

5.2 Numerical study of steel frame model structure

A small scale spacesteel frame model structure was constructed for numerical simulation investigation and experimental studies to demonstrate the accuracy and effectiveness of the proposed finite element model updating method, as shown in Figure 5.1. Analytical model of the tested structure to be updated has been presented in section 3.2. In the tested structure, accelerometers are placed at beam-column joints to measure only translational displacement readings in horizontal directions. The modal data such as frequencies and mode shape readings at measured degrees of freedom are extracted from the acceleration measurements by using modal analysis technique (Reynolds et al. 2002, Pavic and Reynolds2007).

In order to update the physical properties at specific locations in individual structural components, structural updating parameters are chosen to characterise the physical properties at critical point level for beams and columns, i.e. at both ends and in the middle, and at element level for braces. A total number of 104 stiffness updating parameters are introduced for updating the initial finite element model, i.e. 48 for columns, 48 for beams and 8 for braces, while the updating of mass is not considered due to its relatively higher accuracy.

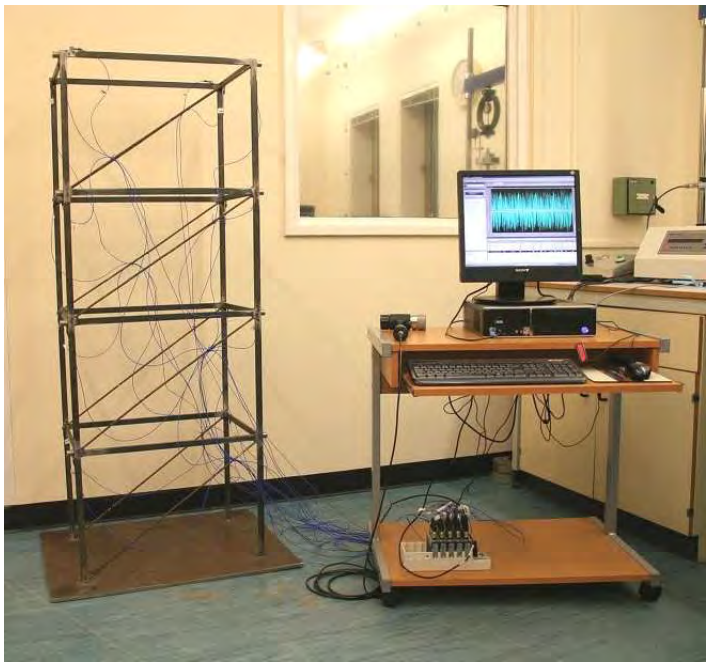

Figure 5.1 Steel frame model structure used for laboratory testing with installed sensors.

In the numerical simulation investigations, three simulation cases with different number of measurement sensors are considered,as shown in Table 5.1, to verify the accuracy of the proposed finite element model updating method.

Table 5.1 Simulations of sensor measurements for the space steel frame model structure

Simulation	Description
1	Simulated sensor measurements at four nodes
2	Simulated sensor measurements at six nodes
3	Simulated sensor measurements at sixteen nodes

5.2.1 Simulation 1: Simulated sensor measurements at four nodes

In this Simulation 1, the stiffness difference to be updated are simulated at different structural elements with various updating levels, i.e. -40% change at both ends of column elements 2, 3, 26 and 27, -10% change at both ends of beam elements 6 and 30, and -20% change in brace elements 33 and 40. Here, the "measured" exact modal data, i.e. frequencies and the corresponding incomplete mode shapes, are obtained from finite element dynamic analysis for the simulated "tested" structure, namely by solving the characteristic equations for the "tested" structure with assumed stiffness changes. The first 10 natural frequencies for the initial finite element model and the simulated "tested" structure are summarized in Table 5.2with an average frequency absolute error of 4.25%. The "measured" incomplete mode shapes are constructed by the degrees of freedom translational displacement readings in only X and Y directions at four nodes, as shown in Figure 5.2.

In structural dynamic testing, frequencies can be measured more accurately than mode shapes. Thus, ability of 6-10 modes is assumed to be used in the numerical simulation. The initial finite elementmodel is adjusted through the proposed model updating method by using the simulated "measured" incomplete modal data. Information about different number of

noise-free incomplete modes, i.e. 6 modes, 8 modes and 10 modes, is utilised for evaluating the chosen stiffness updating parameters. The results show that the updated frequencies are in excellent agreement with the simulated exact values, with average absolute errors of only 0.0013%, 0.0003% and 0.0008% for cases with 6, 8 and 10 modes used, respectively. The errors between measured and updated frequencies are very little due to using simulated analytical modal data. The accuracy of the updated mode shapes is assessed by the results given in Table 5.3where MAC diagonal values and relative and average mode errors are used as the performance indicators compared with simulated exact mode shapes.The correlation between the updated modes and the simulated exact modes is obviously improved for each mode after model updating with maximum possible MAC values of unity. The average mode error of 16.78% between the initial finite element model and the simulated "tested" structure is significantly reduced after model updating to values of 0.0244%, 0.0175%, and 0.0907% for cases with 6, 8, and 10 incomplete modes used, respectively.

In order to investigate the influence of modal measurement uncertainty on the performance of the proposed model updating method, errors in the "measured" modal data are simulated by corrupting the exact analytical modal data with certain standard normally distributed noise levels (i.e. standard deviations). Here, information on a total number of eight corrupted incomplete modes with various noise levels, i.e. 5%, 10% and 15%, are then employed for updating the initial analytical model. The Tikhonov regularisation incorporating the L-curve criterion is adopted in the proposed solution algorithm to obtain robust solutions for the chosen structural updating parameters. The best results data set is selected among the other simulated data sets. The stiffness at some beam members ends need to be adjusted with relatively small absolute values of typically less than 10% , and the stiffness of columns ends however requires relatively large modifications in some members with adjusted stiffness

factor value of up to approximately -45%. The stiffness of brace elements need modifications up to approximately -20% in some members, and other elements only require little modifications. Table 5.4gives results for updated natural frequencies from eight corrupted incomplete modes with various simulated noise levels. The results indicate that the frequencies of the updated finite element model are in good agreement with the simulated noise-free exact values, with a small average frequency absolute error for each simulated noise case. The mode shapes for the updated analytical model also match the simulated exact values, with MAC diagonal values of close to unity and significantly reduced average mode errors after updating, as shown in Table 5.5.

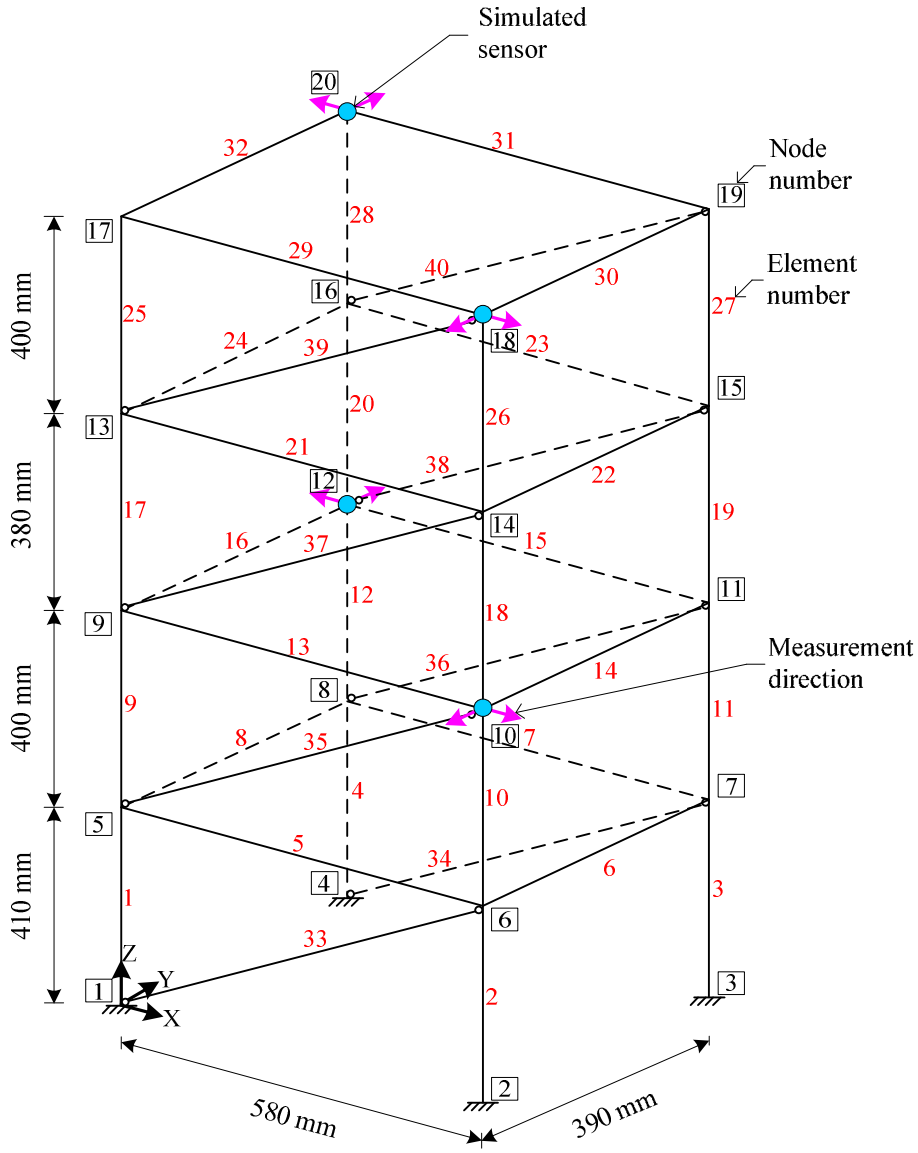

Figure 5.2 The finite element model of the laboratory tested space steel frame model structure with simulated sensors at four nodes adopted for model updating

Table 5.2 Updated natural frequencies of the finite element model of the experimental structure using different number of noise-free incomplete modes extracted from simulated sensor measurements at four nodes

				6 modes used		8 modes used		10 modes used	
Mode	FE (Hz)	Exact (Hz)	Error (%)	Updated (Hz)	Error (%)	Updated (Hz)	Error (%)	Updated (Hz)	Error (%)
1	10.3552	9.7865	5.8111	9.7867	0.0020	9.7866	0.0004	9.7866	0.0002
2	25.9380	25.3668	2.2517	25.3669	0.0005	25.3668	-0.0001	25.3667	-0.0004
3	31.7608	29.3901	8.0662	29.3904	0.0009	29.3902	0.0002	29.3903	0.0005
4	45.2475	43.6114	3.7515	43.6115	0.0002	43.6113	-0.0002	43.6110	-0.0008
5	51.8179	47.6142	8.8287	47.6128	-0.0028	47.6139	-0.0005	47.6155	0.0029
6	65.5716	62.9209	4.2126	62.9200	-0.0015	62.9208	-0.0003	62.9204	-0.0009
7	70.6418	68.6193	2.9474	/	/	68.6194	0.0000	68.6191	-0.0003
8	72.1780	70.4225	2.4929	/	/	70.4219	-0.0008	70.4209	-0.0022
9	85.2298	83.3627	2.2398	/	/	/	/	83.3626	-0.0001
10	86.5838	84.9609	1.9102	/	/	/	/	84.9607	-0.0002
Average error E_{ω} (%)			4.2512		0.0013		0.0003		0.0008

The adjusted stiffness parameters of the critical points and elements are then compared with the assume values, as shown in Figure 5.3, where information on eight simulated noise-free incomplete modes is adopted for model updating. The results indicate that the updated stiffness parameters match well the assumed exact values for stiffness changes at different levels and at various specific locations, such as beam-column joints. However, ill condition problem significantly affects the accuracy of structural updating parameters and leads to

produce more errors than simulated results. The results for adjusted stiffness parameters of the all updating points and elements are also plotted in Figure 5.4. The results give consistent indications that the updated stiffness parameters agree well with the simulated exact value for stiffness changes at different levels in various specific locations.

Table 5.3 Updated mode shape properties of the finite element model of the experimental structure using different number of noise-free incomplete modes extracted from simulated sensor measurements at four nodes

			6 modes used		8 modes used		10 modes used	
Mode	MAC initial, exact	Error E_{ϕ}^{i} (%)	MAC updated, exact	Error E_{ϕ}^{i} (%)	MAC updated, exact	Error E_{ϕ}^{i} (%)	MAC updated, exact	Error E_{ϕ}^{i} (%)
1	0.9992	2.8867	1.0000	0.0207	1.0000	0.0173	1.0000	0.0494
2	0.9823	13.2940	1.0000	0.0165	1.0000	0.0157	1.0000	0.0446
3	0.9273	26.9679	1.0000	0.0282	1.0000	0.0249	1.0000	0.0447
4	0.9838	12.7441	1.0000	0.0280	1.0000	0.0240	1.0000	0.0731
5	0.9587	20.3162	1.0000	0.0361	1.0000	0.0232	1.0000	0.0655
6	0.9262	27.1664	1.0000	0.0167	1.0000	0.0086	1.0000	0.0736
7	0.8994	31.7249	/	/	1.0000	0.0124	1.0000	0.0755
8	0.9915	9.1992	/	/	1.0000	0.0142	1.0000	0.0828
9	0.9794	14.3371	/	/	/	/	1.0000	0.2069
10	0.9915	9.2034	/	/	/	/	1.0000	0.1910
Average error E_{ϕ} (%)		16.7838		0.0244		0.0175		0.0907

The stiffness at some beam members ends need to be adjusted with relatively small absolute values of typically less than 10%, and the stiffness of columns ends however requires relatively large modifications in some members with adjusted stiffness factor value of up to approximately -45%. The stiffness of brace elements need modifications up to approximately -20% in some members, and other elements only require little modifications.

Table 5.4 Updated natural frequencies of the finite element analytical model of the experimental structure using eight incomplete modes extracted from simulated sensor measurements at four nodes with various noise levels

				5% noise		10% noise		15% noise	
Mode	FE (Hz)	Exact (Hz)	Error (%)	Updated (Hz)	Error (%)	Updated (Hz)	Error (%)	Updated (Hz)	Error (%)
1	10.3552	9.7865	5.8111	9.7752	-0.1163	9.7698	-0.1711	9.7621	-0.2499
2	25.9380	25.3668	2.2517	25.3728	0.0236	25.3792	0.0487	25.3880	0.0836
3	31.7608	29.3901	8.0662	29.3970	0.0236	29.5330	0.4862	29.5775	0.6374
4	45.2475	43.6114	3.7515	43.6306	0.0440	43.6475	0.0828	43.6573	0.1053
5	51.8179	47.6142	8.8287	47.6688	0.1147	48.2065	1.2440	48.4057	1.6625
6	65.5716	62.9209	4.2126	62.9347	0.0219	62.9110	-0.0159	62.9259	0.0079
7	70.6418	68.6193	2.9474	68.6452	0.0377	68.6405	0.0309	68.6660	0.0680
8	72.1780	70.4225	2.4929	70.4158	-0.0095	70.3770	-0.0645	70.3957	-0.0380
Average error E_{ω} (%)			4.7953		0.0489		0.2680		0.3566

Table 5.5 Updated mode shape properties of the finite element model of the experimental structure using eight incomplete modes extracted from simulated sensor measurements at four nodes with various noise levels

			5% noise		10% noise		15% noise	
Mode	MAC initial, exact	Error E_{ϕ}^{i} (%)	MAC updated, exact	Error E_{ϕ}^{i} (%)	MAC updated, exact	Error E_{ϕ}^{i} (%)	MAC updated, exact	Error E_{ϕ}^{i} (%)
1	0.9992	2.8867	1.0000	0.5989	0.9999	0.9596	0.9999	1.1734
2	0.9823	13.2940	0.9999	1.0479	0.9990	3.1671	0.9984	3.9547
3	0.9273	26.9679	0.9997	1.6157	0.9963	6.0452	0.9944	7.4601
4	0.9838	12.7441	0.9999	1.0360	0.9995	2.2659	0.9992	2.8687
5	0.9587	20.3162	1.0000	0.3617	0.9995	2.2940	0.9987	3.5526
6	0.9262	27.1664	0.9988	3.4073	0.9952	6.9333	0.9915	9.2333
7	0.8994	31.7249	0.9992	2.8356	0.9976	4.9102	0.9956	6.6673
8	0.9915	9.1992	0.9989	3.3632	0.9991	3.0501	0.9984	3.9794
Average error E_{ϕ} (%)		18.0372		1.7833		3.7032		4.8612

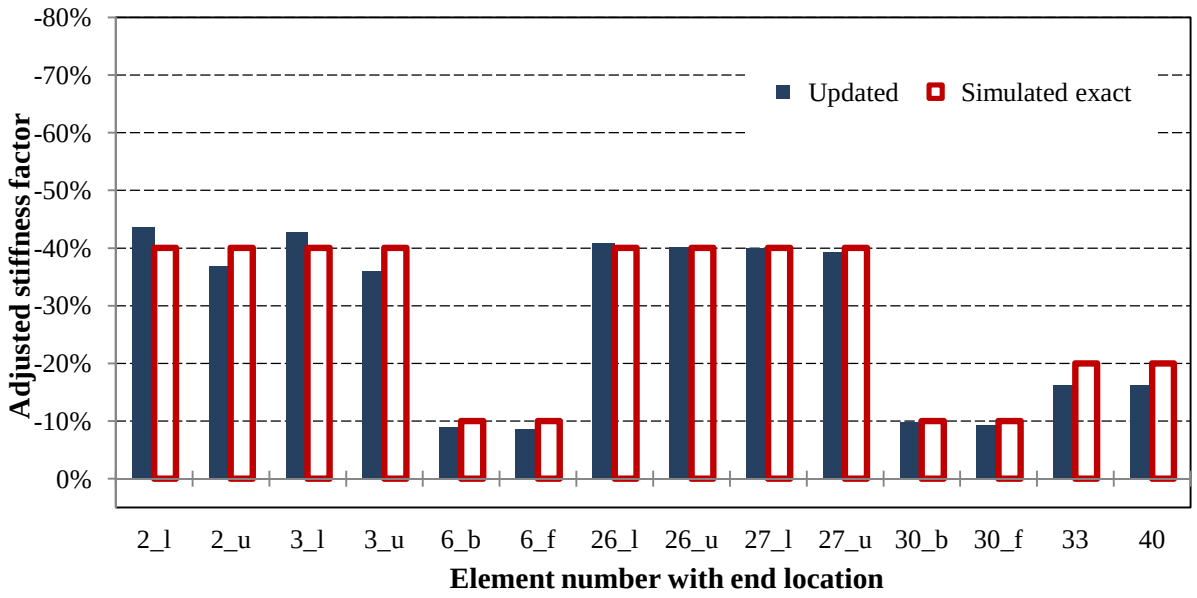

Figure 5.3 Comparison of updated stiffness parameters of the finite element model and simulated exact stiffness parameters, using eight noise-free incomplete mode extracted from simulated sensor measurements at four nodes (end location *l*, *u*, *b* and *f* represent low, upper, back and front ends, respectively)

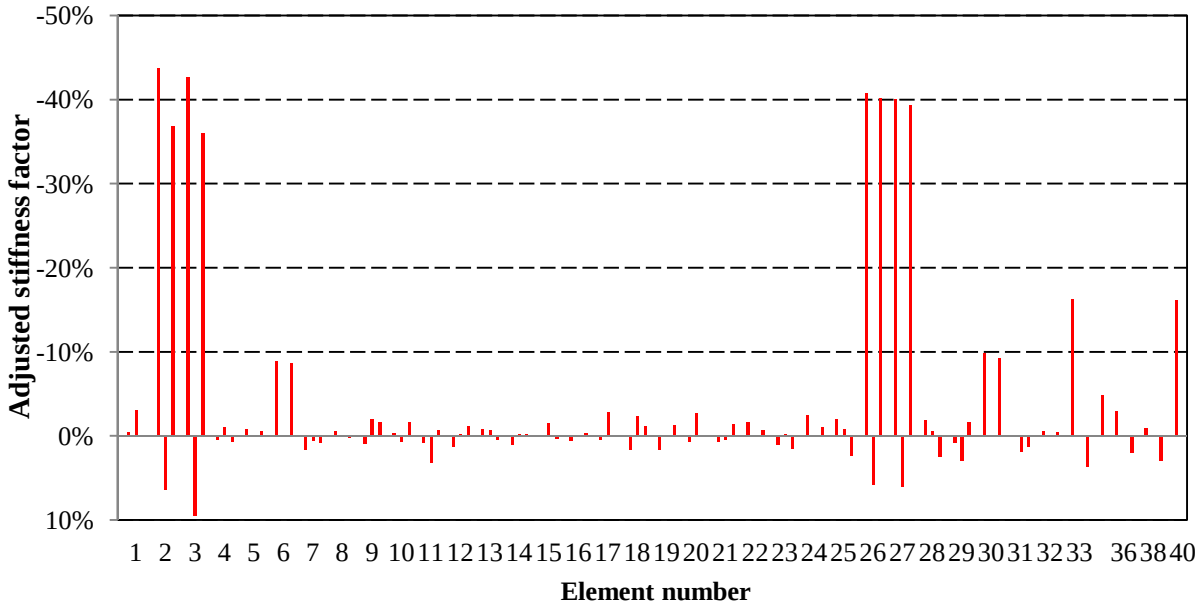

Figure 5.4 Updated stiffness parameters of the finite element model of the laboratory tested structure (three stiffness updating parameters for each beam or column, one parameter for each brace), using eight noise-free incomplete modes extracted from simulated sensor measurements at four nodes

5.2.2 Simulation 2: Simulated sensors measurements at six nodes

In Simulation 2, the stiffness difference to be updated are simulated at different structural elements with various updating levels, i.e. -50% changes at upper and lower ends of column elements 2, 3, 18 and 19, -10% changes at both ends of beam elements 6 and 22, and -30% changes in brace elements 34 and 38. The first 6, 8 and 10 "measured" exact frequencies and the corresponding incomplete mode shapes are obtained from the simulated measurements only in X and Y directions at six nodes, as shown in Figure 5.5. The results in Table 5.6show that the updated frequencies are in excellent agreement with the simulated exact values, with average absolute errors of only 0.0039%, 0.0049% and 0.0173% for cases with 6, 8 and 10 modes used, respectively. The accuracy of the updated mode shapes is assessed by the results given in Table 5.7. The correlation between the updated modes and the simulated exact modes is obviously improved for each mode with MAC values close to unity. The average mode error of 31.87% between the initial finite element model and the simulated "tested" structure is significantly reduced after model updating to values of 0.1408%, 0.0980%, and 0.2393% for cases with 6, 8, and 10 incomplete modes used, respectively.

In this simulation, errors in measurements are considered as the same in Simulation 1. Again, information on eight corrupted incompleted modes is employed to update the initial finite element model. The results in Table 5.8 indicate that the frequencies of the updated finite element model are in well agreement with the simulated noise-free exact values, with a small average frequency absolute error for each simulated noise-polluted case. Similarly, Table 5.9 gives the results of mode shapes for the updated analytical model which are also match the simulated exact values, with MAC diagonal values of close to unity and small average absolute mode error for each simulated noise-polluted case.

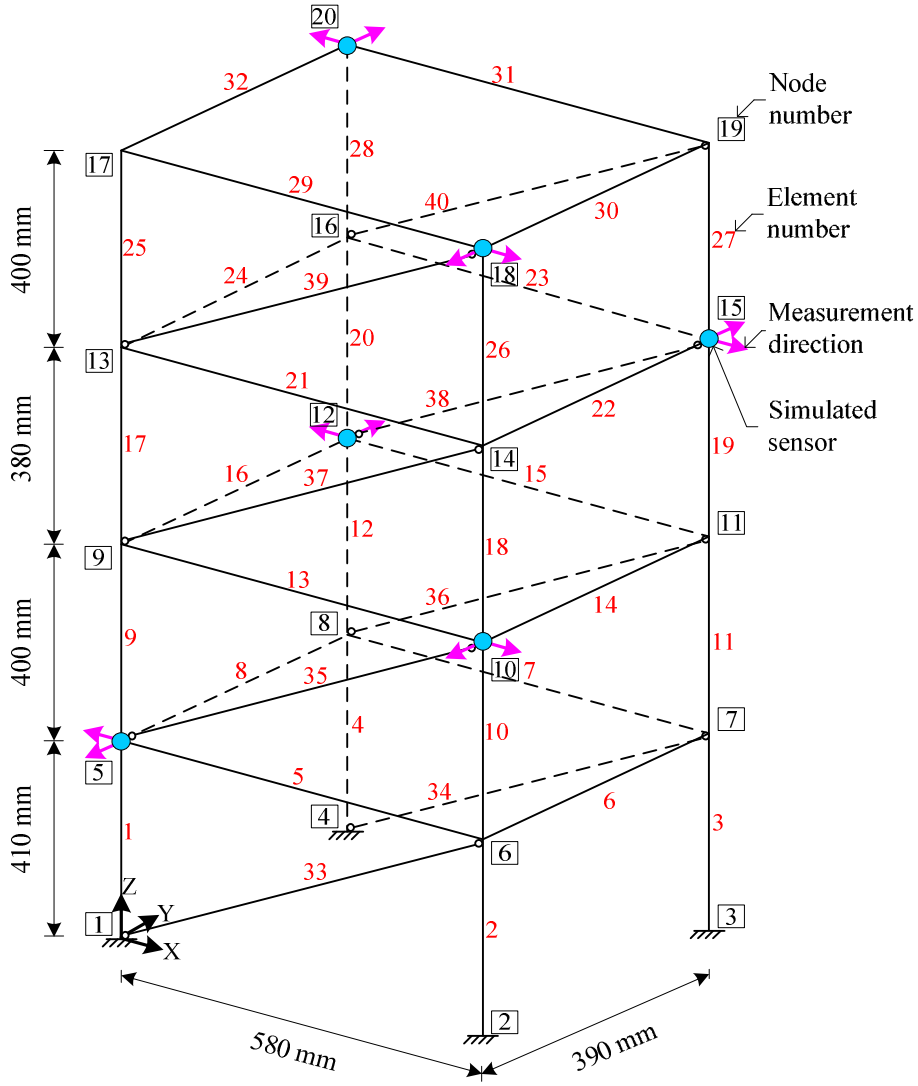

Figure 5.5 The finite element model of the laboratory tested space steel frame model structure with simulated sensors at six nodes adopted for model updating

Comparison of adjusted stiffness parameters with the assumed values is shown in Figure 5.6, where information on eight simulated noise-free incomplete modes is employed for model updating. The results indicate that the updated stiffness parameters match well the assumed exact values for stiffness changes at different levels and at various specific locations. Moreover, the results for all adjusted stiffness parameters are also plotted in Figure 5.7. The results show that the stiffness at beam ends need to be modified with relatively small absolute

values of typically less than 10%. The stiffness of columns ends however requires relatively large modifications in some members with adjusted stiffness factor value of up to approximately -55%. The stiffness of braces in some members also require large alterations with adjusted stiffness factor values of up to approximately -30%.

Table 5.6 Updated natural frequencies of the finite element model of the experimental structure using different number of noise-free incomplete modes extracted from simulated sensor measurements at six nodes

				6 modes used		8 modes used		10 modes used	
Mode	FE (Hz)	Exact (Hz)	Error (%)	Updated (Hz)	Error (%)	Updated (Hz)	Error (%)	Updated (Hz)	Error (%)
1	10.3552	9.4554	9.5170	9.4552	-0.0017	9.4553	-0.0006	9.4569	0.0162
2	25.9380	25.1115	3.2912	25.1145	0.0120	25.1116	0.0006	25.1128	0.0052
3	31.7608	28.0390	13.2734	28.0411	0.0074	28.0410	0.0070	28.0395	0.0018
4	45.2475	42.4984	6.4686	42.4986	0.0004	42.4973	-0.0028	42.4996	0.0028
5	51.8179	50.4929	2.6240	50.4932	0.0006	50.4915	-0.0029	50.5101	0.0340
6	65.5716	63.5167	3.2351	63.5177	0.0016	63.5168	0.0000	63.5508	0.0536
7	70.6418	65.0895	8.5303	/	/	65.0884	-0.0017	65.0888	-0.0011
8	72.1780	68.3407	5.6149	/	/	68.3569	0.0236	68.3278	-0.0189
9	85.2298	81.7057	4.3133	/	/	/	/	81.7166	0.0134
10	86.5838	83.9274	3.1652	/	/	/	/	83.9491	0.0259
Average error E_{ω} (%)			6.0033		0.0039		0.0049		0.0173

Table 5.7 Updated mode shape properties of the finite element model of the experimental structure using different number of noise-free incomplete modes extracted from simulated sensor measurements at six nodes

			6 modes used		8 modes used		10 modes used	
Mode	MAC initial, exact	Error E_{ϕ}^{i} (%)	MAC updated, exact	Error E_{ϕ}^{i} (%)	MAC updated, exact	Error E_{ϕ}^{i} (%)	MAC updated, exact	Error E_{ϕ}^{i} (%)
1	0.9985	3.8326	1.0000	0.0774	1.0000	0.0582	1.0000	0.0782
2	0.9821	13.3652	1.0000	0.2038	1.0000	0.1069	1.0000	0.1723
3	0.8851	33.8940	1.0000	0.1310	1.0000	0.0888	1.0000	0.1375
4	0.8998	31.6542	1.0000	0.1217	1.0000	0.0580	1.0000	0.1199
5	0.9217	27.9819	1.0000	0.1169	1.0000	0.0858	1.0000	0.2326
6	0.3957	77.7367	1.0000	0.1937	1.0000	0.1068	1.0000	0.5359
7	0.6176	61.8349	/	/	1.0000	0.1118	1.0000	0.2842
8	0.9562	20.9219	/	/	1.0000	0.1677	1.0000	0.3762
9	0.9257	27.2557	/	/	/	/	1.0000	0.1290
10	0.9589	20.2707	/	/	/	/	1.0000	0.3275
Average error E_{ϕ} (%)		31.8748		0.1408		0.0980		0.2393

Table 5.8 Updated natural frequencies of the finite element model of the experimental structure using eight incomplete modes extracted from simulated sensor measurements at six nodes with various noise levels

				5% noise		10% noise		15% noise	
Mode	FE (Hz)	Exact (Hz)	Error (%)	Updated (Hz)	Error (%)	Updated (Hz)	Error (%)	Updated (Hz)	Error (%)
1	10.3552	9.4554	9.5170	9.4407	-0.1556	9.4351	-0.2150	9.4344	-0.2223
2	25.9380	25.1115	3.2912	25.1035	-0.0320	25.1010	-0.0418	25.1004	-0.0441
3	31.7608	28.0390	13.2734	28.0772	0.1359	28.1546	0.4120	28.2505	0.7541
4	45.2475	42.4984	6.4686	42.4576	-0.0961	42.4396	-0.1385	42.4300	-0.1609
5	51.8179	50.4929	2.6240	50.5017	0.0174	50.5054	0.0248	50.5036	0.0211
6	65.5716	63.5167	3.2351	63.4923	-0.0385	63.4907	-0.0409	63.5170	0.0004
7	70.6418	65.0895	8.5303	65.2266	0.2107	65.4059	0.4860	65.6214	0.8172
8	72.1780	68.3407	5.6149	68.4002	0.0870	68.6235	0.4137	83.9093	0.8320
Average error E_{ω} (%)			6.5693		0.0967		0.2216		0.3565

Table 5.9 Updated mode shape properties of the finite element model of the experimental structure using eight incomplete modes extracted from simulated sensor measurements at six nodes with various noise levels

			5% noise		10% noise		15% noise	
Mode	MAC initial, exact	Error E_{ϕ}^{i} (%)	MAC updated, exact	Error E_{ϕ}^{i} (%)	MAC updated, exact	Error E_{ϕ}^{i} (%)	MAC updated, exact	Error E_{ϕ}^{i} (%)
1	0.9985	3.8326	1.0000	0.4768	1.0000	0.5973	0.9999	0.8280
2	0.9821	13.3652	0.9995	2.1480	0.9990	3.1915	0.9985	3.9144
3	0.8851	33.8940	0.9998	1.5371	0.9990	3.1778	0.9976	4.9439
4	0.8998	31.6542	0.9998	1.4864	0.9990	3.1439	0.9973	5.2135
5	0.9217	27.9819	0.9998	1.3211	0.9993	2.6923	0.9984	4.0619
6	0.3957	77.7367	0.9988	3.4043	0.9970	5.5220	0.9938	7.8493
7	0.6176	61.8349	0.9997	1.6778	0.9985	3.9061	0.9960	6.3421
8	0.9562	20.9219	0.9991	2.9778	0.9978	4.7076	0.9958	6.4845
Average error E_{ϕ} (%)		33.9027		1.8787		3.3673		4.9547

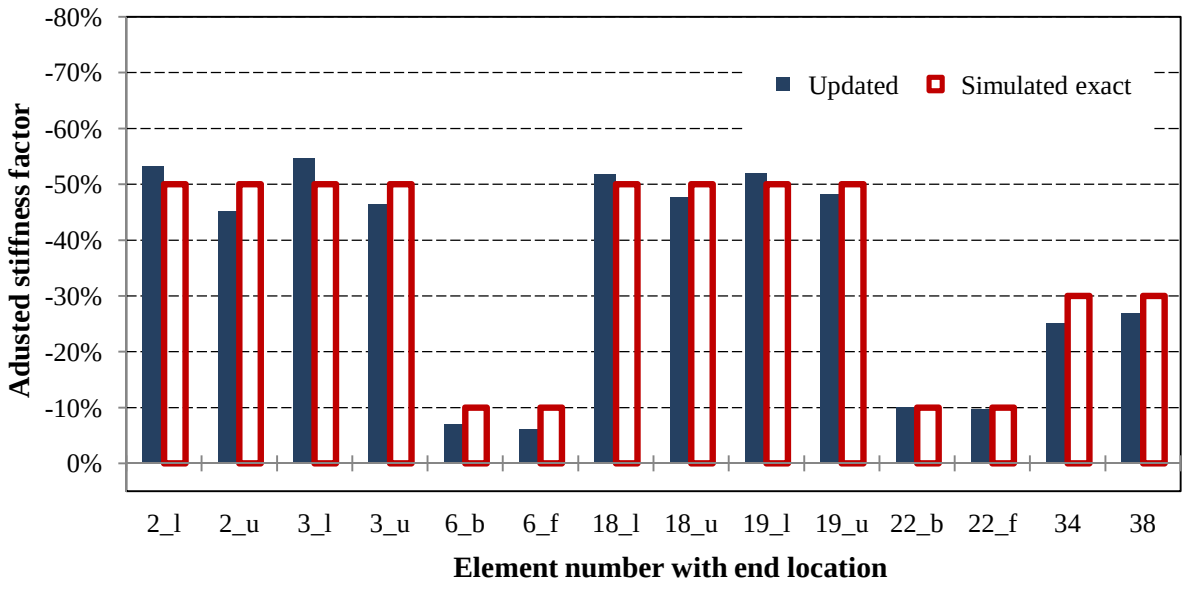

Figure 5.6 Comparison of updated stiffness parameters of the finite element model and simulated exact stiffness parameters, using eight noise-free incomplete mode extracted from simulated sensor measurements at six nodes (end location *l*, *u*, *b* and *f* represent low, upper, back and front ends, respectively)

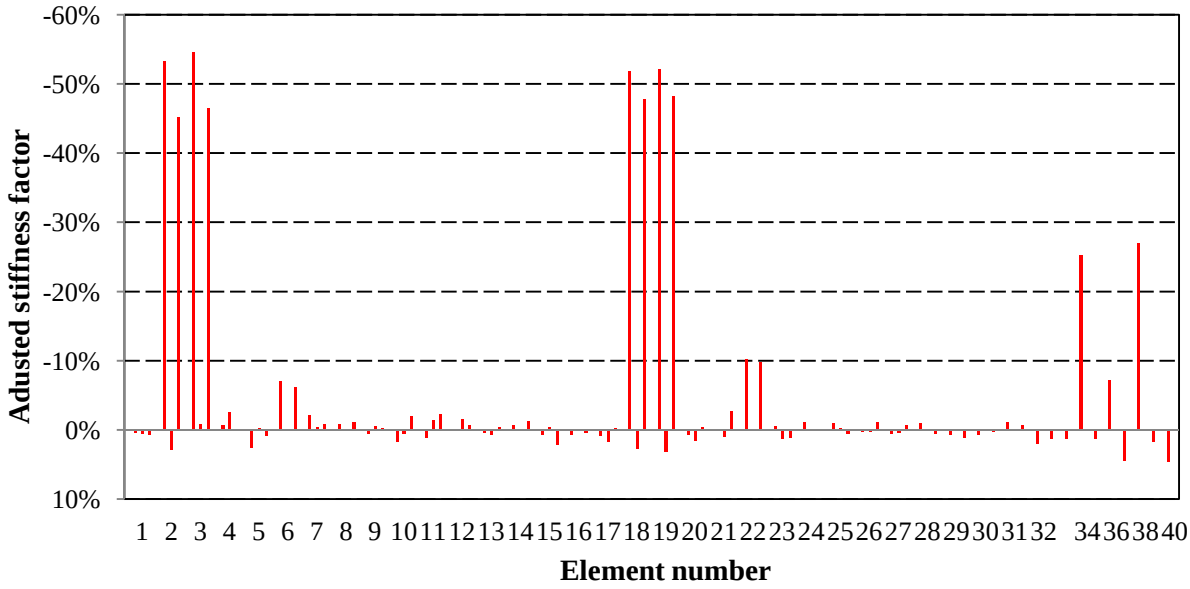

Figure 5.7 Updated stiffness parameters of the finite element model of the laboratory tested structure (three stiffness updating parameters for each beam or column, one parameter for each brace), using eight noise-free incomplete modes extracted from simulated sensor measurements at six nodes

5.2.3 Simulation 3: Simulated sensors measurements at sixteen nodes

In this simulation, the stiffness difference to be updated are simulated at different structural elements with various updating levels, i.e. -50% change at upper and lower ends of column 10,11,26, and 27, -10% change at both ends of beam elements 6 and 30, -20% change in brace elements 33 and 40. The first 6, 8 and 10 “measured” exact frequencies and the corresponding incomplete mode shapes are obtained from the total ofsixteen simulated sensor measurements at nodes 5,7,9,11,13,15,17 and 19 in X direction,andat nodes 6,8,10,12,14,16,18 and 20 in Y direction, as shown in Figure 5.8. The results in Table 5.10 indicate that the updated frequencies agree well with the simulated exact values, with average absolute errors of only 0.055%, 0.0007% and 0.0008% for cases with 6, 8 and 10 modes used, respectively. Furthermore, the accuracy of the updated mode shapes is assessed by the results given in Table 5.11. The correlation between the updated modes and the simulated exact modes is greatly improved with MAC values close to unity. The average mode error of 26.67% between the initial finite element model and the simulated “tested” structure is significantly reduced after model updating to values of 0.4109%, 0.043%, and 0.0334% for the cases with 6, 8, and 10 incomplete modes used, respectively.

Here, measurements errors are simulated by corrupting the exact analytical modal data with standard normally distributed noise levels as in the Simulation 1. The results in Table 5.12 show that the updated frequencies agree well with the simulated noise-free exact values, with a small average frequency absolute error for each noise corrupted case. Similarly, high MAC diagonal values, as shown in Table 5.13, indicated that the updated mode shapes are match well with the simulated exact values, with smallerrors for noise corrupted cases.

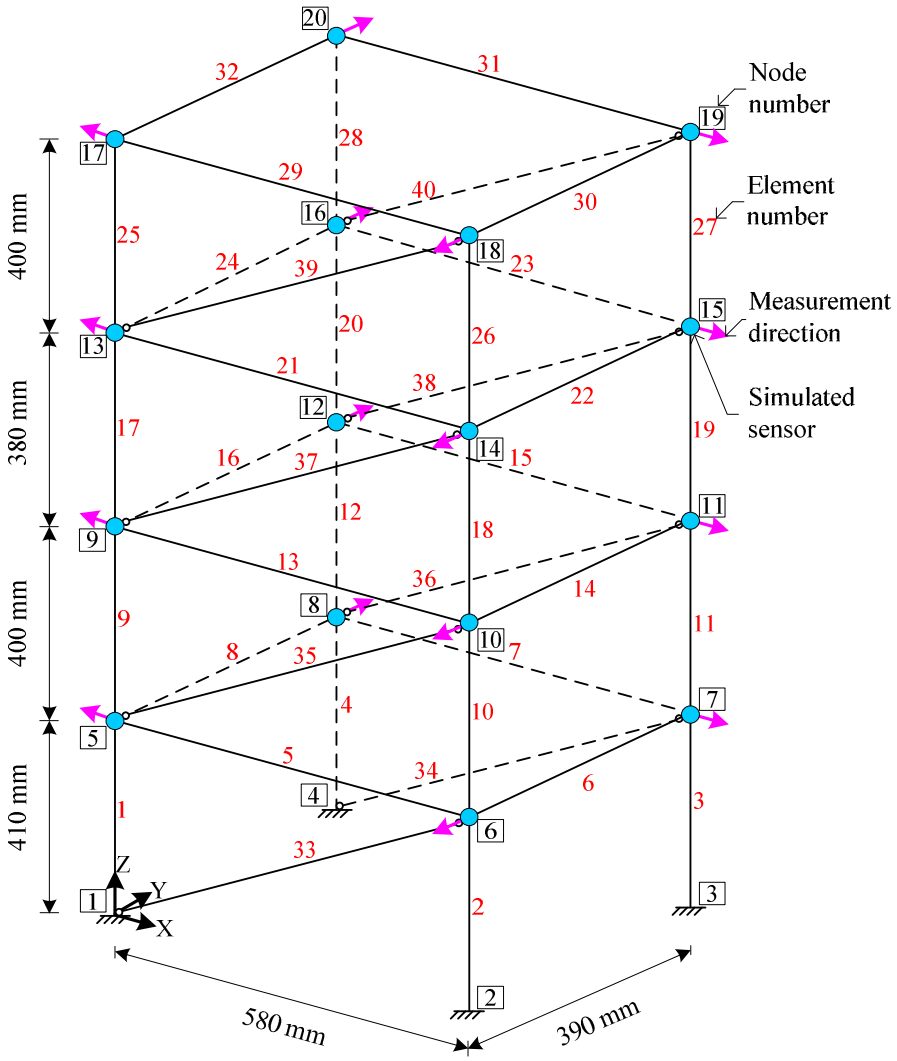

Figure 5.8 The finite element model of the laboratory tested space steel frame model structure with sixteen simulated sensors adopted for model updating

The adjusted stiffness parameters obtained by using the first eight simulated noise-free incomplete modes are plotted in Figure 5.9 and Figure 5.10. The results in Figure 5.9 indicate that the updated stiffness parameters match well with the assumed exact values for stiffness changes at different levels and at various specific locations.Similarly, the results summarised in Figure 5.10 show that the stiffness of the ends of beam elements 6 and 30 need to be modified with relatively small absolute values of approximately -10%. However, the stiffness

of column members 10, 11, 26, and 27 require relatively large modifications with adjusted stiffness factor values of up to approximately -50% in the upper and lower ends. The stiffness of brace elements 33 and 40 also need to be updated large alterations with adjusted stiffness factor values of up to approximately -20% while other brace elements only require very small modifications.

Table 5.10 Updated natural frequencies of the finite elementmodel of the experimental structure using different number of noise-free incomplete modes extracted from simulated sensor measurements at sixteen nodes

				6 modes used		8 modes used		10 modes used	
Mode	FE (Hz)	Exact (Hz)	Error (%)	Updated (Hz)	Error (%)	Updated (Hz)	Error (%)	Updated (Hz)	Error (%)
1	10.3552	9.7504	6.2032	9.7473	-0.0321	9.7504	0.0003	9.7506	0.0015
2	25.9380	25.4704	1.8357	25.4680	-0.0096	25.4701	-0.0013	25.4702	-0.0010
3	31.7608	29.7914	6.6105	29.7580	-0.1122	29.7912	-0.0009	29.7914	-0.0002
4	45.2475	43.2756	4.5567	43.2295	-0.1063	43.2746	-0.0021	43.2749	-0.0015
5	51.8179	46.0823	12.4464	46.0588	-0.0509	46.0823	0.0000	46.0826	0.0007
6	65.5716	62.0041	5.7536	61.9924	-0.0188	62.0034	-0.0011	62.0037	-0.0007
7	70.6418	64.5818	9.3835	/	/	64.5818	0.0000	64.5805	-0.0020
8	72.1780	70.5104	2.3650	/	/	70.5107	0.0003	70.5101	-0.0004
9	85.2298	81.6361	4.4021	/	/	/	/	81.6359	-0.0003
10	86.5838	85.0314	1.8257	/	/	/	/	85.0313	-0.0001
Average error E_{ω} (%)			5.5382		0.0550		0.0007		0.0008

Table 5.11 Updated mode shape properties of the finite elementmodel of the experimental structure using different number of noise-free incomplete modes extracted from simulated sensor measurements at sixteen nodes

			6 modes used		8 modes used		10 modes used	
Mode	MAC initial, exact	Error E_{ϕ}^{i} (%)	MAC updated, exact	Error E_{ϕ}^{i} (%)	MAC updated, exact	Error E_{ϕ}^{i} (%)	MAC updated, exact	Error E_{ϕ}^{i} (%)
1	0.9979	4.6045	1.0000	0.0409	1.0000	0.0243	1.0000	0.0189
2	0.9973	5.2370	1.0000	0.0401	1.0000	0.0299	1.0000	0.0234
3	0.9502	22.3221	1.0000	0.2223	1.0000	0.0599	1.0000	0.0430
4	0.7150	53.3855	1.0000	0.5431	1.0000	0.0602	1.0000	0.0381
5	0.5629	66.1168	0.9999	0.7203	1.0000	0.0676	1.0000	0.0410
6	0.9020	31.3076	0.9999	0.8985	1.0000	0.0414	1.0000	0.0421
7	0.8529	38.3533	/	/	1.0000	0.0374	1.0000	0.0502
8	0.9907	9.6458	/	/	1.0000	0.0234	1.0000	0.0124
9	0.9311	26.2430	/	/	/	/	1.0000	0.0359
10	0.9909	9.5494	/	/	/	/	1.0000	0.0295
Average error E_{ϕ} (%)		26.6765		0.4109		0.0430		0.0334

Table 5.12 Updated natural frequencies of the finite elementmodel of the experimental structure using eight incomplete modes extracted from simulated sensor measurements at sixteen nodes with various noise levels

				5% noise		10% noise		15% noise	
Mode	FE (Hz)	Exact (Hz)	Error (%)	Updated (Hz)	Error (%)	Updated (Hz)	Error (%)	Update d (Hz)	Error (%)
1	10.3552	9.7504	6.2032	9.7429	-0.0768	9.7501	-0.0034	9.7602	0.1006
2	25.9380	25.4704	1.8357	25.4530	-0.0682	25.4622	-0.0324	25.4738	0.0133
3	31.7608	29.7914	6.6105	29.8029	0.0386	29.8280	0.1228	29.8637	0.2425
4	45.2475	43.2756	4.5567	43.3031	0.0636	43.3635	0.2031	43.4397	0.3792
5	51.8179	46.0823	12.4464	46.1581	0.1645	46.2823	0.4341	46.4542	0.8072
6	65.5716	62.0041	5.7536	61.9810	-0.0372	61.9609	-0.0696	61.9478	-0.0908
7	70.6418	64.5818	9.3835	64.6185	0.0569	64.6704	0.1372	64.7442	0.2514
8	72.1780	70.5104	2.3650	70.6925	0.2582	70.9147	0.5734	70.8202	0.4394
Average error E_{ω} (%)			6.1443		0.0955		0.1970		0.2906

Table 5.13 Updated mode shape properties of the finite elementmodel of the experimental structure using eight incomplete modes extracted from simulated sensor measurements at sixteen nodes with various noise levels

			5% noise		10% noise		15% noise	
Mode	MAC initial, exact	Error E_{ϕ}^{i} (%)	MAC updated, exact	Error E_{ϕ}^{i} (%)	MAC updated, exact	Error E_{ϕ}^{i} (%)	MAC updated, exact	Error E_{ϕ}^{i} (%)
1	0.9979	4.6045	1.0000	0.6791	1.000	0.6886	0.9999	0.7378
2	0.9973	5.2370	0.9999	1.1552	0.9998	1.4812	0.9998	1.4003
3	0.9502	22.3221	0.9997	1.7143	0.9992	2.8612	0.9982	4.2821
4	0.7150	53.3855	0.9998	1.5641	0.9985	3.9087	0.9940	7.7162
5	0.5629	66.1168	0.9998	1.3980	0.9984	3.9669	0.9930	8.3913
6	0.9020	31.3076	0.9987	3.6716	0.9953	6.8487	0.9907	9.6182
7	0.8529	38.3533	0.9979	4.5520	0.9927	8.5334	0.9859	11.8779
8	0.9907	9.6458	0.9994	2.3505	0.9997	1.7446	0.9998	1.2276
Average error E_{ϕ} (%)		28.8716		2.1356		3.7541		5.6564

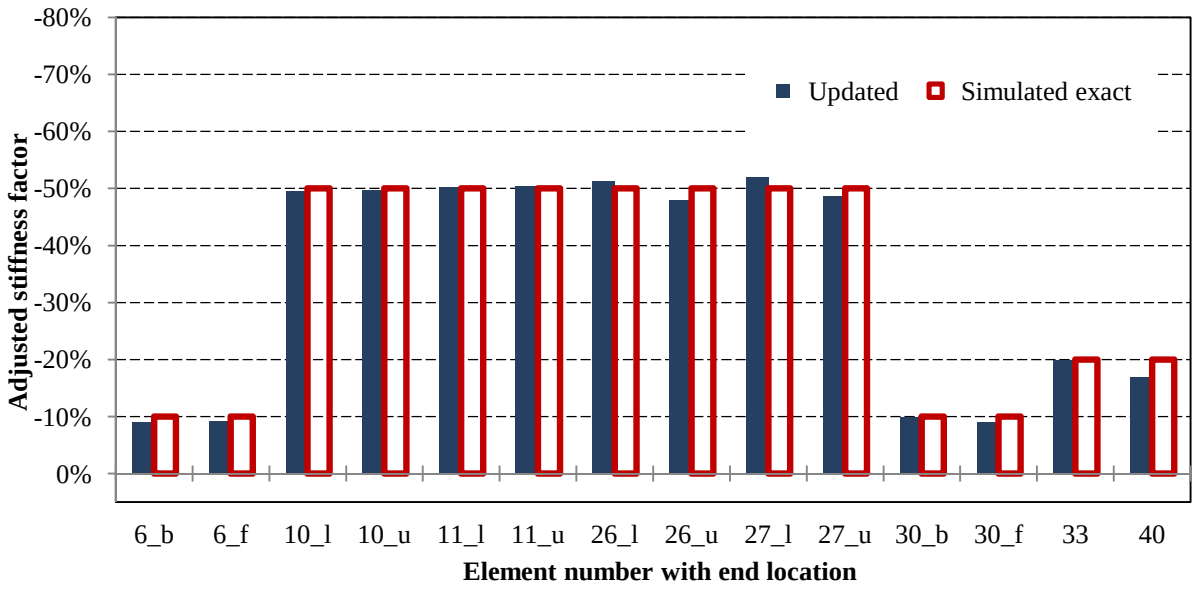

Figure 5.9 Comparison of updated stiffness parameters of the finite elementmodel and simulated exact stiffness parameters, using eight noise-free incomplete mode extracted from simulated sensor measurements at sixteen nodes (end location *l*, *u*, *b* and *f* represent low, upper, back and front ends, respectively)

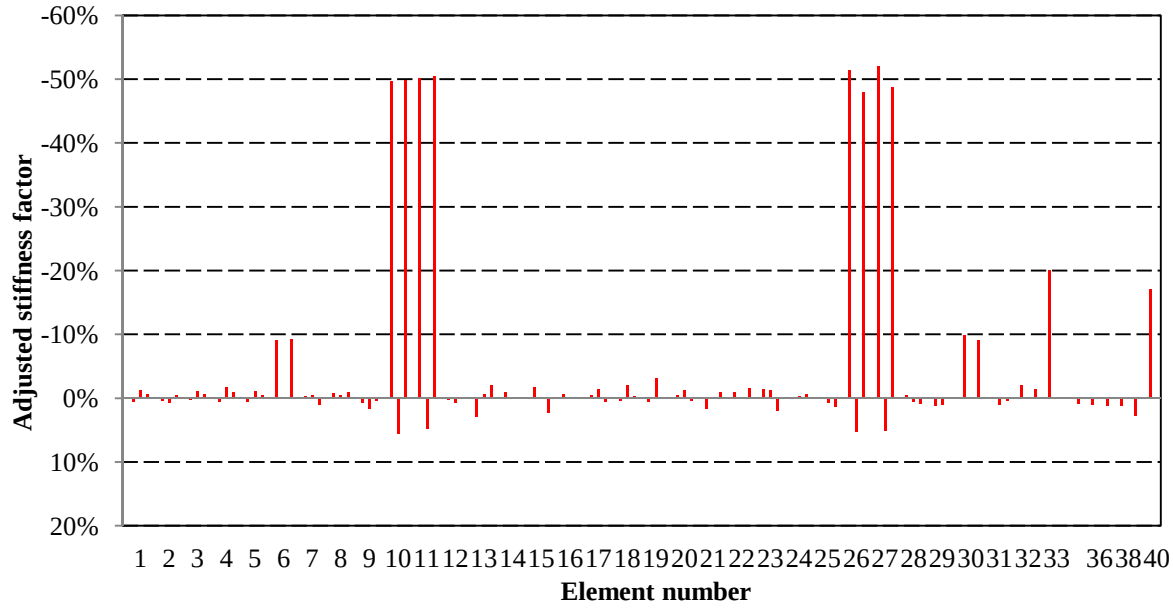

Figure 5.10 Updated stiffness parameters of the finite elementmodel of the laboratory tested structure (three stiffness updating parameters for each beam or column, one parameter for each brace), using eight noise-free incomplete modes extracted from simulated sensor measurements at sixteen nodes

5.3 Experimental study of space steel frame model structure

In the laboratory vibration testing of the space steel frame model structure, a total number of 16 uni-axial accelerometers are installed at the beam-column joints to measure translational displacements in X or Y direction as shown inFigure 3.2. When the model structure is excited by an impact hammer, the data set of acceleration measurements is recorded by using National Instrument (NI) data acquisition device NI-DAQ 9178 with NI-9234 acceleration modules and Labview Signalexpress commercial software as shown in Figure 5.11.

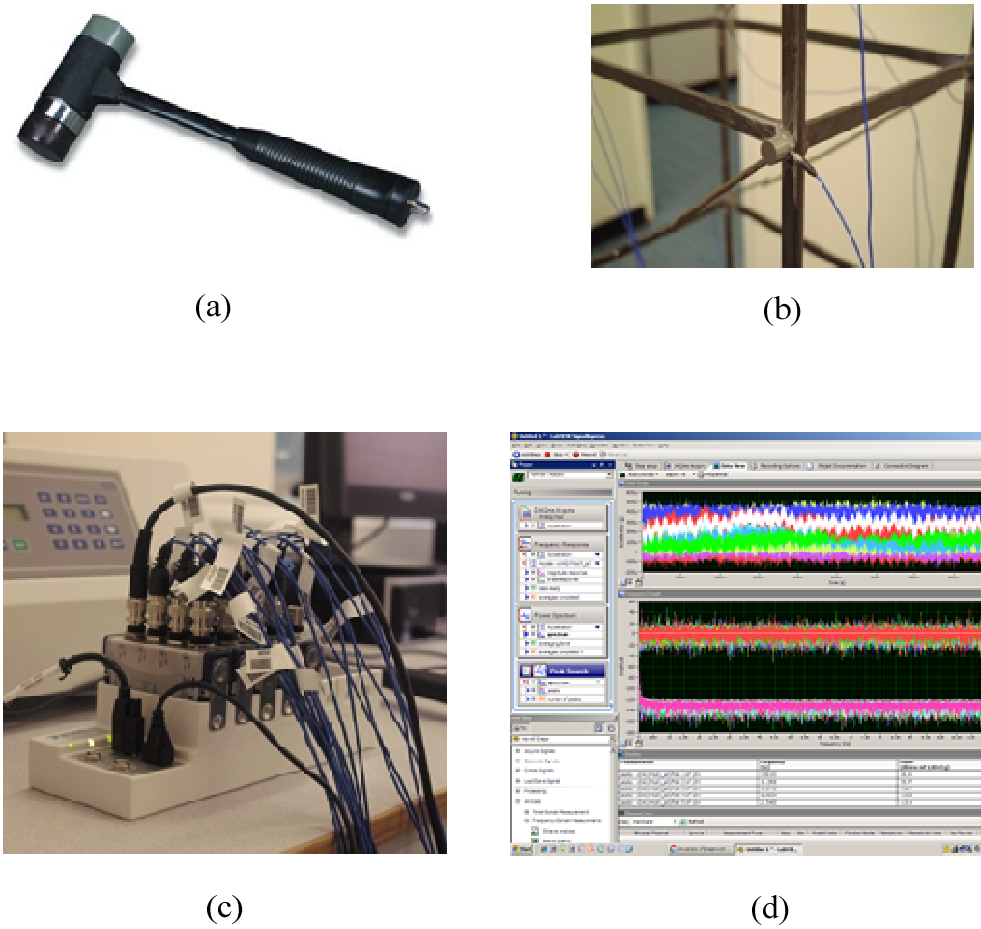

(a) (b)

(c) (d)

Figure 5.11 Structural dynamics testing; (a) Impact hammer; (b) Installed accelerometer; (c) NI data acquisition device; (d) Labview Signalexpress signal processing program

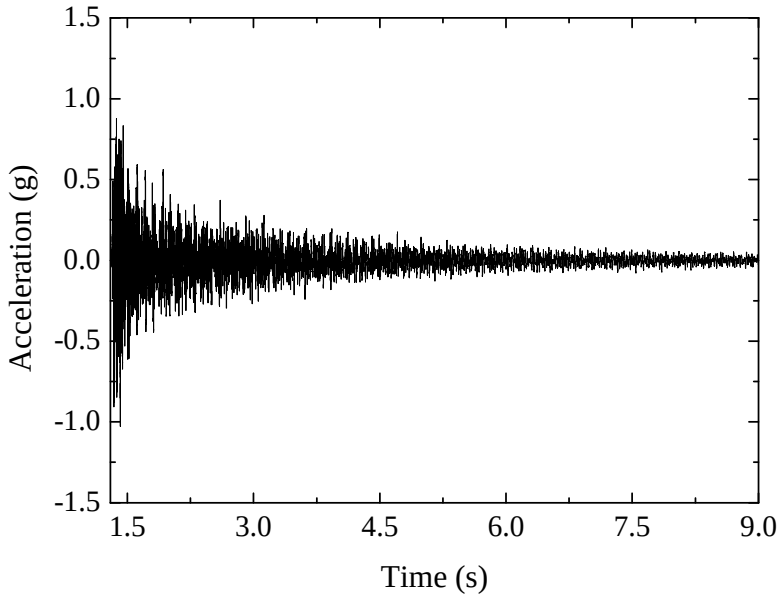

(a) Typical acceleration measurements

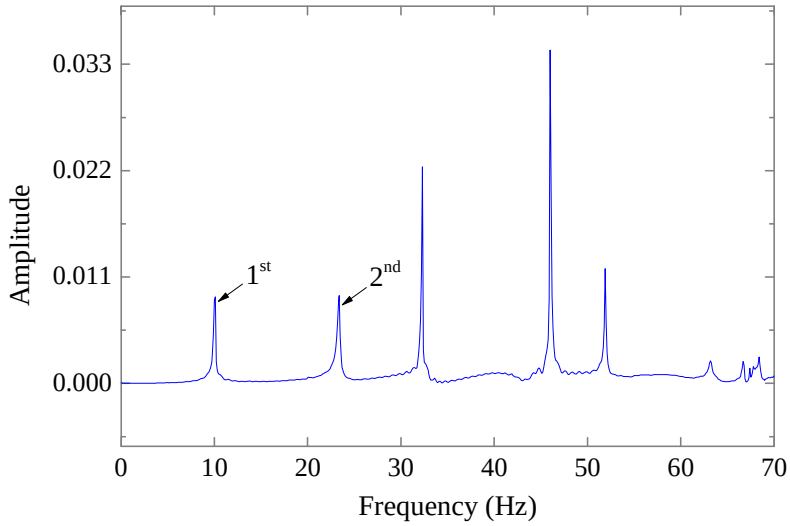

(b) Identified frequencies

Figure 5.12 Laboratory vibration test results for the space steel frame model structure

The experimental modal data including frequencies and mode shape readings at the measured degrees of freedom are extracted from the measured acceleration data by a modal analysis technique. The recorded typical acceleration measurements and the identified natural

frequencies are shown in Figure 5.12. The first four and six measured incomplete modes are adopted for updating the initial finite element model since they correlate well with the corresponding initial analytical modes.

The proposed model updating method can be employed to update the initial analytical model by utilising measured frequencies and incomplete mode shapes. The results in Table 5.14 show the updated modal properties by using four experimental frequencies and incomplete modes. The average frequency absolute error is reduced from an initial value of 2.07% to a value of 0.67% after updating. MAC values closed to unity show that the updated mode shapes are in well agreement with both the initial analytical and experimental modes. Similarly, in the case where first six experimental frequencies and incomplete modes are adopted for model updating, the updated frequencies agree well with the corresponding experimental values and the updated mode shapes have good correlation with both the initial analytical and experimental modes as indicated in Table 5.15.

Table 5.14 Updated modal properties of the finite elementmodel of the experimental structure using four laboratory experimental frequencies and incomplete modes

Mode	FE frequency (Hz)	Tested frequency (Hz)	Initial error (%)	MAC initial, tested	Updated frequency (Hz)	Updated error (%)	MAC updated, initial	MAC updated, tested
1	10.3552	10.569	-2.0224	0.9697	10.5433	-0.2432	0.9997	0.9689
2	25.9380	25.174	3.0348	0.8185	25.7470	2.2760	0.9992	0.8322
3	31.7608	32.258	-1.5413	0.9932	32.2592	0.0036	0.9966	0.9899
4	45.2475	46.018	-1.6744	0.9983	45.9417	-0.1659	0.9983	0.9973
Average error E_{ω} (%)			2.0682			0.6722		

Table 5.15 Updated modal properties of the finite elementmodel of the experimental structure using six laboratory experimental frequencies and incomplete modes

Mode	FE frequency (Hz)	Tested frequency (Hz)	Initial error (%)	MAC initial, tested	Updated frequency (Hz)	Updated error (%)	MAC updated, initial	MAC updated, tested
1	10.3552	10.569	-2.0224	0.9697	10.5333	-0.3374	0.9997	0.9689
2	25.9380	25.174	3.0348	0.8185	25.6105	1.7339	0.9990	0.8294
3	31.7608	32.258	-1.5413	0.9932	32.2388	-0.0596	0.9968	0.9894
4	45.2475	46.018	-1.6744	0.9983	45.9252	-0.2017	0.9973	0.9963
5	51.8179	51.847	-0.0562	0.9844	51.8418	-0.0100	0.9957	0.9850
6	65.5716	65.522	0.0756	0.8351	65.5599	0.0578	0.9875	0.8402
Average error E_{ω} (%)			1.4008			0.4001		

The adjusted stiffness parameters obtained by using first four and six incomplete experimental modes are plotted in Figure 5.13 and Figure 5.14, respectively. The results give consistent indications that the stiffness at beam-column joints needs to be adjusted with relatively small absolute values of typically less than 10%. The stiffness of braces however requires relatively large modifications in some members with adjusted stiffness factor values of up to approximately -20%, which is probably caused by the errors in modelling the welded connections in the laboratory tested structure as the pin-jointed connections are assumed in the initial analytical model.

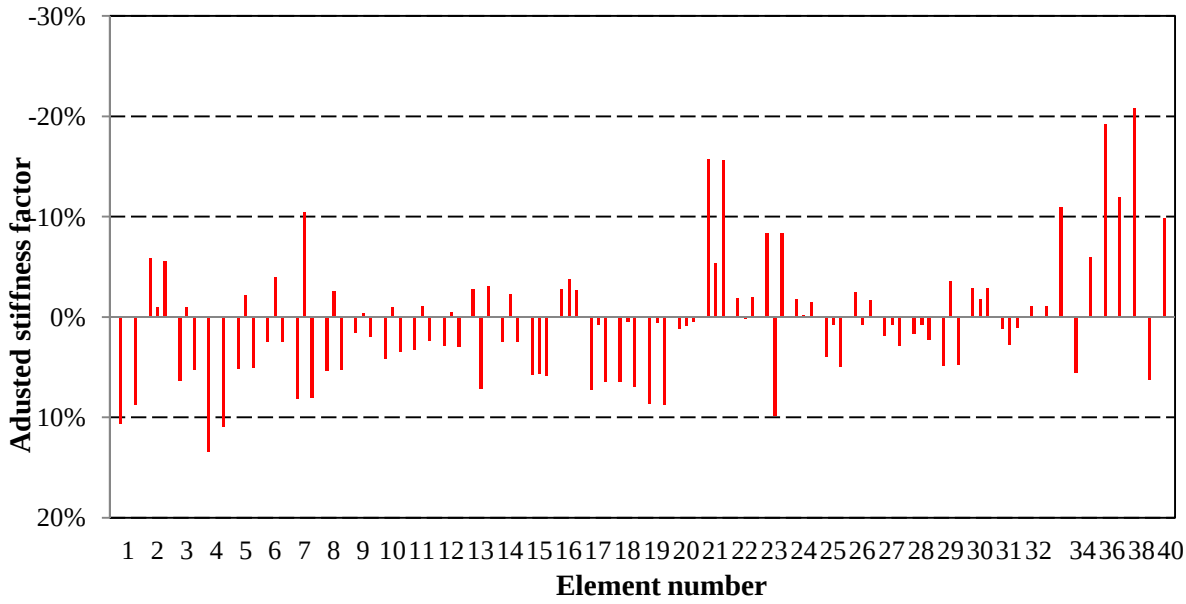

Figure 5.13 Updated stiffness parameters of the finite elementmodel of the laboratory tested structure (three stiffness updating parameters for each beam or column, one parameter for each brace), four experimental frequencies and incomplete modes used

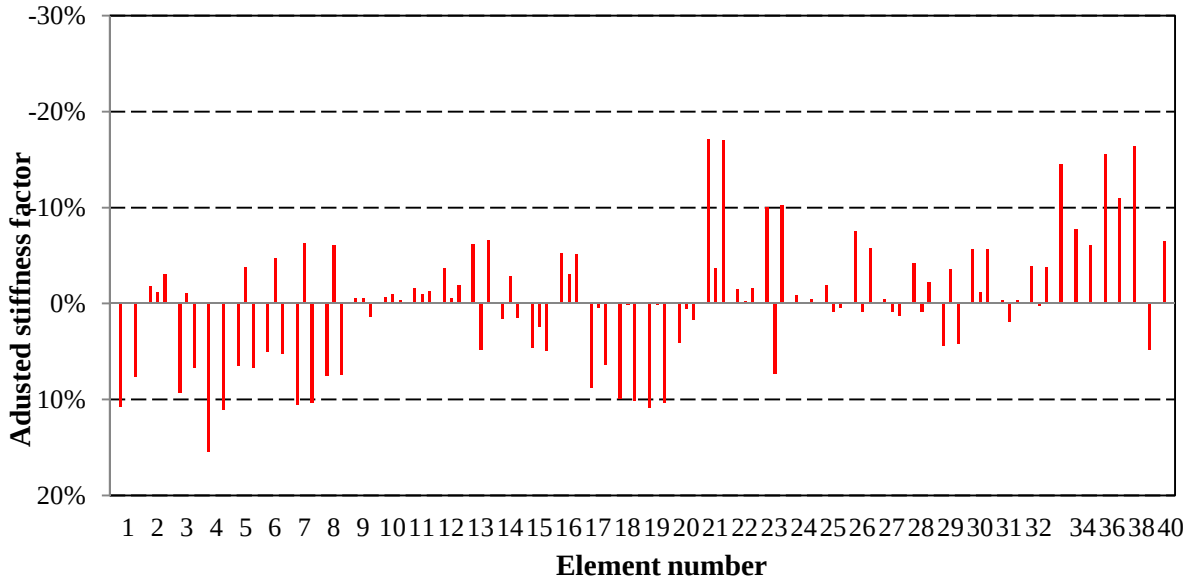

Figure 5.14 Updated stiffness parameters of the finite elementmodel of the laboratory tested structure (three stiffness updating parameters for each beam or column, one parameter for each brace), six experimental frequencies and incomplete modes used

5.4 Practical application by using field measured data

5.4.1 Modal parameter identification of Canton Tower

Canton Tower in China is selected as a case study to demonstrate the applicability of proposed model updating method by using field measured data. Description of Canton Tower is expressed in the Section 2.7. Data processing and modal identification of the Canton Tower are performed by using the modal analysis software MACEC (Peeters and De Roeck 1999, De Roeck and Peeters 1999). The output-only system identification of the structure via Frequency Domain Peak Picking (FDPP) and Stochastic Subspace Identification (SSI) techniques are utilised (Peeters and De Roeck 1999, De Roeck and Peeters 1999). The interested first fifteen frequencies obtained from finite element dynamic analysis of analytical lie between 0 to 2.0 Hz. Thus, re-sampling and filtering of the raw measurement data from 50 to 5 Hz are carried out which lead to desired frequency range. The natural frequencies are simply determined from the observation of the peaks of the spectra, as shown in Figure 5.15. However,disadvantage of FDPP is that it can only extract natural frequencies and is not able to produce mode shapes. On the other hand, SSI method directly works with measured time history data without requiring the conversion into spectra. The SSI technique identifies the state space matrices based on the measurements by using robust numerical techniques, such as Singular Value Decomposition (Van Overschee and De Moor 1996). Once the mathematical description of the structure (the state space model) is determined, it is straightforward to extract natural frequencies, damping ratios and associated mode shapes from the stabilisation diagram, as shown in Figure 5.16.

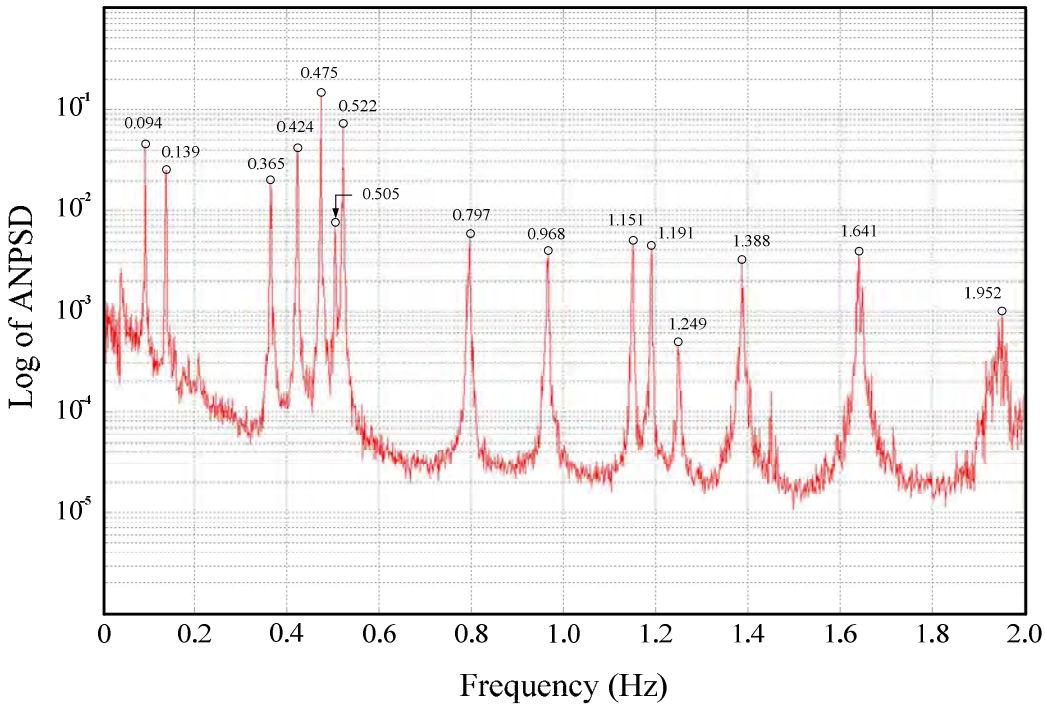

Figure 5.15 Averaged normalized power spectral densities (ANPADs) of the measured acceleration data used for the Frequency Domain Peak Picking (FDPP) technique

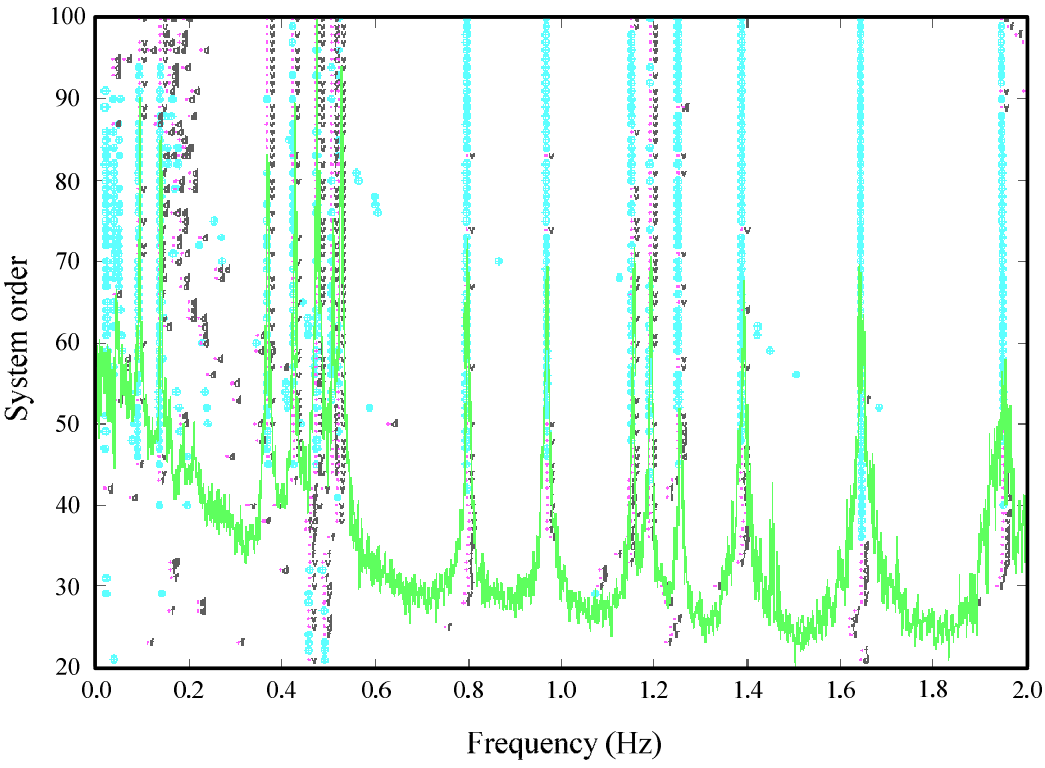

Figure 5.16 The stabilization diagram of measured acceleration data used for the Stochastic Subspace Identification (SSI) technique

The natural frequencies identified by the FDPP technique and the SSI technique are then compared with those obtained from finite element analysis of the reduced-order finite element model, as summarised in Table 5.16. The results show that the differences between the frequencies identified from the ambient vibration measurements and the frequencies obtained from finite element dynamic analysis of analytical model are relatively large. However, the frequencies identified by the SSI technique are very close to the frequencies identified by the FDPP technique. The significant difference between the measured and analytical frequencies requires an updating of the finite element model to improve the correlation. In this study, the modal data identified by the SSI technique are adopted for model updating.

Table 5.16 Comparison of 10 field measured frequencies identified by the FDPP and SSI methods with those calculated from the reduced-order finite elementmodel of the Canton Tower

Mode	FE model (Hz)	FDPP method (Hz)	SSI method (Hz)	FE vs FDPP error (%)	FDPP vs SSI error (%)
1	0.1109	0.094	0.094	17.995	0.000
2	0.1588	0.139	0.140	14.274	-0.714
3	0.3473	0.365	0.367	-4.853	-0.545
4	0.3691	0.424	0.421	-12.952	0.713
5	0.4003	0.475	0.475	-15.724	0.000
6	0.4617	0.505	0.505	-8.575	0.000
7	0.4868	0.522	0.519	-9.746	0.578
8	0.7384	0.797	0.789	-7.358	1.014
9	0.9037	0.968	0.967	-6.641	0.103
10	0.9973	1.151	1.151	-13.354	0.000
Average error E_{ω} (%)				10.847	0.367

5.4.2 Model updating using frequencies and incomplete mode shapes

The proposed model updating method is used to update the numerical model of actually constructed Canton Tower. The updated frequencies and MAC diagonal values of the reduced finite element model are summarised in Table 5.17, where the first five measured

frequencies and incomplete modes are utilised for model updating. The results show that the updated frequencies are much closer to the frequencies identified from vibration measurements, reducing the average frequency absolute error from 12.98% initially to 4.72% after updating. The obtained MAC diagonal values indicate that the updated mode shapes correlate well with the initial modes of the analytical model and also have good correlation with the modes identified from field measurements.

Table 5.17 Initial and updated modal properties of the reduced-order finite element model of the Canton Tower using five field measured incomplete modes

Mode	FE frequency (Hz)	Tested frequency (Hz)	Initial error (%)	MAC initial, tested	Updated frequency (Hz)	Updated error (%)	MAC updated, initial	MAC updated, tested
1	0.1109	0.094	17.9950	0.9004	0.0914	-2.7522	0.9081	0.9846
2	0.1588	0.140	13.4581	0.9341	0.1378	-1.5662	0.8599	0.9875
3	0.3473	0.367	-5.3711	0.9141	0.3655	-0.4079	0.9820	0.8991
4	0.3691	0.421	-12.3321	0.9438	0.3879	-7.8621	0.9856	0.9609
5	0.4003	0.475	-15.7237	0.8811	0.4227	-11.0161	0.9887	0.8689
Average error E_{ω} (%)			12.9760			4.7209		

In order to investigate the influence of the modal information required on the performance of structural model updating, information about first ten measured frequencies and incomplete modes (excluding the 6^{th} torsion mode) is adopted for updating the reduced finite elementmodel. Again, the updated frequencies become closer to the corresponding measured frequencies, with the average frequency absolute errors reduced from 10.8% to 5.12%. The obtained high MAC diagonal values indicate that the updated mode shapes correlate well

with both the initial analytical eigenvectors and measured mode shapes, as shown in Table 5.18.

Table 5.18 Initial and updated modal properties of the reduced-order finite element model of the Canton Tower using ten field measured incomplete modes

Mode	FE frequency (Hz)	Tested frequency (Hz)	Initial error (%)	MAC initial, tested	Updated frequency (Hz)	Updated error (%)	MAC updated, initial	MAC updated, tested
1	0.1109	0.094	17.9950	0.9004	0.0951	1.2036	0.9306	0.9603
2	0.1588	0.140	13.4581	0.9341	0.1401	0.0782	0.8971	0.9747
3	0.3473	0.367	-5.3711	0.9141	0.3635	-0.9607	0.9832	0.8689
4	0.3691	0.421	-12.3321	0.9438	0.4132	-1.8526	0.9977	0.9536
5	0.4003	0.475	-15.7237	0.8811	0.4367	-8.0640	0.9944	0.8519
6	0.4617	0.505	-8.5752	/	0.4614	-8.6259	0.7506	/
7	0.4868	0.519	-6.2068	0.7691	0.4968	-4.2796	0.9712	0.8696
8	0.7384	0.789	-6.4191	0.7792	0.7776	-1.4454	0.9881	0.8206
9	0.9037	0.967	-6.5440	0.7717	0.9301	-3.8203	0.9825	0.8477
10	0.9973	1.151	-13.3545	0.7015	0.9932	-13.7136	0.9889	0.6776
11	1.0375	1.190	-12.8175	0.7519	1.0434	-12.3207	0.9889	0.8203
Average error E_{ω} (%)			10.7998			5.1241		

The results for the updated stiffness parameters of the analytical model are shown in Figure 5.17 where the two cases with five and ten measured frequencies and incomplete modes used for model updating are considered. The values of stiffness updating parameters are relatively

small and reasonably consistent for both cases. In the case with five measured modes used in model updating, the obtained stiffness updating parameters range from -8.77% to 8.24% with an average of the absolute values of 2.70%. For the case with ten measured modes used, similar results are obtained and the updated stiffness parameters vary between -10.08% and 11.36% with an average of the absolute values of 3.41%. The results for the adjusted stiffness parameters for both cases are reasonably close to each other.

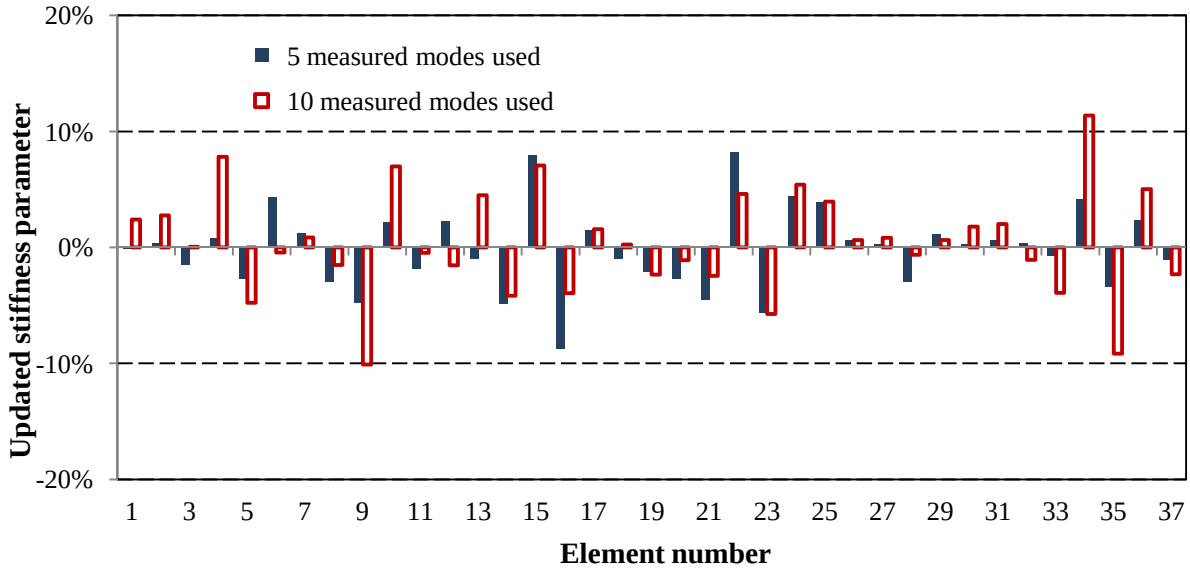

Figure 5.17 Updated stiffness parameters of the finite element model of the Canton Tower, 5 and 10 measured incomplete modes used

5.5 Conclusions

Space steel frame model structure is utilised to demonstrate the accuracy and effectiveness of the proposed model updating method to adjust the analytical model by using incomplete modal data obtained from numerical simulation investigations and experimental studies. The practical application of the proposed technique is demonstrated by correctly updating

thereduced finite element model of Canton Tower benchmark problem by using the operational modal properties identified from ambient vibration measurements.Based on the numerical simulations, experimental studies and practical applications, the following conclusions are drawn. 1) The proposed method is able tocorrectly update the structural parameters such as stiffness at both element and critical point levels, so that the stiffness at the connections of structural members such as beam-column joints can be modified from limited information of measured incomplete modes. 2) The proposed approach needs only little computational effort to estimate the structural updating parameters, and provides optimised solutions for model updating in the least squares sense without requiring objection functions or optimisation techniques. 3) The proposed technique performs well for various scenarios considered and providesrobust predictions of structural updating parameters even in the cases where relatively large modifications in structural parameters and/or modal properties exist between the finite element model and tested structure. 4) Tikhonov regularisation algorithm incorporating the L-curve criterion, is employedin order to reduce the influence of measurements errors in the modal data and provided stable solution for structural updating parameters. 5) Finally, the proposed model updating method provides reasonably small modifications of structural properties to minimise the relatively large difference between the modal data calculated from the initial finite elementmodel and those identified from the vibration measurements of actually constructed structures.

Chapter 6 Real-Time Structural Damage Detection

6.1 Introduction

The performance of existing structural systems is deteriorating with time due to the degradation of resistance capacity caused by the operation environments or severe loading events such as impact and earthquake. Structural damage detection methods are employed to detect the damage that may have occurred due to the severe loading events. A number developed damage detecting methods have been discussed in the Chapter 2 Literature Review. Most of those existing methods require the measured modal data such as frequencies and mode shapes, which have to be extracted from vibration measurements such as acceleration by using modal analysis techniques. In addition, these existing methods may not be able to deal with the evolution of structural damage during a dynamic loading event. Therefore, there is a need to develop an effective method for correctly quantifying the evolution of structural damage over time at specific locations in the structure directly from the monitored dynamic response data.

This chapter presents the development of effective method for identifying structural damage evolution over time directly from noisy dynamic response measurements such as accelerations. Based on the governing equations of motion, the relationship between the change in stiffness due to structural damage evolution and the associated dynamic response measurements of the monitored structural system is developed. Structural damage parameters associated with the elements stiffness matrices are selected to reflect the evolution of structural damage and to contain information about both damage location and severity development. The recorded dynamic response measurements can be directly adopted in the

developed equation to solve for the chosen structural damage parameters without requiring a modal analysis technique. The Newmark time step integration method is introduced to evaluate the structural damage parameters at each time step during dynamic loading period. The Tikhonov regularisation technique incorporating the L-curve criterion is then employed to provide stable solutions for the structural damage parameters from measured vibration data with uncertainties at each time step. Therefore, structural damage evolution with time, represented here by the obtained time-dependent damage parameters, is determined from the continuously monitored dynamic response data. The proposed real-time damage detection method requires measured dynamic responses in all degrees of freedom of the structure and same applied force for both undamaged and damaged structures.

6.2 Inversely detecting structural damage using expanded mode shapes

Recently, significant research works have been done in the area of detecting damages in the structures using dynamic response data (Humar et al. 2006, Yu et al. 2007). However, the measured data set is normally incomplete as the numbers of measured locations of the tested structure are usually less than the number of degrees of freedom of the analytical model (Yuen 2012). The data set of measurements only exists at degrees of freedom associated with the tested locations. Therefore, it is desirable to expand the measured data set onto the associated full analytical coordinate set because model reduction process produces the modelling errors and also destroys the original sparse pattern in mass and stiffness matrices.

This study uses the new mode shape expansion technique for detecting damage in the structure. The process of damage detection utilises the complete mode shapes at all degrees

of freedom of the damaged structure that is expanded from the measured incomplete modal data. Two damage detection techniques, i.e. mode shape curvature change and modal strain energy method (Cornwell et al. 1999) are employed in the inverse detection of structural damage. The results from the numerical example show that damage location can be detected from the expanded mode shapes.

6.2.1 Mode shape expansion

Mode shape expansion is useful in many applications, such as for finite element model updating and structural damage detection. Most mode shape expansion methods utilise transformation matrix to obtain the unmeasured mode components of the actual tested dynamic system. The characteristic equation of a dynamic structural system is expressed as

$$(\mathbf{K} - \omega_i^2 \mathbf{M})\boldsymbol{\phi}_i = \mathbf{0} \tag{6.1}$$

where ω_i and $\boldsymbol{\phi}_i$ are the i^{th} natural frequency and the associated eigenvector of the original structure, respectively. Similarly, the characteristic equation for the tested structure is

$$(\tilde{\mathbf{K}} - \tilde{\omega}_i^2 \tilde{\mathbf{M}})\tilde{\boldsymbol{\phi}}_i = \mathbf{0} \tag{6.2}$$

where the superscript '~' denotes the quantitative of the tested structure. It is assumed here that $\tilde{\omega}_i$ and the incomplete set of measured degrees of freedom $\tilde{\boldsymbol{\psi}}_i$ of the tested structure are obtained from the structural dynamic testing. Then, $\tilde{\boldsymbol{\psi}}_i$ needs to be factored by mode scale

factor υ_i in order to make the measured mode shapes close to the corresponding part of the analytical mode shapes $\boldsymbol{\phi}_i^a$, as

$$\tilde{\boldsymbol{\phi}}_i^a = \upsilon_i \tilde{\boldsymbol{\psi}}_i \quad \text{in which} \quad \upsilon_i = \frac{\boldsymbol{\phi}_i^T \mathbf{M} \boldsymbol{\phi}_i^a}{\boldsymbol{\phi}_i^T \mathbf{M} \tilde{\boldsymbol{\psi}}_i} \tag{6.3}$$

The incomplete set of modal measurements $\tilde{\boldsymbol{\phi}}_i^a$ can then be expanded by using mode shape expansion approach (Chen 2010) onto the full set of analytical model, as

$$\tilde{\boldsymbol{\phi}}_i = \mathbf{T}_p \tilde{\boldsymbol{\phi}}_i^a \tag{6.4}$$

Here, the transformation matrix, $\mathbf{T}_p$, for mode shape expansion is defined as

$$\mathbf{T}_p = \begin{bmatrix} \mathbf{I} \\ \mathbf{T}' \end{bmatrix} \quad \text{in which} \quad \mathbf{T}' = \sum_{k=1}^{N} \frac{\boldsymbol{\phi}_k^u \boldsymbol{\phi}_k^T \mathbf{S}^+}{(\tilde{\omega}_i^2 - \omega_k^2)} \tag{6.5}$$

where $\boldsymbol{\phi}_k^u$ is the analytical mode shape associated with the unmeasured partition and *N* denotes number of original eigenvectors available. The matrix $\mathbf{S}^+$ is the Moore-Penrose pseudo inverse of sensitivity coefficient matrix **S**, calculated from

$$\mathbf{S} = \sum_{k=1}^{N} \frac{\boldsymbol{\phi}_k^a \cdot \boldsymbol{\phi}_k^T}{(\tilde{\omega}_i^2 - \omega_k^2)} \tag{6.6}$$

The MAC factors are used here to verify the correlation between the expanded measured mode shapes $\tilde{\boldsymbol{\phi}}_i$ and the analytical mode shapes $\boldsymbol{\phi}_k$, defined in Eq.(2.1).

6.2.2 Damage detection

From the beam theory, the curvature of beam deformation is inversely proportional to the flexural stiffness of the beam. The reduction in stiffness caused by damage tends to increase the curvature of the mode shape around the damaged region. A curvature change can be used to detect the damage location in the structure (Qiao et al 2007, Gandomi et al. 2008).It can be estimated numerically by using central difference quotient method from the displacement of mode shapes. Expanded mode shapes are required in order to calculated the mode shape curvature which is defined for the i^{th} expanded mode $\tilde{\boldsymbol{\phi}}_i$ as

$$\tilde{\boldsymbol{\phi}}''_{x,i} = \frac{\tilde{\boldsymbol{\phi}}_{x+1,i} - 2\tilde{\boldsymbol{\phi}}_{x,i} + \tilde{\boldsymbol{\phi}}_{x-1,i}}{\Delta x^2} \tag{6.7}$$

where$x$, x+1 and x-1 are coordinate difference of the curvature of the i^{th} mode shape (Carden and Fanning 2004, Jag et al. 2006). Furthermore, the extent of damage can be estimated by measuring the amount of change in the mode shape curvature at the damaged region. Moreover, the modal strain energy (*MSE*), defined as the product of the elemental stiffness matrix and its mode shape component in (Shi et al. 2000), is also employed for structural damage detection. For the j^{th} element and i^{th} mode shape of undamaged structure, the *MSE* is given as

$$MSE_{ij} = \boldsymbol{\phi}_i^T \mathbf{K}_j \boldsymbol{\phi}_i \tag{6.8}$$

Since the damaged element is not known, the undamaged elemental stiffness matrix $\mathbf{K}_j$ is used instead of damaged one to approximate *MSE* for j^{th} damaged element and i^{th} damaged mode shape, expressed as

$$\tilde{MSE}_{ij} = \tilde{\boldsymbol{\phi}}_i^T \mathbf{K}_j \tilde{\boldsymbol{\phi}}_i \tag{6.9}$$

The elemental modal strain energy ratio (*MSECR*) then can be utilised as an indicator for damage localization, defined as (Shi et al. 2000)

$$\tilde{MSECR}_{ij} = \frac{\left| \tilde{MSE}_{ij} - MSE_{ij} \right|}{MSE_{ij}} \tag{6.10}$$

The location of damage in the structure then could be detected by using the indicators discussed above.

6.2.3 Numerical example

In structural dynamic testing, dynamic responses are obtained from installed sensors. Due to economic constraint, limited number of sensors are available and measured mode shapes are

usually incomplete. Those incomplete mode shapes can be expanded by using mode shape expansion method. For the purpose of inversely detecting damage in the structure by utilising incomplete measured data and mode shape expansion method, a numerical example of steel bridge structure is selected as shown inFigure 6.1. In this example, the numerically generated modal data of the damaged structure, replacing experimental measurements, are adopted in the calculations.

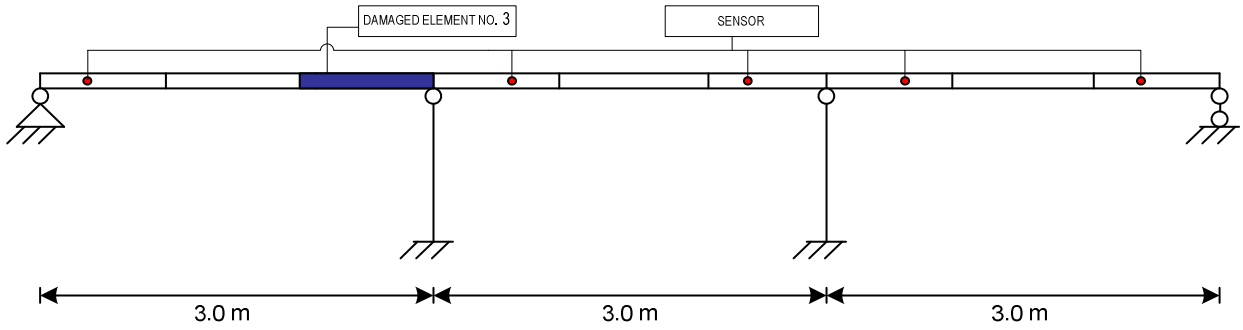

Figure 6.1 Finite element model of three span bridge with simulated sensors and damaged element

To evaluate the effectiveness of the damage detection method discussed above, one damage case is simulated by assuming that a single element (element No.3) in the 1st span is damaged by reducing *EI* value of -50%. Finite element dynamic analysis is performed in order to compute the analytical mode shapes of the damaged structure. The incomplete mode shapes of damaged structure are obtained by selecting the mode values at degrees of freedom of five sensors from the complete analytical mode shapes. Those incomplete mode shapes are fully expanded by using the mode shape expansion method (Chen 2010) and then the expanded mode shapes are utilised for detecting the simulated damage in the structure. The results inFigure 6.2given by the 4th expanded mode shape for the damaged structure, indicate that the

deformation of the damaged mode shape curvature in the region of damaged element No. 3 is clearly larger than the undamaged mode shape curvature. The possible damage location could be identified from the largest percent of curvature change at element No. 3, as indicated inFigure 6.3, and largest modal strain energy ratio at element No. 3 as shown in Figure 6.4Similar results can also be seen in the Figure 6.5toFigure 6.7 given by the 6th expanded damaged mode.

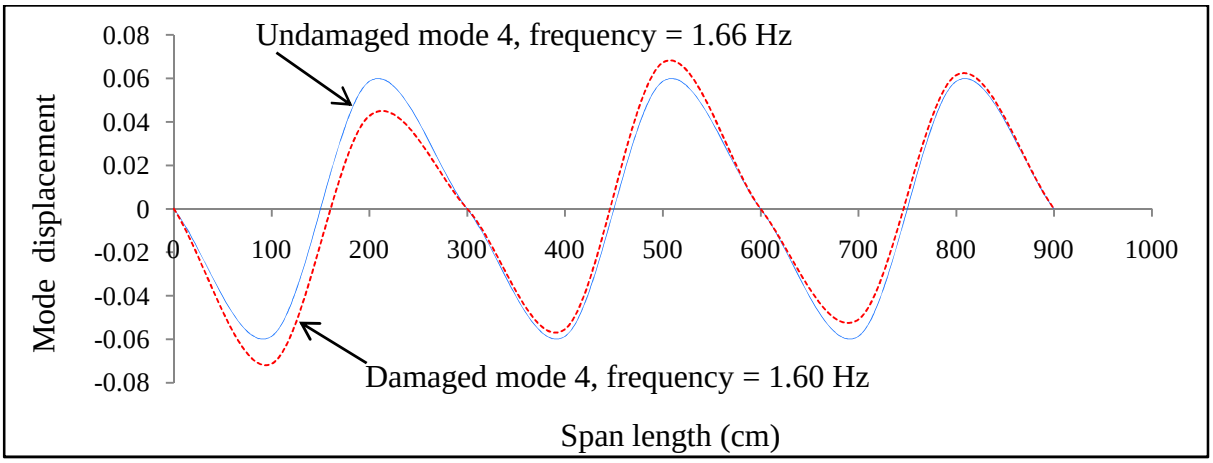

Figure 6.2 4th undamaged and damaged mode shapes

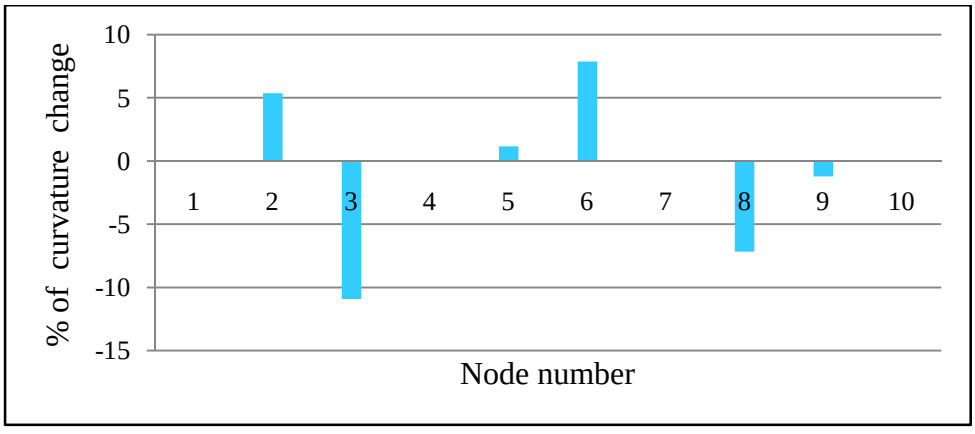

Figure 6.3 Percentage of mode shape curvature change for the 4th expanded mode

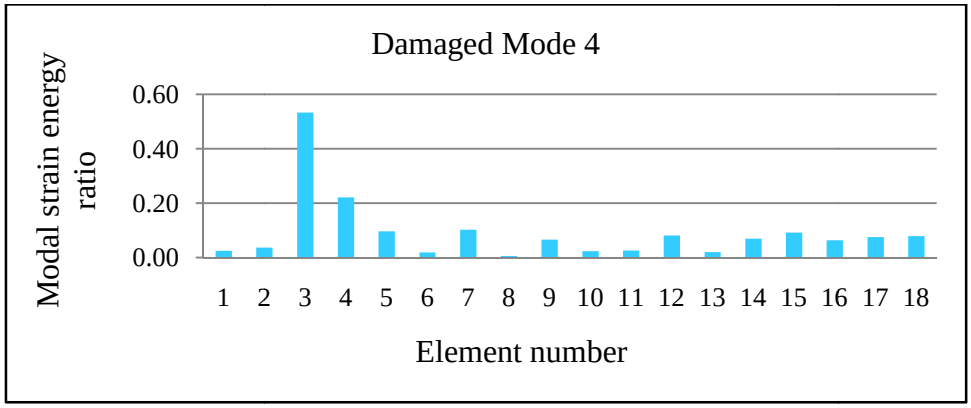

Figure 6.4 Modal strain energy ratio using damaged mode 4

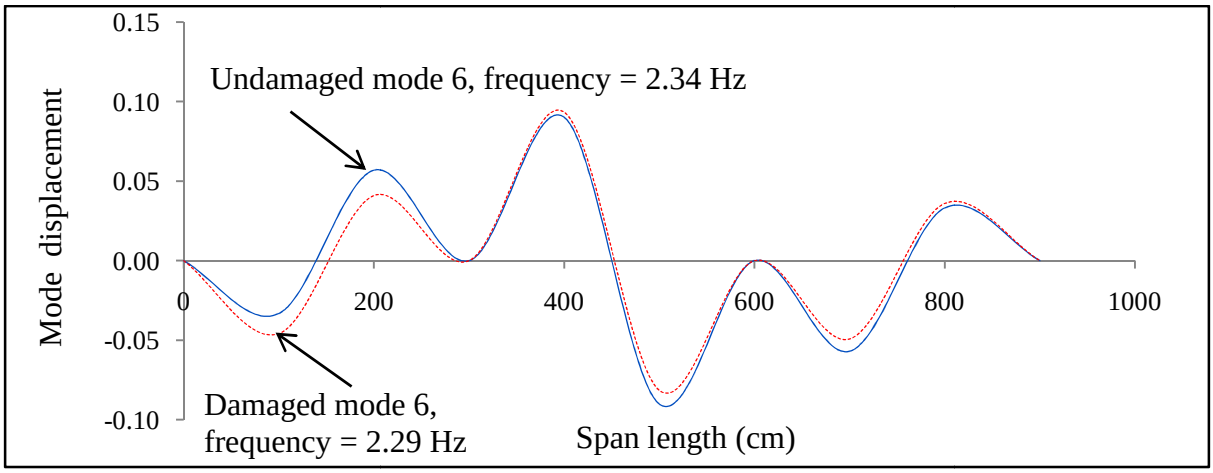

Figure 6.5 6th undamaged and damaged mode shapes

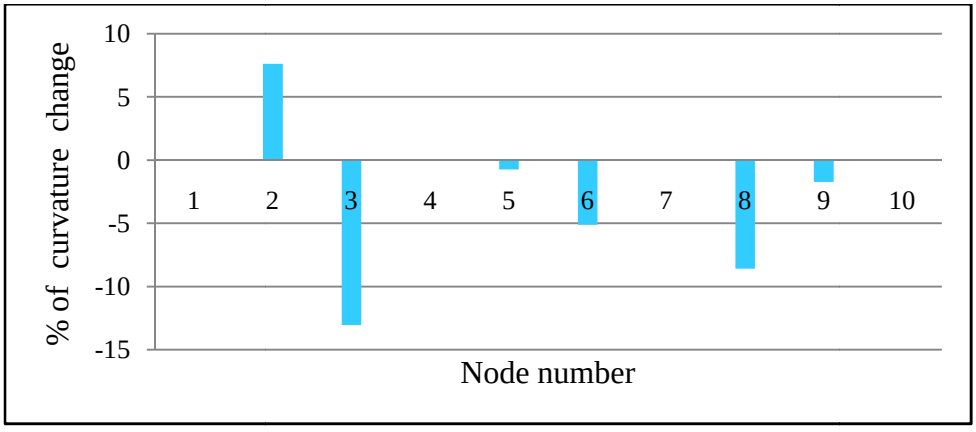

Figure 6.6 Percentage of mode shape curvature change for the 6th expanded mode

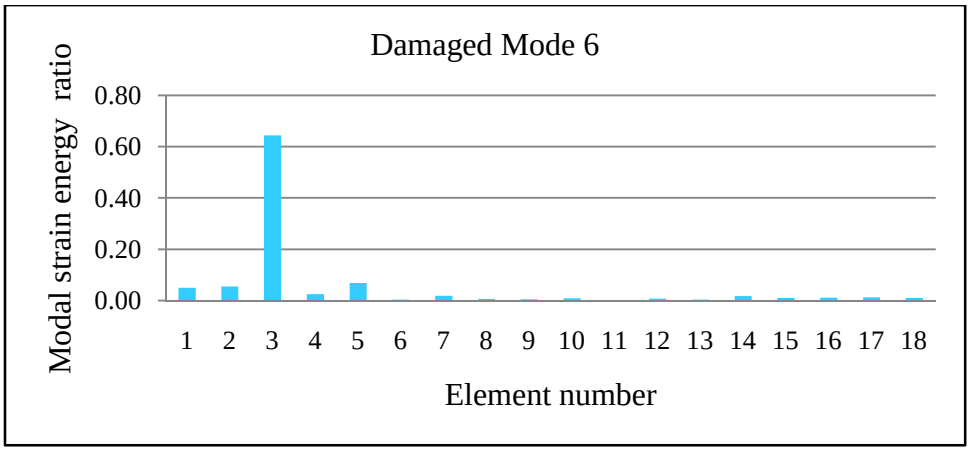

Figure 6.7 Modal strain energy ratio using damaged mode 6

The numerical simulation results of a bridge modelled with plane beam elements show that damage in the structure could be located from the limited vibration measurements utilising changes in mode shape curvatures and modal strain energy calculated from the expanded mode shapes.

6.3 Basic equation

The equation of motion for the structural dynamics system is given by

$$\mathbf{M}\ddot{\mathbf{U}}_i + \mathbf{C}\dot{\mathbf{U}}_i + \mathbf{K}\mathbf{U}_i = \mathbf{F}_i \tag{6.11}$$

where "i" represents the time step at t_i, $\mathbf{C}$ and $\mathbf{F}_i$ are global damping matrix and applied force vector respectively. Time dependent variable $\mathbf{U}_i$, $\dot{\mathbf{U}}_i$, and $\ddot{\mathbf{U}}_i$ are nodal displacement,

velocity and acceleration, respectively.Similarly, equation of motion for the damaged structure can also be given by

$$\mathbf{M}^d\ddot{\mathbf{U}}_i^d + \mathbf{C}^d\dot{\mathbf{U}}_i^d + \mathbf{K}^d\mathbf{U}_i^d = \mathbf{F}_i^d \tag{6.12}$$

For the damaged structure, $\mathbf{K}^d$ and $\mathbf{M}^d$ are expressed as

$$\mathbf{K}^d = \mathbf{K} + \Delta\mathbf{K} \tag{6.13}$$

$$\mathbf{M}^d = \mathbf{M} \tag{6.14}$$

In which mass matrix is assumed to remain unchanged.The change in the structural stiffness matrix $\Delta\mathbf{K}$ is given by (Chen and Bicanic 2006, Maung et al. 2012)

$$\Delta\mathbf{K} = \sum_{j=1}^{NE} \alpha_j \mathbf{K}_j \tag{6.15}$$

where *NE* is the total number of structural elements in the system, $\mathbf{K}_j$ is the contribution of the j^{th} element to the global stiffness matrix and α_j is the damage parameter associated with the j^{th} element which ranges from "0" to "-1". Damage parameter α_j can provide information about the location and extent of damage in the structure. For damage location, the j^{th} element is considered as damaged element if the value of damage parameter α_j is not equal to zero, whereas for the damage quantification, the damage extent of the j^{th} element is determined by

the magnitude of the damage parameter α_j. As a result, structural damage can be detected by determining the damage parameter α_j.

Newmark (1959) introduced a time integration method for solving structural dynamic problems (Clough and Penzien 1975). Here, Newmark's method is implemented into the formulation of new damage detection technique. A harmonic force is considered as applied force on both undamaged and damaged structures. In the Newmark's method, displacement and velocity for the next time step are given by

$$\mathbf{U}_{i+1} = \mathbf{U}_i + \Delta t\dot{\mathbf{U}}_i + (0.5-\delta)\Delta t^2\ddot{\mathbf{U}}_i + \delta\Delta t^2\ddot{\mathbf{U}}_{i+1} \tag{6.16}$$

$$\dot{\mathbf{U}}_{i+1} = \dot{\mathbf{U}}_i + \Delta t[(1-\gamma)\ddot{\mathbf{U}}_i + \gamma\ddot{\mathbf{U}}_{i+1}] \tag{6.17}$$

where "$i+1$" denotes the next time step $t_i + \Delta t$. In Newmark's method coefficients $\delta = \frac{1}{4}$ and $\gamma = \frac{1}{2}$ are required for the algorithm to be second order accuracy and unconditionally stable. The time history is divided into a sequence of equal time steps Δt.

In the case of using displacement sensors, acceleration and velocity can be computed from measured displacement data by using the following derivation based on Newmark's method. $\mathbf{U}_{i+1}$, $\dot{\mathbf{U}}_{i+1}$, and $\ddot{\mathbf{U}}_{i+1}$ can be expressed as incremental form

$$\mathbf{U}_{i+1} = \mathbf{U}_i + \Delta\mathbf{U}_i \tag{6.18}$$

$$\dot{\mathbf{U}}_{i+1} = \dot{\mathbf{U}}_i + \Delta\dot{\mathbf{U}}_i \tag{6.19}$$

$$\ddot{\mathbf{U}}_{i+1} = \ddot{\mathbf{U}}_i + \Delta\ddot{\mathbf{U}}_i \tag{6.20}$$

where $\Delta\mathbf{U}_i$, $\Delta\dot{\mathbf{U}}_i$, and $\Delta\ddot{\mathbf{U}}_i$ are incremental displacement, velocity and acceleration, respectively. Substituting $\mathbf{U}_{i+1}$ in Eq.(6.18) into Eq.(6.16) gives

$$\Delta\ddot{\mathbf{U}}_i = \frac{1}{\delta\Delta t^2}\Delta\mathbf{U}_i - \frac{1}{\delta\Delta t}\dot{\mathbf{U}}_i - \frac{1}{2\delta}\ddot{\mathbf{U}}_i \tag{6.21}$$

Similarly, substituting Eq.(6.19) into Eq.(6.17) leads to

$$\Delta\dot{\mathbf{U}}_i = \Delta t\ddot{\mathbf{U}}_i + \gamma\Delta t\Delta\ddot{\mathbf{U}}_i \tag{6.22}$$

From $\Delta\ddot{\mathbf{U}}_i$ in Eq.(6.21), Eq.(6.22) becomes

$$\Delta\dot{\mathbf{U}}_i = \frac{\gamma}{\delta\Delta t}\Delta\mathbf{U}_i - \frac{\gamma}{\delta}\dot{\mathbf{U}}_i + \Delta t(1-\frac{\gamma}{2\delta})\ddot{\mathbf{U}}_i \tag{6.23}$$

Equation of motion for the time step "i+1" can be described by

$$\mathbf{M}\ddot{\mathbf{U}}_{i+1} + \mathbf{C}\dot{\mathbf{U}}_{i+1} + \mathbf{K}\mathbf{U}_{i+1} = \mathbf{F}_{i+1} \tag{6.24}$$

The difference between Eqs.(6.11) and(6.24) gives the incremental equilibrium equation of motion

$$\mathbf{M}\Delta\ddot{\mathbf{U}}_i + \mathbf{C}\Delta\dot{\mathbf{U}}_i + \mathbf{K}\Delta\mathbf{U}_i = \Delta\mathbf{F}_i \tag{6.25}$$

where $\Delta\mathbf{F}_i$ is incremental applied force. From $\Delta\ddot{\mathbf{U}}_i$ in Eq.(6.21) and $\Delta\dot{\mathbf{U}}_i$ in Eq.(6.23), Eq.(6.25) is rewritten as

$$^{*}\mathbf{K}\Delta\mathbf{U}_i = {}^{*}\mathbf{F}_i \tag{6.26}$$

where

$$^{*}\mathbf{K} = \frac{1}{\delta\Delta t^2}\mathbf{M} + \frac{\gamma}{\delta\Delta t}\mathbf{C} + \mathbf{K} \tag{6.27}$$

$$^{*}\mathbf{F}_i = \Delta\mathbf{F}_i + [\frac{1}{2\delta}\mathbf{M} + \Delta t(\frac{\gamma}{2\delta} - 1)\mathbf{C}]\ddot{\mathbf{U}}_i + [\frac{1}{\delta\Delta t}\mathbf{M} + \frac{\gamma}{\delta}\mathbf{C}]\dot{\mathbf{U}}_i \tag{6.28}$$

with the knowledge of system properties, $\dot{\mathbf{U}}_i$ and $\ddot{\mathbf{U}}_i$ at the initial time, $\Delta\mathbf{U}_i$ at time step "i"can be computed by inverting $^{*}\mathbf{K}$ in Eq.(6.26) as

$$\Delta\mathbf{U}_i = {}^{*}\mathbf{K}^{-1}{}^{*}\mathbf{F}_i \tag{6.29}$$

In which, ${}^{*}\mathbf{K}^{-1}$ is a square matrix. Once $\Delta\mathbf{U}_i$ is known $\Delta\ddot{\mathbf{U}}_i$ and $\Delta\dot{\mathbf{U}}_i$ can be computed from Eq.(6.21) and Eq.(6.23), respectively. Similarly, $\mathbf{U}_{i+1}$, $\dot{\mathbf{U}}_{i+1}$, and $\ddot{\mathbf{U}}_{i+1}$ can also be computed from Eq.(6.18), Eq.(6.19) and Eq.(6.20).

6.4 Inverse prediction of damage parameter

Substitution of damaged stiffness $\mathbf{K}^d$ from Eq.(6.13) into Eq.(6.12) and assuming unchanged mass and damping for the damaged dynamic system lead to

$$\mathbf{M}\ddot{\mathbf{U}}_i^d + \mathbf{C}\dot{\mathbf{U}}_i^d + (\mathbf{K}+\Delta\mathbf{K})\mathbf{U}_i^d = \mathbf{F}_i \tag{6.30}$$

Evidently, the right-hand side equality of Eq.(6.11) and Eq.(6.30) gives

$$\mathbf{M}\ddot{\mathbf{U}}_i^d + \mathbf{C}\dot{\mathbf{U}}_i^d + (\mathbf{K}+\Delta\mathbf{K})\mathbf{U}_i^d = \mathbf{M}\ddot{\mathbf{U}}_i + \mathbf{C}\dot{\mathbf{U}}_i + \mathbf{K}\mathbf{U}_i \tag{6.31}$$

Simply, Eq.(6.31) can be rewritten in the following form

$$\Delta\mathbf{K}\mathbf{U}_i^d = \mathbf{M}(\ddot{\mathbf{U}}_i - \ddot{\mathbf{U}}_i^d) + \mathbf{C}(\dot{\mathbf{U}}_i - \dot{\mathbf{U}}_i^d) + \mathbf{K}(\mathbf{U}_i - \mathbf{U}_i^d) \tag{6.32}$$

From $\Delta\mathbf{K}$ in Eq.(6.15), Eq.(6.32) becomes

$$\sum_{j=1}^{NE} \alpha_j \mathbf{K}_j \mathbf{U}_i^d = \mathbf{M}(\ddot{\mathbf{U}}_i - \ddot{\mathbf{U}}_i^d) + \mathbf{C}(\dot{\mathbf{U}}_i - \dot{\mathbf{U}}_i^d) + \mathbf{K}(\mathbf{U}_i - \mathbf{U}_i^d) \tag{6.33}$$

Only damage parameter α_j is an unknown vector in the above equation. Therefore, Eq.(6.33) can be expressed as a set of linear algebraic equation in the following form

$$\mathbf{A}\boldsymbol{\alpha} = \mathbf{b} \tag{6.34}$$

in which row vectors $\mathbf{a}_j$ in matrix **A** and vector **b** are defined as

$$\mathbf{a}_j = \mathbf{K}_j \mathbf{U}_i^d \tag{6.35}$$

$$\mathbf{b} = \mathbf{M}(\ddot{\mathbf{U}}_i - \ddot{\mathbf{U}}_i^d) + \mathbf{C}(\dot{\mathbf{U}}_i - \ddot{\mathbf{U}}_i^d) + \mathbf{K}(\mathbf{U}_i - \mathbf{U}_i^d) \tag{6.36}$$

In Eq.(6.34), the inverse of **A** may not exist since the coefficient matrix **A** may not be square. In these cases, the inverse will befound via the Moore-Penrose pseudoinverse method and the damage parameters can be estimated from

$$\boldsymbol{\alpha} = \mathbf{A}^{+}\mathbf{b} = (\mathbf{A}^T\mathbf{A})^{-1}\mathbf{A}^T\mathbf{b} \tag{6.37}$$

where $\mathbf{A}^+$ is the Moore-Penrose pseudoinverse matrix in a least squares sense, which can be calculated from SVD. Consequently, the location and amount of damage can be determined by the obtained damage parameters at detailed level.

6.4.1 Flowchart for calculation of damage parameter

In order to understand more clearly on the process of proposed method, a flowchart of computational procedure for damage parameter α_j from the developed equation is presented as

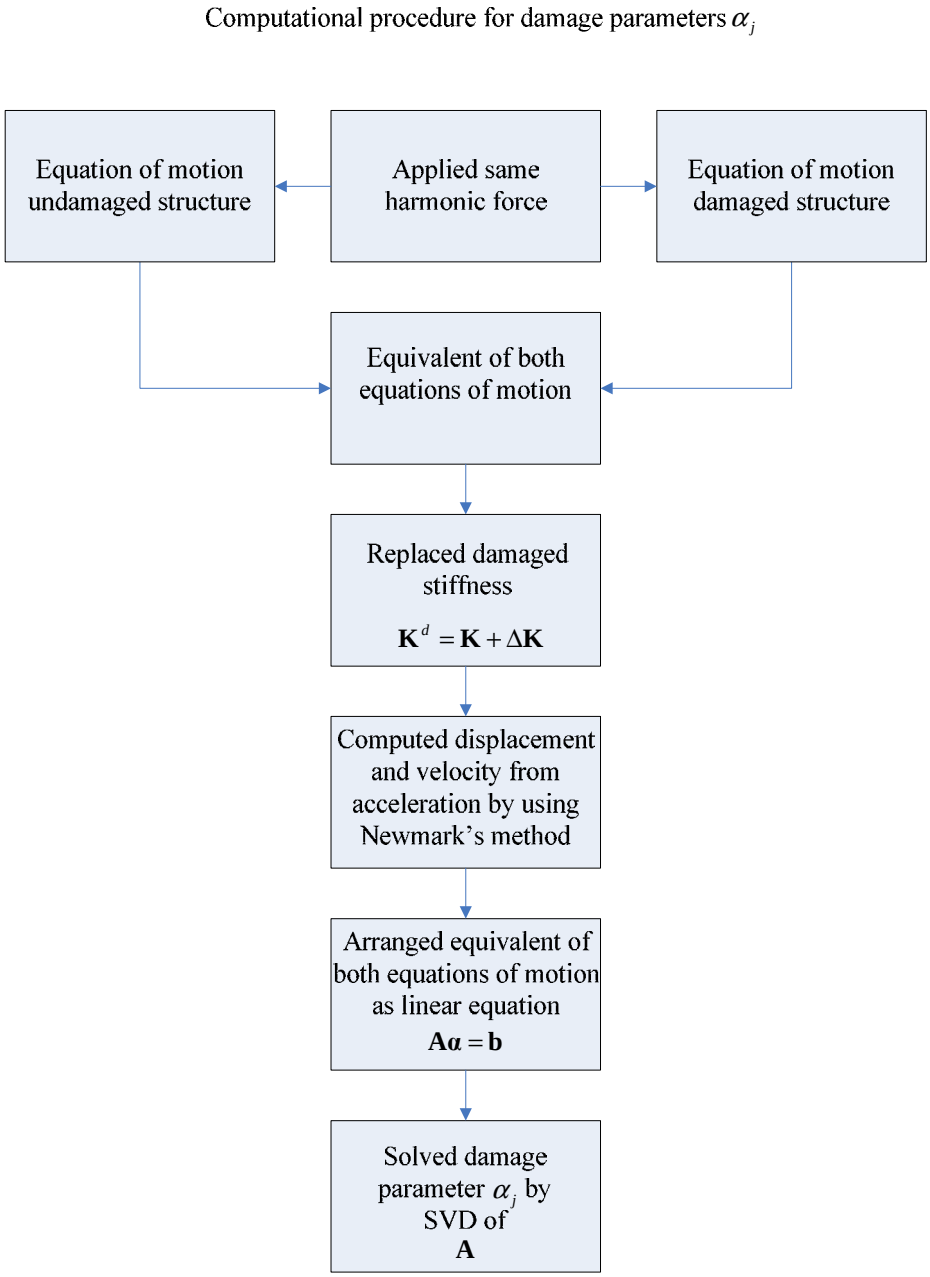

Figure 6.8 Flowchart for calculation of damage parameters α_j

6.5 Numerical example

A cantilever beam comprising of 10 elements is selected as a numerical example to demonstrate the applicability of proposed approach.Assumed set of geometric and material properties for the beam structure is adopted as cross sectional area $A = 64.9\,\text{cm}^2$, area moment of inertia $I = 1.4136\,\text{x}\,10^4\ \text{cm}^4$, Young's modulus $E = 2.0\,\text{x}\,10^4\ \text{kN/cm}^2$, and density $\rho = 7.850\,\text{x}\,10^{-3}\ \text{kg/cm}^3$ .In order to understand how the procedure works, three damage scenarios are considered as summarised in Table 6.1. Structural damages are assumed reduction in stiffness and mass remained unchanged.

Table 6.1 Simulated damage scenarios for the cantilever beam

Damage scenario	Element number	Damage amount (%)
1	1	-10
2	1	-10
	3	-20
	4	-30
3	1	-10
	3	-5
	4	-5

Only the first element is assumed to be damaged 10% damage in damage scenario 1. In damage scenario 2, elements 1, 3 and 4 are assumed as 10%, 20% and 30% damage, respectively. Additional damage scenario 3 based on the damage scenario 2 is

assumedelement 1 unchanged and element 3 and 4 damaged with the same amount of 5% damaged. For simplicity and future purpose of laboratory experiment using harmonic input force, same harmonic force is applied on both undamaged and damaged structures. Noise is not considered for this example but will be included for the next examples. The location and amount of the simulated damage are then determined from the inverse calculations of the damage parameter α_j.

6.5.1 Damage scenario 1

Firstly, the simulated damage scenario 1 is considered, as shown in Figure 6.9 .The proposed approach is employed to inversely identify the simulated damage in the structure. Figure 6.10 shows the results for inverse predictions of damage parameter α_j without considering the damping effect in the structure. The damaged element 1 with damage amount of 10% is clearly identified while the other elements are identified as undamaged elements. This gives an excellent agreement with the assumed simulation. From the results shown inFigure 6.11, the damping of the structure has little influence on the inverse structural damage identification.

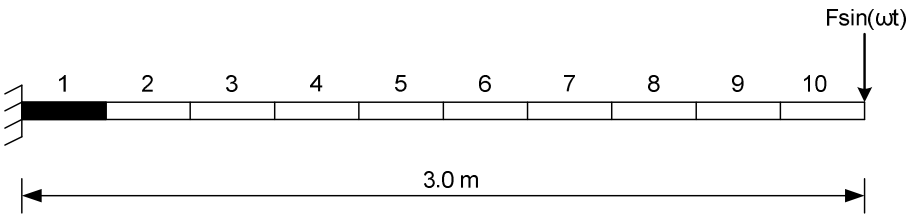

Figure 6.9 Cantilever beam subject to harmonic force with simulated damaged element 1 in damage scenario 1

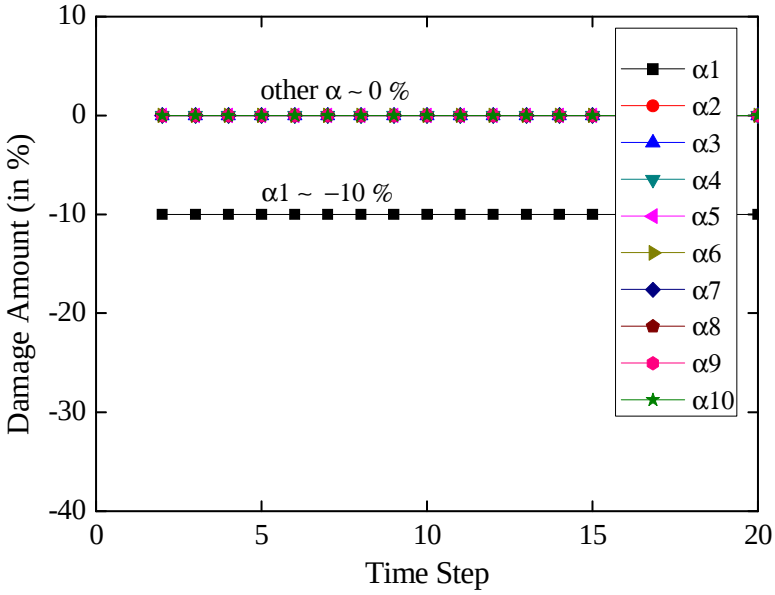

Figure 6.10 Inversely identified damage parameters in real time for damage scenario 1 without damping where only element 1 damaged by 10%

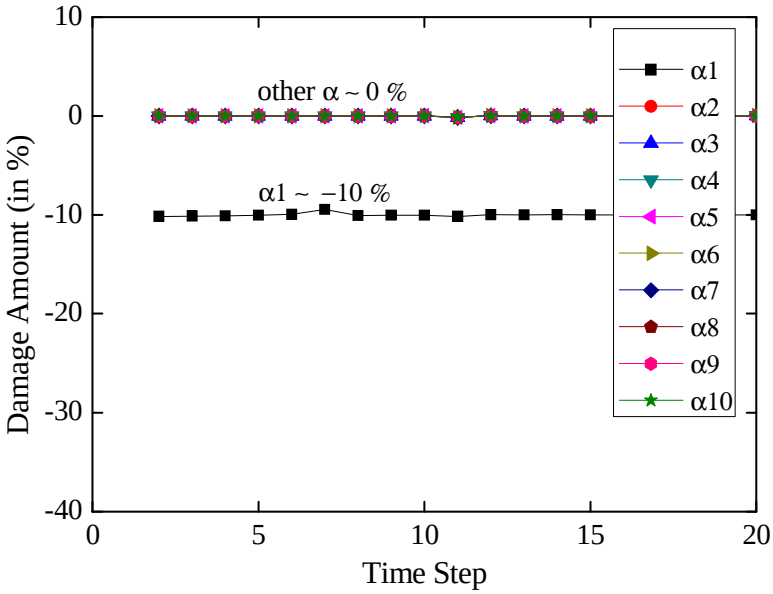

Figure 6.11 Inversely identified damage parameters in real time for damage scenario 1 with damping where only element 1 damaged by 10%

6.5.2 Damage scenario 2

In damage scenario 2, structural damage at multiple locations in various damage magnitudes is considered, as shown in Figure 6.12. The results for inverse predictions damage parameter α_j with no damping effect in the structure are indicated inFigure 6.13 and Figure 6.14. Again, the proposed approach provides accurate inverse predictions of the simulated damage for this complex case, and the obtained results agree well with the locations and magnitudes of simulated structural damage. The results also show that the inverse predictions for the undamped structure are better and stable, comparing with the results of damped structure as shown in Figure 6.14. The damping therefore may affect the structural damage identification in the cases of severe damage at multiple locations. The identified damage parameter for element 2 is slightly influenced by the damping with oscillation at the beginning of time steps due to the severe damage inthe neighbor elements 1, 3 and 4.

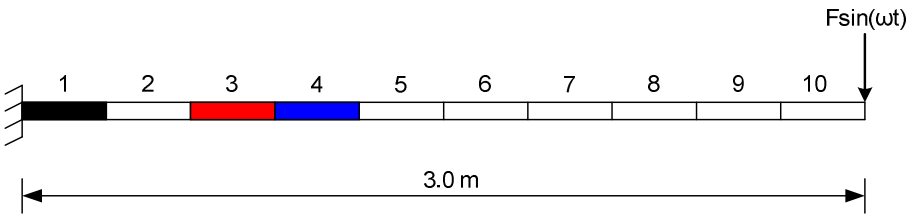

Figure 6.12 Cantilever beam subject to harmonic force with simulated damagedelements 1, 3 and 4 in damage scenario 2

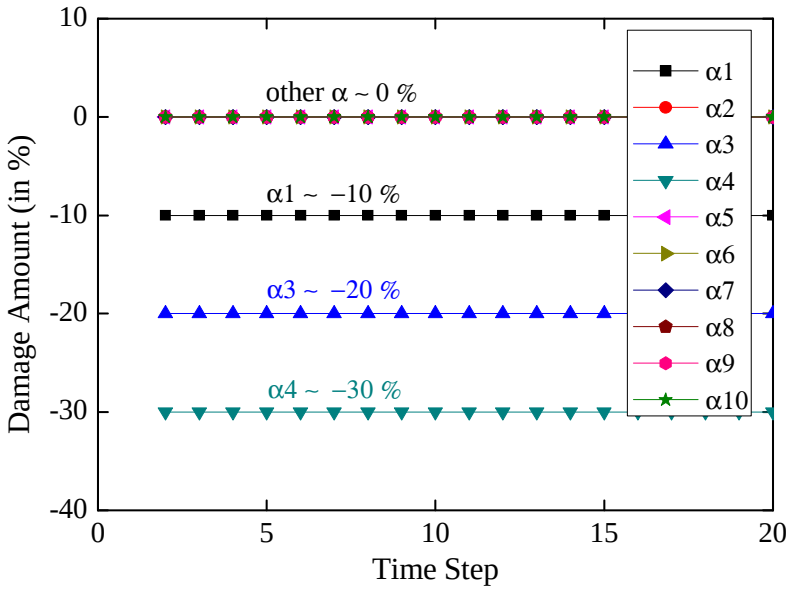

Figure 6.13 Inversely identified damage parameters in real time for damage scenario 2 without dampingwhere elements 1, 3 and 4 damaged in 10%, 20% and 30%, respectively

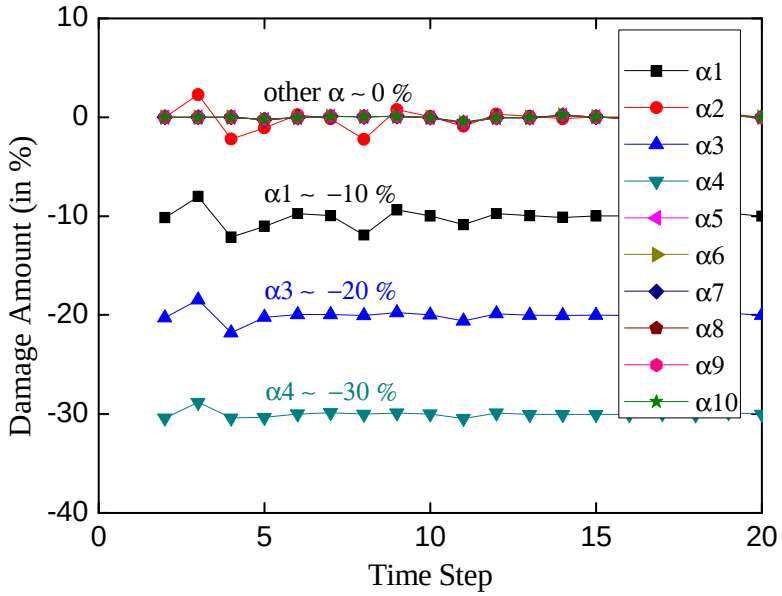

Figure 6.14 Inversely identified damage parameters in real time for damage scenario 2 with damping where elements 1, 3 and 4 damaged in 10%, 20% and 30%, respectively

6.5.3 Damage scenario 3

For the additional damage scenario 3 assuming element 1 damaged 10%, both elements 3 and 4 damaged equal amount of 5%, the identified damage parameters are presented in Figure 6.15 and Figure 6.16by using the proposed technique without and with damping, respectively. It can be seen that influence of surrounding damaged elements on the predictions of damage parameter for element 2 is reduced significantly and stable predictions are then obtained for all damage parameters for all elements concerned.

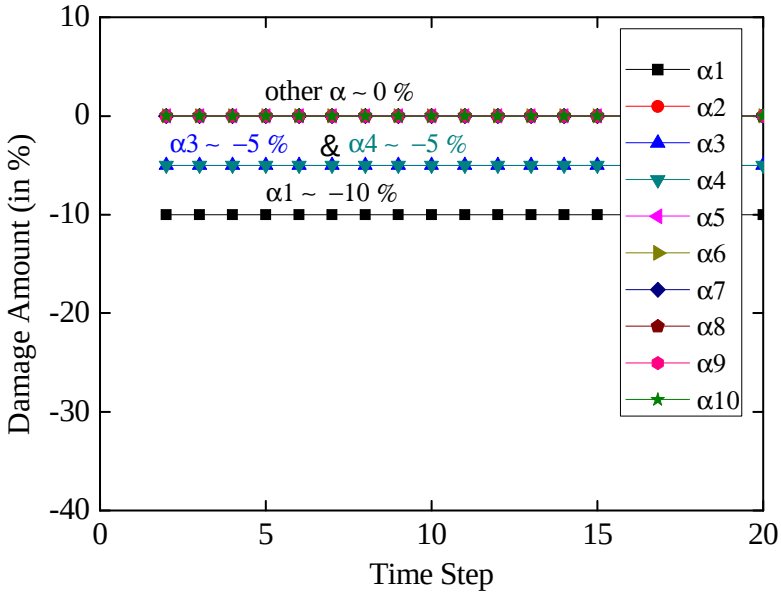

Figure 6.15 Inversely identified damage parameters in real time for damage scenario 3 without damping where elements 1, 3 and 4 are damaged in 10%, 5% and 5%, respectively

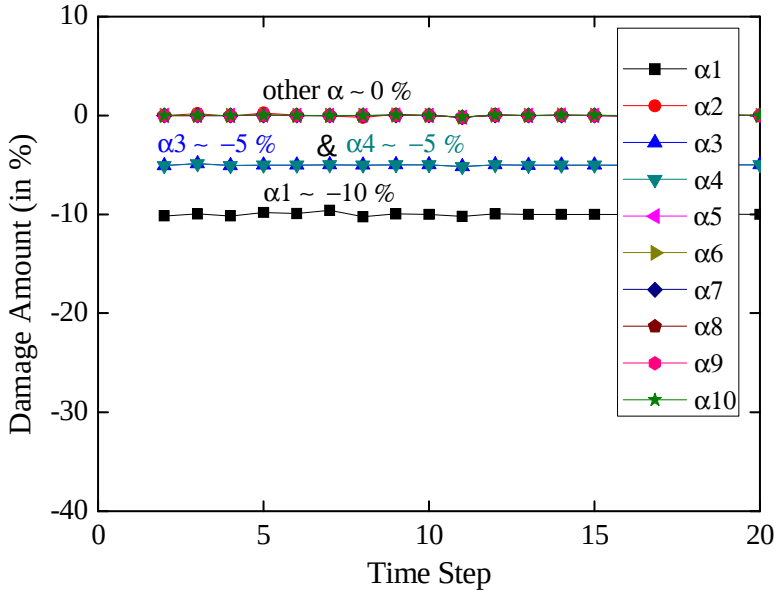

Figure 6.16 Inversely identified damage parameters in real time for damage scenario 3 with damping where elements 1, 3 and 4 are damaged in 10%, 5% and 5%, respectively

6.6 Further damage parameter equation

In this study, Rayleigh damping matrix is used in the formulation of damage parameter equation (Clough and Penzien 1975). Subtraction of Eq.(6.12) from Eq.(6.11) gives

$$\mathbf{M}\ddot{\mathbf{U}}_i - \mathbf{M}^d\ddot{\mathbf{U}}_i^d + \mathbf{C}\dot{\mathbf{U}}_i - \mathbf{C}^d\dot{\mathbf{U}}_i^d + \mathbf{K}\mathbf{U}_i - \mathbf{K}^d\mathbf{U}_i^d = \mathbf{F}_i - \mathbf{F}_i^d \tag{6.38}$$

In which, damping matrix is assumed to be proportional to a combination of mass and the stiffness matrices as

$$\mathbf{C} = c_m \mathbf{M} + c_k \mathbf{K} \tag{6.39}$$

$$\mathbf{C}^d = c_m^d \mathbf{M}^d + c_k^d \mathbf{K}^d \tag{6.40}$$

Substituting $\mathbf{K}^d$ in Eq.(6.13) into Eq.(6.40) gives

$$\mathbf{C}^d = c_m^d \mathbf{M} + c_k^d \mathbf{K} + c_k^d \Delta\mathbf{K} \tag{6.41}$$

The above damping factors c_m and c_k can be calculated from

$$c_m = \frac{2\varsigma\omega_m\omega_n}{\omega_m + \omega_n} \tag{6.42}$$

$$c_k = \frac{2\varsigma}{\omega_m + \omega_n} \tag{6.43}$$

where ς is the damping ratio of the structural system. ω_m is generally taken as fundamental circular frequency and ω_n is set among the higher circular frequencies of the analytical structural system (Clough and Penzien 1975). ω_m and ω_n can be obtained from the finite element analysis of analytical model. In the calculation, c_m^d and c_k^d are assumed same value as c_m and c_k. Substituting $\mathbf{M}^d$, $\mathbf{C}^d$ and $\mathbf{K}^d$ into Eq.(6.38) leads to

$$\mathbf{M}(\ddot{\mathbf{U}}_i - \ddot{\mathbf{U}}_i^d) + \mathbf{C}\dot{\mathbf{U}}_i - (c_m^d\mathbf{M} + c_k^d\mathbf{K})\dot{\mathbf{U}}_i^d + \mathbf{K}(\mathbf{U}_i - \mathbf{U}_i^d) - \Delta\mathbf{K}(c_k^d\dot{\mathbf{U}}_i^d + \mathbf{U}_i^d) = \mathbf{F}_i - \mathbf{F}_i^d \quad (6.44)$$

Furthermore, Eq.(6.44) is rewritten as

$$\Delta\mathbf{K}(c_k^d\dot{\mathbf{U}}_i^d + \mathbf{U}_i^d) = \mathbf{M}(\ddot{\mathbf{U}}_i - \ddot{\mathbf{U}}_i^d) + \mathbf{C}\dot{\mathbf{U}}_i - (c_m^d\mathbf{M} + c_k^d\mathbf{K})\dot{\mathbf{U}}_i^d + \mathbf{K}(\mathbf{U}_i - \mathbf{U}_i^d) - (\mathbf{F}_i - \mathbf{F}_i^d) \quad (6.45)$$

From $\Delta\mathbf{K}$ in Eq.(6.15), Eq.(6.45) becomes

$$\sum_{j=1}^{NE}\mathbf{K}(c_k^d\dot{\mathbf{U}}_i^d + \mathbf{U}_i^d)\alpha_j = \mathbf{M}(\ddot{\mathbf{U}}_i - \ddot{\mathbf{U}}_i^d) + \mathbf{C}\dot{\mathbf{U}}_i - (c_m^d\mathbf{M} + c_k^d\mathbf{K})\dot{\mathbf{U}}_i^d + \mathbf{K}(\mathbf{U}_i - \mathbf{U}_i^d) - (\mathbf{F}_i - \mathbf{F}_i^d) \quad (6.46)$$

In structural dynamic testing, the data acquisition instruments generally take the signal from the specific transducer type, and giving displacement, velocity or acceleration. Conversion from displacement to acceleration and velocity requires numerical differentiation as

$$\dot{\mathbf{U}}_i = \frac{d\mathbf{U}_i}{dt} \quad (6.47)$$

$$\ddot{\mathbf{U}}_i = \frac{d\dot{\mathbf{U}}_i}{dt} \quad (6.48)$$

On the other hand, velocity and displacement can be obtained from numerical integration of acceleration and can be described as

$$\dot{\mathbf{U}}_i = \int_{t_i}^{t_{i+1}} \ddot{\mathbf{U}}_i dt \tag{6.49}$$

$$\mathbf{U}_i = \int_{t_i}^{t_{i+1}} \dot{\mathbf{U}}_i dt \tag{6.50}$$

But those methods produce significant errors in the conversion process (Han 2003). In order to obtain dynamic responses from measured data, Newmark's time step integrating method is implemented into the formulation of a new damage detection technique (Clough and Penzien 1975).

Here, Δt for this example is roughly estimated as $\Delta t = \frac{2\pi}{f_n}$ where f_n is natural frequency at *"n"* number of mode which is selected among the higher modes for the harmonic applied force. In the case of velocity sensors are used, the following equation is derived from Eq.(6.17) to compute $\ddot{\mathbf{U}}_{i+1}$.

$$\ddot{\mathbf{U}}_{i+1} = \frac{1}{\gamma \Delta t}(\dot{\mathbf{U}}_{i+1} - \dot{\mathbf{U}}_i) - (\frac{1}{\gamma} - 1)\ddot{\mathbf{U}}_i \tag{6.51}$$

Then, $\ddot{\mathbf{U}}_{i+1}$ in Eq.(6.51) is substituted in to Eq.(6.16) to compute $\mathbf{U}_{i+1}$. In this study, accelerometer is utilised as a sensor to acquire measured acceleration data. In this case, Eq.(6.16) and Eq.(6.17) can be directly employed to compute velocity and displacement from acceleration. In the case of undamaged and damaged structures are subjected to identical loading as

$$\mathbf{F}_i = \mathbf{F}_i^d \tag{6.52}$$

Then, Eq.(6.46) becomes

$$\sum_{j=1}^{NE} \mathbf{K}_j (c_k^d \dot{\mathbf{U}}_i^d + \mathbf{U}_i^d)\alpha_j = \mathbf{M}(\ddot{\mathbf{U}}_i - \ddot{\mathbf{U}}_i^d) + \mathbf{C}\dot{\mathbf{U}}_i - (c_m^d \mathbf{M} + c_k^d \mathbf{K})\dot{\mathbf{U}}_i^d + \mathbf{K}(\mathbf{U}_i - \mathbf{U}_i^d) \tag{6.53}$$

Here, α_j is only unknown damage parameter. Thus, Eq.(6.53) can be expressed as a set of linear algebraic equation in the following form

$$\mathbf{A}\boldsymbol{\alpha} = \mathbf{b} \tag{6.54}$$

whererow vectors in matrix **A** are as follows

$$\mathbf{a}_j = \mathbf{K}_j (c_k^d \dot{\mathbf{U}}_i^d + \mathbf{U}_i^d) \tag{6.55}$$

$$\mathbf{b} = \mathbf{M}(\ddot{\mathbf{U}}_i - \ddot{\mathbf{U}}_i^d) + \mathbf{C}\dot{\mathbf{U}}_i - (c_m^d \mathbf{M} + c_k^d \mathbf{K})\dot{\mathbf{U}}_i^d + \mathbf{K}(\mathbf{U}_i - \mathbf{U}_i^d) \tag{6.56}$$

An inverse prediction procedure is required to compute damage parameter $\boldsymbol{\alpha}$. Here, the SVD is employed to solve for damage parameters $\boldsymbol{\alpha}$.Let the SVD of matrix**A** of dimension *M* x *NE* be

$$\mathbf{A}_{M \text{ x } NE} = \mathbf{U}_{M \text{ x } M} \sum_{M \text{ x } NE} \mathbf{V}^T_{NE \text{ x } NE} = \sum_{j=1}^{NE} \sigma_j \mathbf{u}_j \mathbf{v}_j^T \tag{6.57}$$

where $\sum$ is the diagonal matrix containing strictly non-negative and non-increasing singular values σ_j, i.e. $\sigma_1 \geq \sigma_2 \geq ... \geq \sigma_n \geq 0$. $\mathbf{U}$ and $\mathbf{V}$ are the matrices of orthonormal left and right vectors $\mathbf{u}_j$ and $\mathbf{v}_j$ respectively. Ordinary least squares solution in Eq.(6.54) can then be described in the form

$$\boldsymbol{\alpha} = \sum_{j=1}^{NE} \frac{\mathbf{u}_j^T \mathbf{b}}{\sigma_j} \mathbf{v}_j \tag{6.58}$$

Therefore, the damage parameters are obtained from Eq.(6.58).

6.7 Numerical example

One-bay plane frame model, shown in Figure 6.17, is utilised to demonstrate the applicability of the proposed damage identification approach using measured acceleration data. The structure concerned is a two-story model comprising beams and columns which are divided into 60 elements in total. The structure has 3.0 m width and 6.0 m height. For simplicity, beams and columns are considered same material properties as shown in Table 6.2. The damage parameters are chosen to characterize structural damage at element level. A total number of 60 damage parameters indicating the location and extent of structural damage are employed for the damage identification of the plane frame model structure. In the example, five simulated damage scenarios are defined for the structure model by reducing the stiffness of elements at various locations in the structure as summarised in Table 6.3. For simplicity, noise effect on inverse damage predictions is not considered in this example.

Table 6.2 Material properties of the structure

Cross-sectional area A (mm^2)	4.70×10^3
Moment of inertia I (mm^4)	2.21×10^7
Density ρ (kg/mm^3)	7.85×10^{-6}
Young's modulus E (N/mm^2)	2.10×10^5

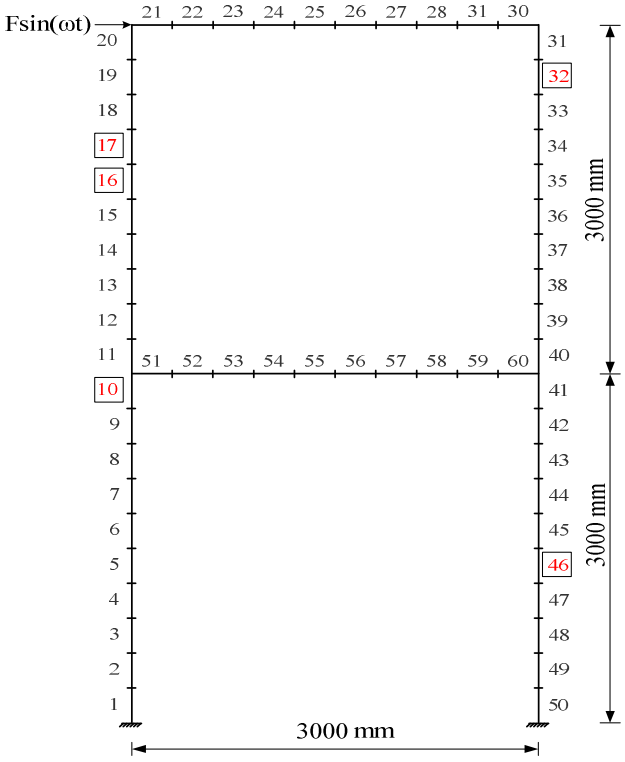

Figure 6.17 One-bay plane frame subjected to harmonic force with simulated damage at elements 10,16,17,32 and 46

Table 6.3 Simulated damage scenarios for the one-bay plane frame structure

Damage scenario	Damage description (stiffness reduction)	Element number	Damage amount (%)
1	1st column in 1st story	10	-5
2	1st column in 2nd story	16	-10
	2nd column in 1st story	46	-10
3	1st column in 1st story	10	-5
	1st column in 2nd story	17	-25
	2nd column in 2nd story	32	-10
4	beam in 2nd story	24	-10
5	beam in 2nd story	23	-10
	beam in 2nd story	28	-20

6.7.1 Damage scenario 1

For the first damage scenario, element number 10 is assumed to be damaged with the amount of 5% in the simulated example. Damage location and amount identified for damage scenario 1 are shown inFigure 6.18, where the inverse damage predictions at element level are plotted. It can be seen that the predictions of the location and amount of the considered damage are identified by the proposed method. Also, damping of the structure has little influence with oscillation on the inverse structural damage identification at the beginning of the time steps.

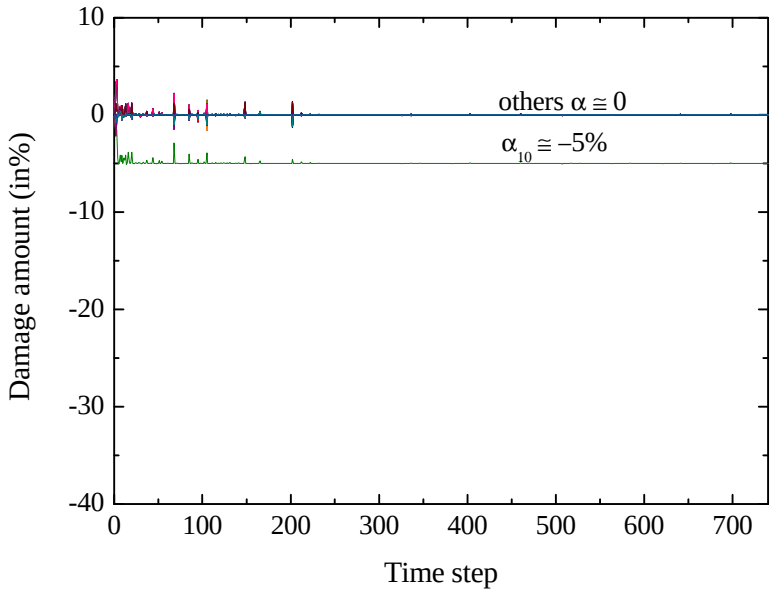

Figure 6.18 Inversely identified damage parameters in real time for damage scenario 1 where only element 10 is damaged by 5%

6.7.2 Damage scenario 2

Figure 6.19 gives the results for inverse predictions of damage scenario 2 for structural elements. Two elements, i.e. element number 16 and 46, are assumed to be damaged in the same amount of 10%. The results show that the proposed approach is capable of giving good predictions of the damage using modal data measurements.

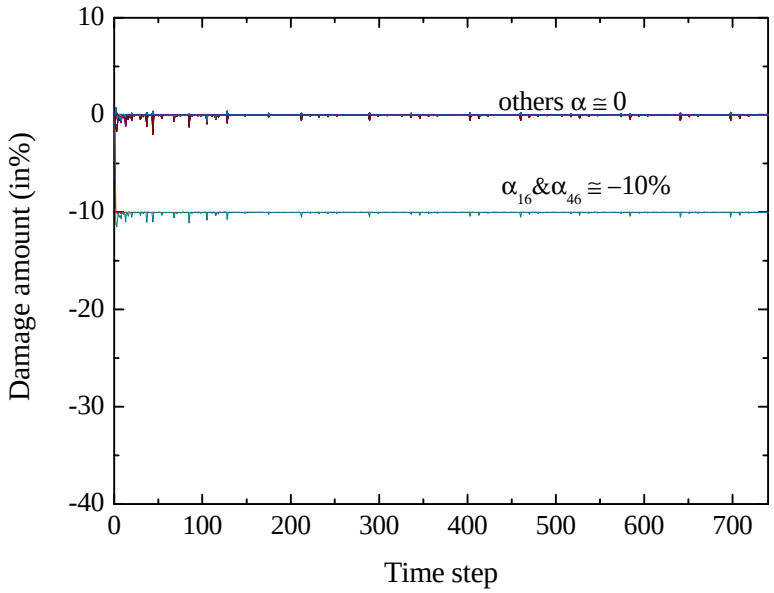

Figure 6.19 Inversely identified damage parameters in real time for damage scenario 2 where elements 16 and 46 are damaged by the same amount of 10%

6.7.3 Damage scenario 3

Damage scenario 3 involves the loss of stiffness in three elements namely 10, 17 and 32 with 5%, 25% and 10%, respectively. This is a difficult damage case to be identified due to increasing damaged elements in the structure. Again, damaged elements are clearly identified as shown in Figure 6.20. The proposed approach provides accurate predictions of the location and extent of structural damage, when comparing with the simulated damage.

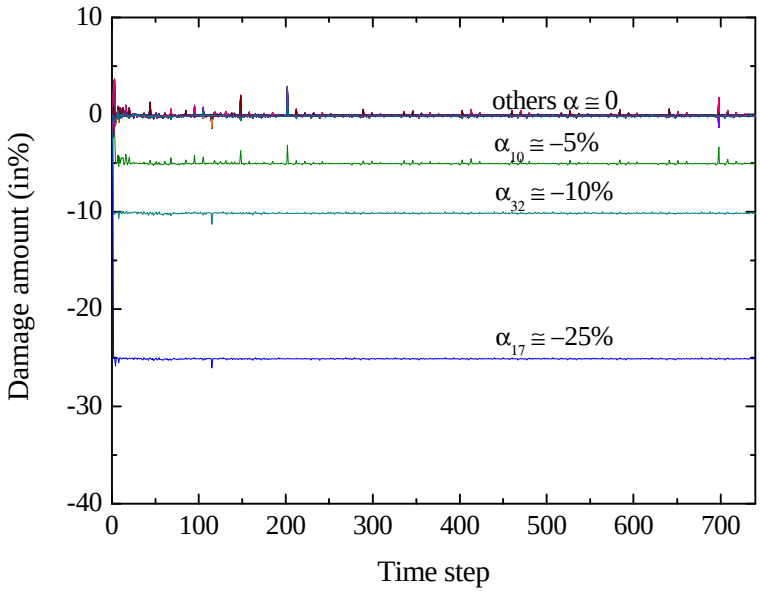

Figure 6.20 Inversely identified damage parameters in real time for damage scenario 3 where elements 10, 17 and 32 are damaged by 5%, 25% and 10%, respectively

6.7.4 Damage scenario 4

In order to effectively identify damage existing on beam, harmonic loading is applied vertically on the top story as show in Figure 6.21. In the simulated damage scenario 4, the proposed approach is employed again to inversely identify the simulated damage in the structure. Figure 6.22 shows the results for inverse prediction of the simulated damaged element. The damaged element 24 with damage amount of 10% is clearly identified while the other elements are indicated as undamaged elements. This gives an excellent agreement with the simulated damage.

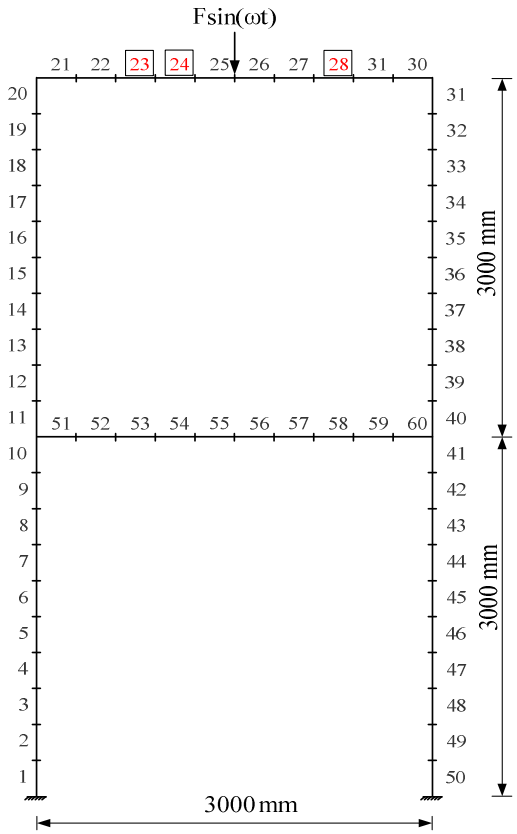

Figure 6.21 One-bay plane frame subject to harmonic force with simulated damaged elements 23, 24 and 28

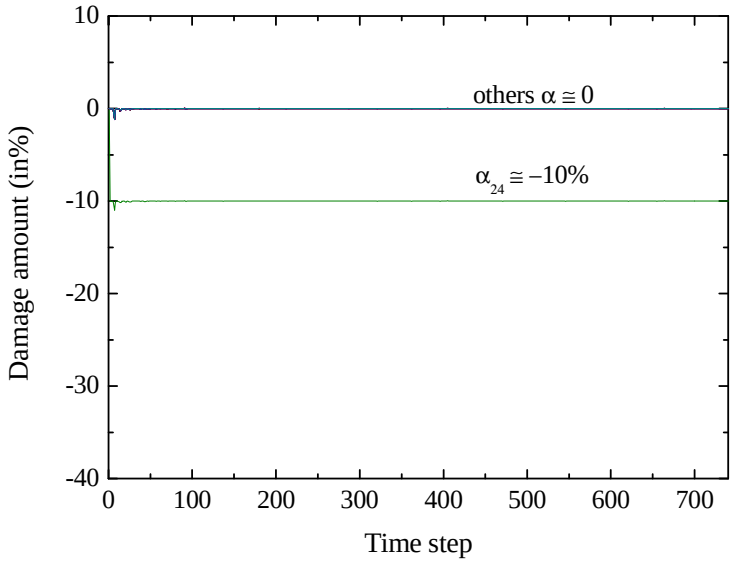

Figure 6.22 Inversely identified damage parameters in real time for damage scenario 4 where element 24 is damaged by 10%

6.7.5 Damage scenario 5

The structural damages at multiple locations in various damage magnitudes are considered in simulated scenario 5. The results of inverse predictions for the simulated damage scenario 5 are shown in Figure 6.23. Again, the proposed approach provides accurate inverse predictions of the damaged elements 23 and 28 with simulated damaged amount of 10% and 20%, respectively,for this complex case, and the obtained results agree well with the locations and magnitudes of simulated structural damage.

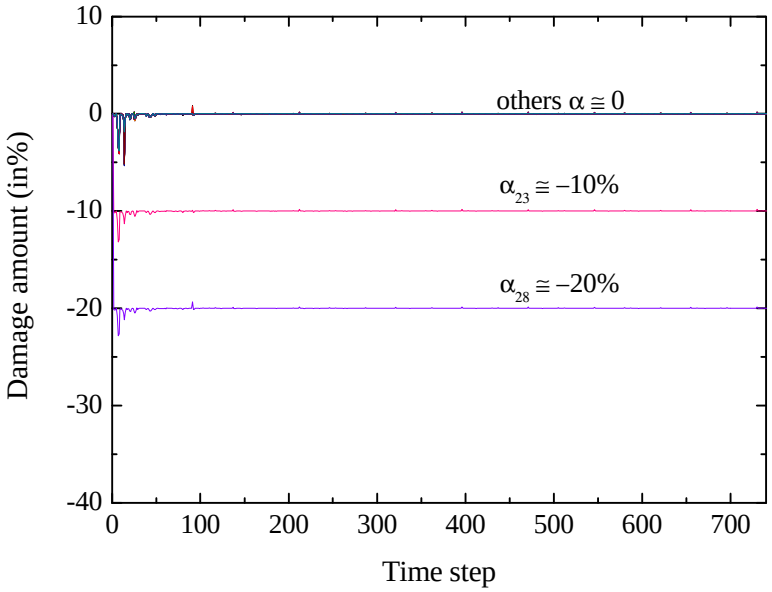

Figure 6.23 Inversely identified damage parameters in real time for damage scenario 5 where element 23 and 28 are damaged by 10% and 20%, respectively

6.8 Regularized damage identification

Extreme catastrophic events such as earthquake, impact and blast are regarded as the most destructive disasters and can cause severe damages in the structures. Damage related to

stiffness change with time during a short period is more difficult to identify.The extent of damages needs to be assessed immediately during and/or after the event. Therefore, there is a strong need to develop robust methods for real time detecting and evaluating of damage to monitor the safety and integrity of the structures.

Vibration response such as acceleration measurements can be used for real time detection of damage in the structure. However, noise often exist in the vibration measurements, therefore, a regularization algorithm is needed to reduce the influence of noise on the damage identification.Tikhonov regularization algorithm incorporating the L-curve criterion is employed here to filter out the measurements errors (i.e. noise) in the modal data (Hansen 1998, 2000, 2007, Tikhonov and Arsenin 1993). The more detailed about regularisation algorithm has been discussed in Section 5.3.3. Structural damage evolution with time in the element is determined from continuously monitored data, and the condition of the structure is then further assessed and updated. Those damage parameters could also be used to monitor real time damages caused by extreme loading such as earthquake, impact and blast (Ma et al. 2005).The algebraic equation in Eq.(6.54) can be rewritten as a general form of

$$\mathbf{A}_{M \times NE}\boldsymbol{\alpha}_{NE} = \mathbf{b}_{M} \tag{6.59}$$

where$M$ ranges from 1 to total number of measured degrees of freedom readings of the structural system. The system of linear equation becomes discrete ill-posed problem as singular values of the matrix $\mathbf{A}$ decay gradually to zero and the ratio between the largest and the smallest non-zero singular values become larger(Chen 2008, Chen and Bicanic 2010). In practice, the vector$\mathbf{b}$ is often contaminated by certain level of measurement errors which are assumed to be noise here (Sanliturk and Cakar 2004). To investigate the effect of noise-

polluted measurements, simulated noise is added in the acceleration data and then velocity and displacement are computed by using Eq.(6.16) and Eq.(6.17). Noise contaminated acceleration can be defined as

$$\ddot{\mathbf{U}}_i^d = \overline{\ddot{\mathbf{U}}}_i^d (\mathbf{1} + \varepsilon\zeta) \tag{6.60}$$

where $\overline{\ddot{\mathbf{U}}}_i^d$ is noise-free acceleration for the damaged structure. The noise level is represented as standard deviation $\varepsilon > 0$ and random numbers ζ are generated from standard normal distribution. The terms with small singular values will make the computed solution unstable because the ordinary solution coefficients $\frac{\mathbf{u}_j^T \mathbf{b}}{\sigma_j}$ in Eq.(6.58) become increasingly large when the singular values σ_j decrease. Thus, the regularization of the ill-posed problem is required to filter out the contribution of the inevitable noise contained in **b**. For this case, Tikhonov regularization algorithm incorporating L-curve criterion is one of the most commonly used method. This method utilises a continuous regularisation parameter which replaces the original operation with a better-conditioned and produces regularised solution to the original problem (Hansen and O'Leary 1993).The procedure discussed in section 4.3.3 will be used to evaluate regularization parameter λ.

6.9 Numerical examples

6.9.1 One-bay braced frame

A ten-story one-bay braced frame building model, shown inFigure 6.24 is utilised to demonstrate the applicability of the proposed damage identification approach. The structure

concerned has 6.0m width and 3.0 m story height comprising beams, columns and braces which are divided into 40 elements in total. The damage parameters defined in Eq.(6.54) are chosen to characterise structural damage at element level. A total number of 40 damage parameters are employed for damage identification. For simplicity, all elements are considered same material properties as summarized in Table 6.4.

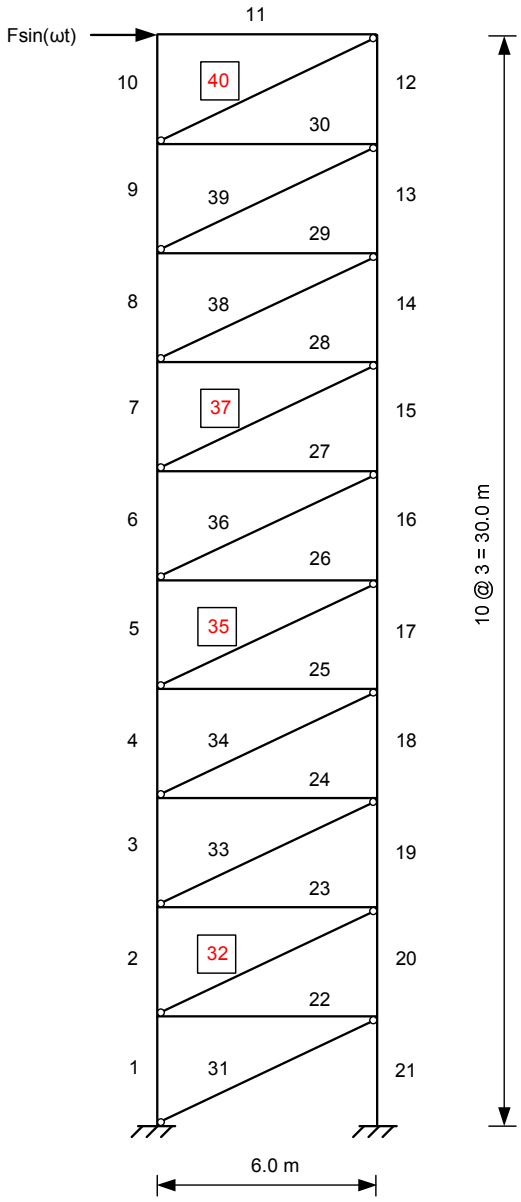

Figure 6.24 One-bay braced frame structure with simulated damage at elements 32, 35, 37 and 40 subjected to harmonic force

Table 6.4 Material properties of the structure

Cross-sectional area A (m^2)	1.740×10^{-2}
Moment of inertia I (m^4)	3.281×10^{-4}
Density ρ (kg/m^3)	7850
Young's modulus E (N/m^2)	2.100×10^{11}

Table 6.5 Simulated damage scenarios for the structure

Damage scenario	Damage description (stiffness reduction)	Element number	Damage amount
1	brace in 2nd story	32	0%-20%
2	brace in 2nd story	32	0%-20%
	brace in 5th story	35	0%-25%
3	brace in 2nd story	32	0%-13%
	brace in 5th story	35	0%-20%
	brace in 7th story	37	0%-25%
	brace in 10th story	40	0%-32%

In the example, the bracing is formed by inserting diagonal structural members between each story to resist lateral forces. The brace members are pin-jointed at both ends and therefore primarily subject to axial force. The connection joints of beams and columns are modelled as rigid joints to maintain bending moments. For the braced frame structure, structural damage is assumed to occur at brace members. Here, three damage scenarios are considered for the

structural damage problems. In the simulated damage scenarios, damage is introduced by gradually reducing the stiffness in the brace elements at every time step as summarised in Table 6.5. The dynamic responses before and after the damage are obtained by performing finite element dynamic analysis of analytical model. Simulated noise level 1% and 3% are adopted in the acceleration data as measurement error in all assumed cases. Tikhonov regularization method incorporating the L-curve criterion for determining the regularization parameter is employed to produce stable and robust solutions for damage parameters.

Damage scenario 1

For the first damage scenario, only brace element 32 is assumed to be damaged. Simulated damage is gradually increased from 0 to 20% in every time step. The results for the damage location and amount identified are shown in Figure 6.25 to Figure 6.27where the damage predictions associated with the elements are plotted. In the case free of noise, as shown in Figure 6.25, the damaged element 32 with increasing damage magnitude is clearly identified while the other elements are identified as undamaged elements. This prediction agrees well with the assumed simulation.

The results of inverse predictions for the damage parameters with noise level 1% and 3% are shown in Figure 6.26 and Figure 6.27 respectively. Presence of noise in the measurements causes some false predictions on damage parameters providing unstable solutions. More unstable solution for damage parameters are appeared when noise level rises from 1% to 3% in measured modal data. In this case, the proposed method incorporating the regularisation method is capable of giving good predictions of the severe damage using modal data measurements with realistic errors.

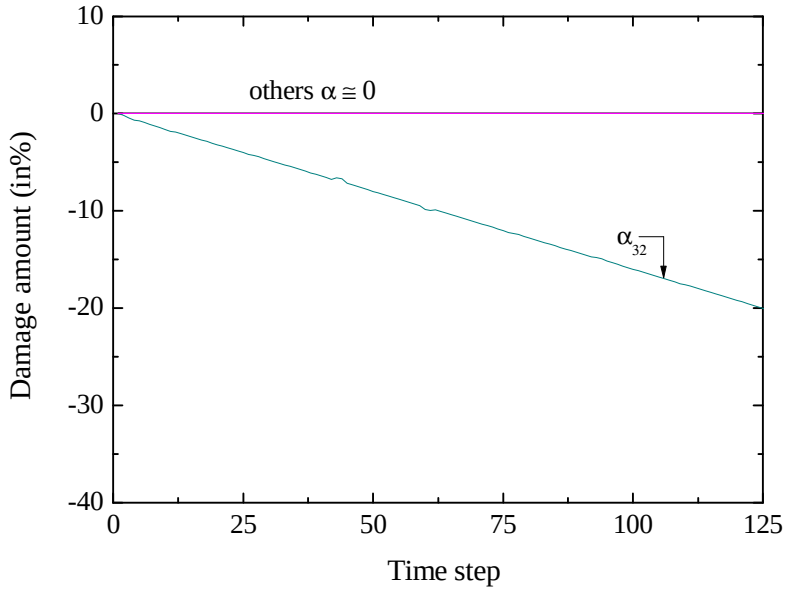

Figure 6.25 Inversely identified damage parameters in real time without noise in acceleration where element 32 is damaged

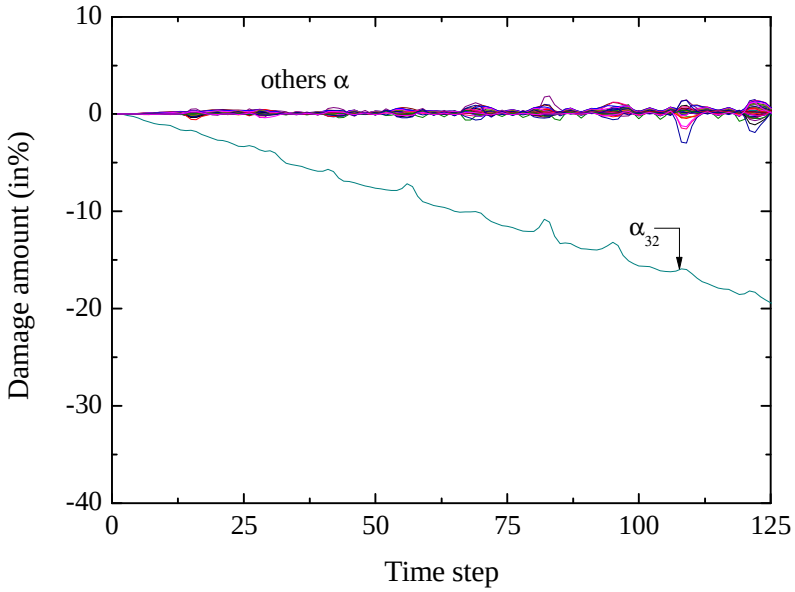

Figure 6.26 Inversely identified damage parameters in real time with 1% noise in acceleration where element 32 is damaged

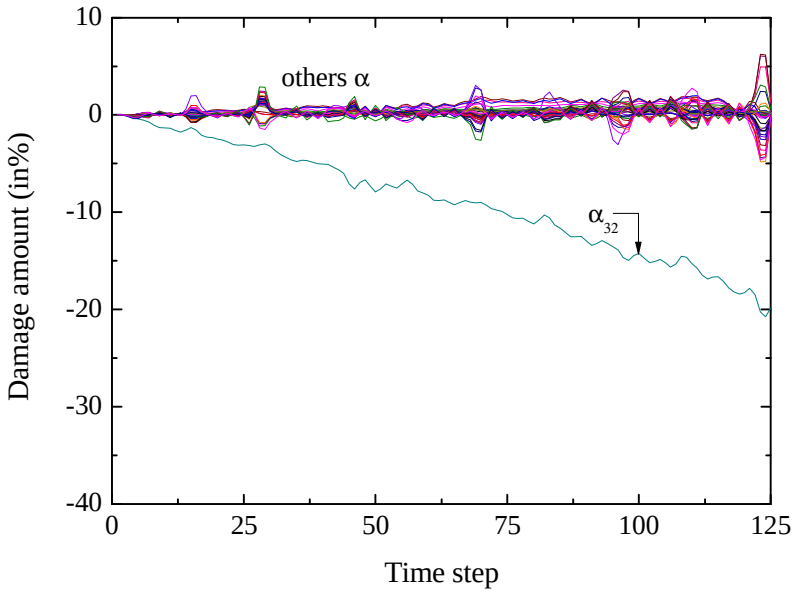

Figure 6.27 Inversely identified damage parameters in real time with 3% noise in acceleration where element 32 is damaged

Damage scenario 2

Damage scenario 2 involves two damaged brace members with various damage magnitudes at different stories. Simulated damage from 0 to 25% at element 35 is considered in addition to damaged element 32 in damage scenario1. Figure 6.28 gives the result of noise free case for inverse predictions of structural damage. Two damaged elements 32 and 35 are clearly identified as predicted. The results in Figure 6.29 and Figure 6.30 show some false damage detections in the inverse prediction of damage parameters due to the noise effect in modal data. False indications become more when noise level rises to 3%. However, the predictions of the location and amount of the considered damaged elements are correctly identified by the proposed method.

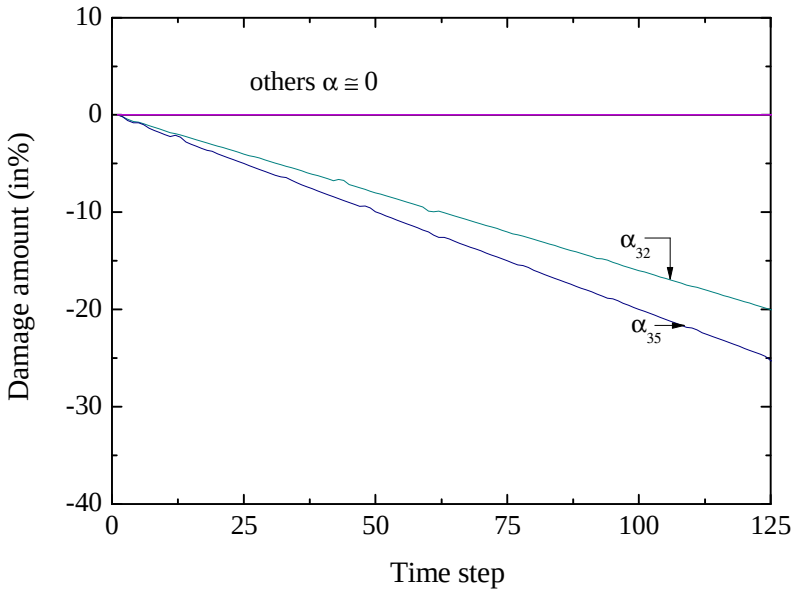

Figure 6.28 Inversely identified damage parameters in real time without noise in acceleration where elements 32 and 35 are damaged

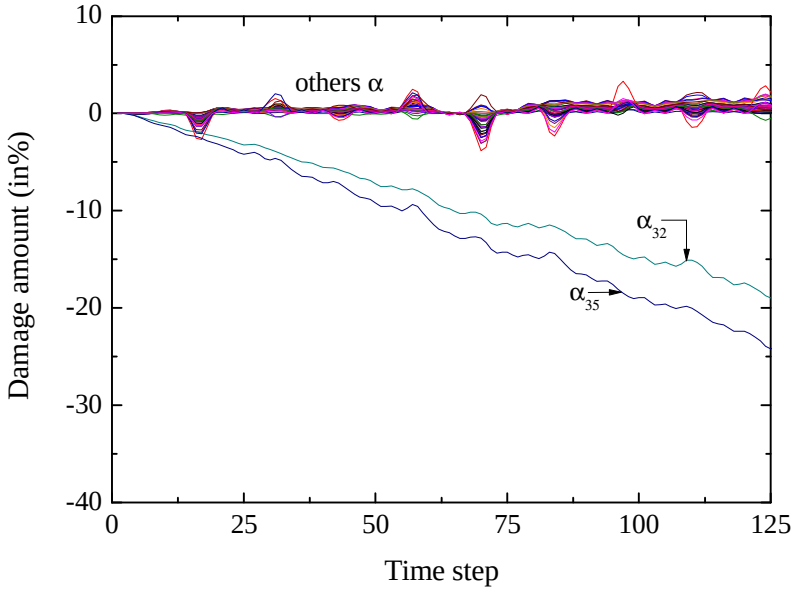

Figure 6.29 Inversely identified damage parameters in real time with 1% noise in acceleration where elements 32 and 35 are damaged

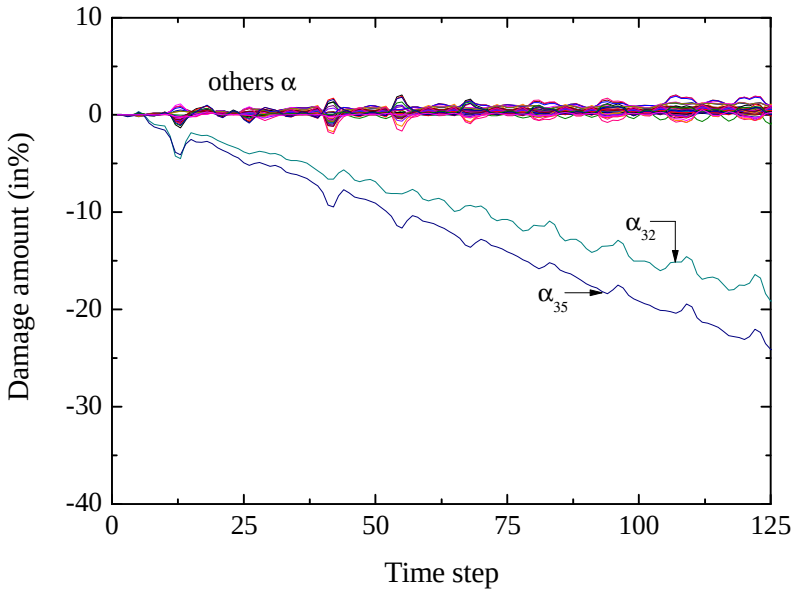

Figure 6.30 Inversely identified damage parameters in real time with 3% noise in acceleration where elements 32 and 35 are damaged

Damage scenario 3

In damage scenario 3, multiple damaged elements 32, 35, 37 and 40 with different damage magnitudes are considered. This is more difficult damage pattern to be identified due to increasing damaged elements in the structural system when compared with the other damage patterns discussed. The results for identified damage parameters in noise free case arepresented in Figure 6.31. There are some unstable predictions of damage parameters for damage elements as more damaged elements are involved. It can be seen that the proposed approach provides results agreeing well with the locations and magnitudes of simulated structural damage for this complex case too.

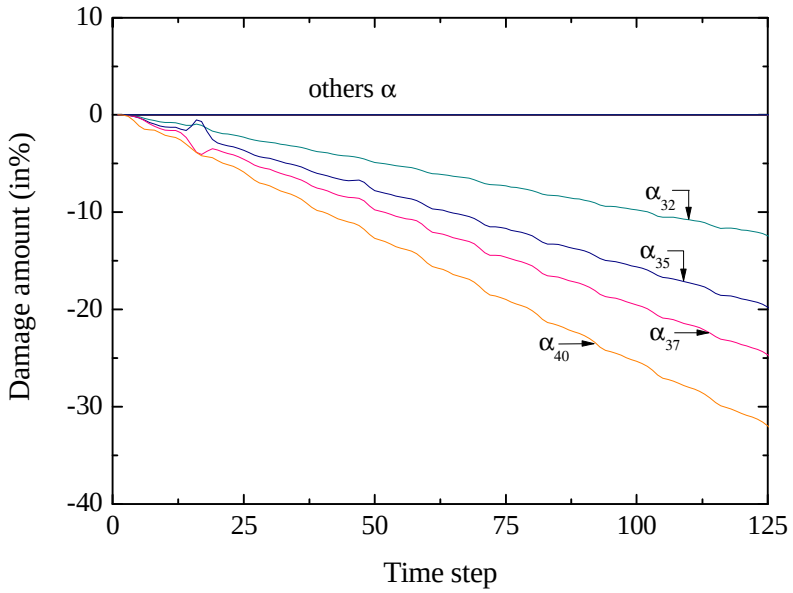

Figure 6.31 Inversely identified damage parameters in real time without noise in acceleration where elements 32, 35, 37 and 40 are damaged

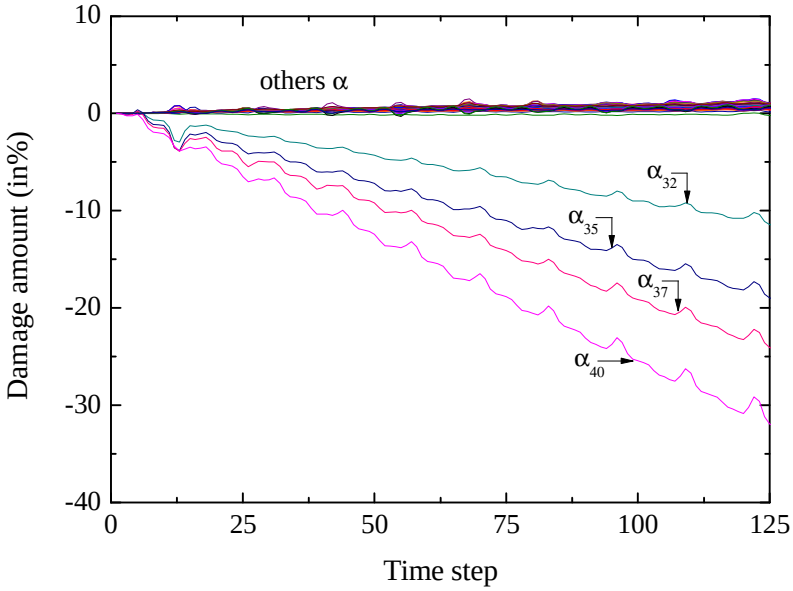

Figure 6.32 Inversely identified damage parameters in real time with 1% noise in acceleration where elements 32, 35, 37 and 40 are damaged

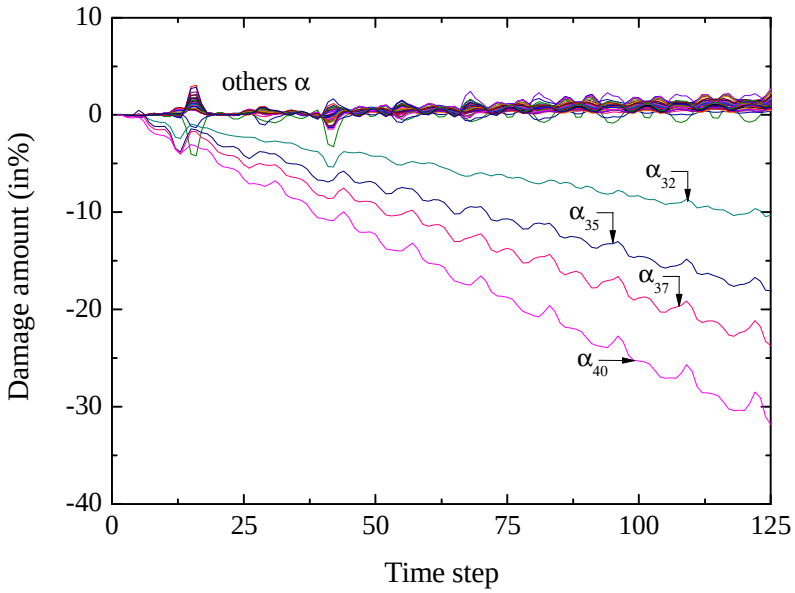

Figure 6.33 Inversely identified damage parameters in real time with 3% noise in acceleration where elements 32, 35, 37 and 40 are damaged

Again, Figure 6.32 and Figure 6.33 show some false damage indications due to existence of noise but the magnitudes of the false damage are small. The results show that all four damaged brace elements are clearly identified and the magnitudes of damage are correctly estimated.

6.9.2 Cantilever beam

Cantilever beam example is reselected to illustrate the further progress of proposed method for detecting damage evolution with time. The structure is divided into a number of elements for damage detection in detailed level. For simplicity, same material properties as shown in Table 6.4are utilised. In order to understand how the procedure works, two damage scenarios for the cantilever beam as summarised in Table 6.6. Damage is simulated by gradually

reducing the stiffness of assumed damaged element during a short time period of 0-25s. Dynamic responses before and after the damage are obtained by performing finite element dynamic analysis of the structure. Simulated noise level 1%, 3% and 5% are adopted in the acceleration data as measurement errors in all assumed cases. Tikhonov regularization algorithm incorporating with the L-curve criterion is utilised to filter out the noise on the inversely predictions of damage parameters.

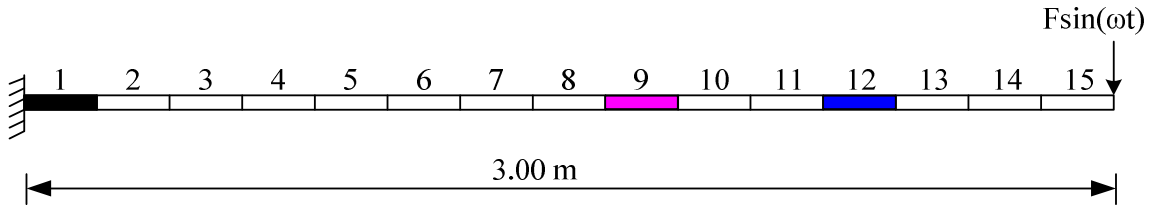

Figure 6.34 Cantilever beam with simulated damaged elements 1, 9, and 12

In the cantilever beam example as shown in Figure 6.34, member is divided in to 15 elements. Only one element is assumed to be damage in damage scenario 1. In damage scenario 2, various structural damages at multiple locations are considered. The undamaged and damaged structures are subjected to the same harmonic force. The location and amount of the simulated damage are then determined from the inverse calculation of the damage parameter α_j.

Table 6.6 Damage scenarios for cantilever beam

Damage scenario	Damage description	Element number	Damage amount (during 0-25s)
1	stiffness reduction	1	0%-12%
2	stiffness reduction	1	0%-12%
	stiffness reduction	9	0%-20%
	stiffness reduction	12	0%-32%

Damage scenario 1

In damage scenario 1, element 1 is assumed to be damaged by gradually reducing its stiffness up to 12% for the duration of 0-25s. Figure 6.35 shows the results for inverse predictions of damage parameters in noise-free case. Increasing damage amount of element 1 is clearly identified while the other elements are identified as undamaged elements. This gives an excellent agreement with the assumed simulation. Results of noise effect in measurements show some false indications of damage parameters as shown in Figure 6.36 to Figure 6.38. In this case, the proposed method incorporating the regularization algorithm is capable of giving good predictions of the damage using modal data measurements with realistic errors.

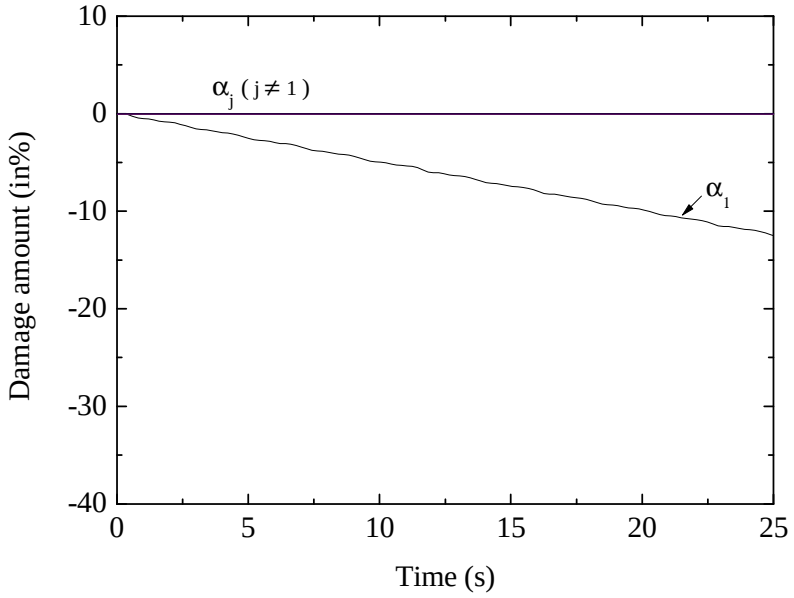

Figure 6.35 Inversely identified damage parameters in real time for damage scenario 1 without noise in acceleration where element 1 damaged 0-12% in cantilever beam

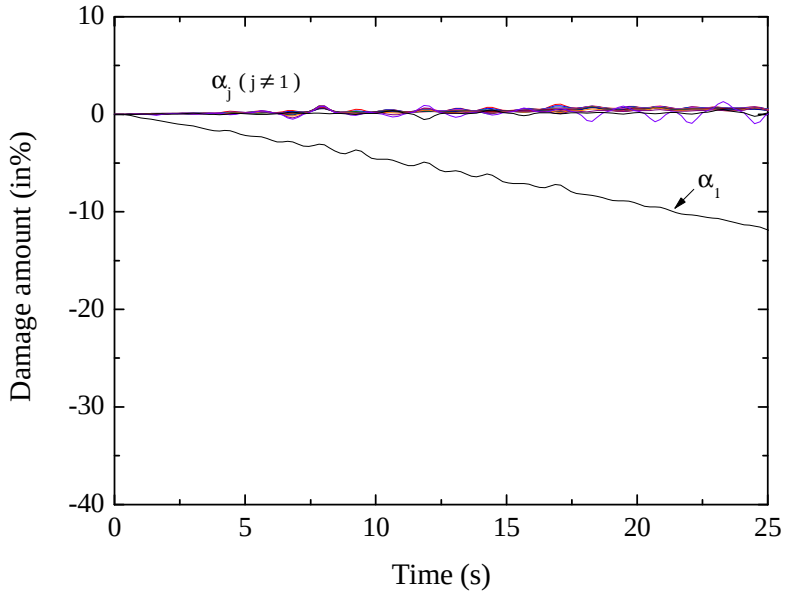

Figure 6.36 Inversely identified damage parameters in real time for damage scenario 1 with 1% noise in acceleration where element 1 damaged 0-12% in cantilever beam

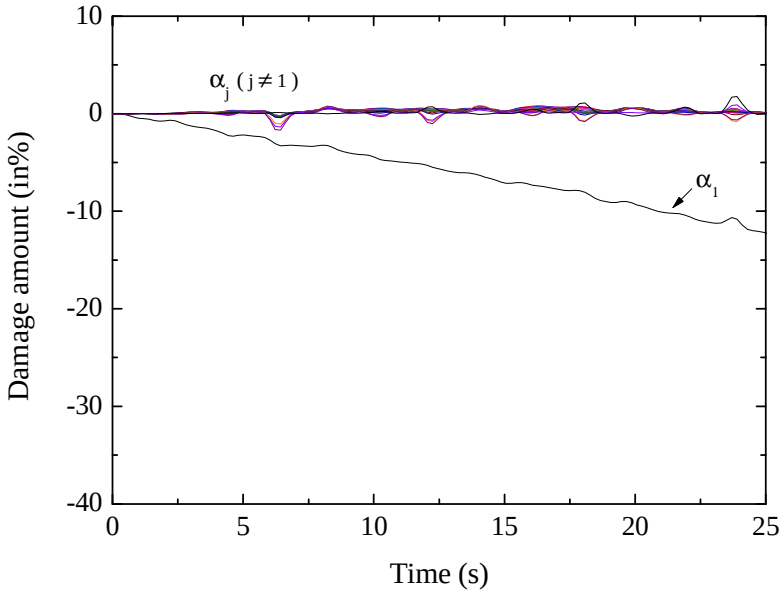

Figure 6.37 Inversely identified damage parameters in real time for damage scenario 1 with 3% noise in acceleration where element 1 damaged 0-12% in cantilever beam

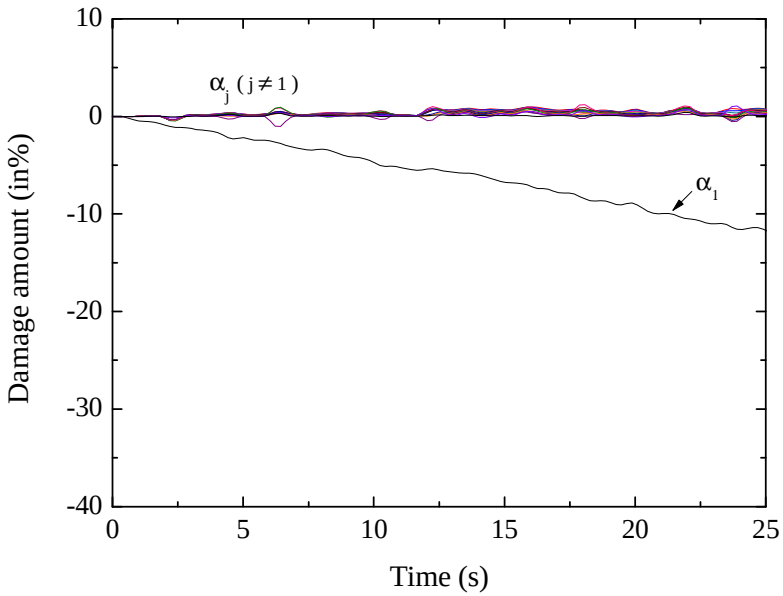

Figure 6.38 Inversely identified damage parameters in real time for damage scenario 1 with 5% noise in acceleration where element 1 damaged 0-12% in cantilever beam

Damage scenario 2

In damage scenario 2, elements 9 and 12 are selected as damaged elements in additional to damage scenario 1. The results of inverse predictions for damage parameters in noise-free case are indicated in Figure 6.39. All damaged elements with different magnitudes are clearly identified. Unstable predictions of damage parameters due to noise effect are shown in Figure 6.40 to Figure 6.42. Although noise existin acceleration, the proposed approach provides good predictions of the simulated damage for this multiple damage case, and the obtained results agreeing well with the locations and magnitudes of simulated structural damages.

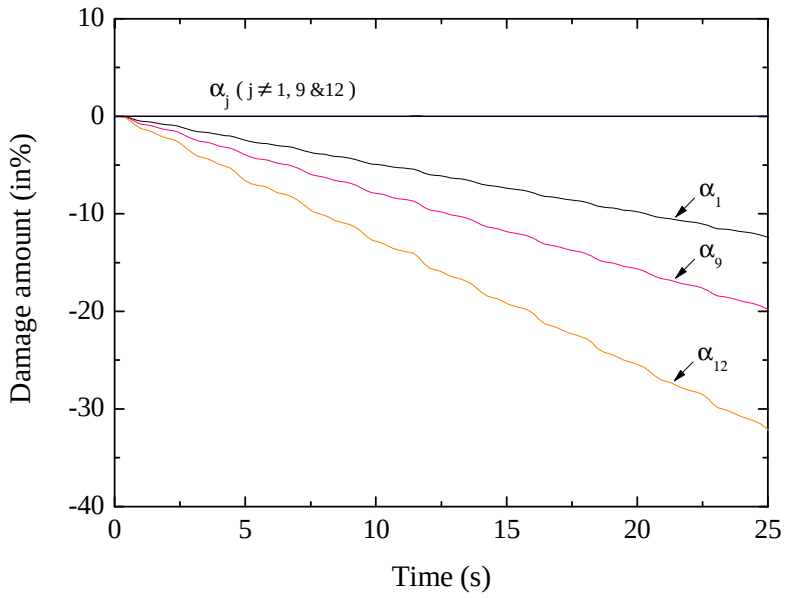

Figure 6.39 Inversely identified damage parameters in real time for damage scenario 2 without noise in acceleration where elements 1, 9 and 12 damaged 0-12%, 0-20% and 0-32% in cantilever beam respectively

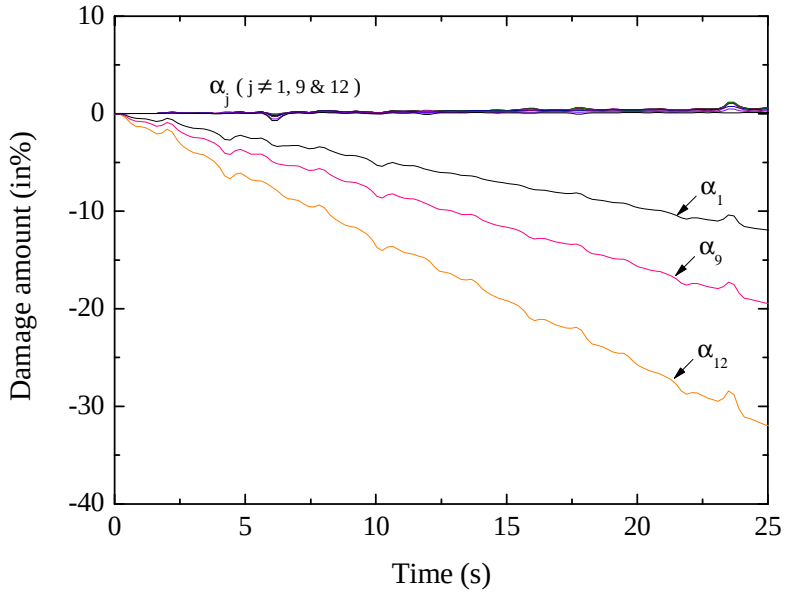

Figure 6.40 Inversely identified damage parameters in real time for damage scenario 2 with 1% noise in acceleration where elements 1, 9 and 12 damaged 0-12%, 0-20% and 0-32% in cantilever beam respectively

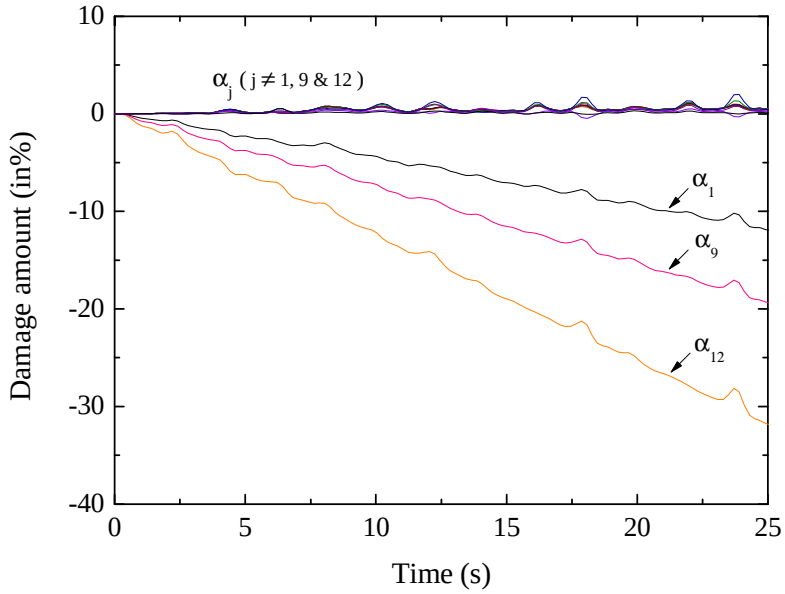

Figure 6.41 Inversely identified damage parameters in real time for damage scenario 2 with 3% noise in acceleration where elements 1, 9 and 12 damaged 0-12%, 0-20% and 0-32% in cantilever beam respectively

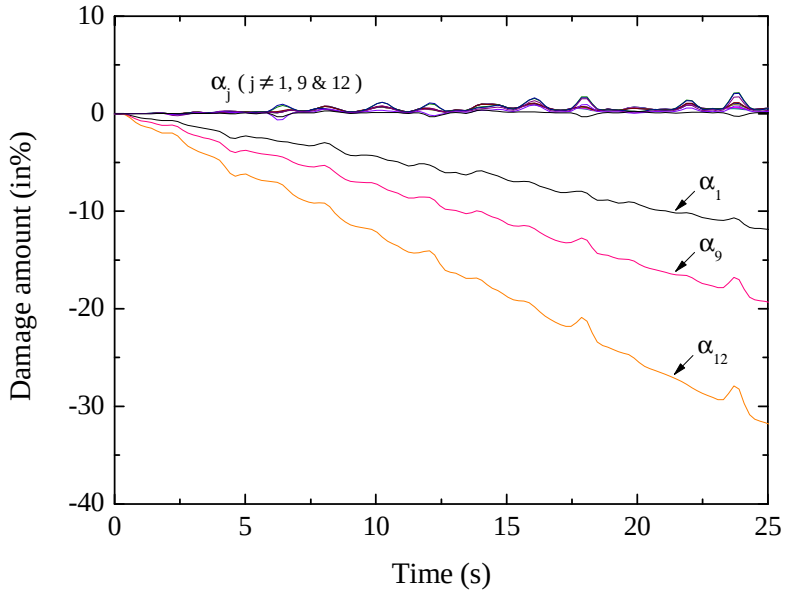

Figure 6.42 Inversely identified damage parameters in real time for damage scenario 2 with 5% noise in acceleration where elements 1, 9 and 12 damaged 0-12%, 0-20% and 0-32% in cantilever beam respectively

6.9.3 Three-bay braced frame

A three-bay braced frame building model, as shown inFigure 6.43, is utilised as a numerical example to demonstrate the applicability of the proposed damage identification method. The structure concerned has nine stories comprising beams, columns and braces which are divided into 72 elements in total. The damage parameters defined in Eq.(6.54) are chosen to characterize structural damage at element level. In this example, the bracing is formed in the middle bay by inserting diagonal structural members between stories to resist lateral forces generated by strong excitation such as earthquake or wind. The brace members are pin-jointed at the ends and therefore primarily subjected to axial force. The connection joints of beams and columns are modelled as rigid joints to maintain bending moments. The braced

frame structure is subject to the lateral force as shown inFigure 6.43. Thus, structural damages are assumed to be occurring in the brace members.

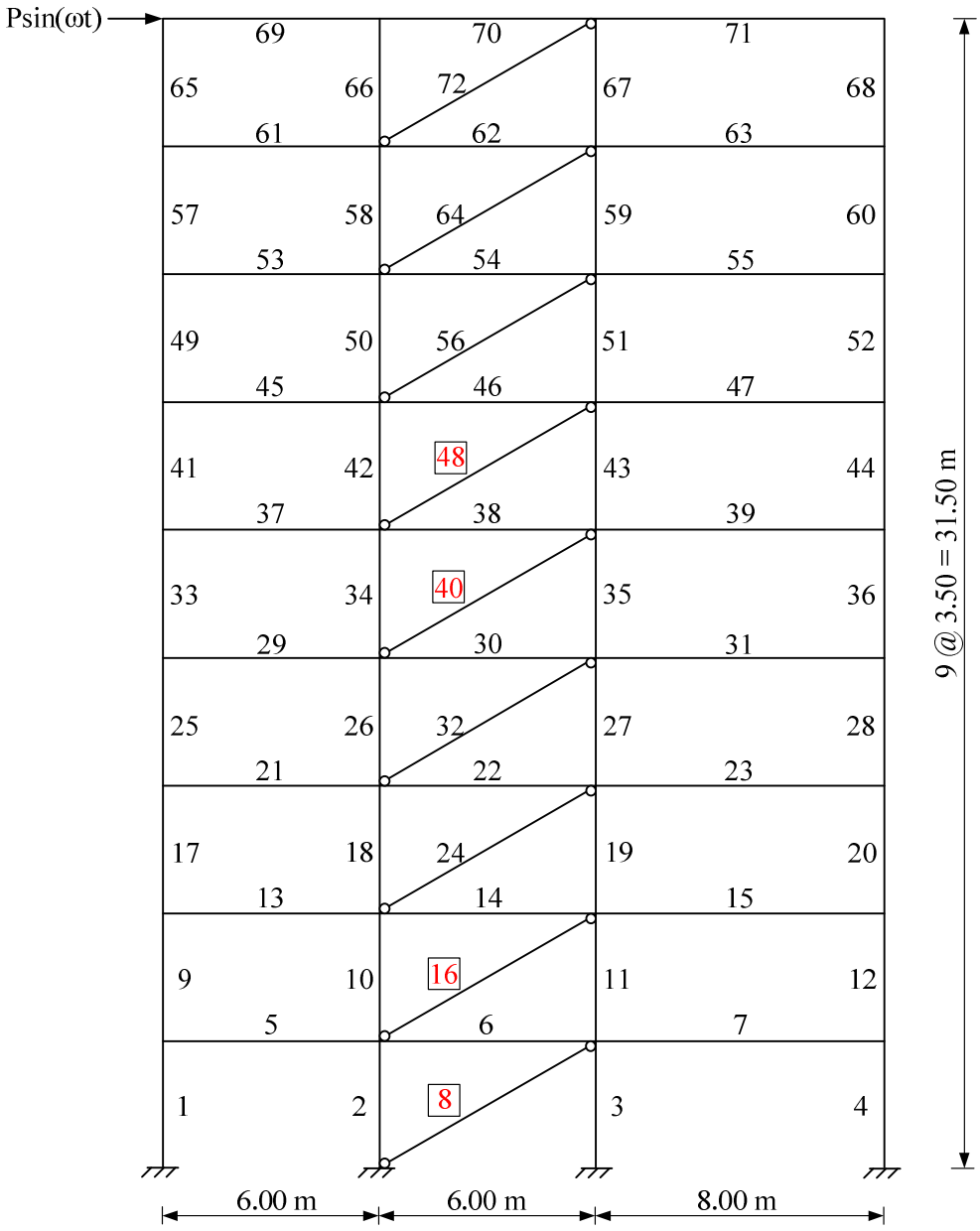

Figure 6.43 Nine-story three-bay braced frame structure with simulated damage at elements 8, 16, 40, and 48 is subject to harmonic force

Here, three damage scenarios are considered for the structural damage problems. Simulated damage scenarios are introduced by gradually reducing the stiffness of the assumed damaged elements in every time step as summarised in Table 6.7.

Table 6.7 Damage scenarios for three-bay braced frame structure

Damage scenario	Damage description (stiffness reduction)	Element number	Damage amount (during 0-25s)
1	brace in 1st story	8	0%-12%
2	brace in 1st story	8	0%-12%
	brace in 2nd story	16	0%-20%
3	brace in 1st story	8	0%-12%
	brace in 2nd story	16	0%-20%
	brace in 5th story	40	0%-25%
	brace in 6th story	48	0%-33%

Damage scenario 1

In damage scenario 1, only brace element 8 is assumed to be damaged. Structural damage is gradually increased from 0% to 12% for the short duration of 0-25s. In noise-free case, increasing damage magnitude ofelement 8 is correctly predicted while the other elements are identified as undamaged elements as shown in Figure 6.44. This agrees well with the assumed damage simulation.The results of inverse predictions for the damage parameters with noise level 1%, 3% and 5% are shown in Figure 6.45 to Figure 6.47respectively where the damage predictions associated with the elements are plotted. Presence of noise in the measurements occurs some false predictions on damage parameters providing unstable solutions. More unstable predictions for damage parameters appear when higher noise levels are existed in the measured data.

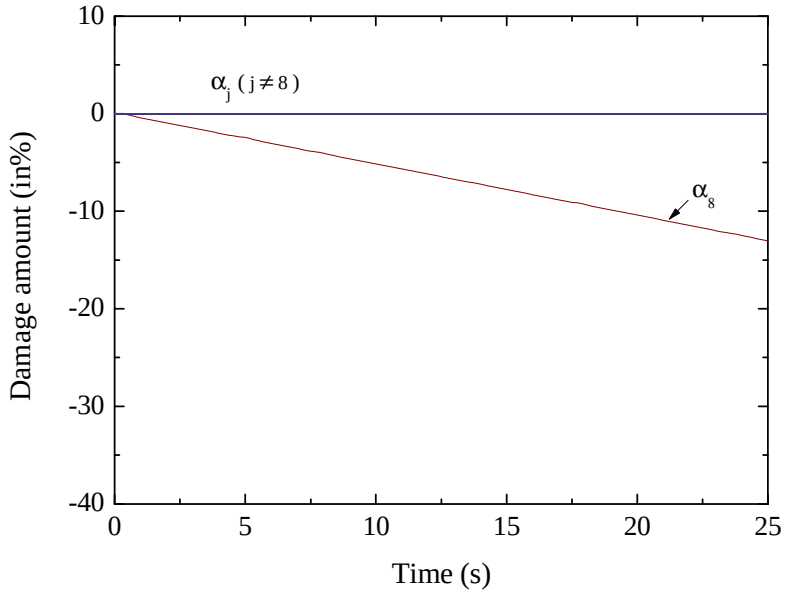

Figure 6.44 Inversely identified damage parameters in real time for damage scenario 1 without noise in acceleration where element 8 damaged 0-12% in braced frame structure

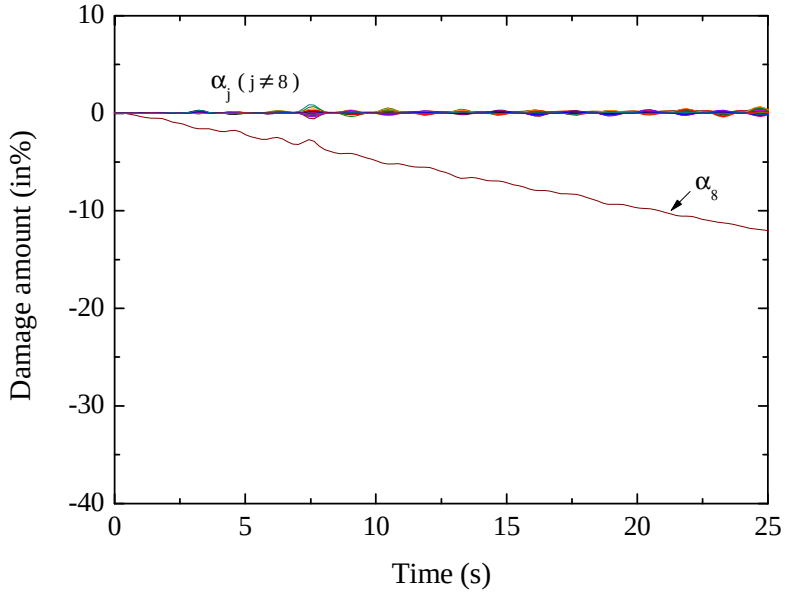

Figure 6.45 Inversely identified damage parameters in real time for damage scenario 1 with 1% noise in acceleration where element 8 damaged 0-12% in braced frame structure

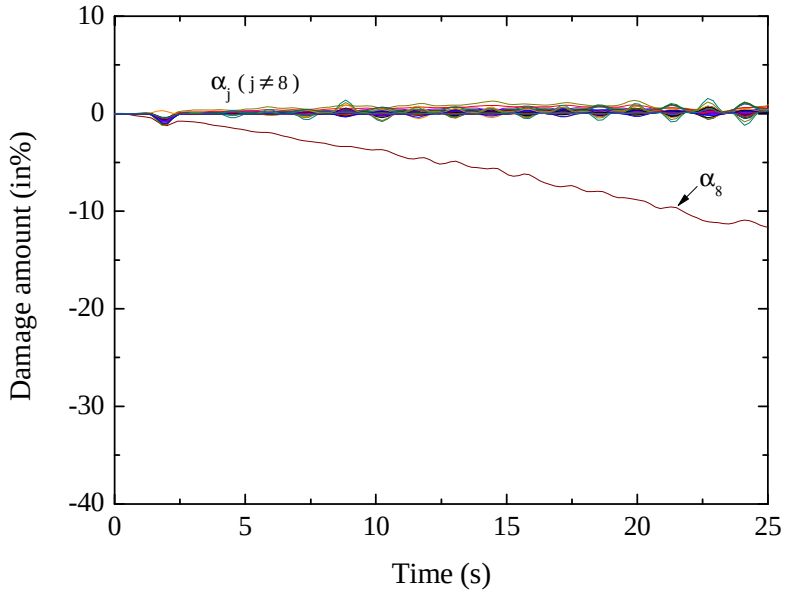

Figure 6.46 Inversely identified damage parameters in real time for damage scenario 1 with 3% noise in acceleration where element 8 damaged 0-12% in braced frame structure

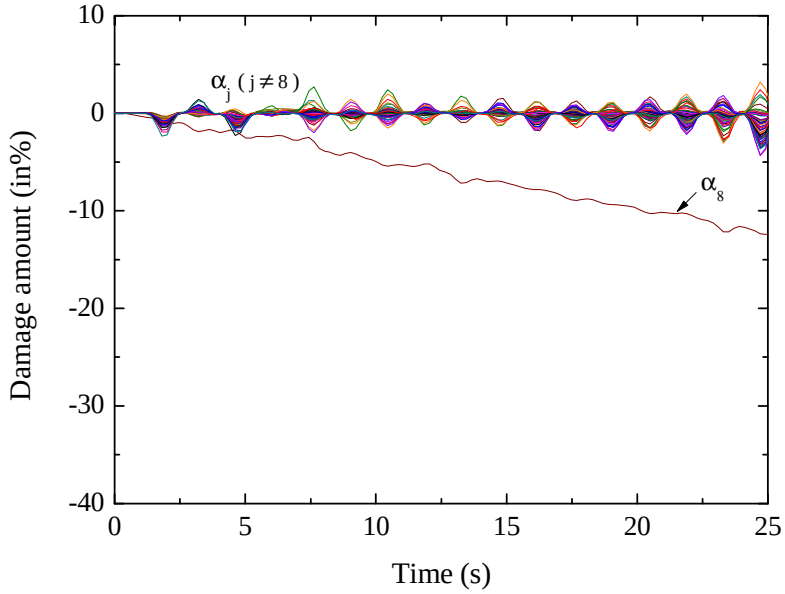

Figure 6.47 Inversely identified damage parameters in real time for damage scenario 1 with 5% noise in acceleration where element 8 damaged 0-12% in braced frame structure

Damage scenario 2

Damage scenario 2 involves two damaged brace members with different damage magnitudes. Simulated damage from 0% to 20% at element 16 is considered in addition to damaged element 8 in damage scenario1. Figure 6.48 gives the result of noise-free case for inverse predictions of structural damage. Two damaged elements 8 and 16 are clearly identified as predicted. The results in Figure 6.49 to Figure 6.51show some false damage detections in the prediction of damage parameters due to the noise effect in measurements. More false predictions are indicated at higher noise level. However, the predictions for location and amount of the considered damaged elements are correctly identified by the proposed method.

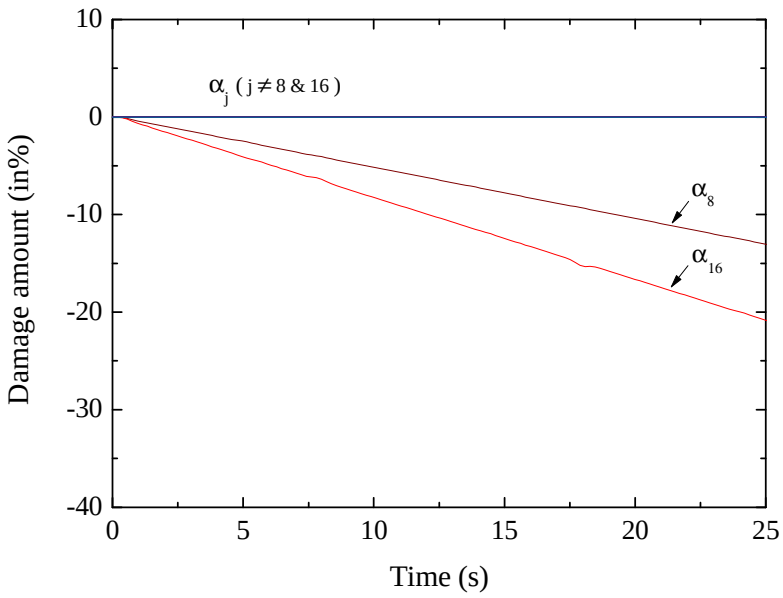

Figure 6.48 Inversely identified damage parameters in real time for damage scenario 2 without noise in acceleration where elements 8 and 16damaged 0-12% and 0-20% in braced frame structure respectively

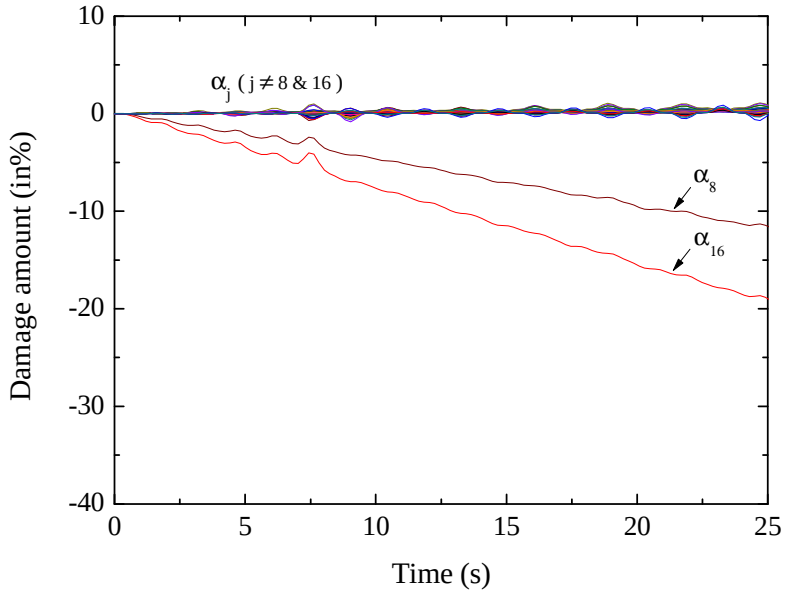

Figure 6.49 Inversely identified damage parameters in real time for damage scenario 2 with 1% noise in acceleration where elements 8 and 16 damaged0-12% and 0-20% in braced frame structure respectively

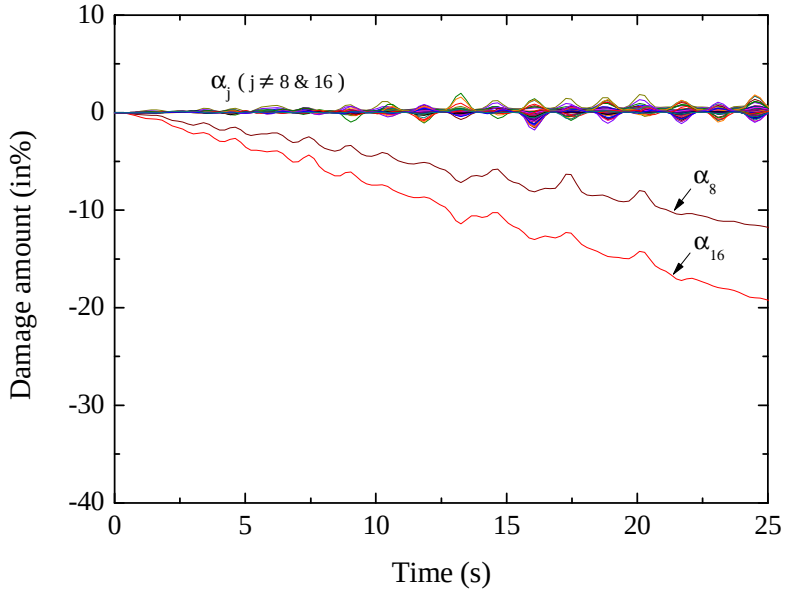

Figure 6.50 Inversely identified damage parameters in real time for damage scenario 2 with 3% noise in acceleration where elements 8 and 16 damaged0-12% and 0-20% in braced frame structure respectively

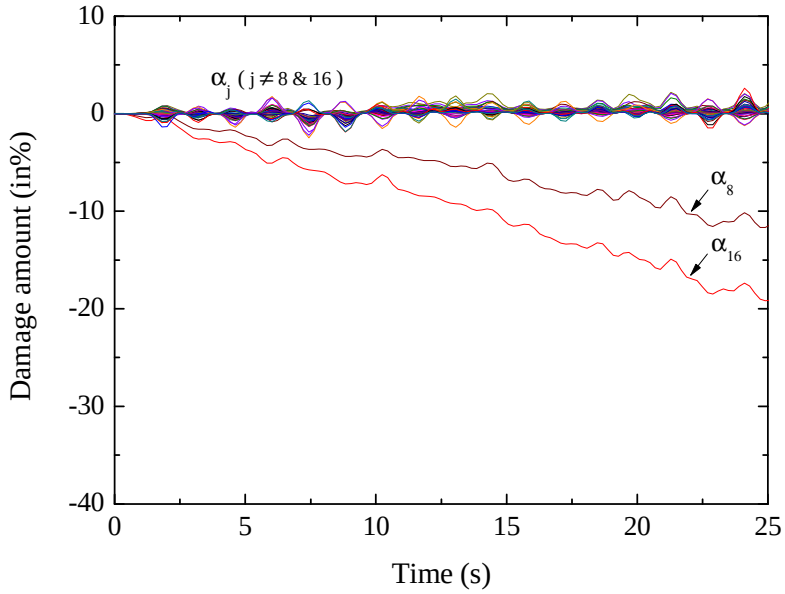

Figure 6.51 Inversely identified damage parameters in real time for damage scenario 2 with 5% noise in acceleration where elements 8 and 16 damaged0-12% and 0-20% in braced frame structure respectively

Damage scenario 3

In damage scenario 3, multiple damaged elements 8, 16, 40 and 48 with various damage magnitudes are considered. Simulated damage magnitudes of above damaged elements are summarised in Table 6.7. This is more difficult damage pattern to be identified due to increasing damaged elements in the structure when compared to the above damage patterns discussed. The result for identified damage parameters in noise-free case is plotted in Figure 6.52. There are some unstable predictions of damage parameters as more damaged elements are involved. Again, Figure 6.53 to Figure 6.55show some false damage indications due to existence of noise but the magnitudes of all damaged elements are clearly identified. It can be seen that the proposed approach provides results agreeing well with the locations and magnitudes of simulated structural damage for this complex case too.

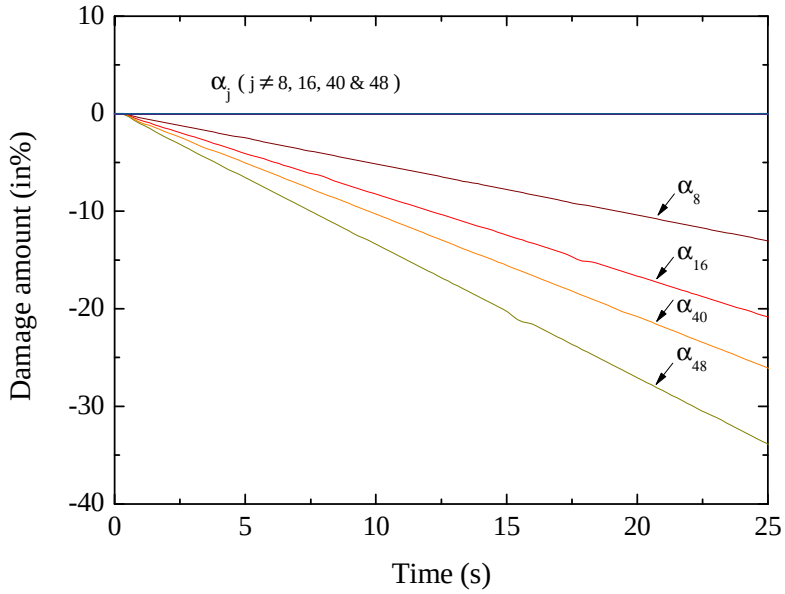

Figure 6.52 Inversely identified damage parameters in real time for damage scenario 3 without noise in acceleration where elements 8, 16, 40 and 48 damaged 0-12%, 0-20%, 0-25% and 0-33% in braced frame structure respectively

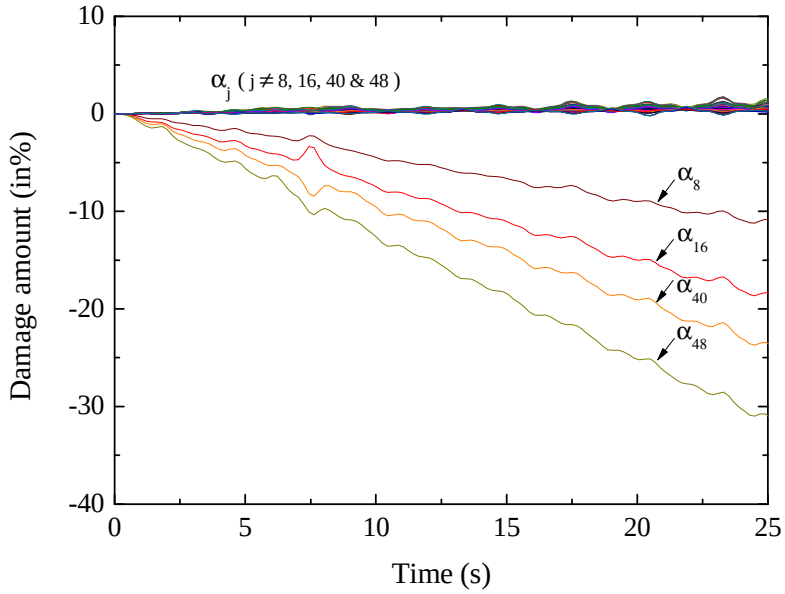

Figure 6.53 Inversely identified damage parameters in real time for damage scenario 3 with 1% noise in acceleration where elements 8, 16, 40 and 48 damaged 0-12%, 0-20%, 0-25% and 0-33% in braced frame structure respectively

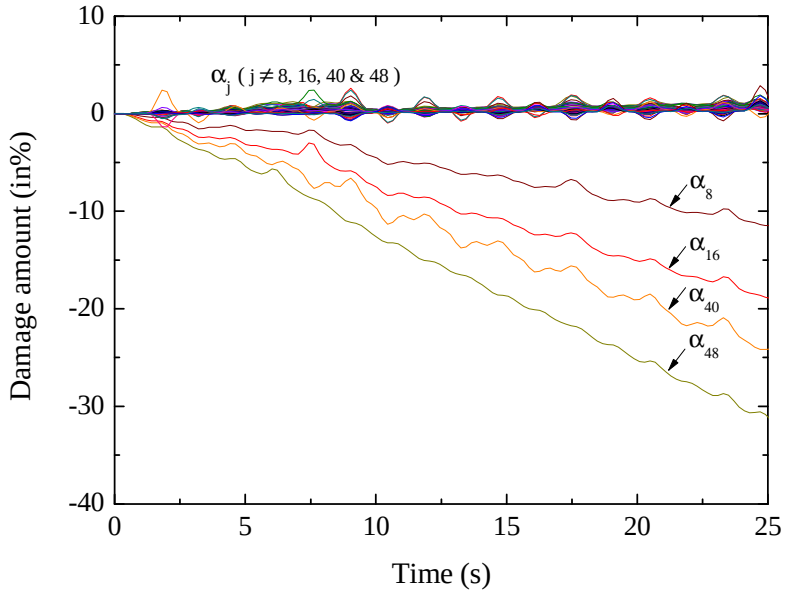

Figure 6.54 Inversely identified damage parameters in real time for damage scenario 3 with 3% noise in acceleration where elements 8, 16, 40 and 48 damaged 0-12%, 0-20%, 0-25% and 0-33% in braced frame structure respectively

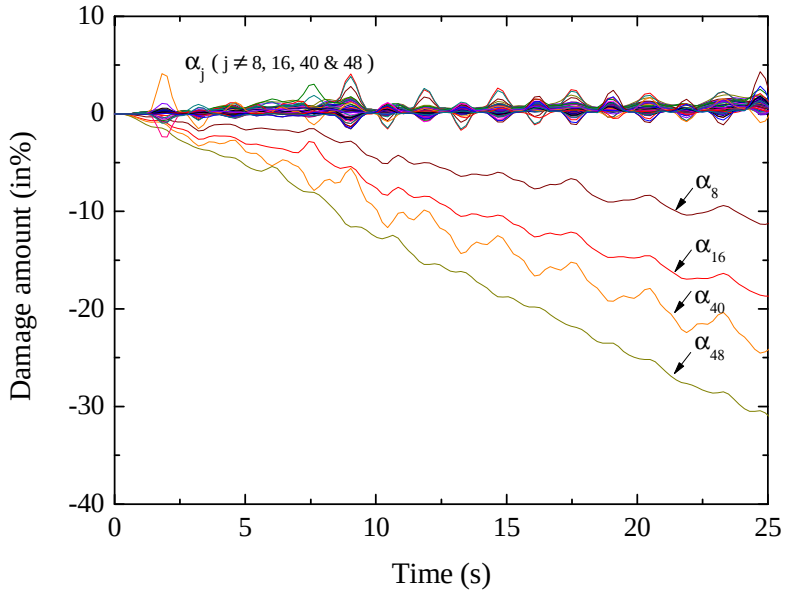

Figure 6.55 Inversely identified damage parameters in real time for damage scenario 3 with 5% noise in acceleration where elements 8, 16, 40 and 48 damaged 0-12%, 0-20%, 0-25% and 0-33% in braced frame structure respectively

6.10 Conclusions

A new method for real-time structural damage identification is presented. In this method, appropriate damage parameters are defined to characterize the local damage evolution for individual structural members by decreasing structural stiffness at element level. A system of linear equations for determining damage parameters is developed by directly adopting vibration measurements such as acceleration. The Tikhonov regularisation algorithm incorporating the L-curve criterion is employed to filter out the influence of noise in the measured data. Then, damage parameters are inversely predicted from the developed equation. Those damage parameters could be used in real time detection of structural damage evolution. Based on the numerical results involving cantilever beams, one-bay plane frame, and one-bay and three-bay braced frame examples, the following conclusions are noted: (1) The proposed new method is capable of successfully detecting the local damage in the structure; (2) It can be used for detecting damage in the structure at early stage; (3) Damage location and magnitude can be identified with relatively high accuracy; (4) The new proposed technique performs well for all simulated damage cases and produces stable and reliable results even though existing certain levels of noise exist in the measurements; (5) It can also be used for real time and rapid damage assessment during operation and immediately after the events of earthquake and explosion. However, the current limitation of the proposed method is that it requires measured dynamic responses in all degrees of freedom of the structure and same applied force for both undamaged and damaged structures. In practice, numbers of sensor available are limited due to economic constraints and difficulty in measuring dynamic responses at all degrees of freedom for a large structure. Moreover, excitation force for actual large structure in structural dynamic testing is usually unknown

and ambient vibration testing is more practical. Therefore, further research developments such as using unknown excitation forces, expansion of incomplete measurements to complete full degrees of freedom measurements or reduction of finite element model to the measured degrees of freedom, and experimental verification utilising real measured data should be continued.

Chapter 7 Summary, Conclusions and Further Works

7.1 Conclusions

In this PhD study, research problems and objectives are presented. Relevant literatures are reviewed. Then methodologies and techniques used in current research are described. Finally, the critical contribution and recommended areas of future research are presented.Initially, numerical simulation investigation and experimental study of a steel frame model structure including intact and four damage scenarios have been conducted. The objectives of the experiments were to determine the modal parameters of tested structure from vibration measurements and apply the modal data into the proposed model updating method. Dynamic characteristics of the analytical models are obtained from finite element dynamic analysis of the tested structure. The optimum sensor arrangement was determined based on the analytical mode shapes and repeatedly moving sensor locations which did not affect significantly the modal data. Modal parameters are identified from the measured acceleration data through modal analysis techniques. Comparison of analytical and measured modal data provides the real dynamic behaviour of the structure. The results show that modal parameters of actually constructed structures can be successfully identified, and are in good agreement with analytical results.

Furthermore, an effective finite element model updating method is presented for adjusting analytical models of the experimental structure by utilising only limited information about measured incomplete mode shapes. Structural updating parameters are chosen to characterise the modifications of the structure at element or integration point level in order to adjust the stiffness at the connections of structural members such as beam-column joints. From the

obtained exact relationship between the perturbation of structural parameters and the modal properties of the actual tested structure, an iterative solution algorithm is developed to solve for the chosen structural updating parameters in the least squares sense. The regularisation algorithm based on the Tikhonov solution incorporating the L-curve criterion is employed to reduce the influence of measurement errors in the modal data and to produce robust solutions for the updating parameters.

The laboratory tested steel frame model structure is utilised to demonstrate the accuracy and effectiveness of the proposed method for updating the finite element model by numerical simulation investigations and experimental studies. The practical application of the proposed method is demonstrated by correctly updating the Canton Tower benchmark problem using the operational modal properties identified from ambient vibration measurements. Based on the numerical simulations, experimental studies and practical applications, the following conclusions are drawn. The new effective model updating procedure discussed here is capable of successfully updating structural parameters such as stiffness at both element and critical point levels. The proposed approach converges quickly to evaluate the structural updating parameters, and provides optimised solutions for model updating in the least squares sense without requiring optimisation techniques even in the cases where large modifications of structural parameters exit. The proposed model updating method provides reasonably small modifications of structural properties to minimise the relatively large difference between the modal data calculated from the initial analytical model and those identified from the vibration measurements.

For inversely structural damage detection, an inverse damage detection algorithm based on expanded mode shapes is discussed. The incomplete measured modal data are fully expanded

by using a reliable mode shape expansion technique, providing the complete mode shapes at all degrees of freedom of the tested structure. The damage detection technique based on mode shape curvature and modal strain energy calculated from expanded mode shapes is then utilised to detect the damage in the structure. The effectiveness of the proposed method for inverse damage detection is demonstrated by a numerical study of a bridge structure. The results show that the damage in the structure can be detected by utilising only limited vibration measurements and expanded mode shapes.

In addition, a new approach for real-time structural damage detection by using monitored noisy acceleration measurements is presented. In this method, appropriate damage parameters are introduced to characterize the structural damage at element level. The relationship between the damage parameters and the measured dynamic response is then established from the governing equation of the dynamic structure. On the basis of the measured acceleration data, structural dynamic responses such as displacement and velocity are obtained by using Newmark's numerical integration method in order to construct damage equation from the developed equation of motion for the structural system. Tikhonov regularization algorithm incorporating the L-curve criterion for determining the regularisation parameters is employed to filter out the influence of noise in measured data on the predictions of damage parameters. Both the location and extent of the damage are then determined based on the inverse predictions of damage parameters of individual structural elements. Moreover, structural damage evolution with time in the elements is determined from continuously monitored data, and the condition of the structure is then further assessed and updated.

The results from the numerical examples involving a cantilever beam, one-bay plane frame, and one-bay and three-bay braced frame show that damage can be correctly identified in

terms of location and extent in the structure, even in the case when relatively high level of noise exists in the measured vibration data. The new proposed technique performs well and produces stable and reliable results from noisy vibration measurements. Therefore, the developed approach has potential to be used for real-time structural health monitoring such as at the severe loading event of earthquake and blast. However, the limitation of the proposed method is that it requires measured time history dynamic responses such as accelerations at all degrees of freedom of the structure and same applied force for both analytical model and tested structure.

7.2 Further works

The success of the proposed model updating method depends on the accuracy of mode shapes and natural frequencies identified from the limited sensor measurements. Therefore, the development of methods for optimum sensors arrangements is required. The proposed real-time damage detection method is proved to be effective with numerical examples. Further evaluation and implementation of real time measured data for practical damage detection approach should be carried out. The proposed damage detection method has been shown to work under certain circumstances such as requiring same applied forces for analytical model and tested structure. The applied force can be obtained in control vibration testing. However, application of the proposed method is limited in the cases of ambient vibration testing where unknown applied force or input measurements is not available. To make this method more practical, further developments of using unknown excitation force is required.

The proposed real-time damage detection method requires not only acceleration data but also velocity and displacement data at all degrees of freedom. In order to achieve this, more

reliable methods for the calculation of velocity and displacement from measured acceleration and development of more robust model reduction or modal expansion techniques are required. The performances of real-time damage detection algorithm in the controlled laboratory and real operational environments still need to be validated. Finally, the ultimate goal of “Damage Prognosis” needs to be addressed, which estimates the remaining service life of a structure, providing the assessment of its current damaged state and performance predictions in the future loading environments.

References

Agarwal P, Wood S, Kurtulus A, Menq F.Y, Rathje E.M, Stokoe K. 2010. Dynamic field tests of small-scale bridge bents supported on drilled shafts. http://nees.org/ resources/ 1434.

Allemang R.L, Brown D. L. 1983. A correlation coefficient for modal vector analysis.*1st International Modal Analysis Conference*, Bethel, Connecticut, USA, 110-116.

Alvandi A, Cremona C. 2006. Assessment of vibration-based damage identification techniques.*Journal of Sound and Vibration* 292**:**179-202.

Alwash M, Sparling B.F, Wegner L.D. 2009. Influence of excitation on dynamic system identification for multi-span reinforced concrete bridge. *Advances in Civil Engineering*Article ID 859217.

Avitabile P. 2005.Model reduction and model expansion and their applications - part 1: Theory. *23rd Conference and Exposition on Structural Dynamics (IMAC - XXIII),* Florida, USA.

Bakira P.G, Reynders E, De Roeck G. 2007. Sensitivity-based finite element model updating using constrained optimization with a trust region algorithm.*Journal of Sound andVibration* 305**:**211-25.

Bakira P.G, Reynders E, De Roeck G. 2008. An improved finite element model updating method by the global optimization technique “Coupled Local Minimizers”.*Computers andStructures* 86**:**1339-1352.

Baneen U, Kinkaid N.M, Guivant J.E, Herszberg I. 2012. Vibration based damage detection of a beam-type structure using noise suppression method. *Journal of Sound and Vibration*331(8)**:**1777-1788.

Baruch M, Bar Itzhack Y. 1978. Optimal weighted orthogonalization of measured modes.*AIAA Journal* 16(4)**:**346-351.

Baruch M. 1978. Optimization procedure to correct stiffness and flexibility matrices using vibration tests.*AIAA Journal* 16(11)**:**1208-1210.

Berman A. 1979. Comment on "Optimal weighted orthogonalization of measured modes".*AIAA Journal* 17**:**927-928.

Berman A, Nagy E.J. 1983. Improvement of a large analytical model using test data.*AIAA Journal* 21(8)**:**1168-1173.

Brownjohn J.M.W, Magalhaes F, Caetano E, Cunha A. 2010. Ambient vibration re-testing and operational modal analysis of the Humber Bridge.*Engineering Structures* 32(8)**:** 2003-2018.

Bayissa W.L, Haritos N. 2007. Structural damage identification in plates using spectral strain energy analysis.*Journal of Sound and Vibration* 307**:**226-249.

Brownjohn J.M.W, Xia P.Q. 2000. Dynamic assessment of curved cable-stayed bridge by model updating.*Journal of Structural Engineering*126(2)**:**252–260.

Brownjohn J.M.W, Hao H, Pan T.C. 2001. Assessment of structural condition of bridges by dynamic measurements.*Applied Research Project*, Nanyang Technological University, Singapore.

Brownjohn J.M.W, Moyo P, Omenzetter P, Lu Y. 2003. Assessment of highway bridge upgrading by dynamic testing and finite element model updating. *Journal of Bridge Engineering* 8(3)**:**162-172.

Caesar B. 1987. Updating system matrices using modal test data.*5th IMAC* 453-459.

Caesar B, Peter J. 1987. Direct update of dynamic mathematical models from modal test data.*AIAA Journal* 25(11)**:**1494-1499.

Carden E.P, Fanning P. 2004. Vibration based condition monitoring: A review. *Structural Health Monitoring Journal* 3(4)**:**355-377.

Carvalho J, Datta B.N, Gupta A, Lagadapati M. 2007. A direct method for model updating with incomplete measured data and without spurious modes.*Mechanical Systems and SignalProcessing* 21**:**2715-2731.

Cawley P, Adams R.D. 1979. The location of defects in structures from measurement of natural frequency. *Journal of Strain Analysis* 14**:**49-57.

Chandrashekhar M, Ganguli R. 2009. Damage assessment of structures with uncertainty by using mode shape curvatures and fuzzy logic.*Journal of Sound and Vibration* 326**:**939-957.

Chang C.C, Chen L.W. 2005. Detection of the location and size of cracks in the multiple cracked beam by spatial wavelet based approach. *Mechanical Systems and Signal Processing* 19**:**139-155.

Chang P.C, Flatau A, Liu S.C. 2003. Review paper: Health monitoring of civil infrastructure. *Structural Health Monitoring Journal* 2(3)**:**257-267.

Charles R.F, Nick A.J.L. 2006. Damage prognosis: The future of structural health monitoring. *Philosophical Transactions of The Royal Society* A 365**:**623-632.

Chase J. G, Hwang K. L, Barroso L. R, Mander J. B. 2004. A simple LMS-based approach to the structural health monitoring benchmark problem.*Journal of Earthquake Engineering & Structural Dynamic* 34(6)**:**575-594.

Chen H.P, Bicanic N. 2000. Assessment of damage in continuum structures based on incomplete modal information.*Computers and Structures* 74**:**559-570.

Chen H.P. 2005. Nonlinear perturbation theory for structural dynamic systems.*AIAA Journal* 43(11)**:**2412-2421.

Chen H. P, Bicanic N. 2006. Inverse damage prediction in structures using nonlinear dynamic perturbation theory. *Journal of Computation Mechanic* 37(5)**:**455-467.

Chen H.P. 2008. Application of regularization methods to damage detection in large scale plane frame structures using incomplete noisy modal data. *Engineering Structures* 30(11)**:**3219-3227.

Chen H.P. 2010. Mode shape expansion using perturbed force approach.*Journal of Sound andVibration*329(8)**:**1177-1190.

Chen H.P, Bicanic N. 2010. Identification of structural damage in buildings using iterative procedure and regularisation method. *Engineering Computations* 27(8)**:**930-950.

Chen W.H, Lu Z.R, Lin W, Chen S.H, Ni Y.Q, Xia Y, Liao W.Y. 2011. Theoretical and experimental modal analysis of the Guangzhou New TV Tower.*Engineering Structures*33(12)**:**3628-3646.

Chou J, Ghaboussi J. 2001. Genetic algorithm in structural damage detection.*Composite Strucure* 79**:**1335-1353.

Clough R.W, Penzien J. 1975.*Dynamics of Structures*, McGraw-Hill Book Co.

Colombo S, Giannopoulos A, Forde M.C, Hasson R, Mulholland J. 2005.Frequency response of different couplant materials for mounting transducers. *NDT & E International* 38(3)**:**187-193.

Conte J, He X, Moaveni B, Masri S, Caffrey J, Wahbeh M, Tasbihgoo F, Whang D, Elgamal A. 2008. Dynamic testing of Alfred Zampa memorial bridge. *Journal of Structural Engineering* 134(6)**:**1006-1015.

Cooley J.W, Tukey J.W. 1965. An algorithm for the machine calculation of complex Fourier series.*Mathematics of Computation* 19(90)**:**297-311.

Cornwell P, Doebling S.W, Farrar C.R. 1999. Application of the strain energy damage detection method to plate like structures. *Journal of Sound and Vibration* 224**:**359-374.

De Roeck G, Peeters B. 1999. *MACEC2.0—Modal Analysis on Civil Engineering Constructions,* Department of Civil Engineering, Catholic University of Leuven,Belgium.

De Roeck G, Peeters B, Maeck J. 2000. Dynamic monitoring of civil engineering structures.*Computational Methods for Shell and Spatial Structures,* IASS-IACM, Chania, Crete, Greece.

Darwin C. 1859.The Origin of Species.

Dong Y, Song R. 2010.Bridges structural health monitoring and deterioration detection synthesis of knowledge and technology.*Report.*University of Alaska Fairbanks.

Esfandiari A, Bakhtiari-Nejad F, Sanayei M, Rahai A. 2010.Structural finite element model updating using transfer function data.*Computers and Structures*88**:**54-64.

Ettouney M, Daddazio R, Hapij A, Aly A. 1998. Health monitoring of complex Structures.*Smart Structures and Materials: Industrial and Commercial Applications of Smart Structures Technologies, Proceedings of SPIE,* 326(3)**:**368-379.

Ewins D.J. 2000. Modal testing: theory, practice and application. Baldock, Research Studies Press.

Fan W and Qiao P. 2009. A 2-D continuous wavelet transform of mode shape data for damage detection of plate structures.*International Journal of Solids and Structures* 46**:**4379-4395.

Fan W and Qiao P. 2011. Vibration-based damage identification methods: A review and comparative study. *Structural Health Monitoring Journal* 10(1)**:**83-29.

Fang S.E, Perera R, De Roeck G. 2008. Damage identification of a reinforced concrete frame by finite element model updating using damage parameterization.*Journal of Sound and Vibration* 313**:**544-559.

Farrar C.R, Cone K.M. 1995. Vibration testing of the I-40 bridge before and after the introduction of damage. *13th International Modal Analysis Conference,* Nashville TN 203-209.

Farrar C.R, Doebling S.W. 1999. Damage detection II: Field applications to large structures. In: Silva, J.M.M. and Maia, N.M.M. (eds.), *Modal Analysis and Testing*, Nato Science Series. Dordrecht, Netherlands, Kluwer Academic Publishers.

Farrer C.R, Cornwell P.J, Doebling S.W, Prime M.B. 2000. Structural health monitoring studies of the Alamosa Canyon and I-40 Bridges.*Technical Report LA-13635-MS*, Los Alamos National Laboratory, Los Alamos, NM, USA.

Farrar C.R, Leiven N.A.J.2007. Damage prognosis: the future of structural health monitoring. *Philosophical Transactions of the Royal Society A* 365**:**623-632.

Farrar C.R, Worden K. 2007. An introduction to structural health monitoring. *Philosophical Transactions of the Royal Society A* 365**:**303-315.

Flynn E.B, Todd M.D. 2010. A Bayesian approach to optimal sensor placement for structural health monitoring with application to active sensing.*Mechanical Systems and Signal Processing* 24**:**891-903.

Friswell M.I, Garvey S.D, Penny J.E.T. 1995.Model reduction using dynamic and iterated IRS techniques.*Journal of Sound Vibration* 186(2)**:**311-323.

Friswell M.I, Garvey S.D, Penny J.E.T. 1998.The convergence of the iterated IRS method. *Journal of Sound and Vibration* 211(1)**:**123-132.

Friswell M.I, Mottershead J.E. 1995. *Finite element model updating in structural dynamics*. Kluwer Academic Publishers, Dordrecht, The Netherlands.

Friswell M.I, Inman D.J, Pilkey D.F. 1998. Direct updating of damping and stiffness.*AIAA Journal*36(3)**:**491-493.

Friswell M.I. 2007.Damage identification using inverse methods.*Philosophical Transactions of the Royal Society A* 365**:**393-410.

Fox C.H.J. 1992. The location of defects in structures: A comparison of the use of natural frequency and mode shape data. *10th International Modal Analysis Conference,* San Diego, California, 1**:**522-528.

Gallego R, Rus G. 2004. Identification of cracks and cavities using the topological sensitivity boundary integral equation. *Computational Mechanic* 33(2)**:**154-163.

Gandomi A.H, Sahab M.G, Rahaei A, Safari Gorji M. 2008.Development in modes shape-based structural fault identification technique.*World Applied Sciences Journal*,5(1)**:**29-38.

Girard A, Defosse H. 1993. Frequency response smoothing and structural path analysis: application to beam trusses. *Journal of Sound and Vibration*165(1)**:**165-170.

Guyan R.J. 1965. Reduction of stiffness and mass matrices.*AIAA Journal* 3(2)**:**380.

Guedri M, Bouhaddi N, Majed R. 2006. Reduction of the stochastic finite element models using a robust dynamic condensation method. *Journal of Sound and Vibration* 297(1-2)**:**123-145.

Han S. 2003. Retrieving the time history of displacement from measured acceleration signal. *KSME Journal* 17(2)**:**197-206.

Hansen P.C, O'Leary D.P. 1993. The use of the L-curve in the regularization of discrete ill-posed problem. *SIAM Journal of Scientific Computing* 14 (6)**:**1487-1503.

Hansen P.C.1998. Rank-deficient and discrete ill-posed problems: Numerical aspects of linear inversion. *SIAM*, Philadelphia.

Hansen P.C. 2000. The L-curve and its use in the numerical treatment of inverse problems, Computational inverse problems in electrocardiology, ed. P. Johnston. *Advances in Computational Bioengineering* 4**:**119-142.

Hansen P.C. 2007. Regularization Tools: A Matlab package for analysis and solution of discrete ill-posed problems. *Version 4.1 for Matlab 7.3, Numerical Algorithms* 16**:**189-194.

Hao H, Xia Y. 2002. Vibration-based damage detection of structures by genetic algorithm. *Journal of Computing in Civil Engineering* 16**:**222-229.

Hinton E, Owen D.R.J. 1985. *An introduction to Finite Element Computations*, Pineridge Press, Swansea, UK.

Hogg R.V, Craig A.T. 1978. *Introduction to Mathematical Statistics*. Macmillan.

Holland J. 1975.Adaptation in natural and artificial systems.MIT Press, Cambridge, Massachusetts, USA.

Hu S.L.J, Bao X, Li H. 2010. Model order determination and noise removal for modal parameter estimation.*Mechanical Systems and Signal Processing* 24**:**1605-1620.

Huang M, Guo W, Zhu H, Li L. 2008. Dynamic test and finite element model updating of bridge structures based on ambient vibration. *Frontiersof Architectureand Civil Engineeringin China* 2**:**139-144.

Hugenschmidt J, Mastrangelo R. 2006. GPR inspection of concrete bridges.*Cement and Concrete Composites* 28(4)**:**384-392.

Humar J, Bagchi A, Xu H. 2006. Performance of vibration-based techniques for the identification of structural damage.*Structural Heath MonitoringJournal*5(3)**:**215-241.

Huth O, Feltrin G, Maeck J, Kilic N, Motavalli M. 2005. Damage identification using modal data: Experiences on a prestressed concrete bridge. *Journal of Structural Engineering ASCE* 131**:**1898-1910.

Humar J, Bagchi A, Xu H. 2006. Performance of vibration-based techniques for the identification of structural damage.*Structural Health Monitoring Journal, SAGE* 5(3)**:**215-241.

Huynh D, He J, Tran D.2005. Damage location vector: A non-destructive structural damage detection technique. *Computers and Structures* 83(28-30)**:**2353-2367.

Inman D.J, Minas C.1990. Matching finite element models to modal data. Transactions of the ASME, *Journal of Vibration and Acoustics* 84-92.

Jaishi B. 2005. Finite element model updating of Civil Engineering structures under operational conditions.PhD thesis, Fuzhou University, China.

Jaishi B, Ren W. X. 2005. Structural finite element model updating using ambient vibration test results.*Journal of Structural Engineering* 131**:**617-628.

Jaishi B, Ren W. X. 2006. Damage detection by finite element model updating using modal flexibility residual.*Journal of Sound and Vibration* 290**:**369-387.

Kang J.S, Park S.K, Shin S.B, Lee H.S. 2005. Structural system identification in time domain using measured acceleration. *Journal of Sound and Vibration* 288**:**215-234.

Kessler S.S, Spearing S.M, Atalla M.J, Cesnik C.E.S, Soutis C. 2002.Damage detection in composite materials using frequency response methods.*Composites Engineering* Part B 33**:**87-95.

Kilmer M.E, O'Leary D.P. 1998. Choosing regularization parameters in iterative methods for ill-posed problems. *SIAM Journal on Matrix Analysis and Application* 22(4)**:**1204-1221.

Kim J.T, Stubbs N. 1995. Model uncertainty impact and damage detection accuracy in plate girder. *Journal of Structural Engineering* 121(10)**:**1409-1417.

Kim J.T, Ryu Y.S, Cho H.M, Stubbs N. 2003. Damage identification in beam-type structures: frequency-based method vs. mode-shape based method, *Engineering Structures* 25(1)**:** 57-67.

Lakshmanan N, Raghuprasad B.K, Gopalakrishnan N, Sathishkumar K, Murthy S.G.N. 2012. Detection of contiguous and distributed damage through contours of equal frequency change.*Journal of Sound and Vibration* 329**:**1310-1331.

Lam H.F, Yin T. 2011. Dynamic reduction-based structural damage detection of transmission towers: Practical issues and experimental verification. *Engineering Structures* 33(5)**:** 1459-1478.

Labview 2009. Signalexpress signal processing software. National Instruments Ltd.

Lee Y, Chung M. 2000. A study on crack detection using eigen frequency test data. *Computers and Structures* 77**:**327-342.

Lee U, Shin J. 2002. A frequency response function-based structural damage identification method.*Computers and Structures* 80**:**117-132.

Li H, Wang J, Hu S.L.J. 2008. Using incomplete modal data for damage detection in offshore jacket structures. *Ocean Engineering* 35(1718)**:**1793-1799.

Li J, Wu B, Zeng Q.C, Lim C.W. 2010. A generalized flexibility matrix based approach for structural damage detection. *Journal of Sound and Vibration* 329**:**4583-4587.

Lieven N.A.J, Ewins D.J. 1990. Error location and updating finite element models using singular value decomposition.*Proceeding of the 8th IMAC,* 768-773, Kissimmee, Florida.

Link M, Weiland M, Barragan J.M. 1987. Direct physical matrix identification as compared to phase resonance testing: An assessment based on practical application.*5th IMAC* 804-881.

Liu F. 2011. Direct mode-shape expansion of a spatially incomplete measured mode by a hybrid-vector modification.*Journal of Sound and Vibration* 330(18-19)**:**4633-4645.

Liu P.L, Sun S.C. 1997. The application of artificial neural networks on the health monitoring of bridges.*Structural Health Monitoring, Current Status andPerspectives*, Stanford University, Palo Alto, California, 103-110.

Sohn H, Farrar C.R, Hemez F.M, Shunk D.D, Stinemates D.W, Nadler B.R. 2003. A review of structural health monitoring literature:1996-2001.*Los Alamos national laboratory report LA-13976-MS.*

Lu C.J, Hsu Y.T. 2002. Vibration analysis of an inhomogeneous string for damage detection by wavelet transform. *International Journal of Mechanical Sciences* 44(4)**:**745-754.

Lu K.C, Wang Y. Lynch J.P, Loh C. H, Chen Y.J, Lin P.Y, Lee Z.K. 2006. Ambient vibration study of Gi-Lu cable-stay bridge: Application of wireless sensing units. *Proceeding SPIE 6174, Smart Structures and Materials.*

Ma T.W, Yang H.T, Chang C.C. 2005.Structural damage diagnosis and assessment under seismic excitations.*Journal of Engineering Mechanics* 131(10)**:**1036-1045.

Maeck J, De Roeck G. 1999. Damage detection on a prestressed concrete bridge and RC beams using dynamic system identification.*International Conference on Damage Assessment of Structures (DAMAS 99)*, Dublin, Ireland, 320-327.

Maia N.M.M, Silva J.M.M. 1997. *Theoretical and experimental modal analysis*, ResearchStudies Press, Letchworth.

Mares C, Mottershead J.E, Friswell M.I. 1999.Damage location in beams by using rigid body constraints.*International Conference on Damage Assessment of Structures (DAMAS 99)*, Dublin, Ireland, 381-390.

Maung T.S, Chen H.P, Alani A.M. 2010. Inversely detecting structural damage in bridges based on expanded mode shapes.*18th UK Conference of ACME*, University of Southampton, UK.

Maung T.S, Chen H.P, Tee K.F, Alani A.M. 2011. Updating finite element model from vibration measurements.*19th UK Conference of ACME*, Heriot-Watt University, UK.

Maung T.S, Chen H.P, Alani A.M. 2011. Real time structural damage assessment from vibration measurements.*9th International Conf on Damage Assessment of Structures*, St Anne's College, University of Oxford, UK.

Maung T.S, Chen H.P, Alani A.M. 2012. Structural health monitoring from on-line monitored vibration measurements. *3rd International Symposium on Life-Cycle Civil Engineering, IALCCE 2012 Conference*, Hofburg Palace, Austria.

Maung T.S, Chen H.P, Alani A.M.2012. Structural damage detection using monitored noisy acceleration data. *1st International Conference on Performance-based and Life-cycle Structural Engineering (PLSE 2012),* Hong Kong Polytechnic University, Hong Kong, China.

Maung T.S, Chen H.P, Alani A.M. 2013. Robust dynamic finite element model updating using modal measurements.*International Conference on Computational Mechanics* (CM13), Durham University, UK.

Meo M, Zumpano G. 2005. On the optimal sensor placement techniques for a bridge structure. *Journal of Engineering Structures* 27(10)**:**1488-1497.

ME'scope VES V.5. 2010. Modal analysis software. Vibrant Technology Ltd.

Michel C, Guéguen P, Bard P.Y. 2008. Dynamic parameters of structures extracted from ambient vibration measurements: An aid for the seismic vulnerability assessment of existing buildings in moderate seismic hazard regions. *Soil Dynamics and Earthquake Engineering* 28(8) 593-604.

Miguel L.F.F, De Menezes R.C.R, Miguel L.F.F 2006. Mode shape expansion from data-based system identification procedures. *Mecanica Computacional* 115**:**1593-1602.

Modak S.V, Kundra T.K, Nakra B.C. 2002. Comparative study of model updating methods using simulated experimental data.*Computers and Structures*80**:**437-447.

Mohd-Yasin F, Zaiyadi N, Nagel D.J, Ong D.S, Korman C.E, Faidz A.R. 2009. Noise and reliability measurement of a three-axis micro-accelerometer.*Microelectronic Engineering* 86**:**991-995.

Mottershead J.E, Friswell M.I. 1993. Model updating in structural dynamics: A survey.*Journal of Sound and Vibration* 167(2)**:**347-375.

Mottershead J.E, Link M, Friswell M.I. 2011. The sensitivity method in finite element model updating: A tutorial.*Mechanical Systems and Signal Processing*25**:**2275-2296.

Moore B. C.1976.On the flexibility offered by state feedback in multivariable system beyond closed loop eigenvalue assignment.*IEEE Transactions on Automatic Control* 689-692.

Moyo P, Brownjohn J.M.W, Suresh R, Tjin S.C. 2005. Development of fiber Bragg grating sensors for monitoring civil infrastructure. *Engineering Structures* 27(12)**:**1828-1834.

Newland D.E 1985. An introduction to random vibrations and spectral analysis. 2nd ed, Longman Group Ltd.

Nobahari M, Seyedpoor S.M. 2011. Structural damage detection using an efficient correlation-based index and a modified genetic algorithm.*Mathematical and Computer Modelling*53(9-10)**:**1798-1809.

Ni Y.Q, Xia Y, Liao W.Y, Ko J.M. 2009. Technology innovation in developing the structural health monitoring system for Guangzhou New TV Tower.*Structural Control and HealthMonitoring* 16(1)**:**73-98.

Ni Y.Q, Wong K.Y, Xia Y. 2011. Health checks through landmark bridges to sky-high structures. *Advances in Structural Engineering* 14(1)**:**103-119.

Ni Y.Q, Liao W.Y, Xia Y, Ko J.M. 2011. Structural health monitoring of supertall structures: an engineering paradigm and technology showcase. *Proceedings of the International Symposium on Innovation and Sustainability of Structures in Civil Engineering, Xiamen, China*.*Innovation and Sustainability of Structures* 131-142.

Nikolakopoulos P.G, Katsareas D.E, Papadopoulos C.A. 1997. Crack identification in frame structures. *Computers and Structures* 64(1-4)**:**389-406.

O'Callahan J, Avitabile P, Riemer R. 1989. System equivalent reduction expansion process.*7th International Modal Analysis Conference*, Las Vegas, 29-37, USA.

O'Callahan J.C. 1989. A procedure for an Improved Reduced System (IRS) model.*7th International Modal Analysis Conference*, Las Vegas, 17-21, USA.

Ohm W.S, Wu L, Hanes P, Wong G.S.K. 2006. Generation of low-frequency vibration using a cantilever beam for calibration of accelerometers. *Journal of Sound and Vibration*289(1-2)**:**192-209.

Palmonella M, Friswell M.I, Mottershead J.E, Lees A.W. 2005. Finite element models of spot welds in structural dynamics: Review and updating.*Computers and Structures*83**:**648-661.

Panayirci H.M, Pradlwarter H.J, Schueller G.I. 2011. Efficient stochastic structural analysis using Guyan reduction. *Advances in Engineering Software*42(4)**:**187-196.

Pandey P.C, Barai S.V. 1995. Multilayer perceptron in damage detection of bridge structures.*Computers and Structures* 54(4)**:**597-608.

Park S.A, Choi J.S, Min K.W. 2011.Dynamic Characteristics for Traditional Wooden Structure in Korea by Using Impact Hammer Test. *Procedia Engineering* 14**:**477-484.

Pastor M, Binda M, Harcarik T. 2012. Modal Assurance Criterion.*Procedia Engineering* 48**:**543-548.

Pavic A, Reynolds P. 2007. Appendix C: Dynamic testing of building floors, *Design of Floors for Vibration: A New Approach*. The Steel Construction Institute, 84-96. ISBN 1-85942-176-8.

Peeters B, De Roeck G. 1999. Reference-based stochastic subspace identification for output-only modal analysis.*Mechanical systems and signal processing* 13(6)**:**855-878.

Peeters B, De Roeck G. 2001. Stochastic system identification for operational modal analysis: A review. *Journal of Dynamic Systems, Measurement and Control* 123(4)**:**659-667.

Perera R, Torres R. 2006. Structural damage detection via modal data with genetic algorithms.*Journal of Structural Engineering* 132(9)**:**1491-1501.

Qiao P.Z, Lu K, Lestari W, Wang J. 2007. Curvature mode shape-based damage detection in composite laminated plates.*Composite Structures* 80**:**409-428.

Quek S.T, Tran V.A, Hou X.Y, Duan W.H. 2009. Structural damage detection using enhanced damage locating vector method with limited wireless sensors.*Journal of Sound and Vibration* 328**:**411-427.

Rahai A, Bakhtiari-Nejad F, Esfandiari A. 2007. Damage assessment of structure using incomplete measured mode shapes. *Structural Control and Health Monitoring*14**:**808-829.

Rainieri C, Fabbrocino G, Manfredi G, Dolce M. 2012. Robust output-only modal identification and monitoring of buildings in the presence of dynamic interactions for rapid post-earthquake emergency management.*Engineering Structures* 34**:**436-446.

Rana K.P.S. 2011. Fuzzy control of an electrodynamic shaker for automotive and aerospace vibration testing. *Expert Systems with Applications*38(9)**:**11335-11346.

Rajasekaran S, Varghese S.P. 2005. Damage detection in beams and plates using wavelet transforms. *Computers and Concrete* 2(6)**:**481-498.

Reynders E, De Roeck G. 2010. A local flexibility method for vibration-based damage localization and quantification.*Journal of Sound and Vibration* 329**:**2367-2383.

Reynders E, Teughels A, De Roeck G. 2010. Finite element model updating and structural damage identification using OMAX data.*Mechanical Systems and Signal Processing* 24**:**1306-1323.

Reynolds P, Pavic A, Prichard S. 2002. Dynamic analysis and testing of a high performance floor ftructure. *International Conference on Structural Dynamics Modelling - Test, Analysis, Correlation and Validation*, Madeira Island, Portugal, 339-346.

Rhim J, Lee S.W. 1995. A neural network approach for damage detection and identification

of structures. *Computational Mechanic* 16(6)**:**437-443.

Rizos P.F, Aspragathos N, Dimarogonas A.D. 1990. Identification of crack location and magnitude in a cantilever beam from the vibration modes.*Journal of Sound and Vibration*138(3)**:**381-388.

Ribeiro D, Calcada R, Delgado R, Brehm M, Zabel V. 2012. Finite element model updating of a bowstring-arch railway bridge based on experimental modal parameters. *Engineering Structures* 40**:**413-435.

Robson B.N,Harik I.E. 1998. Pullback testing of seismically isolated P/C I-girder bridge. *Journal of Structural Engineering* 124(8)**:**930-937.

Ross R.G. 1971. Synthesis of stiffness and mass matrices.*SAE conference paper* 710787.

Rytter A.1993. Vibration based inspection of civil engineering structures. Ph.D. Dissertation, Department of Building Technology and Structural Engineering, Aalborg University, Denmark.

Safak E, Hudnut K. 2006. Real-time structural monitoring and damage detection by acceleration and GPS sensors.*8th US National Conference on Earthquake Engineering*, San Francisco, California, USA.

Salawu O.S, Williams C. 1995. Bridge assessment using forced-vibration testing.*Journal of Structural Engineering* 121(2)**:**161-173.

Sanliturk K.Y, Cakar O. 2005. Noise elimination from measured frequency response functions. *Mechanical Systems and Signal Processing* 19**:**615-631.

Sazonov E. S, Klinkhachorn P, Halabe U. B. 2002. Genetic Algorithms based parameter optimization of a non-destructive damage detection method.*Proceedings of the Thirty-Fourth Southeastern Symposium*, 152-156.

Shi Z.Y, Law S.S, Zhang L.M. 2000. Structural damage detection from modal strain energy

change.*Journal of Engineering Mechanics*126(12)**:**1216-1223.

Sidhu J, Ewins D. J. 1984. Correlation of finite element and modal test studies of a practical structure. *Proceeding of the 2nd IMAC* 756-762, Orlando, Florida, USA.

Silva N.R.S.D, Corso L.L, Tamagna A, Gomes H.M. 2006.Genetic algorithms and modal sensitivity for damage detection on portal frames.*Mecanica Computacinoal* 115**:**1879-1892

Spillman W, Huston D, Fuhr P, Lord J. 1993. Neural network damage detection in a bridge element.*SPIE Smart Sensing, Processing, and Instrumentation*1918**:**288-295.

Stoer J, Bulirsch R. 1980. *Introduction to Numerical Analysis* Springer-Verlag, New York.

Stephan C. 2012. Sensor placement for modal identification.*Mechanical System and Signal Processing* 27**:**461-470.

Teughels A, Maeck J, De Roeck G. 2002. Damage assessment by FE model updating using damage functions.*Computers and Structures* 80**:**1869-1879.

Teughels A, De Roeck G. 2004. Structural damage identification of the highway bridge Z24 by FE model updating. *Journal of Sound and Vibration* 278**:**589-610.

Titurus B, Friswell M.I. 2008. Regularization in model updating.*International Journal for Numerical Methods in Engineering* 75(4)**:**440-478.

Thoren A.R. 1972. Derivation of mass and stiffness matrices from dynamic test data.*AIAA conference paper* 72-346.

Tu Z, Lu Y. 2008. FE model updating using artificial boundary conditions with genetic algorithms.*Computers and Structures*86**:**714–727.

Tikhonov AN, Arsenin VY. 1993. Solutions of ill-posed problems.Wiley, New York.

Van Overschee P, De Moor B. 1996. *Subspace identification for linear systems: Theory, implementation and applications*, Kluwer, Dordrecht, The Netherlands.

Verboven P, Guillaume P, Cauberghe B, Vanlanduit S, Parloo E. 2004. Modal parameter estimation from input-output Fourier data using frequency-domain maximum likelihood identification.*Journal of Sound and Vibration* 276(3-5)**:**957-979.

Warren C, Niezrecki C, Avitabile P, Pingle P.2011. Comparison of FRF measurements and mode shapes determined using optically image based, laser, and accelerometer measurements. *Mechanical Systems and Signal Processing* 25(6)**:**2191-2202.

Wang J.Y, Ko J.M, Ni Y.Q. 2000. Modal sensitivity analysis of Tsing Ma Bridge for structural damage detection.*4th Nondestructive Evaluation of Highways, Utilities, and Pipelines Conference,*Newport Beach, 7-9 March.

Wang L, Chan, T. H.T. 2009. Review of vibration-based damage detection and condition assessment of bridge structures using structural health monitoring. *2nd Infrastructure Theme Postgraduate Conference*, Queensland University of Technology, Australia.

Wang Z, Lin R.M, Lim M.K. 1997. Structural damage detection using measured FRF data. *Computer Methods in Applied Mechanics and Engineering* 147(1-2)**:**187-197.

Wendy E. Daniell, John H.G. Macdonald. 2007. Improved finite element modelling of a cable-stayed bridge through systematic manual tuning. *Engineering Structures* 29(3)**:**358-371.

Weng S, Xia Y, Xu Y.L, Zhu H.P. 2011. Substructure based approach to finite element model updating. *Computers and Structures* 89**:**772-782.

Wenzel H, Pichler D. 2005. Ambient vibration monitoring. John Wiley & Sons Ltd, England.

Wu J.R, Li Q.S. 2006. Structural parameter identification and damage detection for a steel structure using a two-stage finite element model updating method. *Journal of Constructional Steel Research* 62**:**231-239.

Wu J.R, Li Q.S. 2004. Finite element model updating for a high-rise structure based on ambient vibration measurements. *Engineering Structures* 26**:**979-990.

Xia Y, Lin R. 2004. Improvement on the iterated IRS method for structural eigensolutions. *Journal of Sound and Vibration*270(4-5)**:**713-727.

Xu Y. G, Liu G. R. 2002. Detection of flaws in composites from scattered elastic-wave field using an improved GA and a local optimizer. *Computer Methods in Applied Mechanics and Engineering* 191**:**3929-3946.

Xu B, He J, Rovekamp R, Dyke S J. 2012. Structural parameters and dynamic loading identification from incomplete measurements: Approach and validation. *Mechanical Systems and Signal Processing* 28**:**244-257.

Yan A.M, Golinval J.C. 2005. Structural damage localization by combining flexibility and stiffness methods.*Engineering Structures* 27(12)**:**1752-1761.

Yan Y.J, Cheng L, Wu Z.Y, Yam L.H. 2007. Development in vibration-based structural damage detection technique.*Mechanical Systems and Signal Processing* 21**:**2198-2211.

Yang Q.W, Liu J.K. 2007. Structural damage identification based on residual force vector. *Journal of Sound and Vibration* 305**:**298-307.

Yang X.F, Swamidas S.J, Seshadri R. 2001. Crack identification in vibrating beams using the energy method. *Journal of Sound and Vibration* 244(2)**:**339-357.

Yang Y.B, Chen Y.J. 2009. A new direct method for updating structural models based on measured modal data. *Engineering Structures* 31**:**32-42.

Yin T, Lam H.F, Chow H.M, Zhu H.P. 2009.Dynamic reduction-based structural damage detection of transmission tower utilizing ambient vibration data.*Engineering Structures* 31(9)**:**2009-2019.

Yu L, Cheng L, Yam L.H, Yan Y.J. 2007. Application of eigenvalue perturbation theory for detecting small structural damage using dynamic responses.*Composite Structures* 78(3)**:**402-409.

Yuen K.V. 2012.Updating large models for mechanical systems using incomplete modal measurement.*Mechanical Systems and Signal Processing* 28**:**297-308.

Yu J, Ziehl P, Zárate B, Caicedo J. 2011. Prediction of fatigue crack growth in steel bridge components using acoustic emission. *Journal of Constructional Steel Research* 67(8)**:**1254-1260.

Zapico-Valle J.L, Abad-Blasco J, González-Martínez M.P, Franco-Gimeno J.M, García-Diéguez M. 2012.Modelling and calibration of a beam-column joint based on modal data.*Computers and Structures* Article in Press.

Zhan J.W, Xia H, Chen S.Y, De Roeck G. 2011. Structural damage identification for railway bridges based on train-induced bridge responses and sensitivity analysis.*Journal of Sound and Vibration* 330**:**757-770.

Zhang L, Brincker R, Andersen P. 2005. An overview of operational modal analysis: Major development and issues. *1st International Operational Modal Analysis Conference,* Aalborg Universitet, Copenhagen, Denmark 179-190.

Zhang Z. Y. 2007. A development of modal expansion method for eigensensitivity analysis of a defective matrix.*Applied Mathematics and Computation* 188(2)**:**1995-2019.

Zhao J, DeWolf J.T. 1999. Sensitivity study for vibrational parameters used in damage detection.*Journal of Structural Engineering* 125(4)**:**410-416.

Zivanovic S, Pavic A, Reynolds P. 2007. Finite element modelling and updating of a lively footbridge: The complete process.*Journal of Sound and Vibration* 301**:**126-45.

Zivanovic S, Pavic A, Reynolds, P. 2006. Modal testing and FE model tuning of a lively footbridge structure. *Engineering Structures* 28(6)**:**857-868.

Appendix

Matlab program for on-line structural damage detection

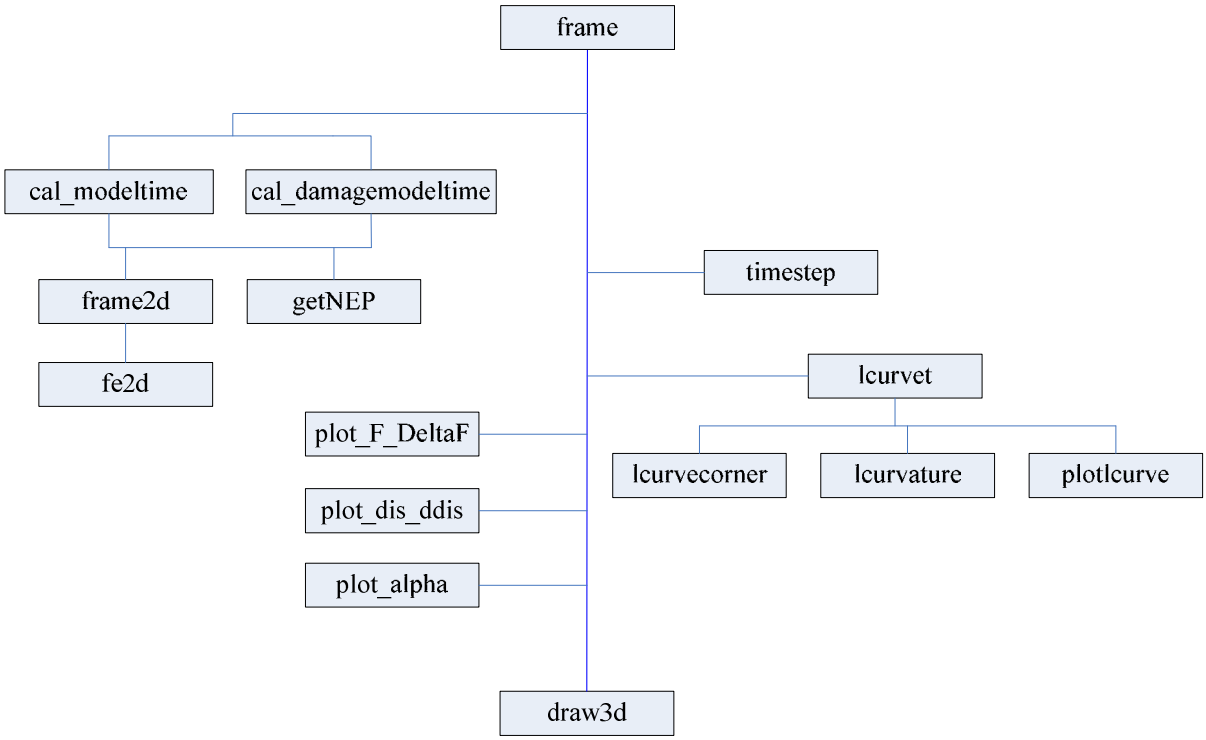

Figure A. Flowchart diagram for online damage detection program

To implement the proposed on-line structural damage detection method inapplication, a program is developed in the Matlab environment. It contains four primary categories: structural modelling, vibration response simulation, damage identification and graphical presentation. In this program, damage refers to loss in stiffness and mass remains unchanged. The following primary functions are included in the Matlab program discussed above.

frame is main function of online damage detection program. It calls sub-functions for analysis and produce results.

cal_modeltime is called by “frame” for the information of the system matrices such as stiffness and mass of the undamaged structure.

cal_damagemodeltime provides information of stiffness and mass matrices of the damaged structure.

getNEPis a sub-function to provide the information of geometry and material properties of the structural system for “cal_modeltime” and “cal_damagemodeltime”.

frame2dassembles stiffness and mass matrices of the structural system and provides those information to “cal_modeltime” and “cal_damagemodeltime”.

fe2d computesstiffness and mass matrices of individual element for “frame2d”.

timestep computes incremental time step for“frame”.

lcurvet is called by “frame” for the information of L-curve.

lcurveconer computes L-curve corner and feeds that information to“lcurvet”.

lcurvature provides information of L-curve curvature to “lcurvet”.

plotlcurveis a sub-function for plotting of L-curve.

plot_F_DeltaF plots applied force and incremental applied force in time domain.

plot_dis_ddisplots displacements of undamaged and damaged structure in time domain.

plot_alphaplots damage parameters in time domain.

draw3d is final sub-function called by “frame” for plotting of structural geometry.

The main part of on-line damage detection in the program is as follow:

```
%*********************************************************************
%                                                                    *
%  frame:   main program for online structural damage detection     *
%                                                                    *
%*********************************************************************
% Remark:                                                           *
%  k_sys       =  system stiffness matrix of undamaged structure    *
%  m_sys       =  system mass matrix of undamaged structure         *
%  d_sys       =  system damping matrix of undamaged structure      *
%                                                                    *
%  dk_sys      =  system stiffness matrix of damaged structure      *
%  dm_sys      =  system mass matrix of damaged structure           *
%  dd_sys      =  system damping matrix of damaged structure        *
%                                                                    *
%  ke_sys      =  element stiffness matrix of the system            *
%                                                                    *
%  X_cur       =  displacement of undamaged structure at current    *
```

```
%                   time step                                          *
%  Xp_cur       =  velocity of undamaged structure at current         *
%                   time step                                          *
%  Xpp_cur      =  acceleration of undamaged structure at current     *
%                   time step                                          *
%                                                                      *
%  X_old        =  displacement of undamaged structure at previous    *
%                   time step                                          *
%  Xp_old       =  velocity of undamaged structure at previous        *
%                   time step                                          *
%  Xpp_old      =  acceleration of undamaged structure at previous    *
%                   time step                                          *
%                                                                      *
%  dX_cur       =  displacement of damaged structure at current     *
%                   time step                                          *
%  dXp_cur      =  velocity of damaged structure at current         *
%                   time step                                          *
%  dXpp_cur     =  acceleration of damaged structure at current     *
%                   time step                                          *
%                                                                      *
%  dX_old       =  displacement of damaged structure at previous    *
%                   time step                                          *
%  dXp_old      =  velocity of damaged structure at previous        *
%                   time step                                          *
%  dXpp_old     =  acceleration of damaged structure at previous    *
%                   time step                                          *
%                                                                      *
%  Iy           =  moment of inertia in the strong axis               *
%  A            =  cross-sectional area                               *
%  E            =  Young's Modulus                                    *
%  rho          =  density                                            *
```

```
%  mbar        =  mass per unit length                              *
%                                                                   *
% Call:  cal_modeltime, cal_damagemodeltime, timestep, lcurvet,     *
%        plot_F_DeltaF, plot_dis_ddis, plot_alpha, draw3d           *
%                                                                   *
% Sub-function: frame2d, getNEP, fe2d, lcurvecorner, lcurvature,    *
%               plotlcurve                                          *
%                                                                   *
%*******************************************************************
```

```
01.for i=1:rdof
02.    tempK(i)=0.;
03. for j=1:rdof
04.if (noiseinput==1)      %without noise
05.   tempK(i) = tempK(i)+((m_sys(i,j)*(Xpp_cur(j)- dXpp_cur(j))+
                (d_sys(i,j)*Xp_cur(j)- d_d_sys(i,j)*dXp_cur(j))+
                k_sys(i,j)*(X_cur(j)-dX_cur(j))));
06.elseif (noiseinput==2)  %with noise
07.    tempK(i) = tempK(i)+((m_sys(i,j)*(Xpp_cur(j)- dXpp_cur(j))+
                (d_sys(i,j)*Xp_cur(j)- d_d_sys(i,j)*dXp_cur(j))+
                k_sys(i,j)*(X_cur(j)-dX_cur(j))));
08.end
09. end
10.   deltaKdX(i,1)=tempK(i);
11.   DeltakdX(TIME,i)= deltaKdX(i);
12. end
13.for k=1:ne
14.    for i=1:rdof
15.        kedx(i,k)=0.0;
16.       for j=1:rdof
```

```
17.          kedx(i,k)= kedx(i,k)+ke_sys(i,j,k)*(dCk*dXp_cur(j)+dX_cur(j));
18.       end
19.    end
20.end
21.    A=kedx;
22.    b=deltaKdX;
23.if (noiseinput==1)
24.    [U,S,V]=svd(kedx); %singular value decomposition
25.    utb=U'*deltaKdX;
26.    for i=1:ne
27.       Y(i,1)=utb(i)/S(i,i);
28.    end
29.    alpha=V*Y; %computing damage parameters
30.elseif(noiseinput>1)
31.    [U,S,V]=svd(A);
32.    utbb= U'*b;
33.for i=1:ne
34.    s(i,1)=S(i,i);
35.    utb(i,1)=utbb(i);
36.end
37.    xi=utb./s;
38.    [reg_c,eta,rho,rho_c,eta_c,kappa,reg_param] = lcurvet(U,utb,b,s,xi);
39.    lambda_l=reg_c;%L-curve corner
40.for j= 1:ne
41.    alpha(j)=0.0;
42.    for i=1:ne     %computing regularised damage parameters
43.        alpha(j)=alpha(j)+s(i)/((s(i)*s(i))+lambda_l^2)*utb(i)*V(j,i);
44.    end
45.end
46. end
47. plot_alpha(T,Alph,TT,enum)%plotting regularised damage parameters
```

In the above Matlab program, line 05 and 06 refer to right hand side of Eq.(7.43) or Eq.(7.46), line 17 refers to left hand side of Eq.(7.43), line 29 refer to Eq.(7.48) and line 43 refers to Eq.(5.55) for the calculation of damage parameter α_j, respectively.

Input information of detecting damaged elements “8” and “16” in the three-bay braced frame example is as follow:

```
% ***** node coordinates and node condition index*****
X1=6.00; X2=8.00; Y=3.50;
%X-coordinate Y-coordinate  X-translation Y-translation theta-rotation
0=fixed, 1=free
node=[
       0            0            0            0            0    %node 1
      X1            0            0            0            0    %node 2
    2*X1            0            0            0            0    %node 3
 2*X1+X2            0            0            0            0    %node 4
%floor 1
       0            Y            1            1            1    %node 5
      X1            Y            1            1            1    %node 6
    2*X1            Y            1            1            1    %node 7
 2*X1+X2            Y            1            1            1    %node 8
%floor2
       0         2*Y            1            1            1    %node 9
      X1         2*Y            1            1            1    %node 10
    2*X1         2*Y            1            1            1    %node 11
 2*X1+X2         2*Y            1            1            1    %node 12
%floor3
```

```
       0          3*Y          1            1            1    %node 13
      X1          3*Y          1            1            1    %node 14
    2*X1          3*Y          1            1            1    %node 15
 2*X1+X2          3*Y          1            1            1    %node 16
%floor4
       0          4*Y          1            1            1    %node 17
      X1          4*Y          1            1            1    %node 18
    2*X1          4*Y          1            1            1    %node 19
 2*X1+X2          4*Y          1            1            1    %node 20
%floor5
       0          5*Y          1            1            1    %node 21
      X1          5*Y          1            1            1    %node 22
    2*X1          5*Y          1            1            1    %node 23
 2*X1+X2          5*Y          1            1            1    %node 24
%floor6
       0          6*Y          1            1            1    %node 25
      X1          6*Y          1            1            1    %node 26
    2*X1          6*Y          1            1            1    %node 27
 2*X1+X2          6*Y          1            1            1    %node 28
%floor7
       0          7*Y          1            1            1    %node 29
      X1          7*Y          1            1            1    %node 30
    2*X1          7*Y          1            1            1    %node 31
 2*X1+X2          7*Y          1            1            1    %node 32
%floor8
       0          8*Y          1            1            1    %node 33
      X1          8*Y          1            1            1    %node 34
    2*X1          8*Y          1            1            1    %node 35
 2*X1+X2          8*Y          1            1            1    %node 36
%floor9
       0          9*Y          1            1            1    %node 37
```

```
      X1          9*Y             1             1             1    %node 38
    2*X1          9*Y             1             1             1    %node 39
 2*X1+X2          9*Y             1             1             1    %node 40
     ];

% ***** element connectivity and element group *****
%startnode  endnode   elementnumber
elem=[
%base
      1           5           1
      2           6           2
      3           7           3
      4           8           4
      5           6           5
      6           7           6
      7           8           7
      2           7           8
%floor 1
      5           9           9
      6          10          10
      7          11          11
      8          12          12
      9          10          13
     10          11          14
     11          12          15
      6          11          16
%floor 2
      9          13          17
     10          14          18
     11          15          19
     12          16          20
```

```
    13          14          21
    14          15          22
    15          16          23
    10          15          24
%floor 3
    13          17          25
    14          18          26
    15          19          27
    16          20          28
    17          18          29
    18          19          30
    19          20          31
    14          19          32
%floor 4
    17          21          33
    18          22          34
    19          23          35
    20          24          36
    21          22          37
    22          23          38
    23          24          39
    18          23          40
%floor 5
    21          25          41
    22          26          42
    23          27          43
    24          28          44
    25          26          45
    26          27          46
    27          28          47
    22          27          48
```

```
%floor 6
     25          29          49
     26          30          50
     27          31          51
     28          32          52
     29          30          53
     30          31          54
     31          32          55
     26          31          56
%floor 7
     29          33          57
     30          34          58
     31          35          59
     32          36          60
     33          34          61
     34          35          62
     35          36          63
     30          35          64
%floor 8
     33          37          65
     34          38          66
     35          39          67
     36          40          68
     37          38          69
     38          39          70
     39          40          71
     34          39          72
    ];

% ***** material properties *****
Iy=32.814E-5;    %305 x 305 x 137 UKC
```

```
Iy1=Iy;   %Iy of undamaged element 1
Iy2=Iy;   %Iy of undamaged element 2
Iy3=Iy;
Iy4=Iy;
Iy5=Iy;
Iy6=Iy;
Iy7=Iy;

Iy9=Iy;
Iy10=Iy;
Iy11=Iy;
Iy12=Iy;
Iy13=Iy;
Iy14=Iy;
Iy15=Iy;

Iy17=Iy;
Iy18=Iy;
Iy19=Iy;
Iy20=Iy;
Iy21=Iy;
Iy22=Iy;
Iy23=Iy;

Iy25=Iy;
Iy26=Iy;
Iy27=Iy;
Iy28=Iy;
Iy29=Iy;
Iy30=Iy;
```

```
Iy31=Iy;


Iy33=Iy;
Iy34=Iy;
Iy35=Iy;
Iy36=Iy;
Iy37=Iy;
Iy38=Iy;
Iy39=Iy;

Iy41=Iy;
Iy42=Iy;
Iy43=Iy;
Iy44=Iy;
Iy45=Iy;
Iy46=Iy;
Iy47=Iy;

Iy49=Iy;
Iy50=Iy;
Iy51=Iy;
Iy52=Iy;
Iy53=Iy;
Iy54=Iy;
Iy55=Iy;

Iy57=Iy;
Iy58=Iy;
Iy59=Iy;
Iy60=Iy;
```

```
  Iy61=Iy;
  Iy62=Iy;
  Iy63=Iy;

  Iy65=Iy;
  Iy66=Iy;
  Iy67=Iy;
  Iy68=Iy;
  Iy69=Iy;
  Iy70=Iy;
  Iy71=Iy;

%Braces
  Iy8=0.0;
  Iy16=0.0;
  Iy24=0.0;
  Iy32=0.0;
  Iy40=0.0;
  Iy48=0.0;
  Iy56=0.0;
  Iy64=0.0;
  Iy72=0.0;

%control decreasing rate
stiffreduc1=0.0010*TIME;
stiffreduc3=0.0021*TIME;
stiffreduc5=0.0030*TIME;

%stiffness decreasing
if stiffreduc1<=1.0
```

```
stiffleft1= 1-stiffreduc1;
else
    stiffleft1=0.0;
end

if stiffreduc3<=1.0
stiffleft3= 1-stiffreduc3;
else
    stiffleft3=0.0;
end

if stiffreduc5<=1.0
stiffleft5= 1-stiffreduc5;
else
    stiffleft5=0.0;
end

A =174.0E-4;        %305 x 305 x 137 UKC
E    =2.10E11;
rho=7850;
mbar =rho*A;
Ab =174.0E-4;
mbarb =rho*Ab;       % for brace element

Eb8 = E;               %brace element
Eb16 = E;
Eb24 = E;
Eb32 = E;
Eb40 = E;
Eb48 = E;
```

```
Eb56 = E;
Eb64 = E;
Eb72 = E;

Eb8 = stiffleft3*E;    %damaged brace element
Eb16 = stiffleft5*E;

%***** element properties for different element group *****
%***** element number must be ascending order
prop=[
      Iy1 A E mbar     %element 1
      Iy2 A E mbar     %element 2
      Iy3 A E mbar     %element 3
      Iy4 A E mbar
      Iy5 A E mbar
      Iy6 A E mbar
      Iy7 A E mbar
      Iy8 Ab Eb8 mbarb % brace element 8
      Iy9 A E mbar
      Iy10 A E mbar
      Iy11 A E mbar
      Iy12 A E mbar
      Iy13 A E mbar
      Iy14 A E mbar
      Iy15 A E mbar
      Iy16 Ab Eb16 mbarb
      Iy17 A E mbar
      Iy18 A E mbar
      Iy19 A E mbar
      Iy20 A E mbar
      Iy21 A E mbar
```

Iy22 A E mbar

Iy23 A E mbar

Iy24 Ab Eb24 mbarb

Iy25 A E mbar

Iy26 A E mbar

Iy27 A E mbar

Iy28 A E mbar

Iy29 A E mbar

Iy30 A E mbar

Iy31 A E mbar

Iy32 Ab Eb32 mbarb

Iy33 A E mbar

Iy34 A E mbar

Iy35 A E mbar

Iy36 A E mbar

Iy37 A E mbar

Iy38 A E mbar

Iy39 A E mbar

Iy40 Ab Eb40 mbarb

Iy41 A E mbar

Iy42 A E mbar

Iy43 A E mbar

Iy44 A E mbar

Iy45 A E mbar

Iy46 A E mbar

Iy47 A E mbar

Iy48 Ab Eb48 mbarb

Iy49 A E mbar

Iy50 A E mbar

Iy51 A E mbar

Iy52 A E mbar

```
 Iy53 A E mbar
 Iy54 A E mbar
 Iy55 A E mbar
 Iy56 Ab Eb56 mbarb
 Iy57 A E mbar
 Iy58 A E mbar
 Iy59 A E mbar
 Iy60 A E mbar
 Iy61 A E mbar
 Iy62 A E mbar
 Iy63 A E mbar
 Iy64 Ab Eb64 mbarb
 Iy65 A E mbar
 Iy66 A E mbar
 Iy67 A E mbar
 Iy68 A E mbar
 Iy69 A E mbar
 Iy70 A E mbar
 Iy71 A E mbar
 Iy72 Ab Eb72 mbarb
];
```